REAL TIME MODULATION RECOGNITION OF RADAR SIGNALS USING DIGITAL TECHNIQUES FOR NEW GENERATION ELINT SYSTEMS

Submitted in partial fulfilment of the requirements
for the award of the degree of

Doctor of Philosophy

by

Ravindra Kumar Niranjan
(Roll No. 717034)

Supervisor(s)

Prof. CB Rama Rao
Professor, Dept. of ECE
Dr. AK Singh
Scientist 'G', DLRL (DRDO)

DEPARTMENT OF ELECTRONICS AND COMMUNICATION ENGINEERING
NATIONAL INSTITUTE OF TECHNOLOGY,
WARANGAL - 506004, INDIA
2021

Approval Sheet

This Thesis entitled **"Real Time Modulation Recognition of Radar Signals using Digital Techniques for New Generation ELINT Systems" by Ravindra Kumar Niranjan, Roll No. 717034** is approved for the degree of Doctor of Philosophy of Electronics and Communication Engineering of National Institute of Technology, Warangal.

Examiners

_____

_____

_____

Supervisor(s)

Dr. A.K. Singh
Scientist-G
DLRL (DRDO), Hyderabad

Prof. C.B. Rama Rao
Professor, Dept. of ECE
NIT, Warangal

Chairman

Prof. L. Anjaneyulu
Head, Department of ECE, NIT, Warangal

Date :_____

Declaration

This is to certify that the work presented in the thesis entitled **"Real Time Modulation Recognition of Radar Signals using Digital Techniques for New Generation ELINT Systems"** is a bonafide work done by me under the supervision of **Prof. C.B. Rama Rao**, **Professor,** Department of Electronics and Communication Engineering, National Institute of Technology, Warangal and **Dr. A.K. Singh, Scientist-G**, Defence Electronics Research Laboratory (DLRL), DRDO, Hyderabad and was not submitted elsewhere for the award of any degree.

I declare that this written submission represents my ideas in my own words and where others ideas or words have been included, I have adequately cited and referenced the original sources. I also declare that I have adhered to all principles of academic honesty and integrity and have not misrepresented or fabricated or falsified any idea / data / fact / source in my submission. I understand that any violation of the above will be a cause for disciplinary action by the Institute and can also evoke penal action from the sources which have thus not been properly cited or from whom proper permission has not been taken when needed.

(Ravindra Kumar Niranjan)

(Roll No. 717034)

Place: Warangal

Date:

DEPARTMENT OF ELECTRONICS AND COMMUNICATION ENGINEERING
NATIONAL INSTITUTE OF TECHNOLOGY,
WARANGAL - 506004, INDIA

Certificate

This is to certify that the thesis entitled "**Real Time Modulation Recognition of Radar Signals using Digital Techniques for New Generation ELINT Systems**" is being submitted by **Mr. Ravindra Kumar Niranjan (Roll No. 717034)**, in partial fulfilment of the requirement for the award of the degree of Doctor of Philosophy of Electronics and Communication Engineering of National Institute of Technology, Warangal, is a record of bonafide research work carried out by him under our supervision.

To the best of our knowledge, the work incorporated in this thesis has not been submitted elsewhere for the award of any degree.

Dr. A.K. Singh
(Co-Supervisor)
Scientist-G
Defence Electronics Research Laboratory (DLRL), DRDO,
Hyderabad - 500005, India

Prof. C.B. Rama Rao
(Supervisor)
Professor
Department of ECE,
National Institute Technology,
Warangal - 506004, India

I would like to dedicate my thesis to my family for their support without them it would have been difficult to carry out this research work.

Acknowledgements

It gives me immense pleasure to convey my deep sense of gratitude and sincere thanks to my supervisor **Prof. C.B. Rama Rao**, Professor, Department of ECE, NIT, Warangal, and **Dr. A.K. Singh, Sc-G**, DLRL-DRDO, Hyderabad, for their perpetual encouragement, guidance, and supervision. Their steady influence throughout my Ph.D. career has oriented me in a proper direction and supported me with promptness and care. They not only gave me the required knowledge to pursue my research work, but also gave me the required moral support during my hard times. I truly appreciate their logical and thought provoking advises both technically and morally which I will follow for the rest of my life.

Also, I take this privilege to thank all my Doctoral Scrutiny Committee members, **Prof. L. Anjaneyulu**, Professor, Head Department of ECE, **Prof. N.V.S.N. Sarma**, Professor, Department of ECE, **Prof. J.V. Ramana Murthy**, Professor, Mathematics Department, **Dr. P. Muralidhar**, Associate Professor, Department of ECE, for their detailed review, constructive suggestions, and excellent advice during the progress of this research work.

I express my heartfelt gratitude to **Prof. L. Anjaneyulu**, Head, Department of ECE, for his valuable suggestions, cooperation, help, and moral support towards the completion of the research work. Also, I extend my thanks to senior Professors of ECE Dept. **Prof. N. Bheema Rao** and **Prof. T. Kishore Kumar** for their continuous support and motivation. I thank all the faculty and non-teaching staff of ECE **Dept. at NIT Warangal** who helped me during the tenure of my research work.

I am grateful to **Dr. K. Maheswara Reddy, Distinguished Scientist & Director DLRL,** and **Sri JRC Sarma, Sc-F, Head HRD** and Members of the HRD for granting me permission for the research work through the development of this thesis in DLRL.

I am immensely thankful to **Sri R. Anand, Sc-G, Additional Director,** Directorate of Radar ECM and RFPS, DLRL, and **Smt. N. Sarada, Sc-G, Head, RFPS Wing,** DLRL for giving me this opportunity and also providing the facilities at RFPS Wing, DLRL.

I am also grateful to all my colleagues, scholars, friends, and well-wishers who helped me to write my thesis with their support. Also, especially I would like to thank Mr. S. Siva

Prasad and Mr. Y.V. Koteswara Rao for their help and support during my Ph.D. I also acknowledge my gratitude to Mr. Kumar Gautam, Mr. Gautam Kumar, and Mr. Lalit Kumar for their support during my research work.

Finally, I am very much grateful to my parent, wife Neelam, my son Priyanshu, and my daughter Vaishnavi for their support, understanding and sacrifice during my research work.

Ravindra Kumar Niranjan

Abstract

This research work considers the problem of accurate estimation of radio frequency (RF), pulse amplitude (PA), angle-of-arrival (AOA), and modulation on pulse (MOP) in the background of its application to new generation electronic intelligence (ELINT) system. The estimation algorithms for the above parameters must be computationally fast, highly accurate, and will need to be implemented using digital hardware for processing.

The received signal is digitized and the signal is preprocessed before signal detection. Noise cancellation using spectral subtraction is performed as part of preprocessing for improvement of signal-to-noise ratio. Noise cancellation is carried out by estimating the average noise from the electromagnetic environment. The estimated average noise magnitude is subtracted from the magnitude of the incoming noisy signal without affecting the phase and restored signal is obtained. It is applied on both in-phase and quadrature-phase channels and restored signal is computed for both the channels. Then moving autocorrelation with different delays is performed on the complex signal to further enhance the signal and reduce the effect of noise. Autocorrelation is computationally intensive but an efficient technique is used for implementation and an instantaneous amplitude profile is obtained.

Noise estimation with different delays are performed using amplitude profile and signal is detected. The leading edge and trailing edge of the pulses are also detected using amplitude profile for pulsed signal. Whereas, to compute an accurate instantaneous frequency profile of the received signal the multilevel autocorrelation algorithm is proposed. This frequency profile is used for modulation identification as the modulation information is lost in the amplitude profile.

Three antenna-based virtual baseline interferometry is proposed as a suitable algorithm for AOA estimation that meets the operational requirements of high altitude electronic intelligence system. However, phase measurements ambiguity occurs in sparse array geometries due to phase wrapping effects. Hence, phase ambiguities are resolved using the extensive ambiguities resolution algorithms using three antennas.

A novel decision-tree algorithm based on the time-domain digital technique is developed for the identification and classification of diverse radar intra-pulse modulated signals in real-time. This includes no-modulation continuous wave (NMCW), frequency

modulated continuous wave (FMCW), no-modulation on pulse (NMOP), linear frequency modulation (LFM), non-linear frequency modulation (NLFM), stepped frequency modulation (SFM), and bi-phase modulation (BPM), LFM with SFM, and SFM with BPM. The proposed algorithm is employed on instantaneous frequency profile and modulations are recognized in real-time. The modulation type and modulation parameter are important for specific emitter identification where similar radars are operating in a dense environments. Simulations are carried out at various signal-to-noise ratio conditions and results are presented for modulation recognition.

This thesis will introduce the noise cancellation technique to improve the signal-to-noise ratio and signal estimation is carried out. Moving autocorrelation will be used to estimate instantaneous amplitude profile and a multilevel autocorrelation technique will be introduced for instantaneous frequency estimation. FFT-based frequency is also estimated using interpolation techniques. The virtual antenna-based baseline interferometry for AOA estimation using three antennas is proposed which is SWaP optimized. The decision-tree algorithm for real-time modulation recognition will be used to estimate the modulation and their parameters. The models for all the algorithms are developed using a system generator and implemented in FPGA. These results are compared with existing digital in-phase and quadrature-phase techniques.

Finally, AOA and MOP parameters are highly useful for specific emitter identification. This will be able to identify emitters operating nearby frequencies in the vicinity because MOP is expected to be different even for similar AOA of emitters.

Keywords: Autocorrelation, Noise cancellation, Digital in-phase quadrature-phase, Virtual baseline interferometry, Modulation recognition, Decision-tree algorithm.

Contents

List of Figures

List of Tables

Abbreviations

Abbreviation	Description
ADC	Analog-to-Digital Converter
ADF	Amplitude Comparison Direction Finding
AOA	Angle of Arrival
BLI	Baseline Interferometry
BPM	Bi Phase Modulation
BRAM	Block Random Access Memory
BW	Bandwidth
CLB	Configurable Logic Block
CORDIC	Coordinate Digital Computer
CPLD	Complex Programmable Logic Device
CRT	Chinese Remainder Theorem
CW	Continuous Wave
DIFM	Digital Instantaneous Frequency Measurement
DIQ	Digital In-phase Quadrature-phase
DOA	Direction of Arrival
DAC	Digital-to-Analog Converter
DSP	Digital Signal Processor
EA	Electronic Attack
EDA	Electronic Design Automation
ELINT	Electronic Intelligence
EOB	Electronic Order of Battle
ES	Electronic Support
ESM	Electronic Support Measure
EP	Electronic Protection
EW	Electronic Warfare
ET	Emitter Type
FER	Front End Receiver
FFT	Fast Fourier Transform
FDOA	Frequency Difference of Arrival
FGA	Fine Grain Analysis

FIR	Finite Input Response
FMCW	Frequency Modulated Continuous Wave
FOV	Field of View
FPGA	Field Programmable Gate Array
HDL	Hardware Description Language
IFM	Instantaneous Frequency Measurement
JTAG	Joint Test Action Group
LFM	Linear Frequency Modulation
LPI	Low Probability of Intercept
LUT	Look Up Table
MAC	Multiply Accumulators
MOP	Modulation On Pulse
MP	Modulation Parameters
MT	Modulation type
NLFM	Non-Linear Frequency Modulation
NMOP	No Modulation On Pulse
PA	Pulse Amplitude
POI	Probability of Intercept
PRF	Pulse Repetition Frequency
PDW	Pulse Descriptor Word
PDOA	Phase Difference of Arrival
PRI	Pulse Repetition Interval
QDR	Quad Digital Receiver
QSHR	Quad Superhetrodyne Receiver
PW	Pulse Width
RDF	Rotary Direction Finding
RF	Radio Frequency
RMS	Root Mean Square
RMSE	Root Mean Square Error
RWR	Radar Warning Receiver
SFM	Stepped Frequency Modulation
SNR	Signal to Noise Ratio
TDOA	Time Difference of Arrival
VBI	Virtual Baseline Interferometer
VHDL	Very High Speed Hardware Description Language

Notations

Notation	Description
$x(t)$	Time domain signal
X_m	Restored signal spectrum
$\overline{N_m}$	Average noise spectrum
Y_m	Noisy signal spectrum
$x(m)$	Restored time domain signal
m, n	Index number
η	SNR of the signal
k	Bin number
ΘY_k	Phase of the Frequency Spectrum
F_s	Sampling Frequency
$\Phi(n)$	Phase of the signal
$d\Phi(n)$	Phase difference
$F_m(n)$	Multilevel Frequency
Θ	Incident angle
Ψ_{ld}	First order virtual phase delay
Ψ_{δ}	Second order virtual phase delay
F	Radio frequency
D	Antenna separation
d_{NL}	Distance between N and 1 antenna's
C	Speed of light
λ	Wavelength
$\lambda_{\min}$	Wavelength of the highest frequency
d_{δ}	Virtual antenna separation
M	Peak frequency bin
S_{f}	Sampling rate
M	FFT number of points
p	Interpolated peak location
S_0	Magnitude of peak bin
S_1	Magnitude of previous peak bin

S_2	Magnitude of next peak bin
$x(nt_s)$	Discrete time signal
t_s	Sampling time
f_s	Sampling frequency
ϕ	Initial phase of the signal
τ	Fixed value in time
α	Ascending chirp rate
β	Descending chirp rate
ω	Angular frequency
T	Time duration
f_c	Centre frequency of IF signal
F_{max}	Maximum frequency of FMCW signal
F_{min}	Minimum frequency of FMCW signal
F_{LE}	Leading Edge Frequency
F_{TE}	Trailing Edge Frequency
F_{IP1}	Frequency at first intermediate point
F_{IP2}	Frequency at second intermediate point
F_{CNT}	Centre frequency during pulse
δf	Frequency deviation
f_m	Sinusoidal modulating frequency
Δf	Frequency tolerance limit
ϕ	Phase tolerance limit

Chapter 1

Introduction

This chapter aims to provide background, introduce electronic intelligence systems, the importance of modulation identification, and motivation. The problem statement, objectives, scope of work presented, and significant contributions have also been revealed in this chapter. Finally, the thesis organization has been presented to give an overview of the individual chapters.

1.1 Introduction

The research work aims to investigate fast and highly accurate modulation on pulse (MOP), radio frequency (RF), and angle-of-arrival (AOA) algorithms that can be implemented in ELINT systems for real-time electronic surveillance or electronic support (ES). This will lead to the correct specific identification of emitters. Though the problem of estimation of the above parameters has been studied extensively in radar, communication, sonar, astrology metrology, it has specific application to the electronic support environment that necessitate additional attention due to the specific and challenging operational requirements of ELINT systems.

The AOA and MOP are the two important parameters to be estimated by ELINT systems. The estimation of AOA is expected from any ELINT systems whereas the estimation of MOP cannot be expected from all ELINT systems in real-time. Both the parameters are exploited and in several strategic and operationally useful ways. However, due to a tradeoff generally exists between accuracy and computational time of algorithms, the accurate algorithm is chosen based on the balance between accuracy and high-speed. The research work aims to investigate high accuracy, but possible sub-optimal, estimation algorithms for AOA and MOP that are computationally fast and that are suited for real-time application for radar ELINT systems.

AOA is the parameter that can’t be camouflaged by radar operators, and MOP is not been identified by most of the intercept receivers in real-time. Both the parameters are helpful

to identify specific emitters in a dense environment where radars with nearby frequencies are operating simultaneously.

MOP identification has become an active area over the two decades. Various researchers have proposed different techniques most of them are frequency domain techniques which are based on spectral analysis. These techniques are useful for offline processing. The details of this research area are described in the literature survey.

1.2 Background

Electronic Warfare (EW) systems preserves the electromagnetic (EM) spectrum for friendly use where same time deny its use to the hostile systems. EW systems are classified based on the functionality, frequency coverage, and their function etc. [1]-[2].

EW systems are categorized into three types of systems Electronic Support (ES), Electronic Attack (EA), and Electronic Protection (EP). ES is also known as Electronic Support Measure (ESM) systems. It does the search of the emissions present in the environment. It does the capturing and detection of the emitters. It locates the emitters present based the signals detected. Further, it record the signals in digital domain and processed parameters which is used to analyse the signals in future or after the mission is completed. This information is used to formulate the electronic order of battle (EOB). It can also provide the information to electronic attack (EA) in real-time for the counter measure. EA systems are used to reduce the impact of hostile systems. It is also known as electronic counter measure (ECM). Electronic Protection (EP) systems are the capability of our own radar systems used to protect own systems. These systems are capable to misguide the hostile systems. It is also known as electronic counter counter measure (ECCM).

EW systems are classified as strategic system or tactical system based on their function. Strategic systems are systems which are used for offline analysis. They measure more parameters with high accuracy. These systems are useful to form the EOB which is useful to build the radar library. The deployment of systems can be obtained based on the available data. Usually ELINT systems are categorized as strategic system. The tactical systems provides the limited information but in real-time. The parameters measured in real-time by ES systems are useful for EA systems for immediate use. Tactical systems are useful for dynamic deployment and dynamic change of mode of emitters. The information obtained by tactical systems can be used to form EOB and threat library also can be prepared. But

presently, the ELINT systems are being used as tactical systems to get the advantage of high sensitivity and measures more parameters compared to ES system.

Radar ES Systems are categorized as Radar Warning Receiver (RWR), Electronic Support Measures (ESM), and Electronic Intelligence (ELINT). The RWR receivers are with quick reaction time, wide frequency coverage, spatial coverage, and with highest probability-of-intercept (POI). It provides the warning to the pilot immediately after detecting the radar which is used to guide the weapons. Once radar main beam looks to the target the receiver with a reasonable sensitivity detects it. It uses the range advantage to detect and indicate a threat. Generally, it is the simplest form of ESM receivers [3].

The ESM systems are mainly wideband, spatial coverage with high POI and also known as ES systems. These systems extracts most of the parameters about radar and establish the EOB. They are more complex and higher measured parameters accuracy than RWR receivers. Basically an ELINT system measures various parameters and these parameters are helpful for strategic planning. The measurement of various parameters are comparatively little slow but helpful for fine grain analysis and requires high SNR compared to ES systems. Its instantaneous bandwidth is less than the ES system and hence its POI is also less. If collected data is not possible to process immediately in the field or collection station due to time constraint, it can be stored and processed later at main station.

In this thesis work, a new generation ELINT system is proposed which can measure most of the parameters including modulation information in real-time. These systems can be used for tactical operations as the mode of adversary radars will be certainly different from peacetime. The need for all adversary radars parameter measurement is important in real-time to recognize the threat in the field itself.

1.3 Electronic Intelligence System

The interception and exploitation of electromagnetic energy of radar signals have been an important objective of military reconnaissance since the existence of radar. Electronic support (ES) systems gathered the information from intercept receivers mainly used by military platforms viz. ground, mobile vehicle, ship borne, airborne, and space borne based to enhance the situation awareness of the operating environment, provide self-protection and contribute to electronic intelligence (ELINT) databases.

A new generation ELINT system identifies the radars by analyzing their signal waveforms. This is achieved by using hardware that can detect reliably and measure the

characteristics of all radar signals in the environment. The characteristics of intercepted radar signals that are generally estimated include the following parameters

- Emitter Type (ET)
- Radio Frequency (RF)
- Pulse Amplitude (PA)
- Pulse width (PW) or Pulse duration
- Time-of-arrival (TOA)
- Angle-of-arrival (AOA)
- Inter-pulse modulation characteristics i.e. Pulse repetition interval (PRI) and PRI type [23]
- Intra-pulse modulation characteristics or modulation on pulse (MOP) parameter i.e. Modulation type (MT) and their modulation parameters (MP) [59], [126], [127]

Among the above parameters modulation on pulse (MOP) parameter is an important evaluation parameter in the proposed research work. Further, RF, PA, and AOA parameters are also used for performance evaluation and all the parameters are SNR dependent.

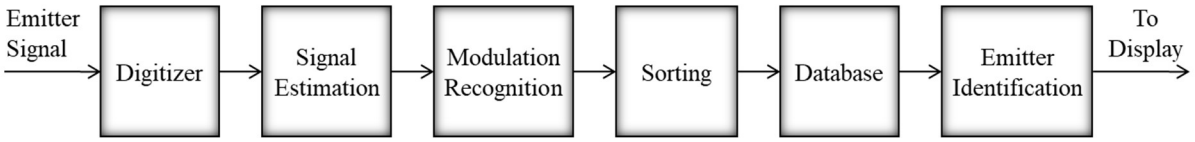

Figure 1.1: Block diagram of functions performed by electronic intelligence receiver.

Once the characteristics of all radar signals have been estimated, electronic intelligence receivers use the estimated parameters to sort the collection of intercepted signals to identify all the intercepts which belong to a single radar emitter. An ELINT database of known radar emitters is then consulted and matched to find a radar emitter that exhibits parameters that best matches estimated characteristics of observed intercept.

ES systems are divided into the category of ELINT system and tactical ES system. The ELINT systems are designed to get the high fidelity data to generate high-quality representations of radar signals. These signals are used to contribute to the ELINT database which is used by ES systems to identify the radars observed in the field. The estimation accuracy is more important compared to execution time for ELINT systems as the analysis can be performed often offline.

On the other hand, the tactical ES systems are designed to provide the operators of military platforms with real-time, early warning of radar receivers that are operating in the vicinity of the platform. Sometimes tactical ES systems are known as Early Warning Receivers. Traditionally, tactical ES systems are designed as Electronic Support Measure (ESM) and Radar Warning receivers (RWR). Usually, ESM systems are interactively operated by human operator whereas RWR systems are fully automated. In extreme operating environments, a tactical ES system may receive over hundreds or thousands of radar intercepts per second. The accuracy of estimation algorithms is important, the data throughput can be sustained is an important consideration. As a result, tactical ES systems may need to trade off some accuracy in the parameter estimation algorithms for the sake of improvements in the data throughput. A new generation ELINT systems emphasize on both estimation accuracy and execution time. The development of computationally fast algorithms for detection and parameter measurements is a major driver of the research presented in this thesis which is implementable for real-time applications.

1.4 Importance of modulation recognition on radar signals

The importance of MOP along with AOA measurements are particularly important parameters among the characteristics of the Radar signals because they can be exploited in many operationally useful ways:

- enhance situational awareness [1]-[3]
- enhance signal de-interleaving (or sorting) algorithms [3]
- enhance identification of emitters operating in the dense environments [3], [12]
- prompt electronic attack (EA) [2], [49], [126], and
- improve signal collection [127], for nearby operating radars are discussed below.

1.4.1 Situational awareness

Situational awareness of the operating environment is critically important to help and determine the engagement priorities, tactics and to formulate electronic order of battle (EOB) [1]-[2], [49]. Correct MOP and accurate AOA estimates can help to improve situational awareness by associating lines of bearing with their intra-pulse characteristics to each detected platform. When MOP from multiple radar intercept receivers is used in conjunction with AOA algorithms, it is possible to further identify the detected platforms.

1.4.2 Sorting or de-interleaving

Radar intercept receivers typically receive anywhere hundreds or thousands of radar intercepts per second from multiple emitters [1], [126]. As part of its typical processing, radar intercept receivers must sort through the collected data and associate all of the intercepts to their respective emitters. This process is known as signal sorting or signal de-interleaving.

Parameters such as the signal radar frequency, pulse duration, pulse train parameters such as PRI and PRI types are traditionally effective de-interleaving parameters [23], [49]. However, the traditional de-interleaving parameters are not effective against radars with similar transmission characteristics or modern parameter-agile radars that are capable of changing their transmission parameters viz. frequency, pulse duration, and PRI on a pulse-by-pulse basis. On the other hand, since the AOA of a signal cannot be camouflaged practically, high precision AOA estimate along with MOP can be used to effectively sort the signal from these types of radars, provided that the radars are sufficiently separated in angle [1], [3], [23], [49]. MOP helps in sorting the intercepts which are coming from the emitters which are marginally separated bearing and frequency in the environment.

1.4.3 Enhance identification of emitter operating in a dense environment

When multiple radars operate in an environment with nearby frequencies and the environment becomes dense. In that condition, identification of emitter with measuring conventional parameters is not sufficient. To overcome this problem, measurement of modulation becomes compulsory. Measurement of MOP using high accuracy RF measurements with AOA provides an advantage to identify the emitter [3], [12]. This also helps in signal sorting.

1.4.4 Electronic attack and electronic protection

Knowing of an adversary bearing and intra-pulse waveform can assist the platform's electronic attack (EA) systems (such as jammers) and electronic protection (EP) systems (such as chaff) by more efficiently directing the platform's resources to deal with a threat from a given bearing and with specific modulation characteristics [2], [49], [126].

1.4.5 Signal enhancement

Preprocessing is exploited prior to the extraction of parameters. As part of preprocessing, noise cancellation is employed for signal enhancement to improve the quality of the signal. Noise cancellation is done by estimating the noise from the system chain. The

estimated noise magnitude is computed for the duration of noise alone. This noise is subtracted from the noisy signal spectrum and signal enhancement is done [127].

1.5 Motivation

The problem of identification of modulation on pulse (MOP) is related to the use of information. This information cannot be utilized for tactical application with the present ELINT systems which is crucial. When hostile radars operate during peacetime, they do not change their operating modes frequently. But hostile radars change their operating modes rapidly during tactical operations. So, the library which is generated over some time for electronic order of battle (EOB) may not be much constructive. The research work on this topic will be helpful, to use this information tactically in the field environment. This proposed research work will identify MOP in real-time which can be used for de-interleaving and specific emitter identification effectively.

Some researchers have proposed techniques for modulation identification using frequency domain techniques and convolutional neural network (CNN) [62]-[64], [74], [84], [92]. These research contributions are only for offline processing and real-time processing is not considered by them. As computational complexities are high for real-time processing. Hence, it is able to reduce the computation's complexities. Further, hardware portability's are also required to test the proposed architecture for modulation recognition in real-time for the ELINT system. The aspect of radar signals modulation recognition in real-time has been motivated to take up this work for classifying various radar signals modulations for a new generation ELINT systems. The noise cancellation technique as part of preprocessing, instantaneous amplitude measurement, noise estimation for adaptive threshold computation, high accuracy instantaneous frequency measurement, FFT based frequency estimation, and three-antenna based virtual baseline interferometry for AOA measurement algorithms are also developed to achieve the above goal. FFT based frequency estimation along with various interpolation techniques enhances the frequency accuracy without increasing the number of FFT points. All the parameters are required to be measured accurately to achieve the objectives of the proposed research work.

1.6 Problem statement

A research problem is proposed as "real-time modulation recognition of radar signals using digital techniques for new generation ELINT systems". The main focus of this thesis is the real-time characterization of radar signals.

1.7 Aim and Objectives

The research work has undertaken aims at developing modulation recognition algorithms of radar signals in real-time.

The following are the aims and objectives of the proposed research work:

- To implement noise cancellation using spectral subtraction technique as part of preprocessing and thus enhancing the radar signal.
- To carry out high accuracy instantaneous frequency measurement and amplitude measurement.
- To estimate noise for the signal duration and compute the adaptive threshold for detection of radar signal (instantaneous amplitude).
- To measure AOA with three antennas BLI algorithm which results in lightweight ELINT system.
- To find out the MOP and their modulation parameter using instantaneous frequency in real-time.

1.8 Scope of work and significant contributions

Scope of work presented and significant contributions are given in this section.

1.8.1 Scope of work presented

The scope of this thesis entails to identify and classify radar signals modulations. Total sixteen types of modulations and their parameters are measured using proposed algorithms. Various radar signals are generated at different SNR conditions and measurements are carried out. The efficacy of these algorithms is also verified using field data. Signal enhancement, frequency estimation, and AOA estimation are also part of the scope of a thesis as these parameter estimations are also important for modulation recognition.

1.8.2 Significant contributions from investigations

The real-time measurement of all the parameters including modulation information is carried out in this research work. The various parameters measurement including direction finding, type of signal, RF frequency, Pulse width, Pulse repletion interval, amplitude, type of modulation, modulation parameter is estimated and formed pulse descriptor word (PDW). All the processing algorithms are designed using a system generator, implemented on a hardware platform, and results are presented.

FPGA provides the hardware environment in which dedicated DSP processing capabilities can be implemented and tested for their functionality. They perform very high-

speed operations that cannot be realized by a DSP processor because of hardware limitations. The primary advantage that FPGA offers is parallel architecture, fine grain resources, availability of MACs known as DSP slices in the order of thousands, re-programmability etc. These capabilities of FPGAs made the preferred choice of hardware platform over DSP processors.

The Digital Signal Processors is the correct choice for the ELINT system for strategic use. But they are not useful for ELINT systems for tactical application. As they are not giving real-time performance because the required sampling rate is high. The reason is, the maximum number of MACs available in the processor is limited and the same MACs is re-used for computation. Whereas in FPGA a large number of MACs are available so that the parallel architecture is possible.

Improving the performance of the ELINT system by measuring all the parameters in real-time. So that the ELINT system can be utilized for tactical applications. Various signal processing algorithms are implemented on the FPGA platform to enhance the speed and maintain the accuracy of parameters. The details of the contribution are explained below:

- Signal enhancement is carried out using spectral subtraction. Spectrum on incoming digitized IF data is computed continuously and an average of noise is estimated. Later, these average noise components are subtracted from the data spectrum and the enhanced signal is achieved by inverse spectrum. This signal enhancement or noise cancellation is implemented and provides an SNR advantage.
- An autocorrelation algorithm is used to generate instantaneous amplitude and a multilevel autocorrelation algorithm is used to generate instantaneous frequency profiles. Again SNR advantage is achieved when performance of autocorrelation algorithm is compared with DIQ technique. The high-frequency accuracy is achieved at lower SNR which is useful for AOA and MOP estimation.
- The noise estimation is done using standard deviation. The fast and easy approach is implemented which gives comparable results with standard deviation implemented. The detection logic is implemented in the FPGA which is based on the comparison with either noise riding threshold or fixed threshold.
- SWaP optimized three antenna-based BLI algorithm is proposed for AOA estimation. This algorithm along with noise cancellation provide an advantage equivalent to four antenna BLI arrays. AOA is useful for emitter sorting.

- Instantaneous frequency profile is used for the MOP estimation using a decision-tree algorithm. Various modulations are identified using the proposed approach which is useful for specific emitter identification.

1.9 Organization of Thesis

The research thesis writing is organized in eight chapters. The following is the brief of each chapter.

Chapter 1, introduces the electronic intelligence systems, importance, and application of these systems. In addition to this, motivation, problem statement, objectives, the scope of work, significant contribution, and chapter organization of thesis have been given in this chapter.

In Chapter 2, a detailed literature survey has been provided. Literature that are related to the work are reviewed carefully and cited in the thesis.

In Chapter 3, the theory of contemporary frequency measurements techniques is presented. This chapter will show the suitable frequency estimation technique, angle-of-arrival measurement technique, and modulation parameter measurement for implementation in radar intercept receivers. The general performance of each technique and its advantages and disadvantages are discussed.

In Chapter 4, the theory of signal estimation techniques is presented which includes noise cancellation, amplitude measurement based on moving autocorrelation, frequency measurement algorithm based on multilevel autocorrelation, AOA measurement using three antennas is presented. SNR advantage using noise cancellation is explained. Noise estimation for pulse detection is also mentioned.

In Chapter 5, proposed modulation recognition is presented. It includes frequency and phase modulation and they are measured in real-time. The type of modulation is measured using a decision-tree based algorithm applied on instantaneous frequency profile along with instantaneous amplitude profile. The results are compared with existing techniques.

In Chapter 6, the ELINT operation methodology is discussed which includes frequency scan operation, test setup hardware, test conditions, and experimental results. Various stages of testing and field data results are also given. The modulation recognition algorithms are applied to the field data to experimentally validate their performance.

Finally, the thesis will be concluded in Chapter 7. The key findings of the thesis and the major contributions of this research will be concluded. This chapter will also identify areas that may warrant further research.

Chapter 2

Review of Literature

This chapter presents a detailed literature review of existing research contributions.

2.1 Introduction

Electronic Intelligence (ELINT) system extracts information related to modulations schemes in detail from electromagnetic (EM) environment for its survivability but denies or limits it to the adversary. The information of measured emitter parameters then can be utilized to affect the hostile operations to block its communication channel and radar can be stopped from firing the weapons.

There is a need for recognition of radar signal modulation for electronic intelligence systems in real-time. During the past two or three decades electronic intelligence system was configured for offline processing. Researchers whose contributions are given in this chapter are offline related. However, the modulation types and their modulation parameters are required to be measured in real-time. Hence, real-time processing systems are needed. Relevant publications in this field are identified and studied. This chapter consists of the details of critical appraisal of previous work published literature pertaining to the topic of the investigation.

2.2 Radar signal modulations estimation

Finding MOP which is an intra-pulse parameter is a useful parameter to classify radar emitters in a dense electromagnetic environment. The inter-pulse parameters alone are not sufficient to classify radar emitters in this environment. Estimation of MOP is a composite work that requires instantaneous frequency measurement, instantaneous amplitude measurement, adaptive threshold estimation, pulse detection, and direction-finding.

The following radar signal modulations are measured using a decision-tree algorithm.

(a) Continuous wave signal

(i) No-Modulation Continuous Wave (NMCW)

(ii) Frequency Modulated Continuous Wave (FMCW)

(b) Pulsed signal

(i) No Modulation on Pulse (NMOP)

(ii) Linear Frequency Modulation (LFM)

(iii) Non-Linear Frequency Modulation (NLFM)

(iv) Stepped Frequency Modulation (SFM)

(v) Phase Modulation (PM)

(vi) Hybridization of LFM and BPM

(vii) Hybridization of SFM and BPM

2.3 Summary of literature review

The summary of a literature review is given in Table 2.1.

Table 2.1: Summary of literature review

S. No.	Study by	Features	Technique	Outcome	Limitations
1.	Nandi & Azzouz (1995, 96) [65, 66]	Automatic Analogue modulation recognition	Decision theoretic algorithm	Success rate more than 90% at SNR of 10 dB	Applicable for communication signals
2.	Chan & Gadbois (1989) [69]	Identification of modulation types	Identification using envelope properties	SNR requirement of 7 dB	Applicable for communication signals
3.	Dubuc, C. et al. (1999) [68]	AMR algorithm for spectrum monitoring	Decision-tree algorithm	Classify with more than 55% at SNR of 5 dB	Applicable for communication signals
4.	Lopez-Risuefio et al. (2003) [115]	CWLFM, Chirp, BPSK, QPSK, and FSK	STFT, AD, and DFT	90% detection up to -11.5 dB SNR	Real-time performance is not achieved
5.	Kawalec &	Intra-pulse	LDA and TKL	90%	Real-time

	Owczarek (2003) [17]	modulation recognition	techniques	recognition accuracy for SEI	performance is not achieved
6.	You, H. et al. (2004) [70]	LFM signals detection	WVD Hough transform	SNR requirement of -3 dB	Real-time performance is not achieved
7.	Gross & Chen (2005) [10]	Comparison of detection techniques	LPI signals	Requirement of detection threshold of 12 dB SNR	SNR requirement is high
8.	Aly, O.A.M. et al. (2006) [5]	Detection and de-noising	Wavelet-based	Detection up to -24 dB SNR	Suitable for offline processing
9.	Carpentieri & Cuomo (2008) [9]	Pulse detection using adaptive threshold	Instantaneous frequency measurement (IFM)	75 dB dynamic range	Modulation measurement is not attempted
10.	Helton, J. et al. (2008) [25]	Frequency measurement	Hilbert transform	2 MHz Frequency accuracy for every 100 ns	Frequency measurement accuracy is not sufficient
11.	Upperman et al. (2008) [36]	Detection of LPI signals	Choi-Williams distribution	LPI signal detection at 0 dB SNR	Suitable for near real-time processing
12.	Simin, Z. et al. (2009) [22]	FPGA based detection	Autocorrelation technique	3 dB SNR required	SNR requirement is high
13.	Mahlooji & Mohammadi (2009) [24]	Frequency measurement	IFM technique	High-frequency accuracy of 43 kHz accuracy at 30 dB high SNR	SNR requirement is high for measurement

14.	Xu S.W., & Shui, P.L. (2010) [71]	Detection of FM signals	Fractional Fourier transform (FrFT)	SNR requirement of -5 dB	Real-time performance is not achieved
15.	Pandolfi, C. et al. (2010) [26]	Comparison of frequency measurement	Analog IFM and digital FM technique	Frequency accuracy achieved at 0 dB SNR (i) IFM: 2 MHz (ii) DFM: 0.5 MHz	Frequency measurement accuracy is not sufficient
16.	Peter, Q.C. et al. (2012) [121]	AOA measurement using 3 Antenna	BLI Technique	RMSE of 1.62^0 at 5 dB SNR	SNR requirement is high
17.	Wang, P. et al. (2016) [92]	Radar pulse modulation classification	Modulation component analysis	96% accuracy at above 2 dB SNR	Real-time implementation is not achieved
18.	Shin, J. et al. (2016) [7]	Detection of LPI signals	Continuous wavelet transform (CWT)	Detection up to -5 dB SNR	Suitable for offline processing
19.	Gurel, A.E. et al. (2017) [52]	FPGA Implementation of DF approach	Amplitude and Phase Comparison DF approaches	A requirement of 10 dB SNR is required	Requirement of high SNR
20.	Fan, X. et al. (2017) [91]	Polyphase and Frank Codes recognition	IQPF and FrFT algorithms	100% recognition above 0 dB of SNR	Real-time implementation is not addressed
21.	Park, B., & Ahn, J.M.	Intra-pulse modulation	Frequency modulation	90% accuracy	SNR requirement is

	(2017) [62]	recognition	identification algorithm	above 10 dB SNR	high
22.	Selim, A. et al. (2017) [94]	Spectrum monitoring for radar bands	Amplitude Phase CNN and Spectrum CNN	Detection at above 5 dB SNR (AP-CNN) and 7 dB (S-CNN)	Real-time implementation is not addressed
23.	Orduyilmaz, A. et al. (2018) [51]	DOA estimation	Concentric Circular Array (CCA)	DOA RMSE of 0.25 degree at 5 dB SNR	SNR requirement is high
24.	Moghaddam & Masoumi (2018) [8]	Detection and frequency measurement	Instantaneous frequency measurement	Detection up to -65 dBm	Modulation measurement is not attempted
25.	Juan Zhang et al. (2018) [64]	Modulation classification for FM signals	Time-frequency distribution and CNN	Classification is good at above 5 dB SNR	Real-time performance is not addressed
26.	Tian Xi et al. (2018) [84]	Intra-pulse intentional modulation recognition	Singular value decomposition (SVD)	Suitable at lower SNR	Real-time implementation is not achieved
27.	E. Yar et al. (2019) [63]	Detection and modulation classification	STFT, Hough transform, and CNN	Accuracy of 93.73% is achieved at 10 dB SNR	Real-time implementation is not achieved
28.	Lauren et al. (2019) [74]	Emitter identification	CNN IQ imbalance estimators	Working well above 10 dB SNR	Real-time implementation is not achieved

2.4 Detailed literature review

ELINT systems which is the division of Radar EW systems measure various parameters [1]-[3]. The waveform generated by radars with magnetron and traveling wave tube (TWT) exhibit differences with the serial number of radars. In other words, waveforms

generated by different serial numbers of radars of the same model will be different. To overcome this, electronic support should have the capability to distinguish among radars of the same model. The features which broadly change from one serial number to another are rise time, fall time, overshoot, and undershoot characteristics of pulses. These features are changed among different serial numbers of radars due to their aging effect and their non-repetitive performances. The non-repetitive performances are basically due to the analog nature of magnetron and TWT.

Advanced radars are based on digital techniques and Transmit/Receive (T/R) module. These multiple T/R modules are combined with multiple active antenna phase array and produce the required gain. Each T/R module provides the gain of the order of 20 to 50 Watts. It produces about 100 dB gain on combining all modules. Their performance is repetitive as they are based on solid-state devices. The radars with these capabilities will generate a similar waveforms with different serial numbers of radars. They will have the same rise time, fall time, overshoot, and undershoot. These radars can generate adaptive waveforms from time to time. Their characteristics also can be changed. To identify the serial number of such radars, the ES system needs to rely on other parameters such as AOA and MOP. These two parameters also help to identify magnetron and TWT-based radars. The fact is that radars based on magnetron and TWT are not repetitive across different serial numbers. Due to the different performances of magnetron and TWT, radar's pulse waveforms are different.

2.4.1 Signal estimation techniques

The basic parameters of radar signals are radio frequency (RF), pulse width (PW), Pulse amplitude (PA), pulse repetition frequency (PRF). These parameters are measured using generated instantaneous amplitude profile and instantaneous frequency profile. The noise reduction is also carried out using spectral subtraction before generating these profiles.

Both inter-pulse and intra-pulse parameters are required to be measured accurately of radar signals. The emitter identification system becomes critical when multiple radars are operating in a dense environment. It becomes a challenging task to uniquely identify them as radars of same kind exhibit minor variations in the transmitted pulses [4]. These systems are required to classify and identify them even with same make and model by utilizing unintentional variations within the pulse. These parameters constitute the fine grain parameters of the radars. The decisions taken based on these fine grain parameters the accurate identification of the radars can be established.

O.A.M. Aly et al. [5], proposed a wavelet-based algorithm for radar pulse detection and de-noising. This algorithm can detect the signal up to -24 dB SNR but it can work on stored data and it is not implementable for real-time applications. Aceros-Moreno & Rodriguez [6], proposed a discrete Chirp Fourier transform (DCFT) detect chirp signals only. But the detection of only chirp signal is not sufficient as the environment is unknown. Shin et al. [7], proposed wavelet-based detection of weak radar signal at -5 dB SNR but this approach is also not implementable for real-time application.

Moghaddam & Masoumi [8], proposed instantaneous frequency measurement for pulse detection using adaptive threshold, detects signal up to -65 dBm power level for 2-4 GHz band, and measures basic parameters. Carpentieri & Cuomo [9], proposed the radar pulse detection up to 75 dB dynamic range using an adaptive threshold. Gross & Chen [10], proposed the various detection techniques which require 12 dB of SNR. But these researchers focussed on basic parameter measurements and have not attempted intra-pulse modulation measurement. Various LPI radar signals [11] are mentioned. These signals are difficult to measure in real-time. It becomes critical to extract these radars and recognize them appropriately in real-time.

M. Conning and F. Potgieter [12], used phase-based detection, measurement using in-phase and quadrature-phase, and identification are done on the measured data. S. Davis and I. Bucher [13], have presented the single tone frequency estimation using the linear least square (LLS) technique. They have been carried out offline processing and are not addressed for hardware implementation. Manish Gupta et al. [14], have presented a statistical solutions for the issues related to drifting and aging of emitters. These researchers considered the offline processing techniques.

J. Dudczyk et al. [15]-[16], have carried out extensive research and presented the identification method using fractal features and graphical representation of the distribution of radar signal parameters. A. Kawalec et al. [17] have presented the emitter recognition using intra-pulse data. S. Deng [18] describes the identification based on the RF fingerprints. Y. Pan [19] has presented the identification based on the high fidelity symbol synchronization. K. Michel and K. Adams [20] have implemented the matched filter in FPGA for a radar systems. These researchers have not concentrated on real-time modulation identification which is required for tactical operations.

An approach based on digital in-phase and quadrature-phase (DIQ) for intra-pulse parameter measurement perform reasonably well for high processing SNR as demonstrated by

RK Niranjan and BR Naik [21]. Z. Simin et al. [22], demonstrated a pulse detection approach which requires 3 dB SNR. J.B.Y. Tsui [23], S. Mahlooji and K. Mohammadi [24], James Helton et al. [25], and C. Pandolfi [26] have presented digital instantaneous frequency measurement techniques for frequency estimation. However, they have shown frequency estimation with high accuracy at high SNR. But their performance is not adequate at lower SNR. These authors have not concentrated on intra-pulse modulation identification.

Various digital receiver front-end configurations and digital receiver techniques are presented by H. Pekau and J.W. Haslett [27], S.G. Kaiser [28], M.A. Sanchez [29], and A.K. Singh and S.K. Rao [30]. These digital receiver configurations used frequency measurement using FFT-based detection. These techniques are good for detection and parameter measurement due to FFT's inherent processing gain. But, intra-pulse modulation measurement is not possible using this technique in real-time. FPGA implementation for the digital IQ method is presented by RK Niranjan and BR Naik [31]. This work is carried out for parameter measurement for 40 MHz bandwidth and not concentrated on intra-pulse parameter measurement.

H. Akima [32] has presented a smooth curve fitting method which is used for frequency estimation. B.G. Quinn [33], shown the estimating frequency by interpolation technique using Fourier coefficient. P. Voglewede [34] has presented a parabola approximation for peak frequency determination. S. Djukanovi has shown frequency estimation of a real sinusoid. These frequency estimation technique does not provide the SNR advantage but these techniques have been used effectively to achieve better frequency accuracy with less FFT number of points.

G.J. Upperman et al. [36], studied Choi-Williams distribution for detection of LPI signals but near real-time performance only could achieve. S.U. Dan et al. [37], have carried out the comparative analysis of frequency estimation techniques. But researcher has not concentrated frequency estimation in real-time. S. Sajedian et al. [38], have presented a frequency estimation technique using a neural network. But it takes about one second processing time.

Frequency estimation techniques presented by H.C. So and K.W. Chan [39], H.C. So et al. [40], H.C. So and K.W. Chan [41], H.C. So et al. [42], L. Liu [43], F.K.W. Chan [44], S.M. Kay [45], R. Stoica and R. Moses [46], and B. Zeng [47], but real-time performance is not achieved using these techniques. These techniques do the frequency estimation offline.

2.4.2 Angle-of-arrival techniques

Minimum two antennas are required for baseline interferometry (BLI). But usually, four antennas are used to get better DF accuracy. A system designed using four antennas with BLI approach requires four antennas, four channel switch filter bank, four channel down-converter, four ADCs for one quadrant. The front-end becomes bulky with four channel, weight and power dissipation will be more. For each quadrant, three different types of antennas are required based on frequency coverage to cover complete 0.5 to 18 GHz range. So, practically twelve antennas are required instead four antennas and their outputs are being switched internally in the switched filter bank. Such four quadrants are required to cover complete 360^0 azimuth.

Three antenna based BLI algorithm is proposed for DOA extraction. In this, three antennas, three channels switch filter bank, three channel down-converters, three ADCs for one quadrant. No. of antenna to cover complete frequency range will be nine. This concept is also known as virtual antenna-based BLI algorithm. The measured error will be more compared to four antennas based BLI algorithms. This is compensated by using noise cancellation technique on raw IF data. This will improve the SNR and it is used only for space ELINT where requirement of FOV is limited. Hence, the performance becomes similar to four antenna based BLI. Total hardware reduction will be around one forth.

High altitude or space-based electronic intelligence (ELINT) systems has the advantage of uninterrupted receiving of airborne radars, tracking radars, etc. These radars can be captured from the high altitude easily and classify them by ELINT systems. The requirement of space-borne systems are small SWaP. The proposed algorithms along with proposed configurations are useful for space ELINT systems. The performance of these systems expected better than ground-based systems [1]-[3], [48]. Many direction-finding techniques and mentioned by Lipsky [49].

K.R. Sundaram [50] et al. has presented a modulo conversion method for resolving phase ambiguity. This modulo conversion method is complex and requires more computations. A. Orduyilmaz et al. [51] has introduced four-channel phase comparison for direction finding. The hardware design using this technique requires four antennas, four coherent down-converters, four-channel processors and hence it becomes bulky. A.E. Gurel et al. [52] presented amplitude and phase comparison direction-finding techniques in real-time. This requires high SNR for processing. S.O. Ata et al. [53] have shown the high-resolution direction of arrival using Concentric Circular Arrays. But this type of array is not

possible for all types of platforms. Q. Yuan et al. [54] have introduced the direction of arrival simulation using an array antenna with arbitrary geometry. But, real-time implementation is not addressed by researchers. H. Sakai [55] has shown the direction of arrival estimation using magic-T circuit's array antenna. This type of arrays antenna is not possible for all types of platforms. L. Osman [56] has shown the multiple signal classification for direction-of-arrival estimation using four antenna array. But this type of hardware configuration is not possible in all types of platforms.

2.4.3 Different techniques used for modulation recognition

Modulation on radar pulse is one of the most important features and one of the vital problems in the analysis of non-cooperative radar signals is modulation classification for emitter identification [3], [13], [15], [18]. The modulation classification plays a very important role in Electronic Intelligence (ELINT) systems. Firstly, the modulation type of a signal is important to identify the radar type. Second, on identifying the correct modulation type the carrier frequency is re-estimated. Third, it helps to distinguish similar radars deployed in proximity. But for radar signals, the modulation classification in real-time is very challenging due to the possibility of various modulations within a very short pulse width.

The earlier generation of Electronic Support (ES) systems was based on instantaneous frequency measurement (IFM) receiver and pulse measurement using log video. The time-domain technique was used for noise estimation and signal detection [21] and frequency was measured using time-frequency analysis [10], [24]-[25]. But during conversion from radio frequency (RF) or intermediate frequency (IF) to log video, the phase and hence the modulation information is lost. Due to this reason these systems measure only basic parameters like radar frequency (RF), Pulse width (PW), Pulse Repetition Interval (PRI), and Pulse Amplitude (PA). These parameters broadly are called inter-pulse parameters. But the measurement of these parameters alone is not sufficient against modern RADARs.

F.B. Gross and K. Chen [57] have demonstrated the comparison of detectability radar waveforms in classic passive receivers. Researcher has not concentrated on modulation identification in his work. X. Fan et al. [58] have shown polyphase pulse compression codes detectability of 90% at above -7 dB SNR using integrated quadratic phase function (IQPF) and fractional Fourier transform (FRFT). But researcher has not concentrated on the real-time processing aspect. L. Nadav and M. Eli [59] have mentioned various radar signals. These signals are used in generator of modern radar waveforms.

E.E. Azzouz and A.K. Nandi [60] have given various techniques of modulation recognition of various signals. L. Yun and M. Chunguang [61] has presented automatic modulation recognition of communication signals using Haar Wavelet Transform (HWT). They have achieved modulation recognition accuracy of more than 90% at more than 5 dB SNR. This high SNR requirement is not sufficient for ELINT systems and researchers have not addressed real-time implementation.

B. Park and J.M. Ahn [62] had demonstrated radar modulation recognition of FSK, LFM, and NLFM using pulse description words and complex waveforms. The recognition accuracy of 90% is achieved at above 10 dB SNR. But researchers have not concentrated on modulation recognition in real-time and SNR requirement is also high. E. Yar et al. [63] have shown the pulse detection and modulation classification for cognitive electronic warfare using short-time Fourier transform (STFT) and Hough transform. Frequency and phase modulations are classified with 93.73% accuracy at 10 dB SNR.

J. Zhang et al. [64] have presented the frequency modulation classification using time-frequency distribution and CNN. Classification accuracy is achieved well at above 5 dB SNR. Real-time classification is not addressed by the researchers. E.E. Azzouz and A.K. Nandi [65] have demonstrated the automatic identification of digital modulation types. The identification accuracy of more than 90% is achieved at above 10 dB SNR. The requirement of 10 dB SNR is not sufficient. The real-time identification of modulation is not addressed by researchers.

A.K. Nandi and E.E. Azzouz [66] did the automatic analog modulation recognition with more than 90% accuracy at above 10 dB SNR. However, this technique is applicable for the recognition of communication signals and this requires high SNR. A.K. Nandi and E.E. Azzouz [67] have presented decision-theoretic algorithms for automatic modulation recognition of communication signals. The recognition is carried out using an artificial neural network (ANN). Total 96% accuracy is achieved at above 15 dB SNR which is not sufficient.

C. Dubuc et al. [68] introduced an automatic modulation recognition algorithm for spectrum monitoring applications using a decision-tree algorithm at 5 dB SNR. In this, researchers have not concentrated on real-time identification. Y.T. Chan and L.G. Gadbois [69] Identification of the modulation type of communication signal using envelope characteristics above 7 dB SNR. The SNR requirement of this technique is more.

Detection of LFM signals is proposed by H. You et al., using Wigner-Ville Distribution (WVD) - Hough Transform at low SNR [70]. But the detection of other signals is

not mentioned. S.W. Xu and P.L. Shui [71] have demonstrated the detection of frequency-modulated signals using fractional Fourier transform at above -8 dB SNR. But researchers have not concentrated on real-time implementation of this technique.

Y. Qun e al. [72] has proposed specific emitter identification using the carrier frequency feature. Fixed and chirp signals are considered for specific emitter identification. The frequency is measured with 140 kHz accuracy but modulation identification is not addressed by researchers. J. Dudczyk and A. Kawalec [73] has proposed a fast-decision identification algorithm of emission source pattern with 92% level accuracy. The algorithm is fast but considered basic radar parameters RF, PW, and PRI. Intra-pulse modulations are not measured and are not considered for identification.

L.J. Wong et al. [74] have presented specific emitter identification using convolutional neural network (CNN) based IQ imbalance estimators. Good SEI performance is achieved at above 15 dB SNR. But researchers have not concentrated on modulation measurement and have not used this parameter for SEI. J. Matuszewski [75] has demonstrated analysis of modern radar signals parameters for electronic intelligence system. The basic parameters RF, PA, PW, PRI, and AOA are measured and modulation parameters are not measured by the researcher.

H. Zanga and Y. Li [76] have presented an overview of radar intra-pulse modulation recognition. Various approaches time domain, frequency domain, time-frequency analysis, delayed sub-autocorrelation, fractal measure, and wavelet transform. All approaches are not possible to implement for real-time applications. Z. Qu et al. [77] have demonstrated radar signal intra-pulse modulation recognition based on convolutional neural network (CNN) and deep Q-learning network (DQN). Recognition accuracy is more than 94% but researchers have not concentrated on the real-time implementation aspect.

R.K. Chilukuri et al. [78] have demonstrated estimation of polyphase and polytime codes of LPI radars using the cyclostationary method. But researcher has not demonstrated algorithms porting on hardware for real-time application. A. Kawalec et al. [79] show the radar-specific emitter recognition using intra-pulse data. The researcher has not shown the intra-pulse measurement approaches for real-time applications. S. Guo et al. [80] have shown the specific emitter identification using signal transients. Intra-pulse modulation measurement is not carried out for identification.

C. Erdem et al. [81] has demonstrated specific emitter identification using the characteristic of video signals. H. Jiang et al. [82] have proposed specific radar emitter

identification based on a digital channelized receiver. The identification is carried out using different shapes of video signals and it is effective at above 20 dB SNR. But the above researchers have not concentrated on basic parameter measurement and modulation measurement.

B.W. Gillespie et al. [83] proposed a classification based on time-frequency features. But the real-time implementation is not addressed by the researchers. T. Xi et al. [84] have demonstrated intra-pulse intentional modulation recognition of radar signals at 5 dB SNR. But the researchers have not shown the real-time implementation of modulation identification.

W. Fenghua et al. [85] have proposed an autocorrelation-based approach for intra-pulse modulation recognition using first and second-order phase differences. The recognition performance is demonstrated better at above 6 dB SNR. K.C. Ho et al. [86] have demonstrated modulation identification using wavelet transform at above 13 dB SNR. The SNR requirement is high for modulation recognition and real-time performance is not demonstrated by these researchers.

Q. Shi and Y. Karasawa [87] have shown the automatic modulation identification using the probability density function of the signal phase. L. Mingquan et al. [88] have demonstrated modulation recognition using cyclic spectral features. H. Haderer et al. [89] have shown the comparison of phase-coded CW radar modulation schemes for integrated radar sensors. Zhou et al. [90] have demonstrated time-frequency atomic dictionary analysis for radar intra-pulse modulation signal sparse representation. But above researchers have not demonstrated the real-time implementation of the proposed approaches.

X. Fan et al. [91] have demonstrated polyphase pulse compression codes modulation recognition using integrated quadratic phase function (IQPF) and fractional Fourier transform (FrFT). Correct recognition of 90% is achieved at above -7 dB SNR. But researcher has not demonstrated the real-time implementation of these approaches. P. Wang et al. [92] have proposed the radar pulse modulation classification using modulation component analysis. Classification accuracy of 96% is achieved at above 2 dB SNR, but real-time implementation is not addressed.

J. Lunden et al. [93] demonstrated automatic radar waveform recognition with 90% accuracy at above 6 dB SNR. A. Selim [94] has shown Spectrum monitoring for radar bands using deep convolutional neural networks (DCNN) at above 7 dB SNR. These researchers also have not demonstrated real-time hardware implementation of these approaches. The requirement of SNR is also high.

Z. Shun [95] has presented a radar signal intra-pulse modulation characteristic analysis method. W. Fenghua et al. [96] have shown an effective method for intra-pulse modulation. Z. Germany et al. [97] have given the identification of intra-pulse modulated signal types based on the phase difference. H. W. Wang et al. [98] have shown identification of radar emitter using pulse envelope characteristics. L. Zheng et al. [99] have demonstrated signal recognition of radiation source based on wavelet transform. But these researchers have not concentrated on real-time implementation of modulation recognition.

Till the earlier generation of EW systems, these offline analysis tools are either add-on or they are integrated with the main ES systems or ELINT systems. Identification of modulations by ELINT system in real-time is still a challenge. Various digital methods are discussed for modern digital implementation [60]-[64] and decision-theoretic approaches are mentioned for modulation classification [65]-[69]. These approaches are used for COMINT systems for measuring communication signal modulations. They are easy to implement as bandwidth is less for these systems.

Modulations can be identified using frequency domain techniques using offline systems for ELINT systems [70]-[99]. Implementation of these techniques in Field Programmable Gate Array (FPGA) for real-time application is not a viable solution as they consume a lot of hardware resources. Due to this reason, the implementation of signal classification techniques is attempted in FPGA using the time-domain technique for real-time application. IF signal is digitized by ADC and samples are captured, processed, and further analysed in FPGA. These are possible to implement in FPGA due to parallelism, high density, and high-speed component cores.

Z. Ge et al. [100] have demonstrated an improved algorithm of radar pulse repetition interval deinterleaving based on pulse correlation. V. Iglesias [101] has demonstrated a real-time radar basic pulse parameter extractor for RWR application. In this work intra-pulse modulation has not been demonstrated by the researchers.

M. Bagheri [102] has presented pulse deinterleaving based on adaptive thresholding. L. Zhang-Meng [103] has presented online pulse deinterleaving with finite automata. F. Fuhua and Y. Xuezhong [104] have demonstrated deinterleaving using stagger PRI. P. Barnwal [105] has shown radar PRI classification based on features estimation. H. Li et al. [106] have given signals deinterleaving using an improved CFSFDP algorithm. G. Noone [107] has demonstrated radar pulse train parameter estimation and tracking using neural networks. S. Wei et al. [108] have shown PRI modulation recognition based on squeeze-and-excitation

networks. Y. Xi et al. [109] have demonstrated an algorithm for multi-signals deinterleaving and two-dimensional imaging recognition based on short-time PRI transform. M. Jawad [110] has shown PRI characteristics analysis under the complex environment of spurious and missing observations. X. Li [111] demonstrated attention-based radar PRI modulation recognition with recurrent neural networks. U.I. Ahmed et al. [112] have shown pulse repetitions interval (PRI) Classification Schemes. X. Li et al. [113] have demonstrated deinterleaving of pulse streams with denoising auto encoders. Z. Shi et al. [114] have shown feature extraction for PRI modes based on the auto-correlation function. G. Lbpez-Risuefio et al. [115] have demonstrated two digital receivers based on time-frequency analysis for signal interception.

The de-interleaving based on the basic parameters (DOA, RF, PW, and PRI) is not very effective due to the dense environment where similar radars are operating in the environment [100]-[114]. Modulations and their parameters measured offline are used for de-interleaving and similar radars can be segregated effectively [70]-[99]. But this information can't be used for tactical application. When these parameters are measured in real-time, they can be used for de-interleaving, and in this case and similar radars can be segregated effectively. This information will be useful for tactical purposes. The advantage in using modulation information for de-interleaving is co-located radars operating with similar frequency can be identified for same reported DOA parameters.

This thesis proposes new processing algorithms i.e. noise cancellation and autocorrelation. The noise cancellation is used to enhance the SNR of the incoming signal. It is being carried out based on spectral subtraction. It is being by estimating the average noise of the system. This estimated noise average is subtracted from the incoming signal and restored signal is obtained without affecting the phase of the signal [117]. Autocorrelation technique is also able to detect the signal at lower SNR. When both the techniques are used together, all the targeted signal is being detected upto 1 dB SNR. Hence, identification is also improved at lower SNR.

Researchers are identifying radar signal modulations using frequency domain techniques, wavelet transforms and convolutional neural network (CNN) based techniques but these techniques can't be implemented on the FPGA platform for real-time application. Literature are available for online modulation identification but they are applicable for communication signals which is used for COMINT systems. Detection and identification of Frank codes, Polyphase codes, and Polytime codes are carried out offline. These techniques

are required resource-intensive hardware for real-time identification. Hence, these techniques are out of the scope of the proposed research work.

2.5 Concluding remarks

In literature, approaches available are frequency domain, wavelet transform, and convolution neural network, etc. for ELINT applications. These approaches cannot be used for real-time application. The comparison of proposed techniques with existing frequency domain techniques is unfair as some existing techniques will get inherent processing gain. As various methods of signal estimations and modulation recognition for radar signals exists, it is difficult to draw meaningful conclusions about the merits of anyone approach over another. The techniques developed in this thesis are useful as this leads to improve the SNR advantage of signal and modulation recognition is carried out in real-time.

Researchers have concentrated on offline processing. In this proposed research work, real-time processing techniques are investigated. With this concluding remark, the research problem is stated as “real-time modulation recognition of radar signals using digital techniques for new generation ELINT systems”.

Chapter 3

Contemporary Parameter Measurement Techniques

Electronic Support (ES) systems have been in development predominantly since world war-II. In this chapter, some of the contemporary frequency measurement receivers, digital frequency measurement techniques, direction-finding techniques, and measurement of modulation techniques for electronic support systems are discussed.

ES systems are designed based on the requirement of frequency and direction finding (DF) measurement techniques. Generally, ES receivers measure quantitatively the following parameters

(a) Radio frequency (RF)
(b) Angle-of-arrival (AOA)
(c) Pulse width (PW)
(d) Pulse amplitude (PA)
(e) Time-of-arrival (TOA)
(f) Pulse repetition interval (PRI)
(g) Modulation information

The frequency is measured using frequency measurement receivers and AOA using the DF receiver technique. The parameters listed from (c) to (f) are measured using the amplitude information. Modulation information is measured using the conventional DIQ technique.

3.1 Frequency measurement receivers

Many microwave receivers exist which are used to measure radio frequency (RF). Various contemporary measurement receivers are described below [1]-[3].

3.1.1 Crystal video receiver

Crystal video receiver is the simplest in structure and most common in use among all types of receivers. The output of the diode detector i.e. crystal detector is amplified enough by a video amplifier. The output voltage of detector is a function of input power since detector operate in a square low region. Crystal video receiver (CVR) consist the series of pulses with amplifier proportional to input RF power. Usually, the sensitivity of CVR is in the range of -35 dBm to -50 dBm. Usually, CRV are used in RWR receivers. The block diagram of the crystal video receiver is shown in Figure 3.1.

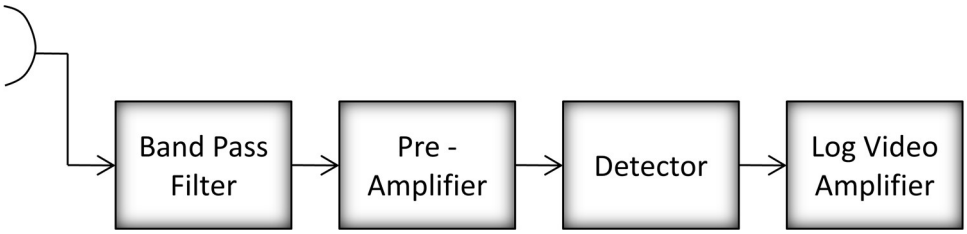

Figure 3.1: Block diagram of Crystal video receiver.

3.1.2 Superheterodyne receiver

Superhet receivers are used in radar receivers as well as communication receivers. Since the instantaneous frequency coverage is very narrow, Superhet provides a high sensitivity of the order of -90 dBm, wide dynamic range, and excellent frequency selectivity & accuracy. The POI is less due to its narrow bandwidth. These receivers are also designed for different bandwidth coverage to enhance POI.

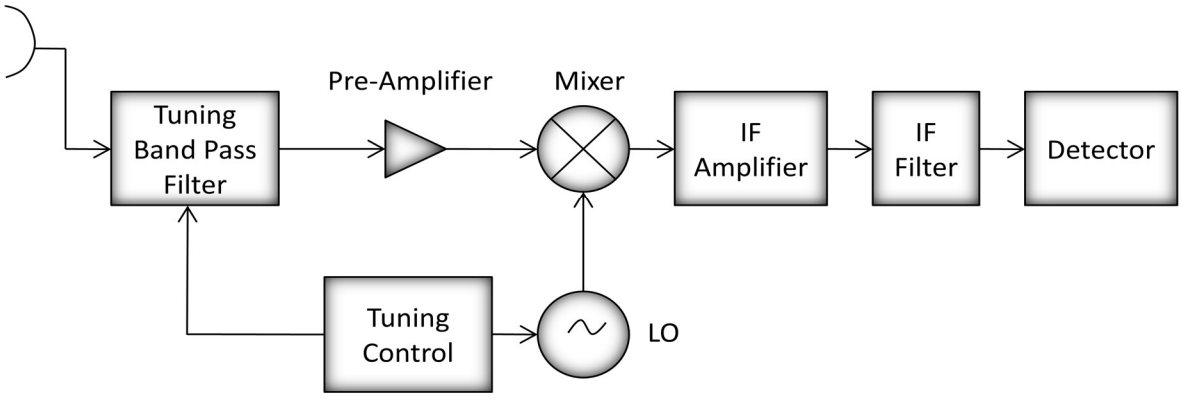

Figure 3.2: Block diagram of Superheterodyne receiver.

The block diagram of the basic Superheterodyne receiver is shown in Figure 3.2. This receiver transforms the information of a portion of its RF frequency into an intermediate

frequency (IF) band using a mixer and tuned local oscillator (LO). A tunable band pass filter (BPF) is used as a pre-selector filter before the pre-amplifier or mixer to avoid and isolate the interfering signals from the other part of the wide RF bandwidth.

Quad-superhet receiver (QSHR) is the four-channel Superhet receiver. This receiver down-converts four RF signals coming from antennas to IF signals simultaneously. These IF signals are used by four-channel digital receivers and parameter measurements are carried out. ELINT systems are designed often using these receivers.

3.1.3 Instantaneous frequency measurement receiver

The instantaneous frequency measurement (IFM) receiver uses the phase delay line and phase differences is measured. The frequency is measured using these phase differences. The RF or IF signal splits into two paths direct path and delayed path (τ). The phase angle between direct and delayed path can be written as $\phi = \omega\tau$. The frequency can be measured using the phase angle (ϕ) and delay time (τ). The Phase relation of sinusoidal waves with constant phase delay for IFM Receiver is shown in Figure 3.3.

The following equations shows the frequency computation of IFM receiver

$$A = x\,Cos\,\phi \tag{3.1}$$

$$B = x\,Sin\,\phi \tag{3.2}$$

$$\phi = tan^{-1}(B/A) \tag{3.3}$$

$$f = \left(\frac{\phi}{2\pi\tau}\right) \tag{3.4}$$

where x is the amplitude information.

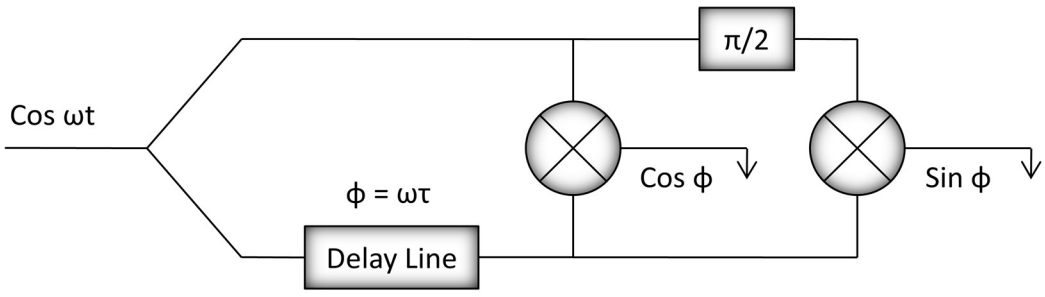

Figure 3.3: Intermediate frequency measurement receiver.

Limiting amplifier is the first component and then power divider is being used. The direct signal and delayed signal are given to phase correlator. Phase correlator multiplies both direct path and delayed path signals and sine and cosine video signals are obtained. Both signals are digitized by the different ADCs. Digitized data is stored in the ROM, which performs $\omega = \left(\frac{1}{\tau}\right) tan^{-1}\left(\frac{Sin\,\phi}{Cos\,\phi}\right)$. The frequency is thus directly computed. Number of phase delay line computes the frequency accuracy and resolution, whereas the shortest delay line are measuring the explicit bandwidth. The frequency measurement is also carried out using the conventional ways by comparing the amplitude in comparators. Grey code equivalent to frequency is obtained. The drawback of IFM is there when number of emitters present in the environment is two or more. It will measure only highest amplitude signals.

3.1.4 Channelized receiver

The basic channelized receiver is shown in Figure 3.4. A switched filter bank is an essential component in this receiver apart from other generic components like pre-amplifier, video detector, etc. This receiver splits the wide input bandwidth into multiple narrow bands through the use of a contiguous filter-bank as part of a fixed tuned Superheterodyne receiver. The sensitivity of the receiver is enhanced using this technique without compromising on wide bandwidth coverage. The channelized receiver has high sensitivity, wide dynamic range, and fine frequency resolution. Parallel video processing blocks for entire channels are required to achieve 100% POI.

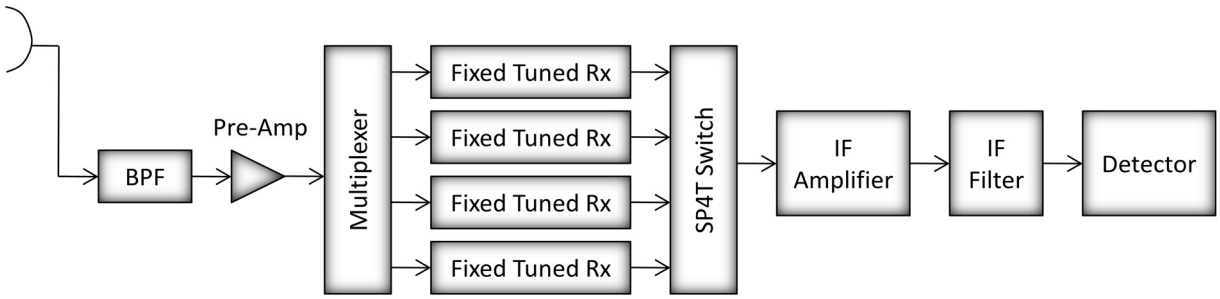

Figure 3.4: Block diagram of Channelized receiver.

The Channelized receiver provides better POI than the Superhet receiver because it's parallel nature. A large number of parallel channels makes this receiver bulky, highly hardware intensive, and expensive which has limited use in current EW applications. However, Surface Acoustic Wave (SAW) devices and millimetric wave integrated circuits (MMICs) hold promise for the future of Channelized receivers which helps in reducing the size and cost.

3.1.5 Homodyne receiver

A Homodyne receiver is a special case of a Superheterodyne receiver. In Superhetodyne receiver, the LO is derived externally. But in the Homodyne receiver, the frequency of the local oscillator (LO) is same as the frequency of the input RF signal. Since the LO is derived from the incoming weak signals with the use of large amplification, the sensitivity is limited which is similar to a wide-open receiver.

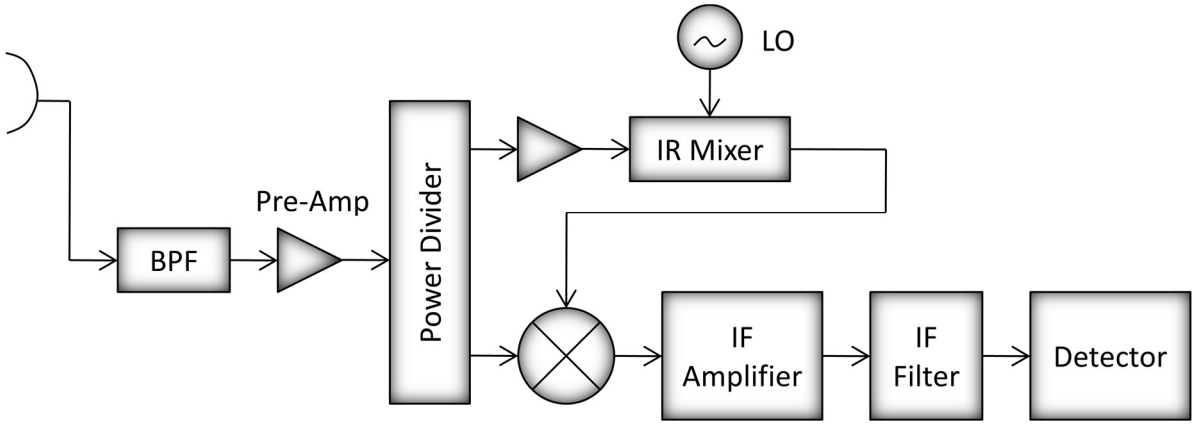

Figure 3.5: Block diagram of Homodyne receiver.

The block diagram of the Homodyne receiver is shown in Figure 3.5. The homodyne reference-LO is the high gain RF front-end and an image rejection (IR) mixer. The homodyne LO is derived from the incoming signal by mixing with an IF frequency of interest as indicated in that figure. The IR mixer rejects that one of the first sidebands (i.e. the image of either RF+IF or RF-IF) of mixer output. These receivers are wideband receivers and work for the complete frequency band. But they suffer from sensitivity due to their wide coverage.

3.1.6 Compressive or Microscan receiver

The compressive receiver is similar to a Superheterodyne receiver but for the rapid tuning, characteristics supported by a compressive filter or dispersive delay line (DDL). The delay time of DDL is inversely proportional to the frequency. It is also called a Microscan because of the use of fast LO to convert RF into frequency modulated (FM) signal before detecting. The detected outputs from a compressive receiver are narrow pulses arriving in series in the time domain. By measuring the positions of these compressed pulses, the frequency of the input signals can be determined. The block diagram of Compressive or Microscan receiver is shown in Figure 3.6.

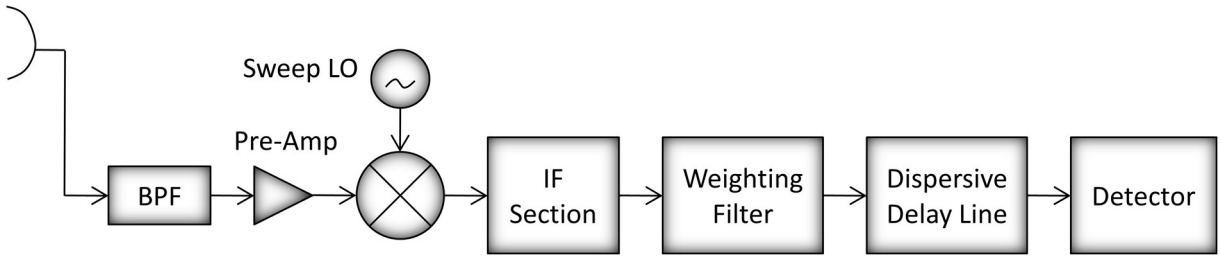

Figure 3.6: Block diagram of Compressive or Microscan receiver.

The structure of this receiver is complicated and high-speed logic circuits are required as the detected pulses are very narrow and very close in time. Advances in Surface Acoustic Wave (SAW) devices technology and high-speed logic circuits have revitalized the interest in developing Compressive receivers.

These receivers can handle signals effectively that are transmitted by pulse compressive radars. The frequency spectrum intercepted by the ESM receiver is scanned at a very high speed to enhance the POI. The sensitivity and dynamic range of these receivers are moderately high and the input bandwidth is moderately wide.

3.1.7 Bragg Cell or Accousto-Optic receiver

Bragg Cell receiver is optical signal processors which perform their function by spatially modulating the phase or amplitude of an optical beam with an input RF signal. The optical or light beam in optical signal processors can be modulated by means of an acoustic (sound) wave, hence this is termed as Accousto-optical receiver. The modulated light beam is then passed through a Bragg Cell that performs an optical Fourier transform to display the frequency domain characteristics of the input signal as a spatial distribution of light energy. The block diagram of Bragg Cell or Accousto-Optic receiver is shown in Figure 3.7.

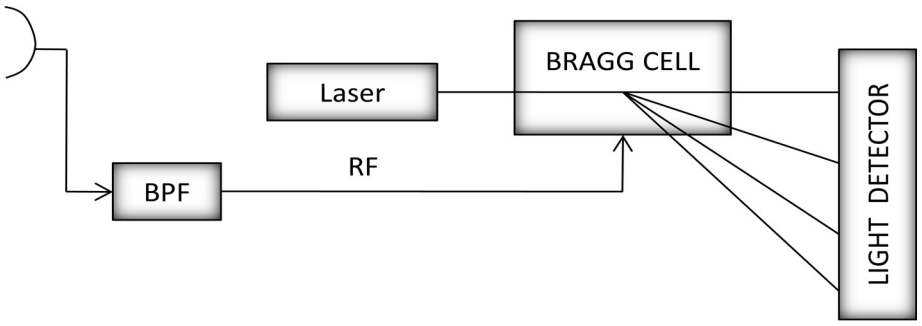

Figure 3.7: Block diagram of Bragg Cell or Accousto-Optic receiver.

The Bragg cell is an Electro-optic device. An entire Bragg cell receiver can be constructed on a single substrate as an integrated optical circuit (IOC) by using modern

integrated circuit technology. The technology is still under development stage. The structure of the Bragg-cell receiver is complicated, but the size is very small. The instantaneous bandwidth of the Bragg-cell receiver is around 2 GHz and provides fine frequency resolution. Simultaneous signals can be processed by this receiver. The sensitivity of Bragg Cell is high but the dynamic range is limited to 25 dB.

3.1.8 Hybrid receiver

To accomplish some specific missions, often one kind of receiver can't fulfil the requirements. The present-day radar threat scenario is highly dense with complex signals and hence demands the need for selection of a combination of ES or ELINT receivers to encounter this situation. Based on the system requirements & technical specifications and considering the size and weight constraints, the ES or ELINT system designer has to optimize the configuration by selecting one or more receiver technologies. Such receiver combinations are called Hybrid receivers.

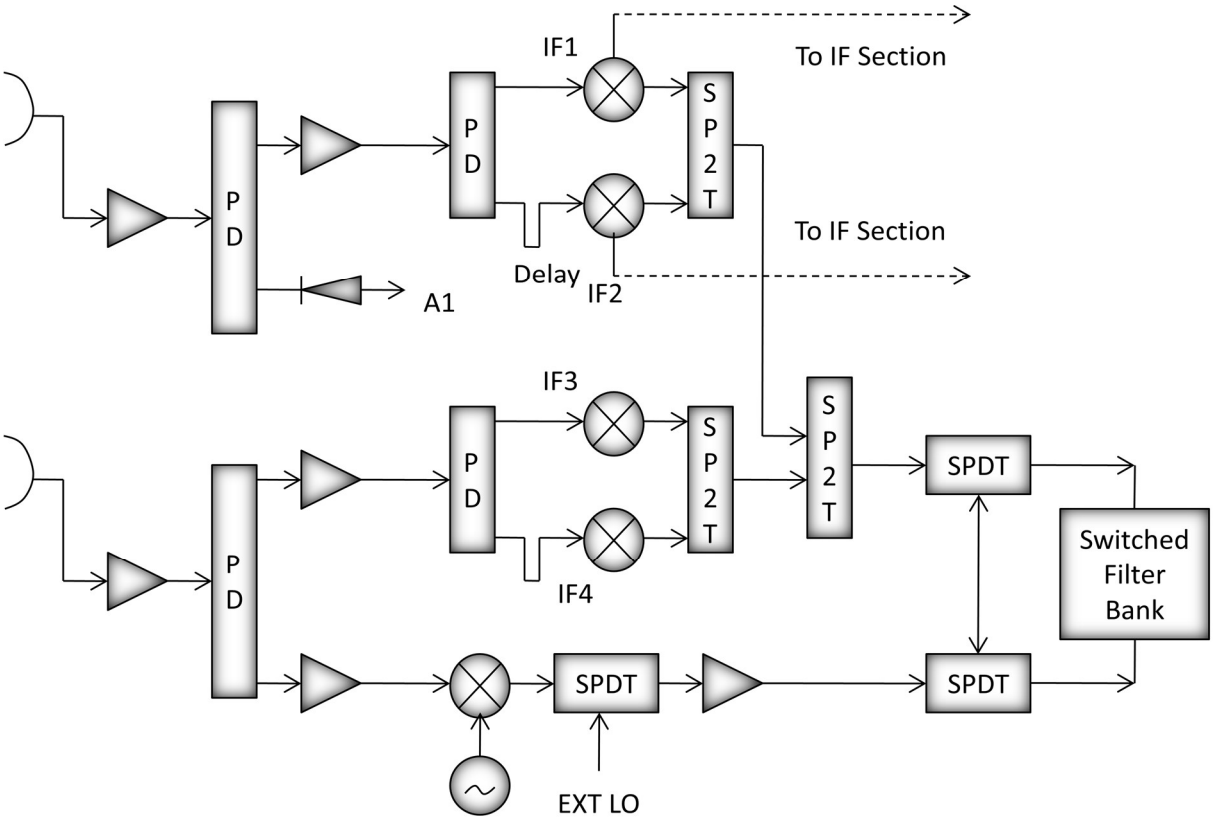

Figure 3.8: Block diagram of Hybrid Receiver.

The typical configuration of a Hybrid receiver is shown in Figure 3.8. The homodyne receiver is the basic structure for the Hybrid receivers, which covers wide bandwidth. By

using the external LO for homodyne-LO, the receiver will be functioning similarly to superheterodyne receiver. Similarly, by inserting a switched-filter-bank at the homodyne LO, the receiver functions as the channelized receiver. By introducing detectors at appropriate places, the crystal video receiver is obtained. Similarly, the IFM receiver is obtained by introducing a few delay lines and mixers.

A Hybrid receiver is configured to have the best combination of salient features of some of the commonly used conventional receivers into a single receiver. Importantly, the hybrid receiver should have superheterodyne receiver feature for higher sensitivity, a crystal video receiver for wide-openness, channelized receiver for handling multiple signal environments, and a digital receiver for handling multiple simultaneous signals within a narrow bandwidth. Also, direction-of-arrival, frequency, and pulse parameters should be measured for all kinds of options. ELINT systems frequently used Digital receivers along with Quad-superhet receivers which is one of the examples of Hybrid receivers.

3.2 Digital Receiver configurations for frequency measurement

Radars employing pulse compression techniques cannot be detected by conventional receivers. The advances in digital hardware and signal processing techniques made it possible to realize digital receivers for the detection and processing of these signals by applying matched filtering and correlation techniques.

In many EW applications, a digital receiver must be able to digitize input signals that can occupy a wide frequency range. Currently, ADC converters do not possess sufficient bandwidth to directly digitize these input signals. Therefore, the A/D converter is usually preceded by a Superhet receiver that down-converts the signal of interest to an IF frequency. The digitized samples of the input signal are usually stored in a digital memory where they are available for analysis. There is a vast array of digital techniques for performing detailed signal analysis [27]-[30]. The block diagram of the digital receiver is shown in Figure 3.9.

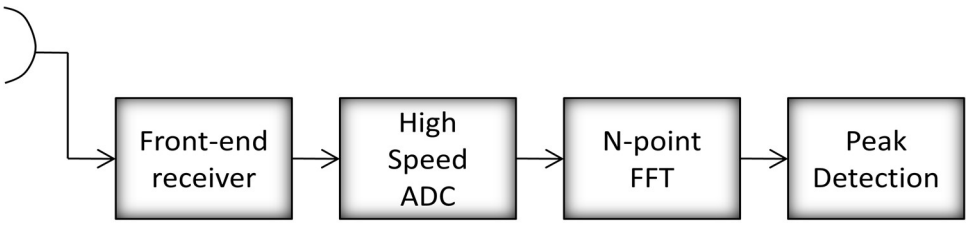

Figure 3.9: Block diagram of Digital receiver.

An extension of the basic digital receiver produces a digital RF memory (DRFM). DRFM allows for the storage of intercepted radar signatures (RF signal) in a digital memory and reconstruct the signal waveform, which is used widely in ECM applications for Jamming radars. Advanced DRFMs are now being configured as ASICs, enhancing the memory size and performance.

In present days the digital receivers are commonly used receiver. A number of frequency measurement algorithms are available for frequency measurement. It includes fast Fourier transform (FFT) based technique, digital instantaneous frequency measurement (DIFM), and digital in-phase quadrature-phase (DIQ).

These measurement algorithms are ported in digital receivers. But digital receivers can't digitize directly RF, whereas it digitizes IF. The RF to IF conversion to lower frequency is carried out using Superhet receiver, Channelized receiver, and IFM receiver. These receivers will be in the front end and Digital receivers are used for digitization and algorithms are used at our choice. The various algorithms are described as below:

3.2.1 Fast Fourier transform technique

FFT is the frequency measurement method and it is the abbreviation of fast Fourier transform. Frequency is measured using FFT has the resolution of (f_s/N), where f_s is the sampling frequency and N is the number of FFT points. It says, if FFT points are more, the resolution will be more. But, keeping more FFT points is not useful from the point of view of pulse width and pulse repetition interval. The accuracy of these two parameters degrades on increasing the N. The frequency is computed from the frequency spectrum as k*(f_s/N). Where k is the bin number.

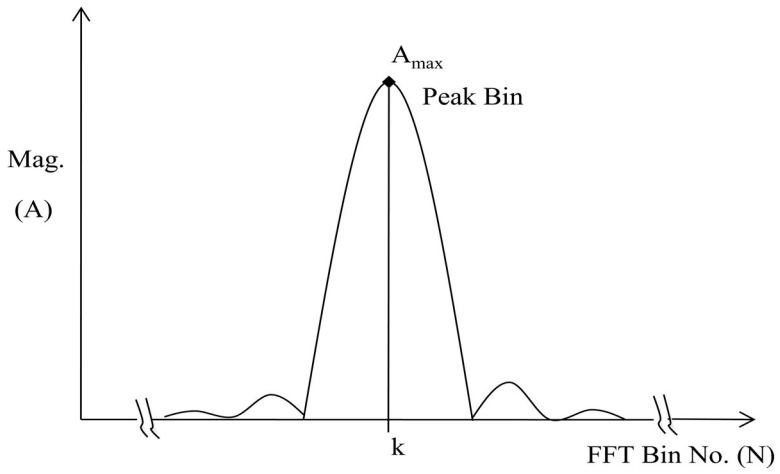

Figure 3.10: Frequency spectrum.

One option to keep the resolution is to use the FFT in an overlap fashion with more N. Another option is to use the interpolation method, where if the frequency falls between two bins it will be measured with higher accuracy.

3.2.2 Digital instantaneous frequency measurement technique

The various types of receivers listed above for frequency measurement, Digital instantaneous frequency measurement (DIFM) is mostly used in frequency measurement receiver in EW system because of its inherent characteristics and makes them suitable for both ESM and ELINT applications. The block diagram of the DIFM Receiver is shown in Figure 3.11.

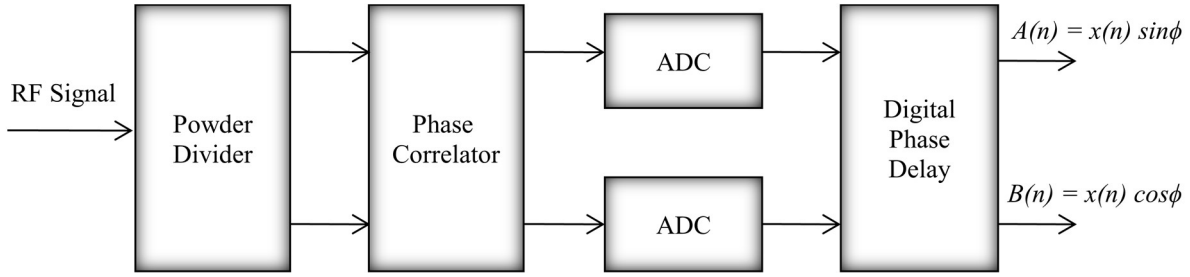

Figure 3.11: Block diagram of DIFM Receiver.

The following are the characteristics of the DIFM receivers

1. Wide instantaneous RF band width
2. Wide instantaneous dynamic range
3. Good frequency accuracy
4. Measure short pulse with high-frequency accuracy
5. Adequate sensitivity for practical applications

The DIFM receiver has only one disadvantage that when multiple signal environments, only one strongest signal will be measured.

3.2.3 Digital In-phase Quadrature-phase technique

In the DIQ technique [21], the digitized IF samples are converted into in-phase and quadrature-phase samples using a numerically controlled oscillator (NCO). These samples are passed through the low pass filter to discard the high-frequency component. The Equations given below describes the DIQ approach for calculating instantaneous phase in radian, frequency in Hertz, and amplitude in Volts. The detection is carried out on this amplitude

profile $R(n)$ and pulse is detected. The block diagram of the DIQ technique is shown in Figure 3.12.

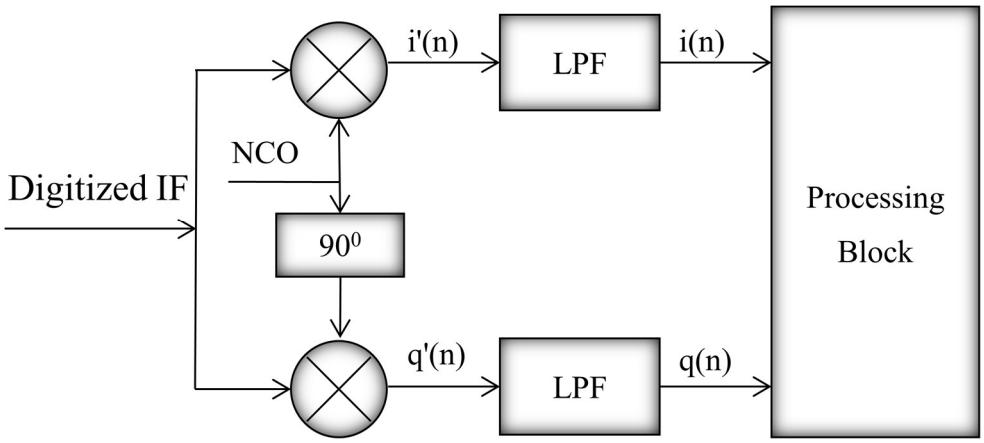

Figure 3.12: Block diagram of DIQ technique.

The input IF signal is defined as $x(t) = A\cos(\theta)$ and the digitized IF sequence is described as $x(nt_s) = x(n) = A\cos(2\pi fnt_s)$. The frequency ($f_c$) of NCO is chosen as $f_c = f_s/4$. Where f is the is signal frequency, t_s is the sampling time, n = 0,1,2,...,N-1, is the sample number, N is the total number of samples, and f_s is sampling frequency. The advantage of choosing NCO frequency as $f_c = f_s/4$ is shown below. The cosine and sine components of NCO becomes as

$$x_c = cos(2\pi f_c nt_s) = [1, 0, -1, 0, 1,.....] \quad (3.5)$$

$$x_s = sin(2\pi f_c nt_s) = [0, 1, 0, -1, 0,.....] \quad (3.6)$$

Finally, the signal x is multiplied with [1, 0, -1] values which is nothing but sign change of input signal. The frequency translation (or multiplier) is performed without any multiplication.

$$i'(n) = x.x_c = [x, 0, -x, 0] \quad (3.7)$$

$$q'(n) = x.x_s = [0, x, 0, -x] \quad (3.8)$$

These signals are passed through low pass filter to filter out $f + f_c$ signal and passes only desired $f - f_c$ signal. Based on i(n) and q(n) signals the following are obtained after filtering:

$$i(n) = LPF\ [i'(n)] \quad (3.9)$$

$$q(n) = LPF\ [q'(n)] \quad (3.10)$$

The instantaneous phase, frequency, and amplitude are obtained using the following equation 3.11 to equation 3.13

$$\text{Phase} \qquad \phi(n) = \tan^{-1}\left(\frac{q(n)}{i(n)}\right) \tag{3.11}$$

$$\text{Frequency} \qquad F(n) = \left(\frac{F_S}{2\pi}\right)\Delta\phi(n) \tag{3.12}$$

$$\text{Amplitude} \qquad R(n) = \sqrt{\{i(n)\}^2 + \{q(n)\}^2} \tag{3.13}$$

There is a requirement of above 12 dB SNR using the DIQ technique for instantaneous phase, frequency, and amplitude measurements of the pulse.

3.3 Direction finding techniques

A direction finding (DF) system gives the direction of emitter [1]-[3], [48]-[49]. It is often important to determine the location of the emitter. Two or more DF systems are necessary to obtain the location of the emitter by triangulation. Alternatively, the DF system can move in space and taking measurement at different times, it is possible to locate the emitter. But this is not possible most of the time. There is a number of ways of determining the AOA. In this section, some of the contemporary direction-finding methods that are suitable for implementation in electronic intelligence receivers are discussed.

3.3.1 Rotary DF

One of the first direction finding (DF) techniques was the mechanically spinning antenna based which is highly directional. It is physically rotated in azimuth (and elevation) to search for radar signals. The AOA for the intercept radar is simply the angle at which the spinning antenna received the radar signal. The modern spinning antenna system can estimate the radar AOA at the accuracy of one-tenth of antenna beam width (typically of the order of 1^0 to 5^0 RMS).

Rotary-based DF systems are easy to understand, easy to implement, low cost, and highly relevant in radar intercept receivers in today's system also. These types of directional antennas provide inherently directional isolation between the intercept radar with other signals coming from the other direction. Hence, they are able to collect the data of intercepted radar only in direction. Intercept receiver antenna receives the signals while rotating and radar system antenna transmit signals also may be rotating. The coincidence of receiving the radar

signal by intercept receiver may or may not be met. The probability of this happening is known as the probability of intercept (POI).

The inherently poor POI performance of this technique is one of the main drawbacks of using spinning antennas for a surveillance system. Ongoing antenna maintenance with the physical wear and tear of mechanical parts also makes the spinning antenna system unattractive.

3.3.2 Amplitude based DF

Amplitude-based DF measurement requires 4 to 16 directional antennas. The beam width of each antenna BW is given by, BW=(360/N) where N is the number of antennas. A larger number of antennas will also give better DF accuracy due to narrower beam width and resultant greater amplitude gradient. More number of antennas will also give better system sensitivity due to higher antenna gain. Spiral antennas are used for ultra-broadband (multi-octave) performance and constant beam width horn antennas are used for medium bandwidth (octave) and narrow bandwidth. Designing a DF system to cover 360^0 azimuth is simpler than for partial azimuth. Outputs of two to three antennas (maximum signal amplitude) are processed for AOA estimation. Single antenna output can also be processed for signals close to bore sight of any one of the antennas especially if 12 element or 16 element arrays are used. The front-end hardware has to be calibrated to remove bias errors and to improve DF accuracy. DF accuracy degradation is graceful for larger amplitude mismatch between the front-end hardware. Loss of sensitivity (in dB) is one-half of the peak-to-peak gain mismatch among front-end hardware components.

Using twelve antenna ADF system AOA is computed as below

$$AOA = \theta_n \pm [15 - 1.25 * (\Delta A)] \tag{3.14}$$

Where θ_n is the principal direction in which the antenna with the highest amplitude faces (0^0, 30^0, 60^0, etc.) and ΔA is the amplitude difference between highest peak and second peak amplitude in $\pm 15^0$ roll-off regions. The + or – sign is used depending on whether the second peak occurs from the antenna to the left of the peak amplitude antenna or the right. Ultra-broadband coverage using spiral antennas reasonably good accuracy of 2^0 to 5^0 RMS simple processing algorithms. But this approach is prone to DF errors due to reflections, multi-path effects, and DF accuracy heavily dependent on calibration.

3.3.3 FDOA based DF

Frequency difference of arrival (FDOA) techniques exploit the Doppler effects to estimate the AOA of the received signal. In this system, one antenna is physically rotated around a reference antenna. The circular motion of the moving antenna causes a sinusoidal Doppler shift relative to the frequency measured by the reference antenna. The angle at which the Doppler shift goes from positive to negative is the AOA of the signal. In practical systems, the rotating antenna can be replaced by a circular array of antennas that are switched sequentially into the receiver. Direction finding systems have been known to achieve angular accuracies of about 3^0 RMS.

3.3.4 TDOA based DF

The time difference of arrival (TDOA) technique is based on the difference in the time of arrival of the signals received by two sensors due to the physical separation of the antennas. Consider two antennas receiving the same RF signal as signal in Figure 3.13. The difference in time of arrival of the signal at the two antennas 't' is given by:

$$t = d * sin(\theta)/c \tag{3.15}$$

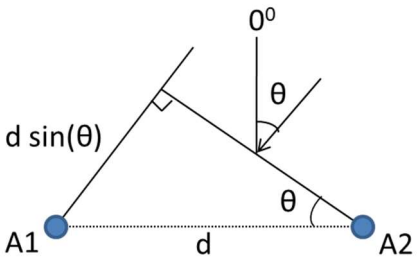

Figure 3.13: Two Antennas based TDOA.

where d is the distance between the antenna in meters, θ is the angle of arrival and c is the velocity of light.

The AOA, θ can be computed as

$$\theta = sin^{-1}(t * c/d) \tag{3.16}$$

The AOA accuracy is given by:

$$\sigma\theta = \sigma t * c/[d * cos(\theta)] \tag{3.17}$$

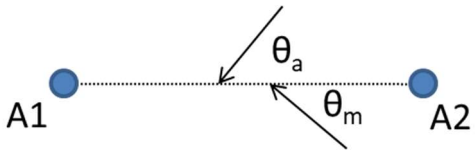

Figure 3.14: Two Antennas based TDOA showing signal arrival from two different directions.

Front to back ambiguity in the AOA will be there because a signal from the mirror image direction also gives identical AOA since the time difference is the same as shown in Figure 3.14 where θ_a and θ_m are the actual AOA and mirror image of AOA.

To resolve these front to back ambiguities a third antenna is introduced so that two (orthogonal) baselines are available. The time delays for the two (orthogonal) baselines are given by: $t_1=d*\sin(\theta)/c$ and $t_2=d*\sin(\theta)/c$. The AOA is given by: $\theta=\tan^{-1}(t_1/t_2)$. Similar equations can be derived for other types of non-orthogonal geometries.

In the TDOA method, the AOA is computed based on the difference in the time of arrival of the intercepted signal by two adjacent antennas. Four antenna based TDOA is shown in Figure 3.15. The difference in the arrival time of the RF signal at each pair of antennas concerning the baseline formed by the two antennas is measured which is proportional to the AOA (i.e. A1-A2, A2-A4, A4-A3, A3-A1, A1-A4, and A2-A3). The time difference arrival in turn depends on the span (distance between the antennas) of the baseline.

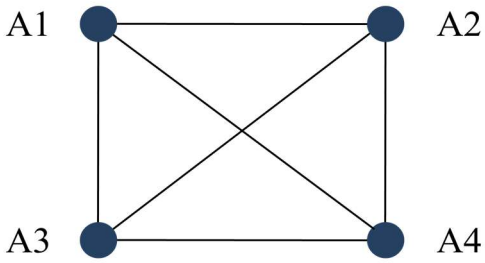

Figure 3.15: Four Antennas based TDOA.

The TDOA approach yields high DF accuracy, but the limitations are the requirement of large baselines and high-speed processing circuits to measure the time difference of the order of nanoseconds very accurately. TDOA approach is useful for pulsed signals only. The present day technology is to use high-speed ECL ICs and GaAs ASICs for time difference measurement. Hence, for platforms where large baselines are available, TDOA DF is highly recommended. DF accuracy for 14 m spans, is less than 2^0 achievable.

3.3.5 BLI based DF

The baseline interferometry (BLI) principle of operation is shown in Figure 3.16. The phase delay ψ across the two antenna outputs is given by,

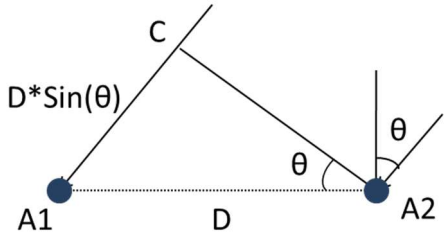

Figure 3.16: BLI principle of operation.

$$\Psi = 2\pi * (D/\lambda) * Sin(\theta) \tag{3.18}$$

where θ is the AOA with respect to the bore-sight axis, λ is the wavelength of the incident signal, and D is the spacing between the two antenna elements. If the phase delay is measured and the frequency (and hence wavelength) is known the Direction of Arrival of the signal can be computed as, $\theta = Sin^{-1}(\Psi\lambda/2\pi D)$. The DF accuracy is computed as below:

$$\sigma_\theta = \sigma_\phi * \lambda / [2 * \pi * D * Cos(\theta)] \tag{3.19}$$

Higher DF accuracy requires a larger baseline. Baseline spacing has to be less than (λ/2) to avoid ambiguous phase measurement. This requirement cannot be met practically for broadband systems with good DF accuracy specifications. Good DF accuracy can be obtained only by large baselines i.e. several wavelengths. Multiple antenna elements (typically 4 to 5 antennas have to be used to resolve phase ambiguity. Maximum likelihood Estimation, Least Mean Square Estimation, and Chinese Remainder Theorem (CRT) are extensively used to resolve the ambiguity in phase measurement. The phase error margin is the single most important criterion in the design of Interferometer DF Systems. This technique gives gross DF errors if the actual phase error exceeds the error margin provided in the algorithm. Phase Error Margin is a function of the Prime Integer Ratio of the Baselines used for resolving ambiguity. A ratio of 1:2 gives a $\pm 60^0$ phase error margin. The general Phase Error Margin $\Delta\phi$ for resolving Mod 2π phase data using CRT is given by $\Delta\phi = 180/(P+Q)$ where $P:Q$ is the prime integer ratio of the baselines whose phase data have to be resolved. Signals coming

from outside the Unambiguous FOV should be suppressed at any cost. The other important parameters to be considered while synthesizing array spacing's are:

Specified DF accuracy, Azimuth coverage (generally $\pm 30^0$ to $\pm 45^0$), Elevation coverage (Including coning errors), Frequency coverage, Antenna Dimensions, Post Calibration Phase errors in antenna and RF Front End hardware components, SNR requirements and Interference immunity, Interference includes reflections, multipath, time coincident signals, mutual coupling, etc.

Phase calibration is a very important requirement in this type of DF system. Calibration is used to remove static bias phase errors in the Front End hardware. Calibration data is stored in a look-up table (LUT) for each frequency. Antenna phase errors are stored in a separate LUT. It is generally possible to bring down phase errors to within 12 degrees (peak) using calibration LUTs. It is to be noted that the phase error margin should not be compromised just because the hardware is calibrated. The phase error margin is required to take care of what happens to the input signal even before it enters the antenna array. Multipath, reflections, Interference, SNR, etc. will alter the phase relationships. A course amplitude based DF system is also required if Inter Sector ambiguity is to be resolved. The peak error in the Amplitude DF system has to be less than half the unambiguous FOV of the Interference.

3.4 Intra-pulse analysis

Intra-pulse analysis of radar signals is carried out in ELINT systems using offline analysis [21]-[23]. RF signal is down-converted into IF signal using front-end i.e. down-converter. This IF signal is digitized by high-speed data acquisition systems and it is stored in the memory. This data is sent to DSP for further analysis. Figure 3.17 shows the block diagram of the conventional ELINT system.

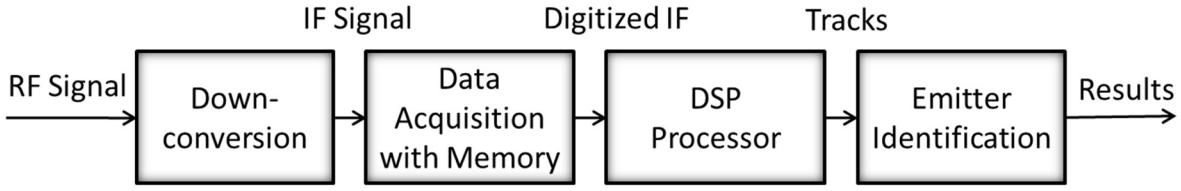

Figure 3.17: Block diagram of conventional ELINT system.

3.4.1 Down-conversion and digitization of IF signal

Superheterodyne receiver, Channelized receiver, or homodyne receiver are tuned for down-conversion and IF signals are obtained. The IF signals are down-converted to the centre frequencies of 1000 MHz ± 250 MHz, 160 MHz ± 20 MHz, or 70 MHz ± 5 MHz. These IF signals are digitized by high-speed data acquisition systems. The IF signal of 1000 MHz is sampled at 1333 MSPS to cater the bandwidth of 500 MHz using band pass sampling. IF signal of 160 MHz or 70 MHz is sampled at 500 MSPS using low pass sampling. In L and S radar bands, the IF of 160 MHz or 70 MHz is used. The IF of 1 GHz is used for higher radar bands.

3.4.2 Storing of IF data and preprocessing

The digitized IF signal is stored in the double data rate DDR SDRAM memory in real-time for pulse data. The pulse data comprises of pulse duration, pre-trigger, and post-trigger. Pre-trigger, and post-trigger data are captured to measure the rise-time or fall-time. Pre-processing is also carried out to measure the course parameters like RF, PW, and PRI. These course measurements are useful for initial plotting.

When the Data acquisition unit completes the acquisition of the required number of pulses, it sends the digitized data to DSP. In case, data is not received within a specified time limit, the timeout interrupt is generated indicating that the emitter is not available and the controller terminates the process.

3.4.3 Modulation measurement

The threshold applied for detection can be either fixed or noise riding. The TOA of each pulse is obtained by applying the selected or calculated threshold on the instantaneous amplitude of the signal and measuring the point where the signal crosses the threshold. From the TOA of each of the pulses in the pulse train, PRF is calculated. The measurement of PW of the signal is similar to that of TOA, where the time duration over which the signal crosses the threshold is measured. As with the other parameters, a statistical analysis of PW and PRF is carried out. The various quantified characteristics thus obtained are passed for post-processing and fine grain data is generated. Block diagram of DSP processor based modulation measurement in shown in Figure 3.18.

The pulse parameter measurement along with modulation measurement is carried out using DSP processors. These processors are having a limited number of Multiply-Accumulate

(MAC) units. The received digitized IF data for the signal is processed. Parameters are measured for each pulse along with intra-pulse modulation and a pulse descriptor word (PDW) is formed.

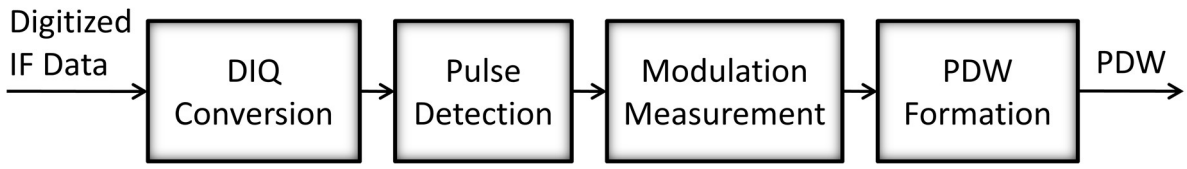

Figure 3.18: Block diagram of DSP processor based modulation measurement.

3.4.4 Sorting

The PDW for each pulse is passed for sorting. De-interleaving is done on the PDW to perform a one-to-many mapping of the track. The initial sorting required for segregating the pulses is done in the primary de-interleaving stage. The parameters used for this segregation are frequency and pulse width. Using these two parameters, emitters are grouped by sorting the pulse data with similar parameters into pulse chains employing the Pigeon Hole technique. After the initial sorting is done, secondary de-interleaving does the task of further sorting and classifying. The process of secondary de-interleaving uses the important parameter, TOA with the techniques of histogram analysis to perform this job. From the TOA parameter of each PDW, the type of PRF and the corresponding parameter for this type of PRF are measured. These tracks are formed based on emitters available in the environment.

3.4.5 Emitter Identification

The Identification unit identifies the incoming radar with the radars stored in the library by using the track parameters, which are measured by the DSP Unit. The controller sends the incoming track parameters to the Identification unit for matching.

The parameters of the library can be scaled and sorted into groups like Frequency, PRI, and PW, etc. For each group, identification is done by passing the parameters through suitable windows and using some distance metrics to find the error between the input parameters and the radar library parameters. The windows for each parameter will depend upon the variance of the parameter, noise, system accuracy, etc. The weights are assigned to each parameter depending upon its importance.

3.5 Summary

This chapter has discussed many contemporary parameter measurements techniques which include frequency measurement receivers, frequency measurement techniques, direction-finding techniques, and modulation measurement techniques. Homodyne receivers are used for wideband coverage and it is frequently used for wideband ES systems but achieves less sensitivity. Superhet receiver is also the most important receiver which is used for the ELINT system. The achieved sensitivity and dynamic range are very high. Superhet receiver is used in conjunction with digital receiver for ELINT system.

The spinning antenna is the simplest of all direction-finding techniques but has a relatively course AOA estimation performance and poor POI performance. However, given spinning antennas are still used due to their low implementation costs. Baseline interferometer is best-suited direction-finding technique among the discussed DF techniques. This provides high DF accuracy.

Existing ELINT receivers use the Superhet receiver due to its feature. This downconverts RF signal into IF signal based on the tuning frequency. The IF signal is digitized by high-speed ADC. This digitized IF data is stored in memory for further processing by the DSP processor. This extracts the features along with modulation which is used for sorting, track formation, and emitter identification. Since, IF data is stored the process after this remains offline. Hence, the modulation measurement is also offline processing. The systems based on DSP hardware is categorized as a strategic system due to offline processing for ELINT systems.

Chapter 4

Signal Estimation and Direction Finding

In the previous chapter contemporary electronic intelligence receivers with digital frequency measurement techniques and direction-finding techniques are described. The modulation measurement techniques are also presented which are useful for offline analysis. In this chapter, noise cancellation technique is used as part of preprocessing of the signal. Further instantaneous amplitude and instantaneous frequency profiles are extracted using the autocorrelation technique. FFT-based frequency estimation using interpolation techniques and three antennas based direction-finding techniques are also described. The simulation results are also presented for all the mentioned techniques and these are implementable for real-time application.

4.1 Introduction

The signal is received and noise cancellation is employed as part of the preprocessing. In noise cancellation, average noise is estimated for fixed time duration by ensuring signal absence. If signal is present during noise estimate the average will be estimated wrongly. The incoming signal spectrum subtraction is carried out with average noise estimate and same time incoming signal phase is not being disturbed. The recovered signal is called as restored signal [117]. This technique is applied for both the I and Q channels as further processing is based on the complex signal. Later, autocorrelation with different delays are computed using both I and Q channels to reduce the impact of noise. Implementation of autocorrelation algorithm consumes more hardware resources. An efficient technique is innovated to reduce the hardware consumption. To measure the highly accurate intra-pulse parameters a new system configuration has been proposed with various proposed signal processing algorithms.

Estimation of frequency is carried out based on the Rectangular window, Hanning window, Curve fitting, Curve fitting with Hanning window interpolation techniques. Interpolation techniques results are compared with FFT measured frequency which improves the accuracy of frequency reporting. The correct frequency is useful for AOA measurement

which is an important parameter because it can't be camouflaged. This parameter can be exploited in many ways which include improving situational awareness, signal sorting or deinterleaving, prompt electronic attack measures (such as jammers) or electronic protection measures (such as chaff), and many more. Accurate DOA measurement is required with available space and resources. There are many contemporary directions finding methods that are suitable for implementation in electronic intelligence receivers such as Rotary Direction Finding (RDF), Amplitude Comparison Direction Finding (ADF), Time Difference of Arrival (TDOA), Phase Difference of Arrival (PDOA), and Frequency Difference of Arrival (FDOA). The PDOA is also known as interferometry [3], [49].

4.2 Preprocessing of signal

Figure 4.1 shows the block diagram of fine grain parameter (FGP) measurement which is carried out by enhancement of signal-to-noise ratio (SNR) and sample-to-sample measurement of amplitude and frequency. The algorithms shown are used on digitized IF signal and instantaneous amplitude and frequency profiles are obtained. Measured parameters constitute the fine grain parameters and computed using both autocorrelation approach and DIQ approach. The signal is pre-processed using the noise cancellation technique before being processed by these algorithms. Noise estimation is also carried out to estimate the noise riding threshold which is used for pulse detection and FGP is measured.

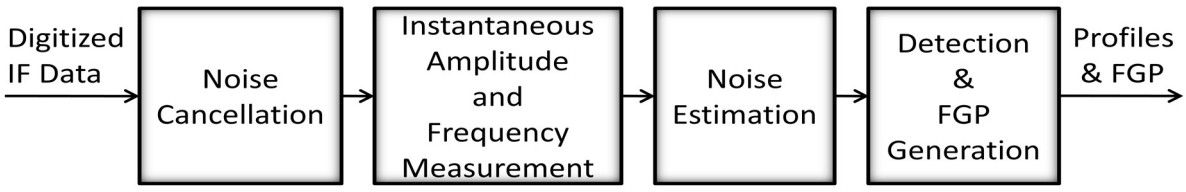

Figure 4.1: Block diagram of fine-grain parameter measurement.

Pre-processing of the signal is carried out at the initial stage just after aligning of data at the FPGA. The data is received thru SERDES in FPGA. Total eight samples are captured four samples at the positive clock and four at the negative clock. Preprocessing is carried out to improve the SNR of the signal.

4.2.1 Noise cancellation by spectral subtraction

Many receivers having the single input channel. Noise has to be estimated with the same input channel. It can reduce the effect of noise in the channel. Hence, the average of noise is estimated for the time duration. This average noise estimate is subtracted from input

signal spectrum. In this process phase of the incoming signal is not distorted. The incoming phase is attached after spectrum subtraction. Hence, this restored signal can be used for direction finding systems also as phase of the input signal will be intact.

Noise cancellation is performed as part of the pre-processing of the signal. Input signal which is noisy and hence it is called a noisy signal. The sum of the clean signal x(m) and the noise n(m) is modelled as noisy signal y(m) i.e. y(m) = x(m) + n(m) where the m is the integer variable known as discrete-time index. The FFT of 1024 points is carried out continuously on the noisy data. An overlap ratio of 75% is considered. Noise data are collected from the system chain when the front-end is connected to the BITE port in signal off condition for a minimum time of 50 us for a good estimate. A total of 50 us of noisy data is considered to carry out the estimated average amplitude of FFT bins. Spectrum subtraction is carried out to get a restored signal which reduces the SNR requirement at the input signal. Then the estimated average of noise spectrum $\overline{N_m}$ is subtracted from the noisy signal spectrum Y_m to get an estimate of the instantaneous magnitude spectrum of restored signal X_m.

$$X_m = Y_m - \overline{N_m} \tag{4.1}$$

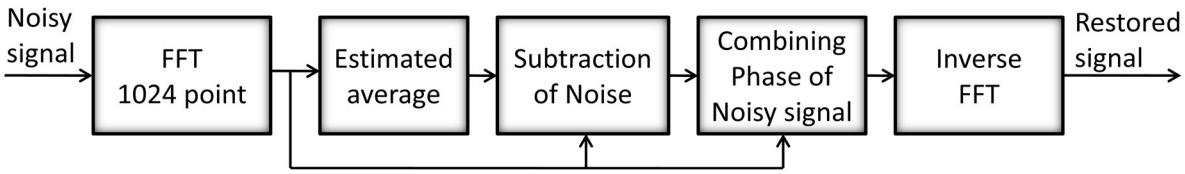

Figure 4.2: Block diagram of noise cancellation using spectral subtraction.

Restored time-domain signal (X_m) is obtained by combining an estimate of the instantaneous magnitude spectrum of restored signal with the phase of the noisy signal, and transforming via an inverse discrete Fourier transform to the time domain [117].

$$x(m) = \sum_{k=0}^{N-1}(X_m e^{j\theta Y_k})(e^{\frac{j2\pi km}{N}}) \tag{4.2}$$

Where, m = 0, 1, 2, ..., N-1

$x(n)$ = Time domain signal

X_m = Restored signal spectrum

$\overline{N_m}$ = Noise spectrum

Y_m = Noisy signal spectrum

$x(m)$ = Restored time domain signal

m, n = Index number

k = Bin number

ΘY_k = Phase of the noisy signal frequency spectrum Y_m

4.2.2 Signal flow graph of noise cancellation

The signal flow graph of the noise cancellation technique is shown in Figure 4.3. The IF data is captured and overlapped FFT of 1024 points is computed continuously upto 50 us of duration. So, the computed number of FFT frames (FF) is compared with incoming FFT frames (Nt). An estimated average of spectrum for all the frames is carried out after completion of FFT computations. This average is subtracted from the incoming signal spectrum and the restored spectrum is obtained. This spectrum is combined with the phase of the incoming signal or noisy signal. Inverse FFT is computed to get the restored time-domain signal. These samples are used for instantaneous measurements and signal detection.

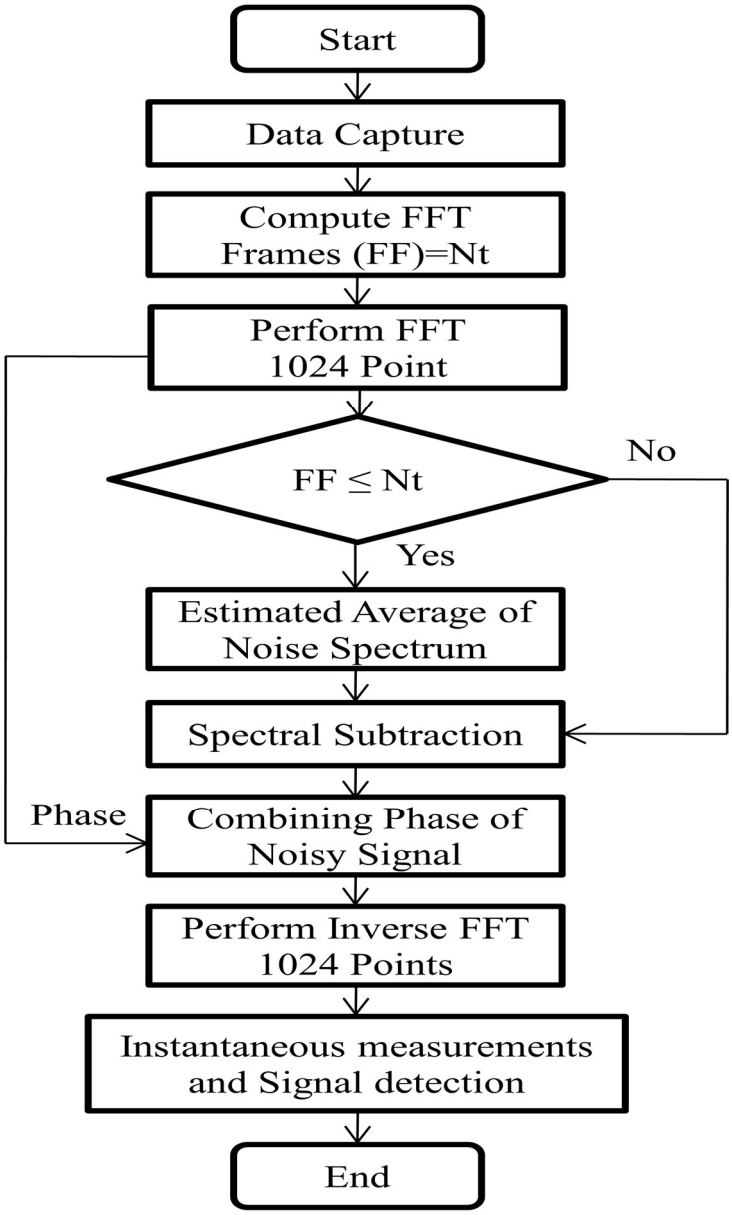

Figure 4.3: Signal flow graph of noise cancellation.

4.2.3 Simulation results of noise cancellation

Noise estimate is computed using the FFT during the noise region as shown in Figure 4.4. These averaged noise estimate is subtracted from input signal spectrum. The output restored signal is produced as shown in Figure 4.5. The 80,000 samples are taken for the pre-trigger region which consists mainly of noise and 8000 samples are taken for the pulse signal which consists of signal as well as noise. Total 33,333 samples are considered for 50 us noise estimates. In this case, only one pulse is taken. The additive white Gaussian noise (AWGN) is considered for this purpose. It is visible in output restored signal that has reduced noise and thus helps in improving the accuracy of further analysis. The restored signal is applied on both baseband signals of In-phase (I) and Quadrature-phase (Q) components.

The noisy signal generated along with for eight pulses as shown in Figure 4.6 at 4 dB SNR. This signal is generated with a total of 150,000 samples. Out of which 33,333 samples are used for noise estimate. Figure 4.7, shows the restored signal obtained using the noise cancellation technique at 4 dB SNR for eight pulses.

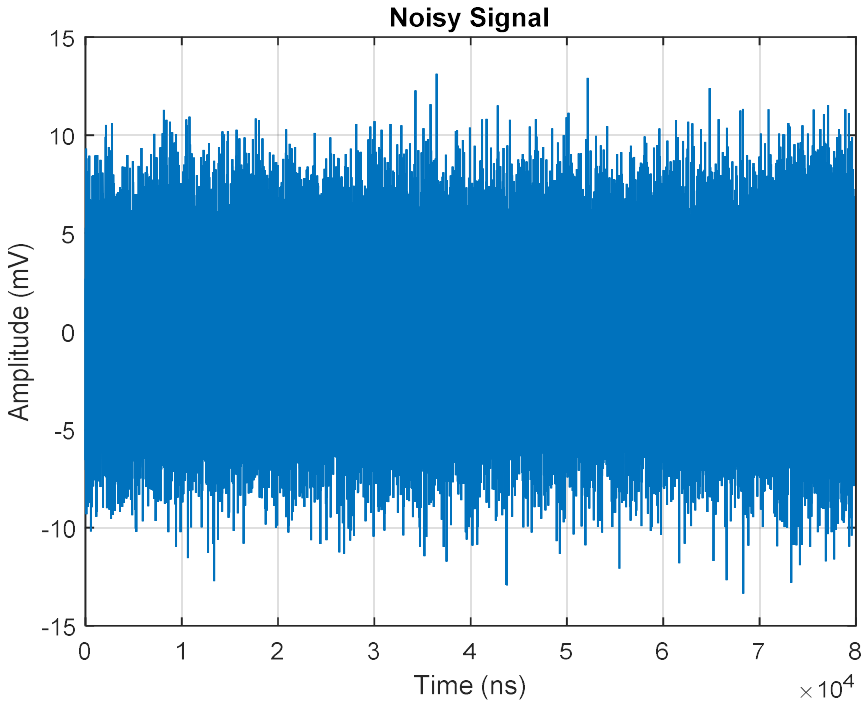

Figure 4.4: Noisy signal (input signal) generated with noise and one pulse. Simulation parameters: f = 1.1 GHz, η = 4 dB, N = 80,000 samples, and t_s = 1.5 ns.

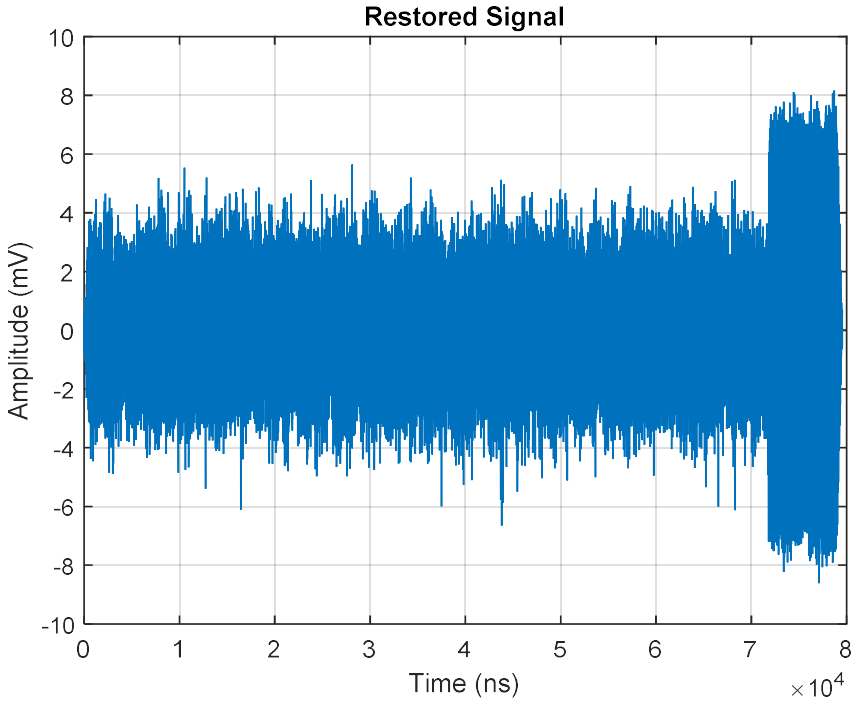

Figure 4.5: Restored signal obtained for noise and one pulse. Simulation parameters: f = 1.1 GHz, η = 4 dB, N = 80,000 samples, and t_s = 1.5 ns.

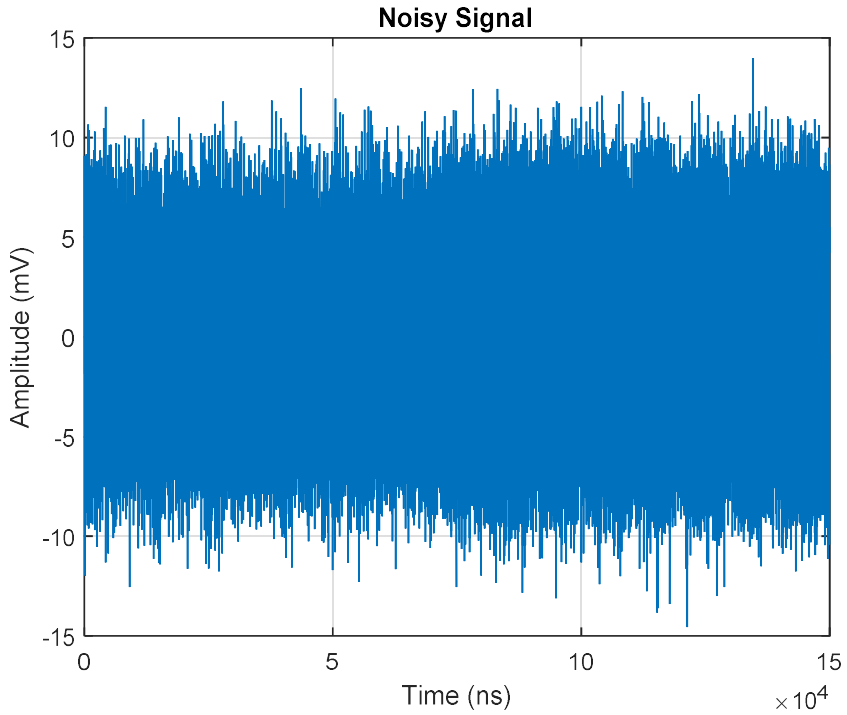

Figure 4.6: Noisy signal (input signal) generated with noise and eight pulses. Simulation parameters: f = 1.1 GHz, η = 4 dB, N = 150,000 samples, and t_s = 1.5 ns.

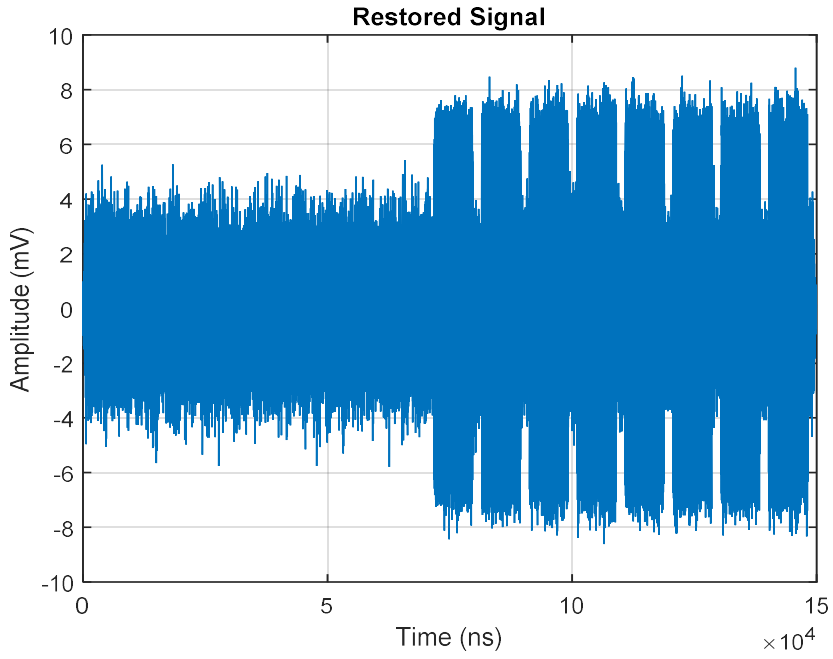

Figure 4.7: Restored signal obtained for noise and eight pulses. Simulation parameters: f = 1.1 GHz, η = 4 dB, N = 150,000 samples, and t_s = 1.5 ns.

The noisy signal generated along with for eight pulses as shown in Figure 4.8 at 2 dB SNR. This signal is generated with a total of 150,000 samples. Out of which 66,666 samples are used for noise estimate. Figure 4.9, shows the restored signal obtained using the noise cancellation technique at 2 dB SNR for eight pulses.

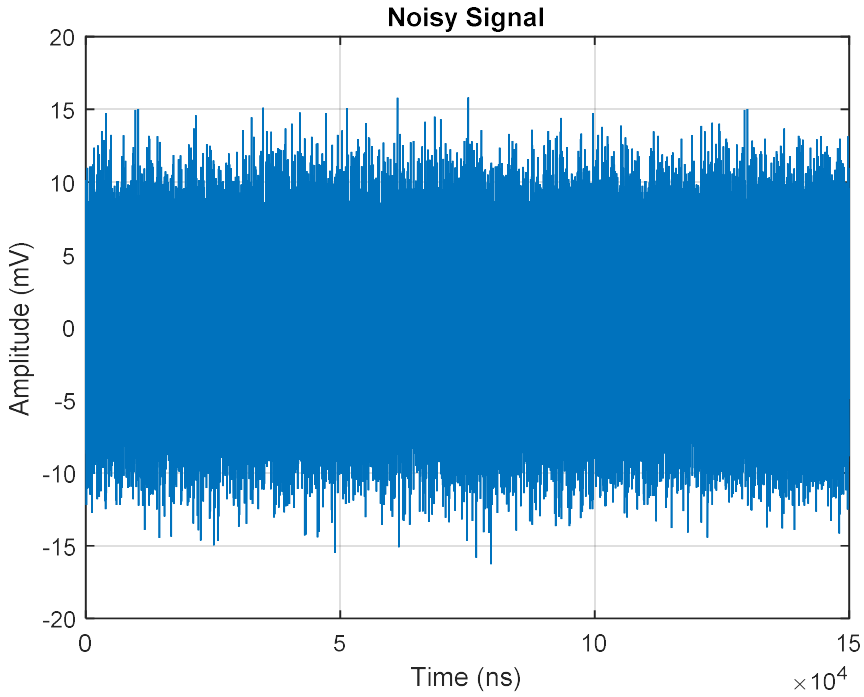

Figure 4.8: Noisy signal (input signal) generated with noise and eight pulses. Simulation parameters: f = 1.1 GHz, η = 2 dB, N = 150,000 samples, and t_s = 1.5 ns.

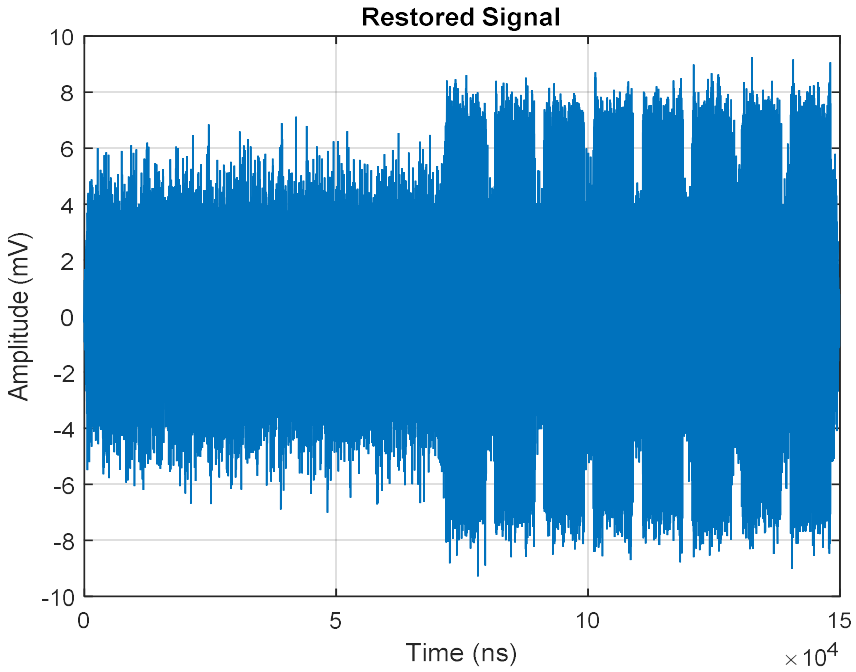

Figure 4.9: Restored signal obtained for noise and eight pulses. Simulation parameters: f = 1.1 GHz, η = 2 dB, N = 150,000 samples, and t_s = 1.5 ns.

Similarly, Figure 4.10 shows the restored signal obtained using noise cancellation technique at 0 dB SNR for eight pulses and Figure 4.11 shows the output restored signal using noise cancellation technique at -2 dB SNR for eight pulses.

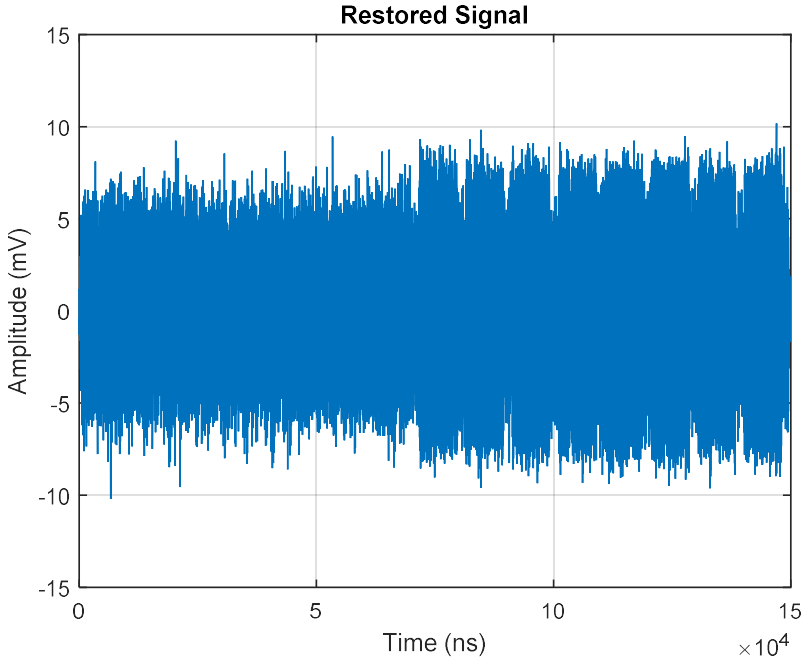

Figure 4.10: Restored signal obtained for noise and eight pulses. Simulation parameters: f = 1.1 GHz, η = 0 dB, N = 150,000 samples, and t_s = 1.5 ns.

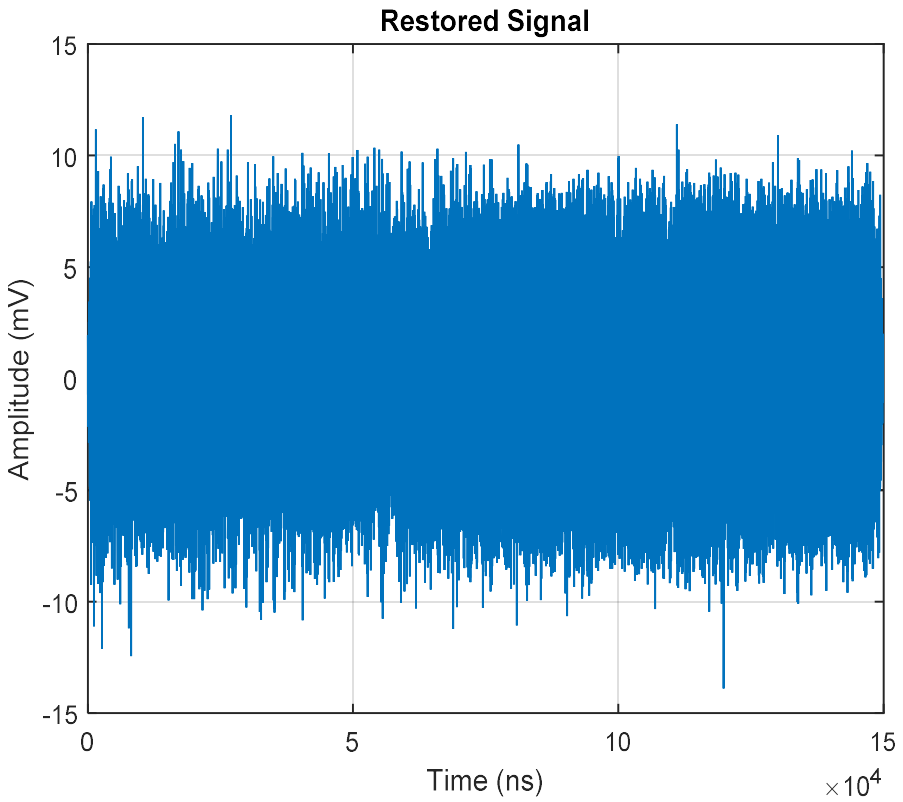

Figure 4.11: Restored signal obtained for noise and eight pulses. Simulation parameters: f = 1.1 GHz, η = -2 dB, N = 150,000 samples, and t_s = 1.5 ns.

4.2.4 Advantage of noise cancellation

The noise cancellation technique traditionally was used for communication signals. But this technique became useful for radar signals also, due to the availability of high density and high-speed processing hardware. This technique gives the SNR advantage and effective upto -2 dB SNR with 1024 point FFT and 75% overlapping ratio. This SNR advantage directly translates into sensitivity improvement. This technique is required to be used as part of preprocessing before detection of the pulse. After detection of pulse, this technique will not provide an advantage at the stage of detection. If FFT-based detection is used, the same FFT output may be used for noise estimate.

In radar signal restoration process, the objective is to estimate the instantaneous signal spectrum. The restored magnitude spectrum is combined with the phase of the incoming signal to form the restored radar signal. Spectral subtraction has to be implemented carefully can result in a substantial improvement in the identification performance. The main attraction of spectral subtraction is its relative simplicity, in that it only requires an estimate of the noise power spectrum.

4.3 Generation of instantaneous amplitude and frequency profiles

The moving autocorrelation technique is used for the generation of instantaneous amplitude profile and instantaneous frequency profile. Amplitude profile is generated on multiplying in-phase and delayed quadrature-phase signals. Since the input signals are in quadrature and hence it is a complex signal. This complex signal after multiplying gives an envelope of the IF signal. In the case of the DIQ technique, the complex signal is generated using a real signal.

Multiplication requirements are reduced compared to the DIQ approach. The multiplications required for the proposed approach are eight for two complex multiplications. Whereas multiplications required for the DIQ approach are more for low pass filters implementations.

4.3.1 Moving autocorrelation technique for amplitude generation

The moving autocorrelation technique is computationally efficient and occupies fewer FPGA resources. It also provides a detection advantage. It is performed on the signal x(n).

The received signal is expressed in complex form as

$$x(n) = Ae^{j2\pi fn\ s}e^{j\emptyset} + w(n) \tag{4.3}$$

Where $Ae^{j2\pi fnt_s}$ is the received signal, A is the signal amplitude, $\emptyset$ is the initial phase, t_s is the sampling interval, f is the carrier frequency, and w(n) is the sampled zero-mean, additive Gaussian white noise (AGWN).

The autocorrelation result is computed based on the absolute value of the pulse and according to the features of a digital wideband pulse. The autocorrelation function is given by [22],

$$X_n(n) = \sum_{i=0}^{N-1} |x(n+i)|\,|x^*(n+i+1)|$$
$$= \sum_{i=0}^{N-1} \left| A^2 e^{j2\pi fn\ s} e^{j\emptyset} + Ae^{j\emptyset} e^{j2\pi f(n+i)t_s}\, w^*(n+i+1) + Ae^{-j\emptyset} e^{-j2\pi(n+i+1)t_s}\, w(n+i) + w(n+i) \right| \tag{4.4}$$

$X_n(n)$ can be updated by iterated means and can be easily implemented on hardware by using,

$$X_n(n+1) = X_n(n) + |x(n+N)x^*(n+N+1)| - |x(n)x^*(n+1)| \tag{4.5}$$

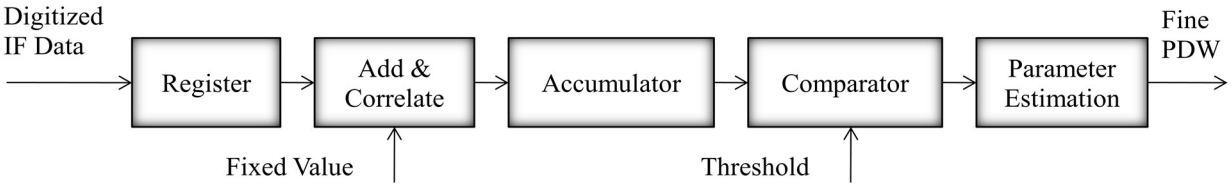

Figure 4.12: Block diagram of autocorrelation-based parameter estimation.

Initial autocorrelation will be performed with length N samples. Then subsequently new autocorrelation output will be obtained by subtracting the first sample autocorrelation output and adding new sample autocorrelation to the correlation value. N samples autocorrelation is performed in a recursive way to reduce the computational burden. The block diagram of autocorrelation-based parameter estimation is shown in Figure 4.12.

Autocorrelation output will be compared with a threshold to check for start of the pulse. If the start of a pulse is detected, then IF data will be stored and the time of arrival will be stored. N should be selected in such a way that it should detect minimum pulse width. As N increases noise reduction is improved. So a selection of N is a trade-off between minimum pulse width and noise suppression. Value of N, more than 16 is optimum. The following equations are rewritten and simplified as below,

$$x(n) = x_i\,(n) + jx_q\,(n) \tag{4.6}$$

$$X_N(n) = \sum_{n=0}^{N-1}\left[x_i(n) + jx_q(n)\right]\left[x_i(n+1) + jx_q(n+1)\right] \tag{4.7}$$

$$X_N(n+1) = X_N(n) + \left[x_i(n+N-1) + jx_q(n+N-1)\right]\left[x_i(n+N) + jx_q(n+N)\right] - \left[x_i(n) + jx_q(n)\right]\left[x_i(n+1) + jx_q(n+1)\right] \tag{4.8}$$

$$Y_N(n) = \left[x_i(n+N-1) + jx_q(n+N-1)\right]\left[x_i(n+N) + jx_q(n+N)\right] \tag{4.9}$$

$$Y_1(n) = \left[x_i(n) + jx_q(n)\right]\left[x_i(n+1) + jx_q(n+1)\right] \tag{4.10}$$

$$X_N(n+1) = X_N(n) + Y_N(n) - Y_1(n) \tag{4.11}$$

$X_N\,(n)$ is computed for every new sample. Here only four real multiplications are required for every new sample.

$$X_N(n+1) = k + Y_N(n) - Y_1(n) \tag{4.12}$$

4.3.2 Multilevel autocorrelation technique for frequency generation

Baseband signal is used to perform the autocorrelation which reduce the impact of noise [22]. Total thirty-two samples are used to perform the autocorrelation recursively to reduce the computational requirement. Thirty-two samples of autocorrelation is selected to cater to the minimum pulse width requirement of 50 ns when sampling time is 1.5 ns. Delay m is 1 in the case of amplitude measurement. The first element of thirty-two samples autocorrelation is calculated as:

$$X_N(n) = \left(\frac{1}{N}\right)\sum_{n=0}^{N-1}\left[x_i(n) + jx_q(n)\right]\left[x_i(n+1) + jx_q(n+1)\right] \tag{4.13}$$

Where, x* is a conjugate of x. It is implemented in recursively as below:

$$X_N(n+1) = X_N(n) + |Y_N(n) - Y_1(n)| \tag{4.14}$$

Typically N is considered 32 which is optimum for all pulse widths varying from 50 ns to 1 ms. Where n varies from 1 to the size of samples. This equation is further optimized by replacing the first element of thirty-two samples autocorrelation with fixed value:

$$X_N(n) = a + jb \tag{4.15}$$

Where *a* and *b* are constant values. This does not require the measurement of an initial average of thirty-two samples autocorrelation output. Measurement of frequency parameters involves the calculation of autocorrelation variables with different delays using baseband signal. Four autocorrelation variables X_1, X_2, X_4, and X_8 with four different delays $m = 1, 2, 4,$ and 8 are calculated from the correlated signal with different delays. Multilevel phase differences are calculated from the correlated signals with different delays, which in turn are used to compute the frequency. Frequency $F_1(n)$ is measured as:

$$F_1(n) = F_s\frac{\Delta\Phi(n)}{2\pi} \tag{4.16}$$

Where, F_s is the sampling frequency and $\Phi(n)$ is the phase derived from X_1, and $\Delta\Phi(n)$ is the phase of the signal. Now $F_1(n)$ measurement determines the zone in which phase belongs according to the following equation.

$$Z_m = Ceil\left(\frac{mF_1(n)}{F_s}\right) \tag{4.17}$$

Here unwrapping of phases which are required for complex signals is not required as different phases are calculated from auto-correlated variables with different delays and are mapped to appropriate zones which are obtained with the help of frequency $F_{m-1}(n)$ [23]-

[24]. Likewise, $F_2(n)$ serves as a guide for Φ_4 by determining the zone it should be merged to. Similarly, $F_4(n)$ determines the zone for Φ_8. The final frequency parameter $F_8(n)$ is based on the mapping of Φ_8.

$$F_m(n) = \left(\frac{F_s}{2\pi m}\right)(\Delta\Phi_m(n) + 2\pi Z_m) \tag{4.18}$$

Using the improved instantaneous frequency, the various intra-pulse modulations. Frequency modulation, bi-phase modulation, and stepped frequency modulations are also classified. The instantaneous frequency is used to extract the modulation of the signal.

4.3.3 Simulation results of amplitude profile generation

An instantaneous amplitude profile is generated for the following four different approaches at different SNR conditions. This will show at what value of SNR particular techniques start generating correct amplitude profile.

(i) DIQ technique without noise cancellation
(ii) DIQ technique with noise cancellation
(iii) Moving autocorrelation technique without noise cancellation
(iv) Moving autocorrelation technique with noise cancellation

Simulation parameters considered to generate following amplitude plots are input frequency (f) = 1.1 GHz, No. of samples (N) = 80,000 samples, and sampling time (t_s) = 1.5 ns. The simulations are carried out for various SNR (η) conditions to establish the benefits of the above techniques with respect to SNR.

4.3.3.1 Simulation results at -2 dB SNR

Figure 4.13 shows the noisy signal generated with eight pulses with SNR of -2 dB. Whereas restored signal is obtained for -2 dB SNR as shown in Figure 4.14 using noise cancellation technique.

The instantaneous amplitude is computed using correlated signal x(n) at the SNR condition of -2 dB. The instantaneous amplitude profile computed using the DIQ technique without noise cancellation is plotted as Figure 4.15 at SNR conditions of -2 dB. The input signal is improved using the noise cancellation technique. Figure 4.16 shows, the instantaneous amplitude profile using the DIQ technique with noise cancellation. This confirms that DIQ technique and DIQ technique with noise cancellation are not working effectively at SNR of -2 dB.

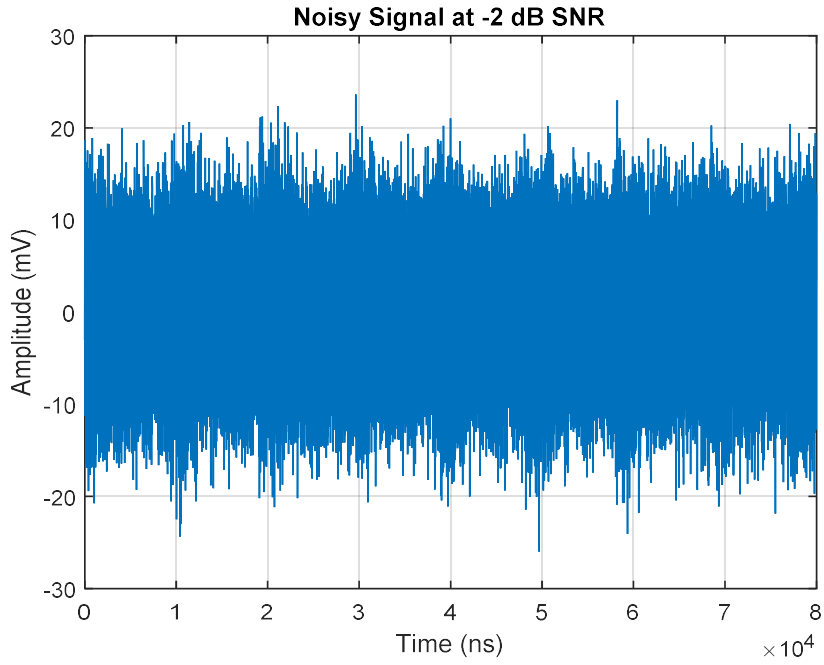

Figure 4.13: Noisy signal (input signal) generated with eight pulses. Simulation parameters: f = 1.1 GHz, η = -2 dB, N = 80,000 samples, and t_s = 1.5 ns.

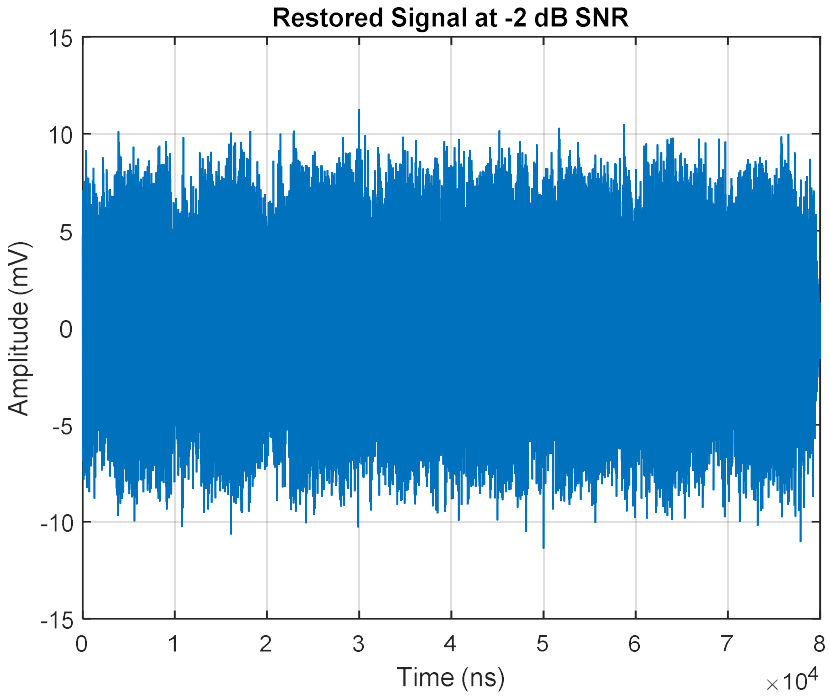

Figure 4.14: Restored signal obtained using noise cancellation for eight pulses. Simulation parameters: f = 1.1 GHz, η = -2 dB, N = 80,000 samples, and t_s = 1.5 ns.

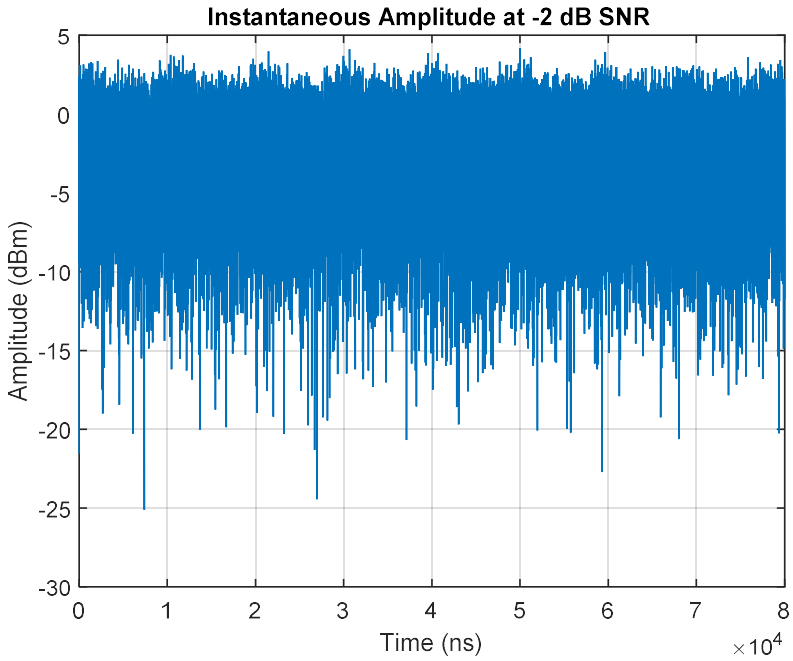

Figure 4.15: Instantaneous amplitude profile using DIQ technique without noise cancellation for eight pulses. Simulation parameters: f = 1.1 GHz, η = -2 dB, N = 80,000 samples, and t_s = 1.5 ns.

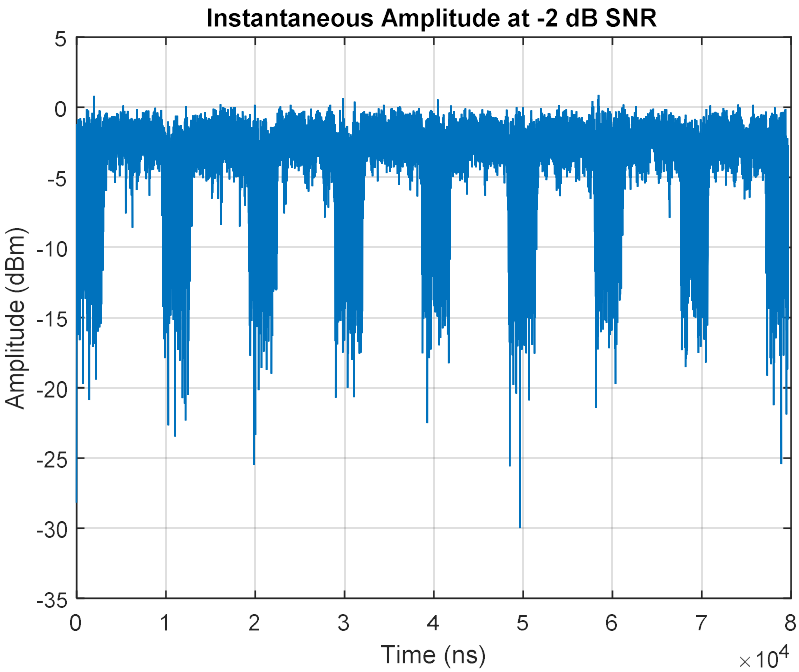

Figure 4.16: Instantaneous amplitude profile using DIQ technique with noise cancellation for eight pulses. Simulation parameters: f = 1.1 GHz, η = -2 dB, N = 80,000 samples, and t_s = 1.5 ns.

The instantaneous amplitude profile computed using autocorrelation technique without noise cancellation is plotted as Figure 4.17 at SNR conditions of -2 dB. It confirms that autocorrelation technique is not working effectively at SNR of -2 dB. Figure 4.18 shows, the instantaneous amplitude profile using the autocorrelation technique with noise cancellation. This confirms that autocorrelation technique with noise cancellation is working effectively at

SNR of -2 dB as there is sufficient clearance between pulse lower amplitude and noise peak amplitude.

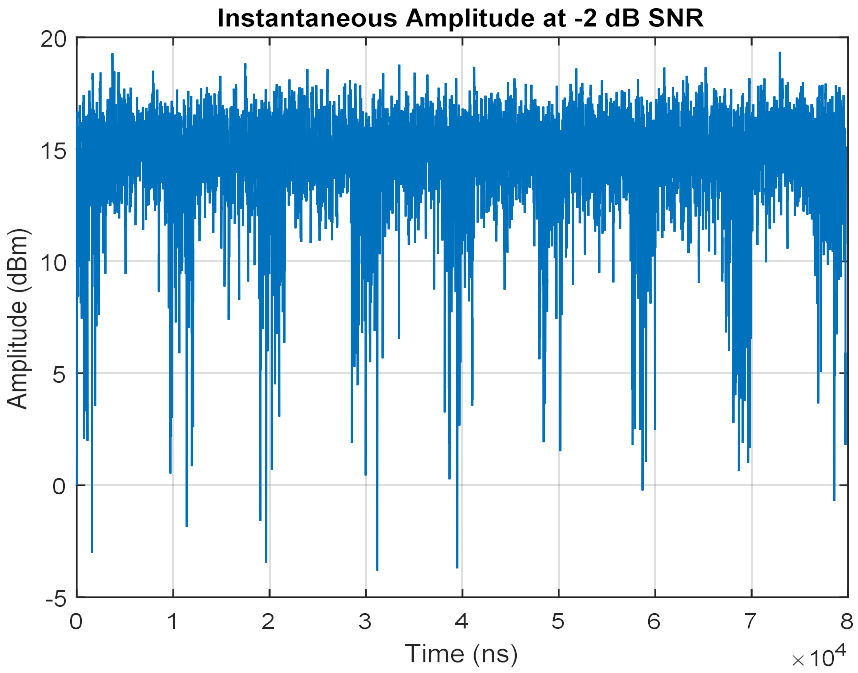

Figure 4.17: Instantaneous amplitude profile using moving autocorrelation technique without noise cancellation for eight pulses. Simulation parameters: f = 1.1 GHz, η = -2 dB, N = 80,000 samples, and t_s = 1.5 ns.

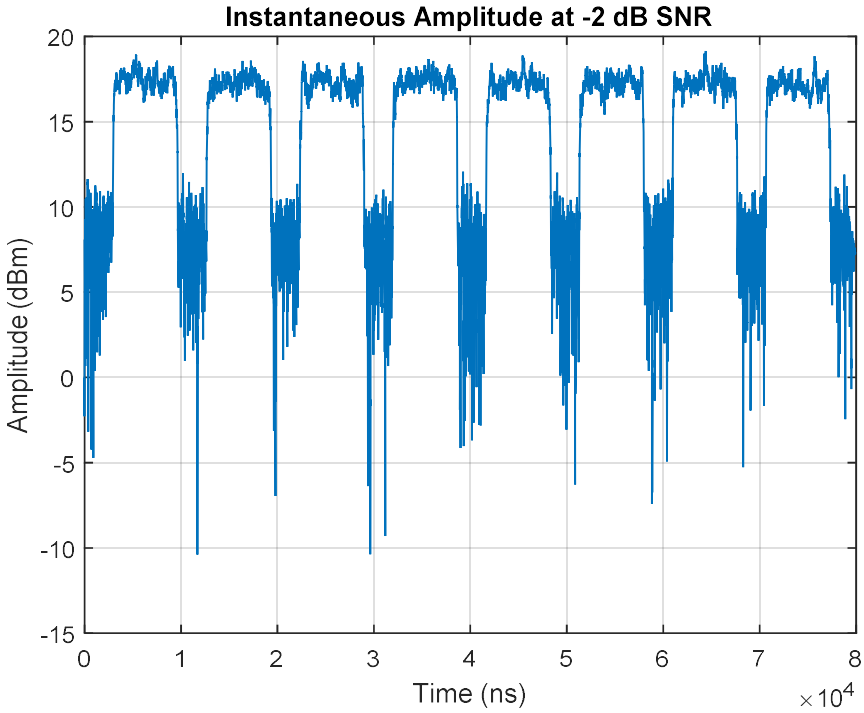

Figure 4.18: Instantaneous amplitude profile using moving autocorrelation technique with noise cancellation for eight pulses. Simulation parameters: f = 1.1 GHz, η = -2 dB, N = 80,000 samples, and t_s = 1.5 ns.

4.3.3.2 Simulation results at 4 dB SNR

A noisy signal is generated at 4 dB SNR and a restored signal is obtained from the noisy signal. The noisy signal is represented in Figure 4.19 and the restored signal is represented in Figure 4.20. Both the DIQ technique and autocorrelation technique is applied to the restored signal and results are shown in subsequent figures.

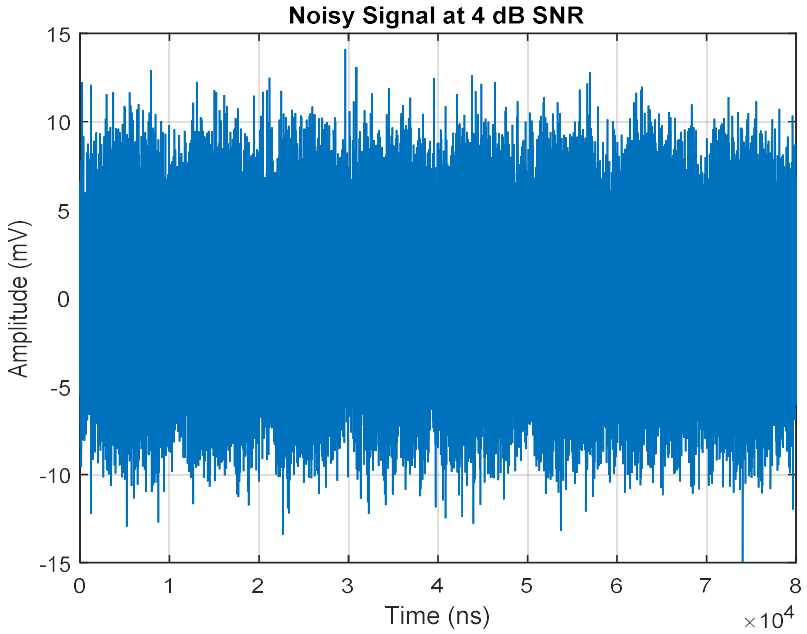

Figure 4.19: Noisy signal (input signal) generated with eight pulses. Simulation parameters: f = 1.1 GHz, η = 4 dB, N = 80,000 samples, and t_s = 1.5 ns.

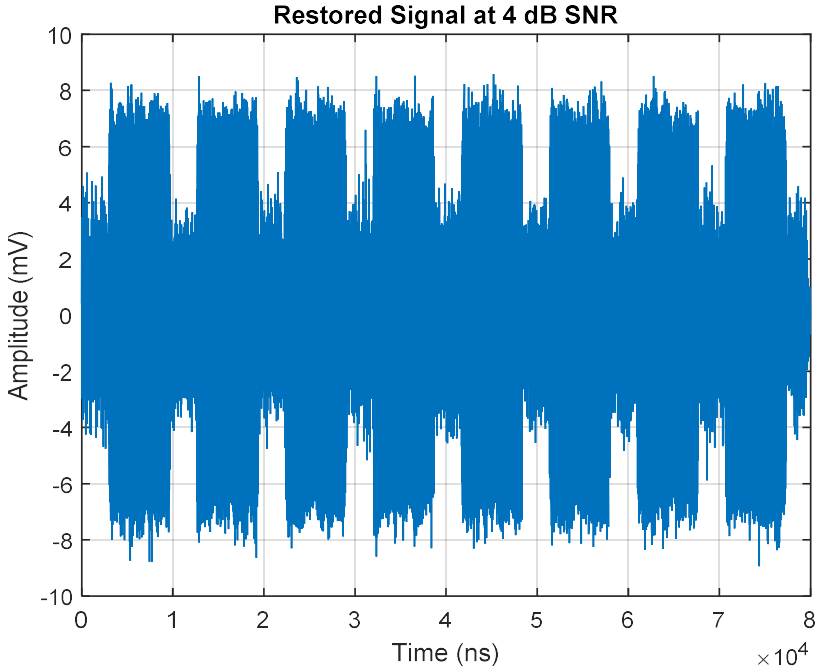

Figure 4.20: Restored signal obtained using noise cancellation for eight pulses. Simulation parameters: f = 1.1 GHz, η = 4 dB, N = 80,000 samples, and t_s = 1.5 ns.

Instantaneous amplitude profile is obtained for 4 dB SNR using DIQ technique and DIQ technique without noise cancellation technique and results are plotted at Figure 4.21 and Figure 4.22 respectively. This confirms that DIQ technique and DIQ technique with noise cancellation are not working effectively at SNR of 4 dB.

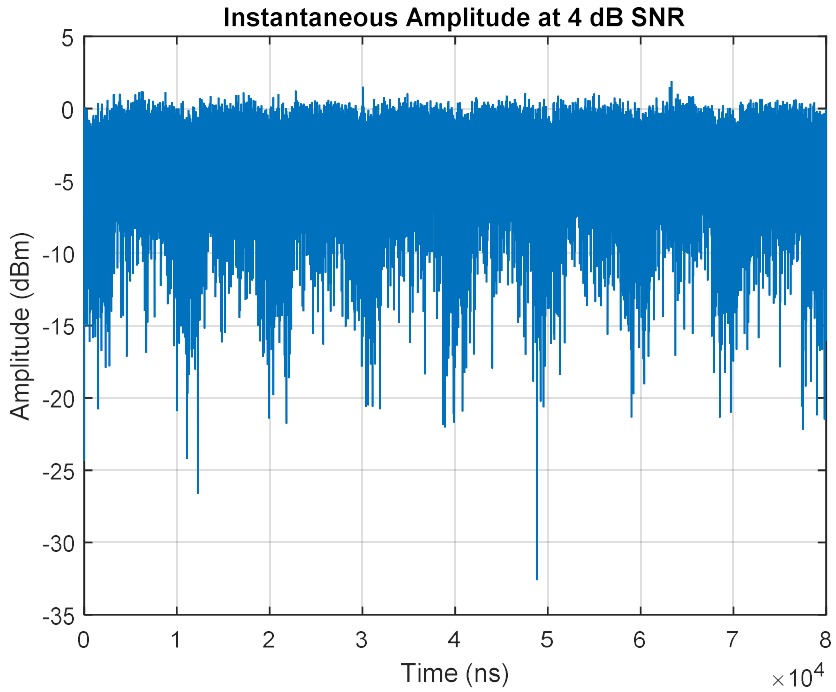

Figure 4.21: Instantaneous amplitude profile using DIQ technique without noise cancellation for eight pulses. Simulation parameters: f = 1.1 GHz, η = 4 dB, N = 80,000 samples, and t_s = 1.5 ns.

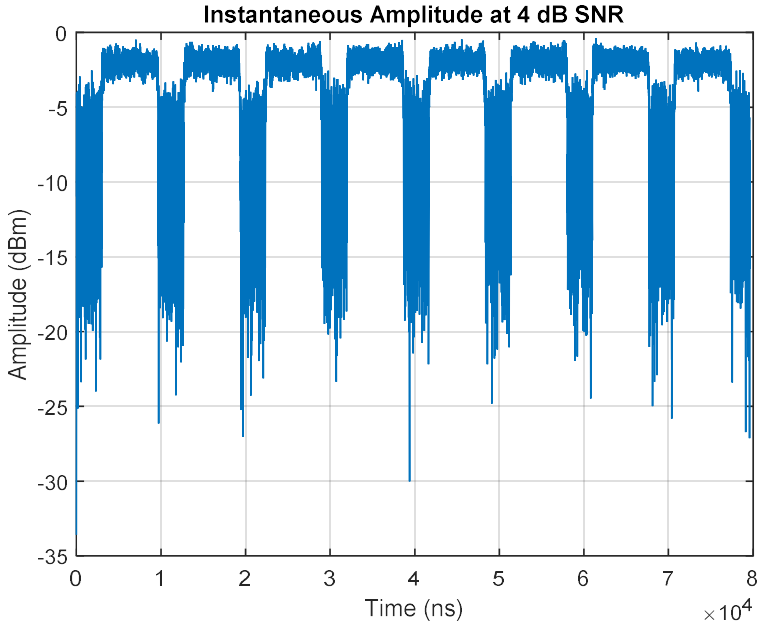

Figure 4.22: Instantaneous amplitude profile using DIQ technique with noise cancellation for eight pulses. Simulation parameters: f = 1.1 GHz, η = 4 dB, N = 80,000 samples, and t_s = 1.5 ns.

Instantaneous amplitude profile is obtained for 4 dB SNR using autocorrelation technique and autocorrelation technique with noise cancellation and results are plotted at Figure 4.23 and Figure 4.24 respectively. This confirms that autocorrelation technique and autocorrelation technique with noise cancellation are working effectively at SNR of 4 dB

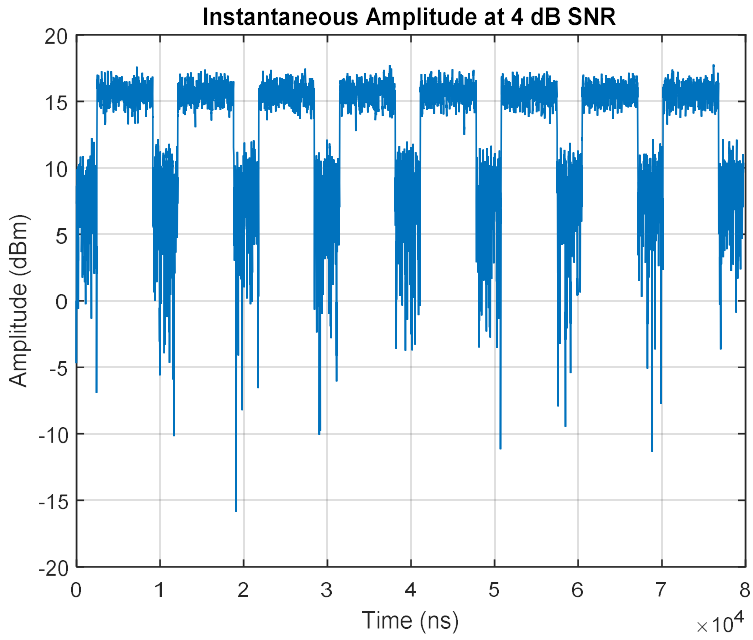

Figure 4.23: Instantaneous amplitude profile using moving autocorrelation technique without noise cancellation for eight pulses. Simulation parameters: f = 1.1 GHz, η = 4 dB, N = 80,000 samples, and t_s = 1.5 ns.

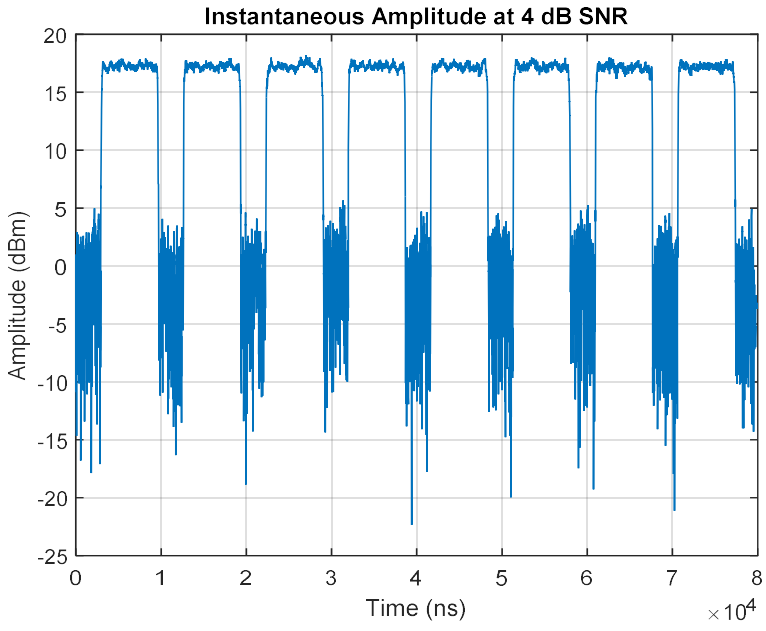

Figure 4.24: Instantaneous amplitude profile using moving autocorrelation technique with noise cancellation for eight pulses. Simulation parameters: f = 1.1 GHz, η = 4 dB, N = 80,000 samples, and t_s = 1.5 ns.

4.3.3.3 Simulation results at 8 dB SNR

The noisy signal is generated at 8 dB SNR and the restored signal is obtained. Figure 4.25 shows the noisy signal at 8 dB SNR and Figure 4.26 shows the restored signal of noisy signal at 8 dB SNR.

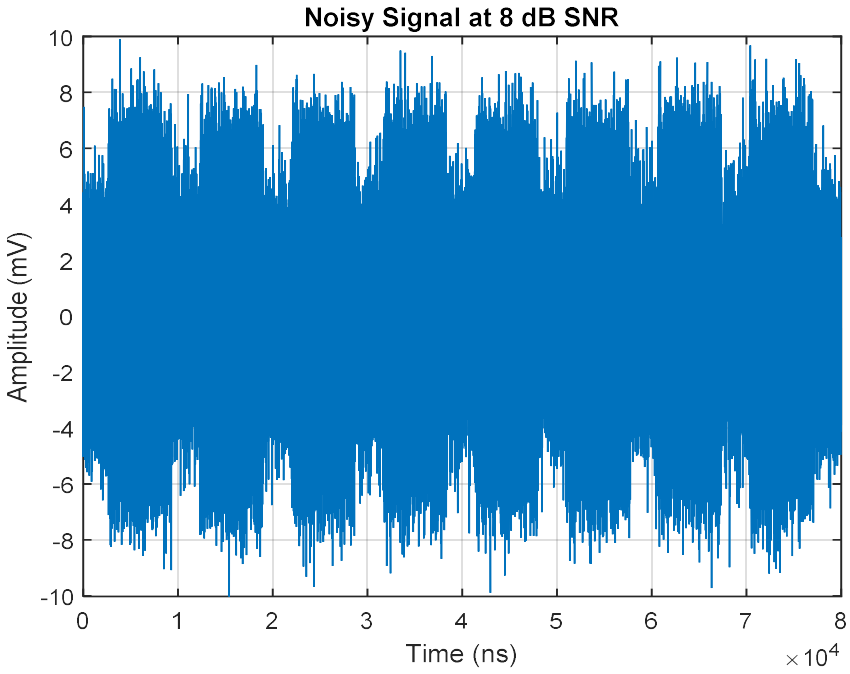

Figure 4.25: Noisy signal (input signal) generated with eight pulses. Simulation parameters: f = 1.1 GHz, η = 8 dB, N = 80,000 samples, and t_s = 1.5 ns.

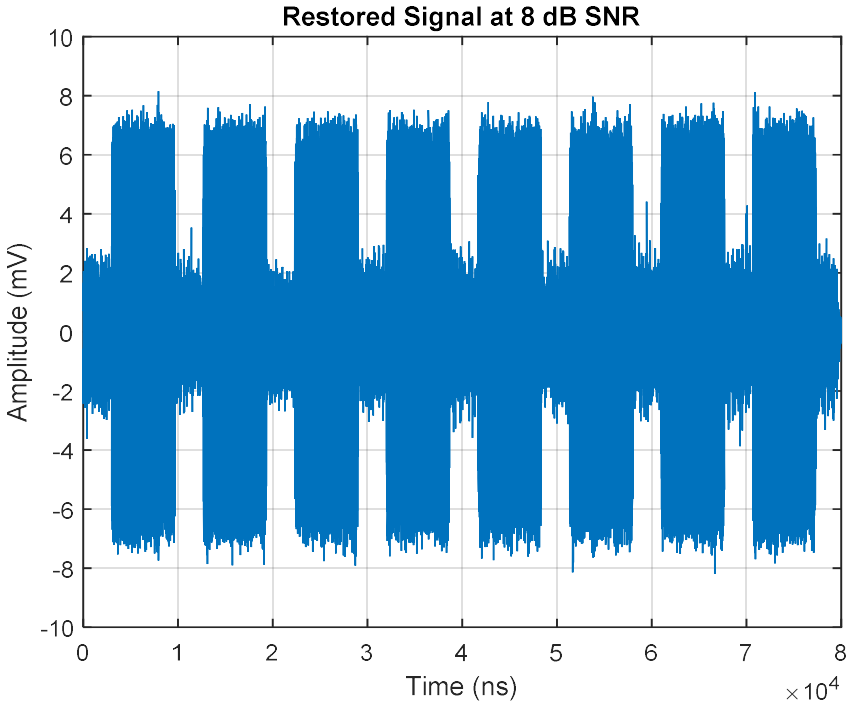

Figure 4.26: Restored signal obtained using noise cancellation for eight pulses. Simulation parameters: f = 1.1 GHz, η = 8 dB, N = 80,000 samples, and t_s = 1.5 ns.

Instantaneous amplitude profile is obtained for 8 dB SNR using DIQ technique and DIQ technique with noise cancellation technique and results are plotted at Figure 4.27 and Figure 4.28 respectively. It confirms that DIQ technique is not working effectively at SNR of 8 dB and DIQ technique with noise cancellation technique is working satisfactorily.

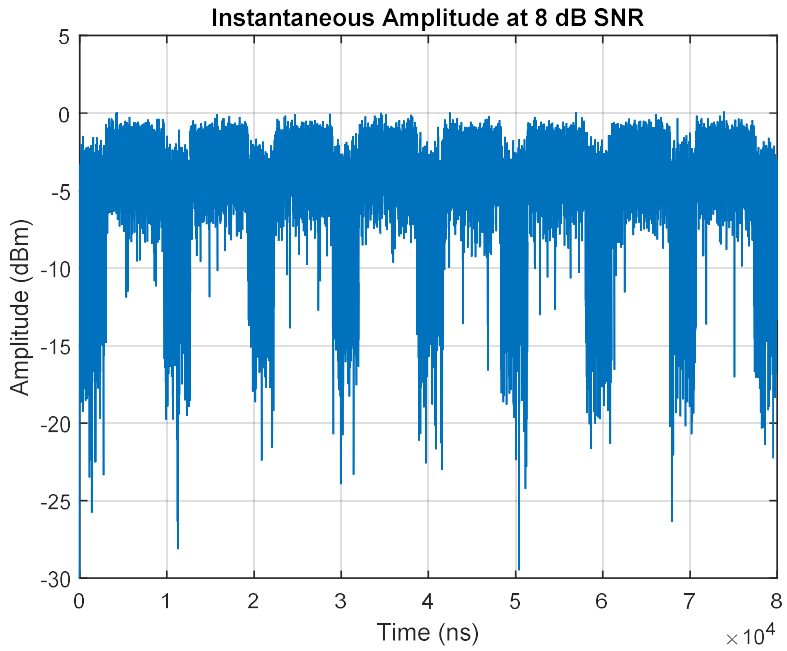

Figure 4.27: Instantaneous amplitude profile using DIQ technique and without noise cancellation for eight pulses. Simulation parameters: f = 1.1 GHz, η = 8 dB, N = 80,000 samples, and t_s = 1.5 ns.

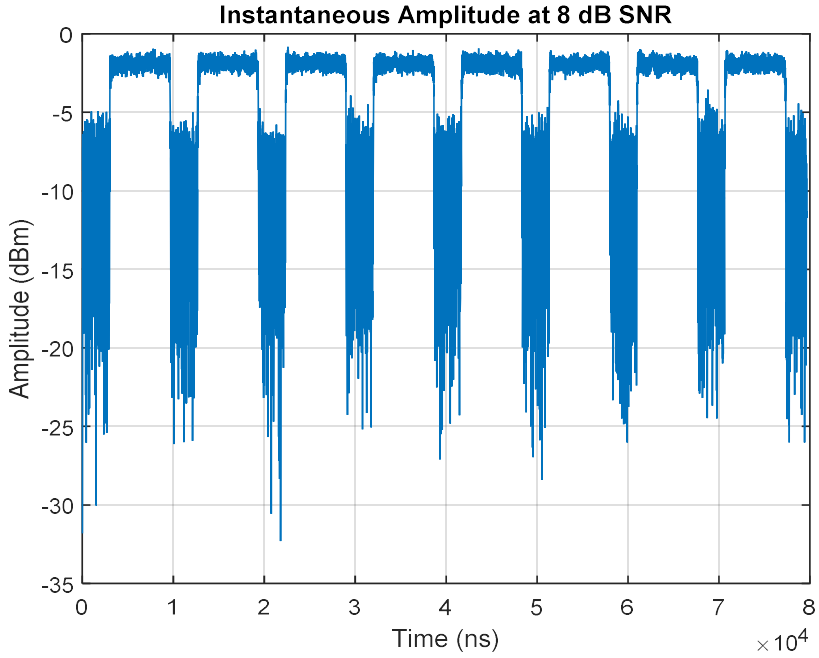

Figure 4.28: Instantaneous amplitude profile using DIQ technique with noise cancellation for eight pulses. Simulation parameters: f = 1.1 GHz, η = 8 dB, N = 80,000 samples, and t_s = 1.5 ns.

Instantaneous amplitude profile is obtained for 8 dB SNR using autocorrelation technique and autocorrelation technique with noise cancellation technique and results are plotted at Figure 4.29 and Figure 4.30 respectively. This confirms that both the techniques are working satisfactorily at 8 dB SNR.

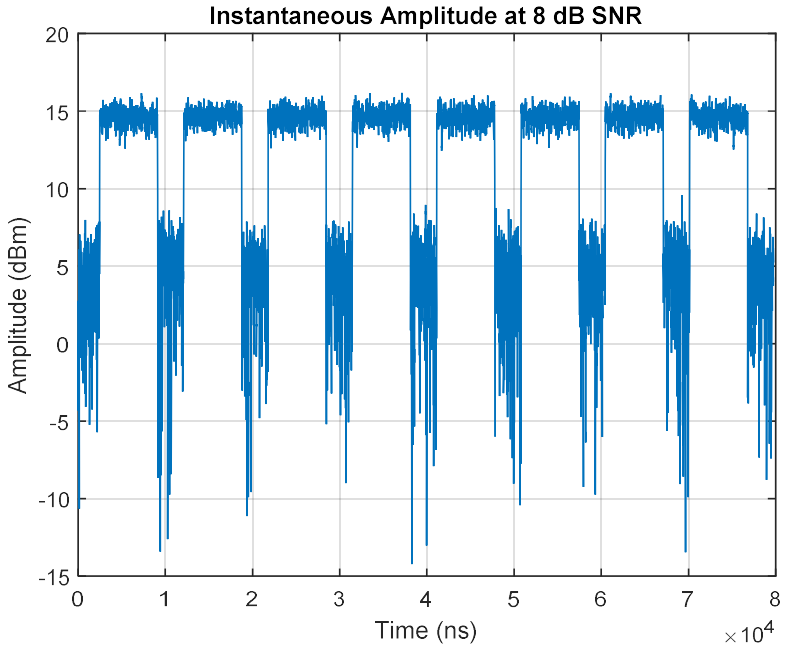

Figure 4.29: Instantaneous amplitude profile using moving autocorrelation technique without noise cancellation for eight pulses. Simulation parameters: f = 1.1 GHz, η = 8 dB, N = 80,000 samples, and t_s = 1.5 ns.

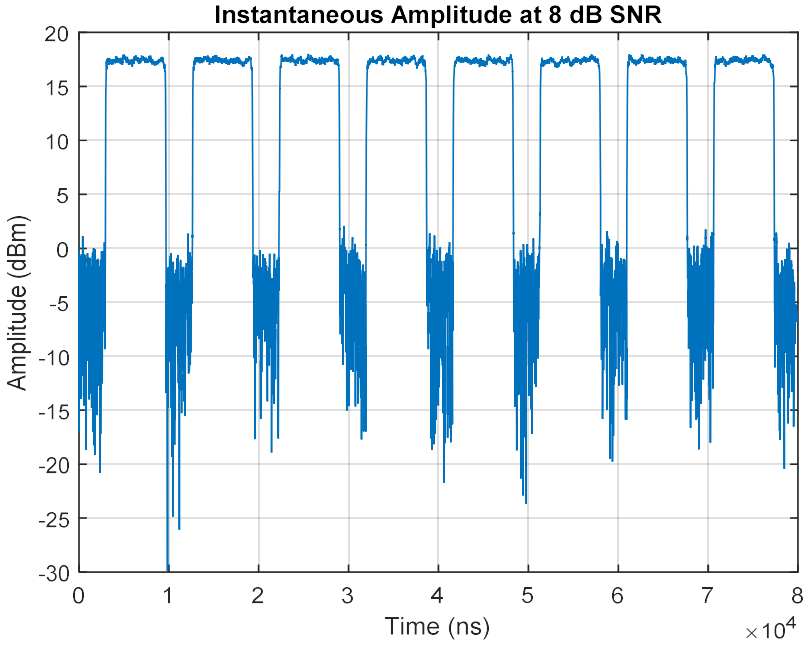

Figure 4.30: Instantaneous amplitude profile using moving autocorrelation technique with noise cancellation for eight pulses. Simulation parameters: f = 1.1 GHz, η = 8 dB, N = 80,000 samples, and t_s = 1.5 ns.

4.3.3.4 Simulation results at 18 dB SNR

The noisy signal is generated at 18 dB SNR and the restored signal is obtained as shown in Figure 4.31 and Figure 4.32 respectively.

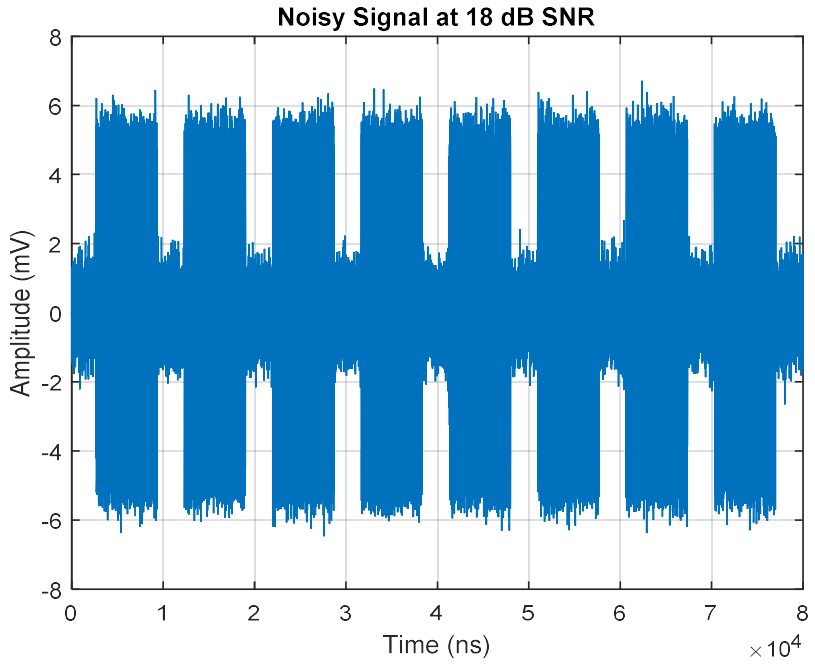

Figure 4.31: Noisy signal (input signal) generated with eight pulses. Simulation parameters: f = 1.1 GHz, η = 18 dB, N = 80,000 samples, and t_s = 1.5 ns.

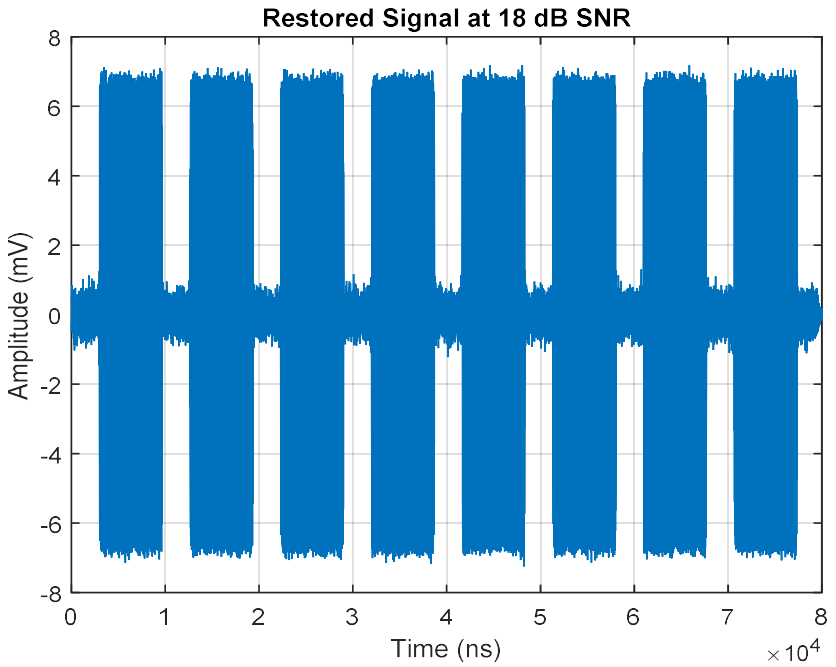

Figure 4.32: Restored signal obtained using noise cancellation for eight pulses. Simulation parameters: f = 1.1 GHz, η = 18 dB, N = 80,000 samples, and t_s = 1.5 ns.

Instantaneous amplitude profile is obtained for 18 dB SNR using DIQ technique and DIQ technique without noise cancellation technique and results are plotted at Figure 4.33 and Figure 4.34 respectively. This confirms that both the techniques are working satisfactorily at 18 dB SNR.

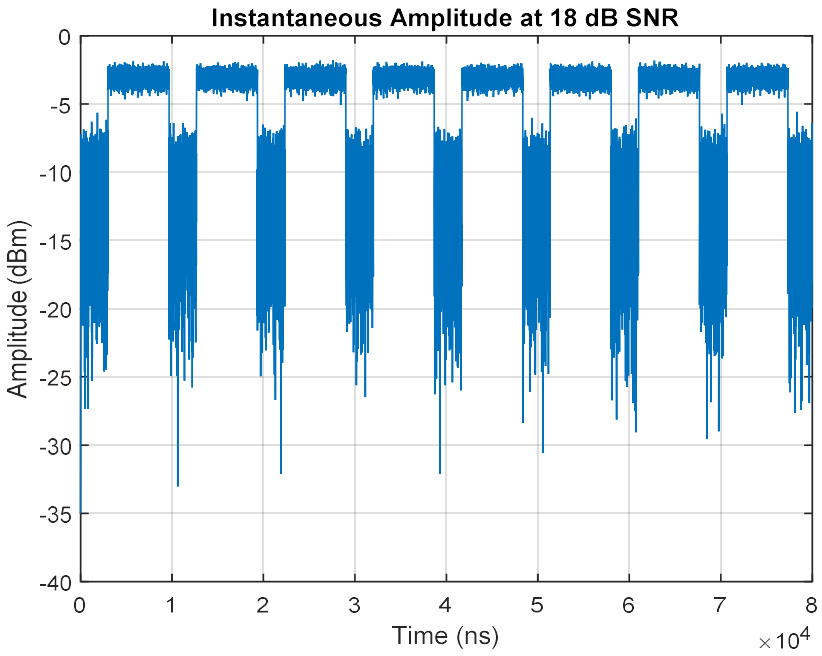

Figure 4.33: Instantaneous amplitude profile using DIQ technique without noise cancellation for eight pulses. Simulation parameters: f = 1.1 GHz, η= 18 dB, N = 80,000 samples, and t_s = 1.5 ns.

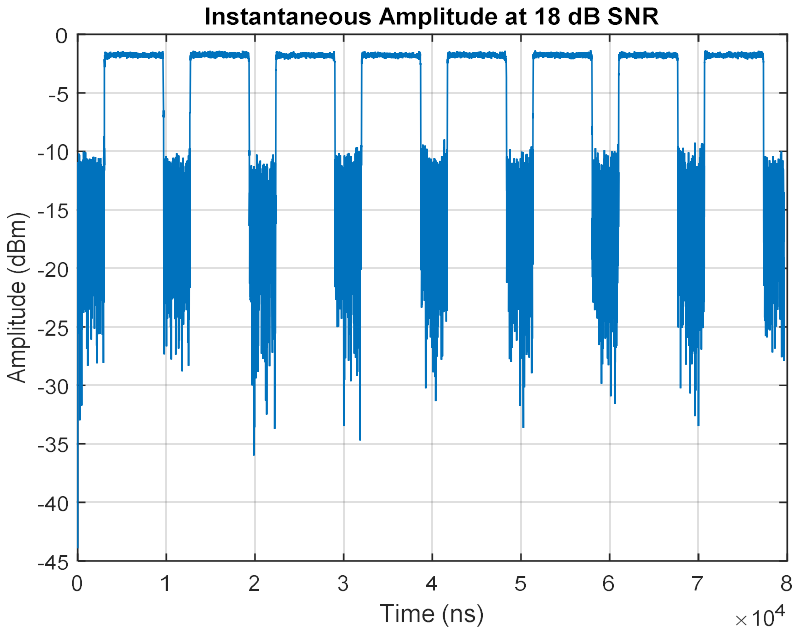

Figure 4.34: Instantaneous amplitude profile using DIQ technique with noise cancellation for eight pulses. Simulation parameters: f = 1.1 GHz, η= 18 dB, N = 80,000 samples, and t_s = 1.5 ns.

Instantaneous amplitude profile is obtained for 18 dB SNR using autocorrelation technique and autocorrelation technique with noise cancellation technique and results are plotted at Figure 4.35 and Figure 4.36 respectively. These figures confirms that both the techniques are working satisfactorily at 18 dB SNR.

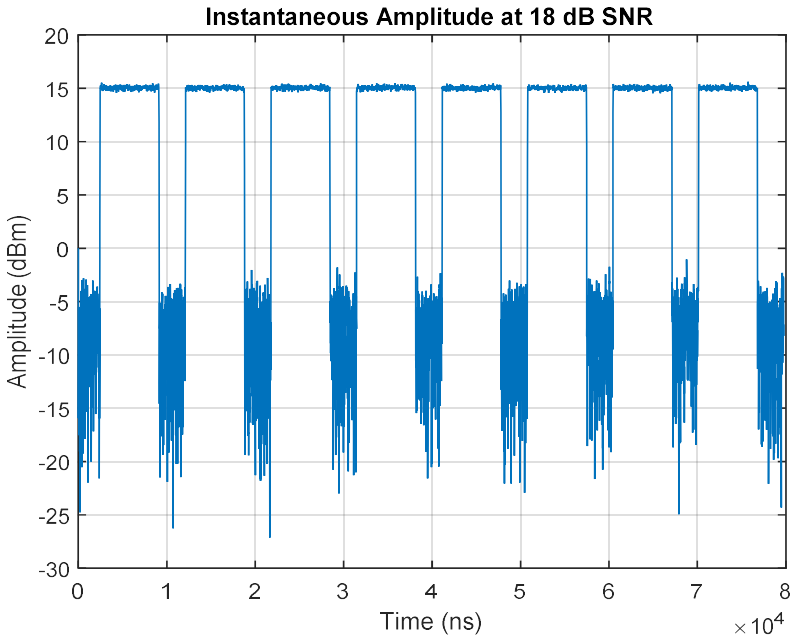

Figure 4.35: Instantaneous amplitude profile using moving autocorrelation technique without noise cancellation for eight pulses. Simulation parameters: f = 1.1 GHz, η = 18 dB, N = 80,000 samples, and t_s = 1.5 ns.

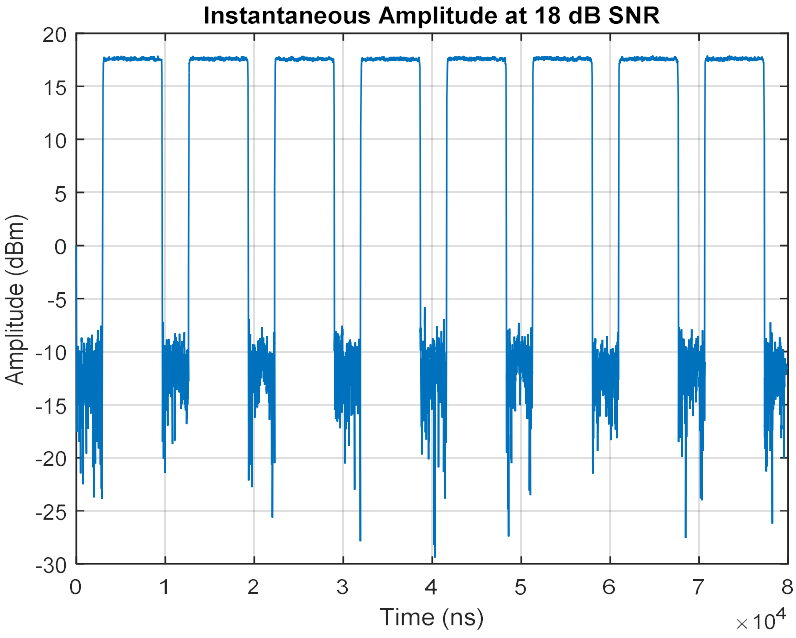

Figure 4.36: Instantaneous amplitude profile using moving autocorrelation technique with noise cancellation for eight pulses. Simulation parameters: f = 1.1 GHz, η = 18 dB, N = 80,000 samples, and t_s = 1.5 ns.

Table 4.1: Amplitude profile generation results suitable for pulse detection for different approaches at various SNR.

Detection Approach	Amplitude Profile Suitable for Correct Detection # SNR(η)											
	-4	-2	0	2	4	6	8	10	12	14	16	18
DIQ without Noise Cancellation	N	N	N	N	N	N	N	N	N	N	N	Y
DIQ with Noise Cancellation	N	N	N	N	N	N	Y	Y	Y	Y	Y	Y
Autocorrelation without Noise Cancellation	N	N	N	N	Y	Y	Y	Y	Y	Y	Y	Y
Autocorrelation with Noise Cancellation	N	Y	Y	Y	Y	Y	Y	Y	Y	Y	Y	Y

The amplitude profile results are summarized in Table 4.1 at various SNR. This shows DIQ technique alone can generate an amplitude profile at 18 dB SNR. When the DIQ technique is used with noise cancellation, it can generate amplitude profile at 8 dB. Similarly, moving autocorrelation technique alone generates an amplitude profile at 4 dB. When this technique is used with noise cancellation, it generates the correct amplitude profile at -2 dB itself. The correct amplitude profile generation means it should have clearance between pulse lowest amplitude and noise highest amplitude which is the requirement for correct detection.

4.3.4 Simulation results of frequency profile generation

Instantaneous frequency profile is generated for the following four different approaches at different SNR conditions. This will show at what value of SNR a particular technique start reporting correct frequency.

(i) DIQ technique without noise cancellation

(ii) DIQ technique with noise cancellation

(iii) Multilevel autocorrelation technique without noise cancellation

(iv) Multilevel autocorrelation technique with noise cancellation

Simulation parameters considered to generate following frequency plots are input frequency (f) = 1.1 GHz, No. of samples (N) = 80,000 samples, and sampling time (t_s) = 1.5 ns. The simulations are carried out for various SNR (η) conditions.

4.3.4.1 Simulation results at -2 dB SNR

Instantaneous frequency profile is computed from the conventional DIQ technique without noise cancellation technique as shown in Figure 4.37. This shows that the frequency plot is broken and it cannot be measured at -2 dB SNR using this technique. Instantaneous frequency profile is computed from the DIQ technique with noise cancellation technique as shown in Figure 4.38. This shows that frequency measurement is not possible at -2 dB SNR using this technique. Frequency variation is very high which is not useful.

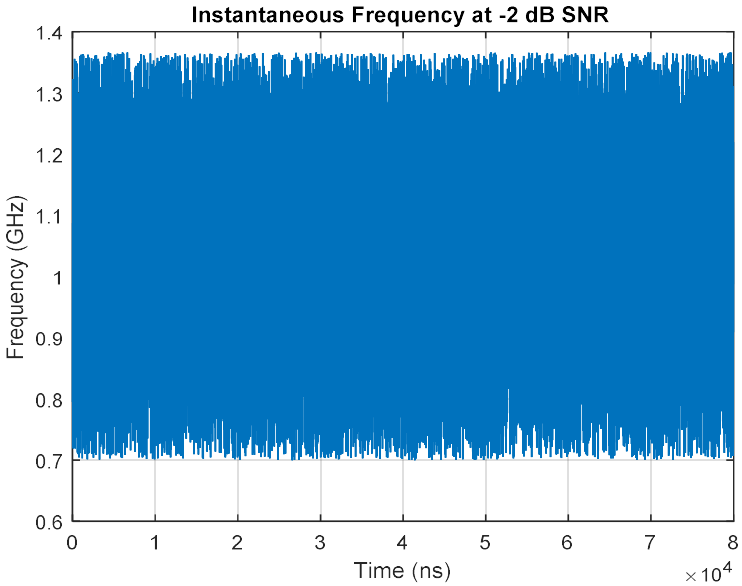

Figure 4.37: Instantaneous frequency profile using DIQ technique without noise cancellation for eight pulses. Simulation parameters: f = 1.1 GHz, η = -2 dB, N = 80,000 samples, and t_s = 1.5 ns.

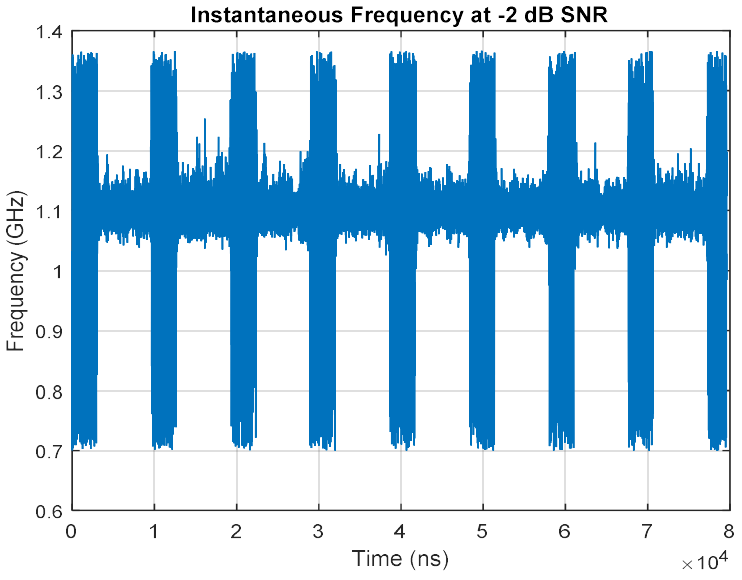

Figure 4.38: Instantaneous frequency profile using DIQ technique with noise cancellation for eight pulses. Simulation parameters: f = 1.1 GHz, η = -2 dB, N = 80,000 samples, and t_s = 1.5 ns.

Instantaneous frequency profile is generated from the multilevel autocorrelation technique without noise cancellation technique as shown in Figure 4.39. This is evident from the figure that frequency measurement is not possible at -2 dB SNR using this technique. Instantaneous frequency profile is generated from the multilevel autocorrelation technique with noise cancellation technique as shown in Figure 4.40. This is evident from the figure that frequency measurement is possible at -2 dB SNR using this technique because there is no break in the frequency. It shows that the correct measurement of frequency for 1.1 GHz input frequency.

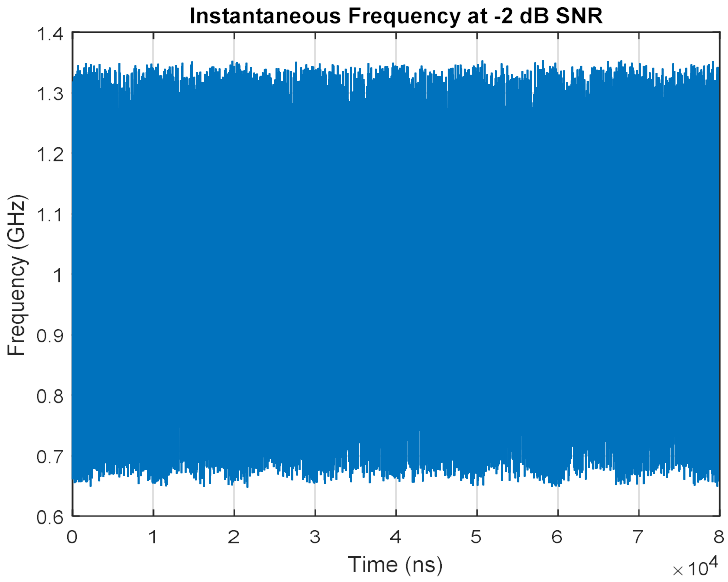

Figure 4.39: Instantaneous frequency profile using moving autocorrelation technique without noise cancellation for eight pulses. Simulation parameters: f = 1.1 GHz, η = -2 dB, N = 80,000 samples, and t_s = 1.5 ns.

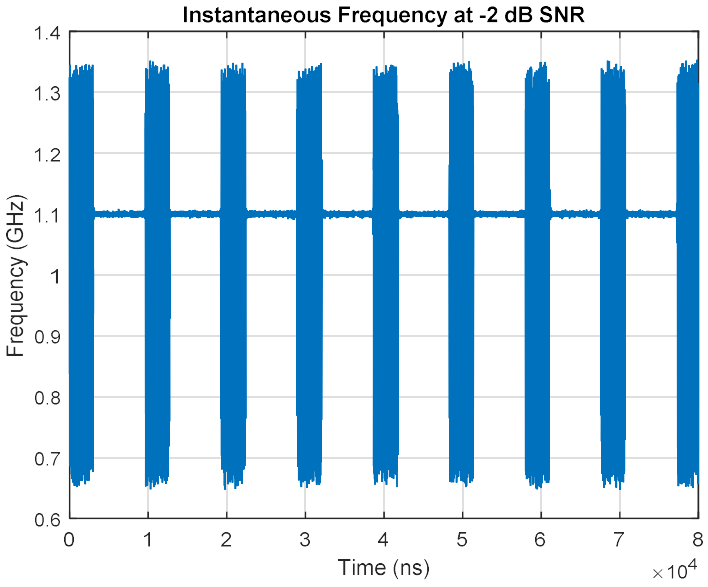

Figure 4.40: Instantaneous frequency profile using moving autocorrelation technique with noise cancellation for eight pulses. Simulation parameters: f = 1.1 GHz, η = -2 dB, N = 80,000 samples, and t_s = 1.5 ns.

4.3.4.2 Simulation results at 4 dB SNR

Instantaneous frequency profile is computed from the conventional DIQ technique without noise cancellation technique as shown in Figure 4.41. This plot shows that frequency is broken and it cannot be measured at 4 dB SNR using this technique. Instantaneous frequency profile is computed from the DIQ technique with noise cancellation technique as shown in Figure 4.42. This plot shows that frequency is measured at 4 dB SNR using this technique. But frequency variation is more which is not useful.

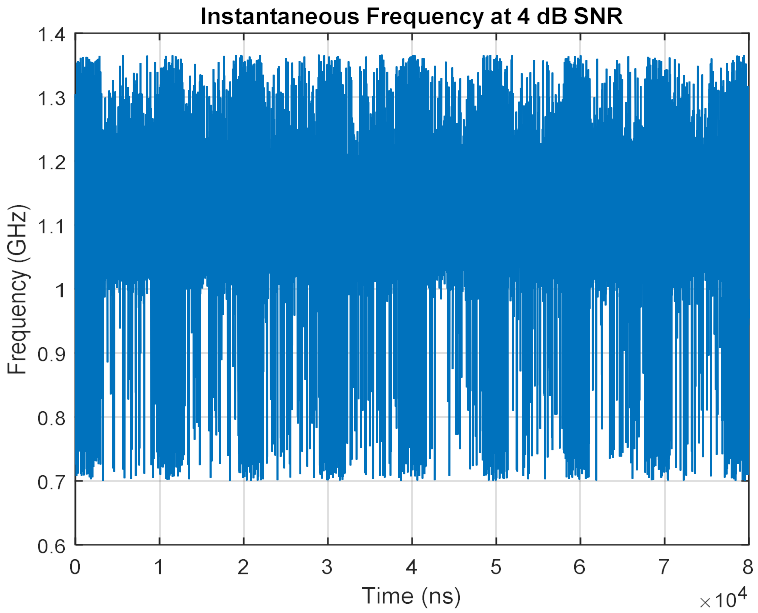

Figure 4.41: Instantaneous frequency profile using DIQ technique without noise cancellation for eight pulses. Simulation parameters: f = 1.1 GHz, η = 4 dB, N = 80,000 samples, and t_s = 1.5 ns.

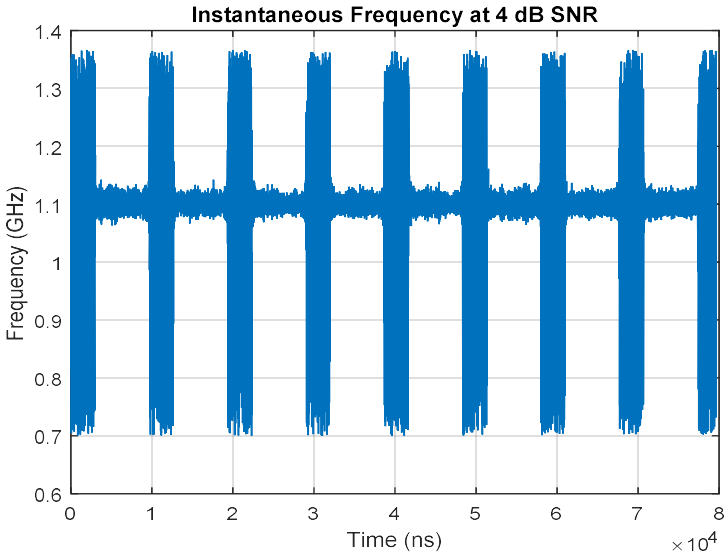

Figure 4.42: Instantaneous frequency profile using DIQ technique with noise cancellation for eight pulses. Simulation parameters: f = 1.1 GHz, η = 4 dB, N = 80,000 samples, and t_s = 1.5 ns.

Instantaneous frequency profile is generated from the multilevel autocorrelation technique without noise cancellation technique as shown in Figure 4.43. This plot shows that frequency is broken and measurement is not possible. Instantaneous frequency profile is generated from the multilevel autocorrelation technique with noise cancellation technique as shown in Figure 4.44. This plot shows frequency measurement is possible at 4 dB SNR using this technique. It shows that the measured frequency is 1.1 GHz against 1.1 GHz input frequency.

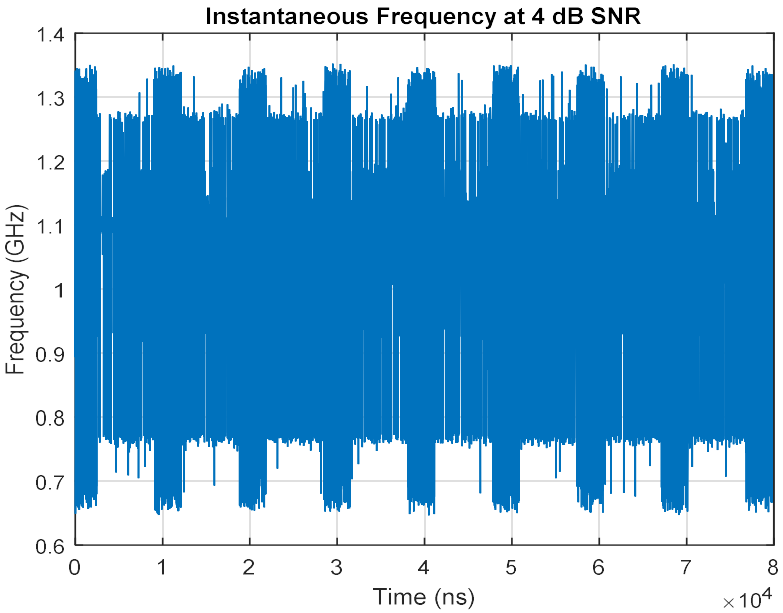

Figure 4.43: Instantaneous frequency profile using moving autocorrelation technique without noise cancellation for eight pulses. Simulation parameters: f = 1.1 GHz, η = 4 dB, N = 80,000 samples, and t_s = 1.5 ns.

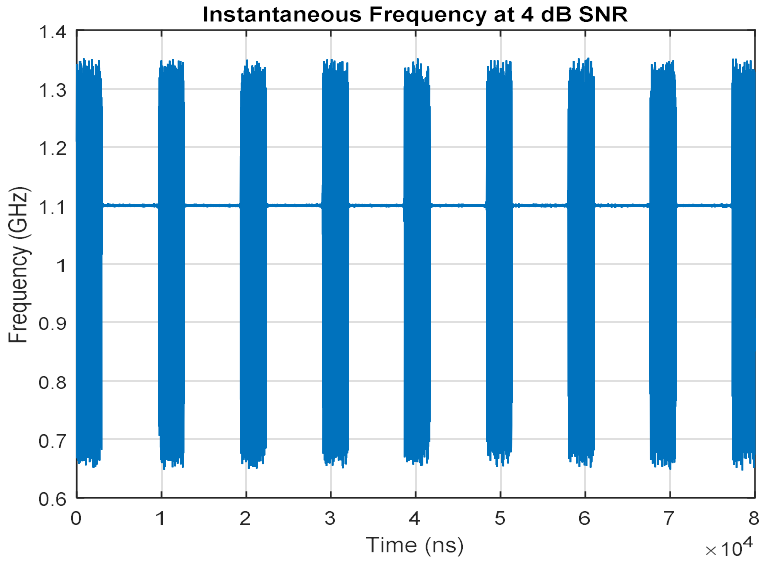

Figure 4.44: Instantaneous frequency profile using moving autocorrelation technique with noise cancellation for eight pulses. Simulation parameters: f = 1.1 GHz, η = 4 dB, N = 80,000 samples, and t_s = 1.5 ns.

4.3.4.3 Simulation results at 10 dB SNR

Instantaneous frequency profile is computed from the conventional DIQ technique without noise cancellation technique as shown in Figure 4.45. This plot shows that frequency is broken and it cannot be measured at 10 dB SNR using this technique. The total frequency variation is about ±100 MHz which is not useful. Instantaneous frequency profile is computed from the DIQ technique with noise cancellation technique as shown in Figure 4.46. This plot show that frequency is measured at 10 dB SNR using this technique.

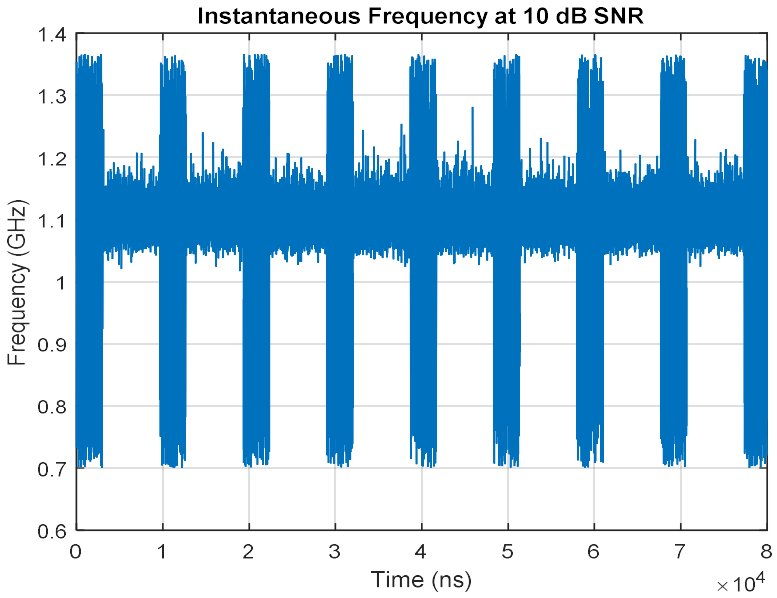

Figure 4.45: Instantaneous frequency profile using DIQ technique without noise cancellation for eight pulses. Simulation parameters: f = 1.1 GHz, η = 10 dB, N = 80,000 samples, and t_s = 1.5 ns.

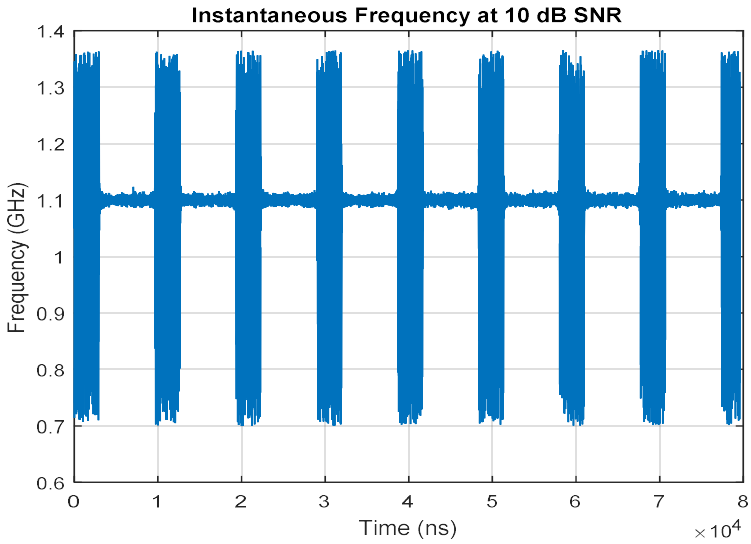

Figure 4.46: Instantaneous frequency profile using DIQ technique with noise cancellation for eight pulses. Simulation parameters: f = 1.1 GHz, η = 10 dB, N = 80,000 samples, and t_s = 1.5 ns.

Instantaneous frequency profile is generated from the multilevel autocorrelation technique without noise cancellation technique as shown in Figure 4.47. Instantaneous frequency profile is generated from the multilevel autocorrelation technique with noise cancellation technique as shown in Figure 4.48. This plot shows frequency measurement is possible at 10 dB SNR using these techniques. It shows that the measured frequency is 1.1 GHz against 1.1 GHz input frequency.

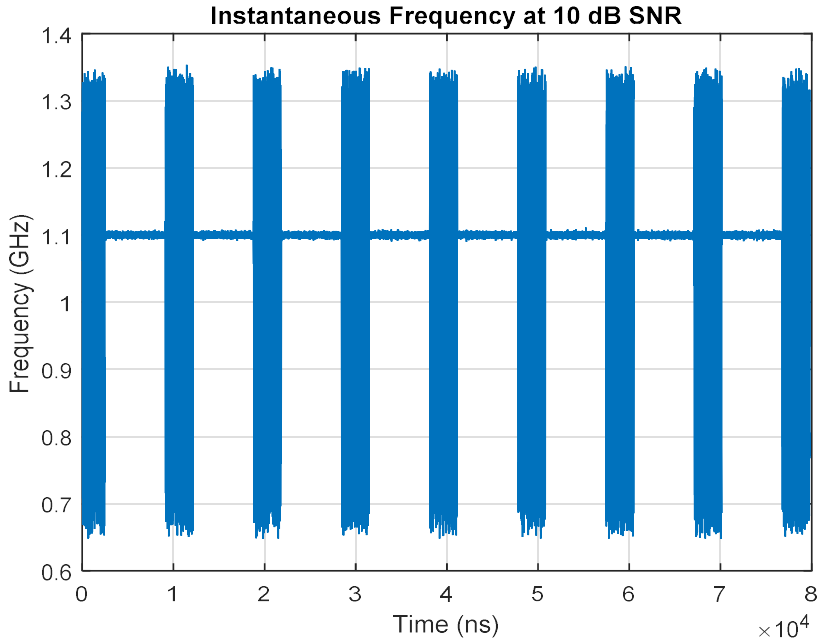

Figure 4.47: Instantaneous frequency profile using moving autocorrelation technique without noise cancellation for eight pulses. Simulation parameters: f = 1.1 GHz, η = 10 dB, N = 80,000 samples, and t_s = 1.5 ns.

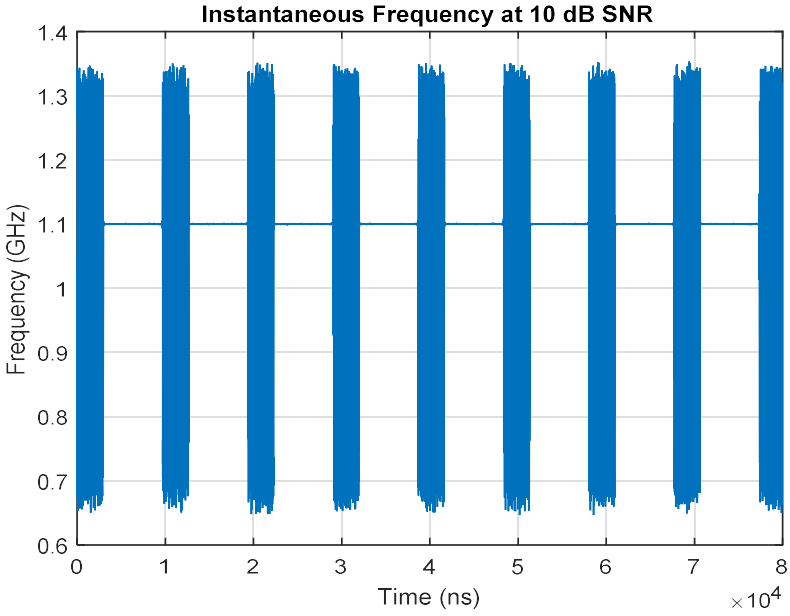

Figure 4.48: Instantaneous frequency profile using moving autocorrelation technique with noise cancellation for eight pulses. Simulation parameters: f = 1.1 GHz, η = 10 dB, N = 80,000 samples, and t_s = 1.5 ns.

4.3.4.4 Simulation results at 18 dB SNR

Instantaneous frequency profile is computed from the conventional DIQ technique without noise cancellation technique as shown in Figure 4.49. Instantaneous frequency profile is computed from the DIQ technique with noise cancellation technique as shown in Figure 4.50. These plots show that frequency is measured correctly at 18 dB SNR using these techniques.

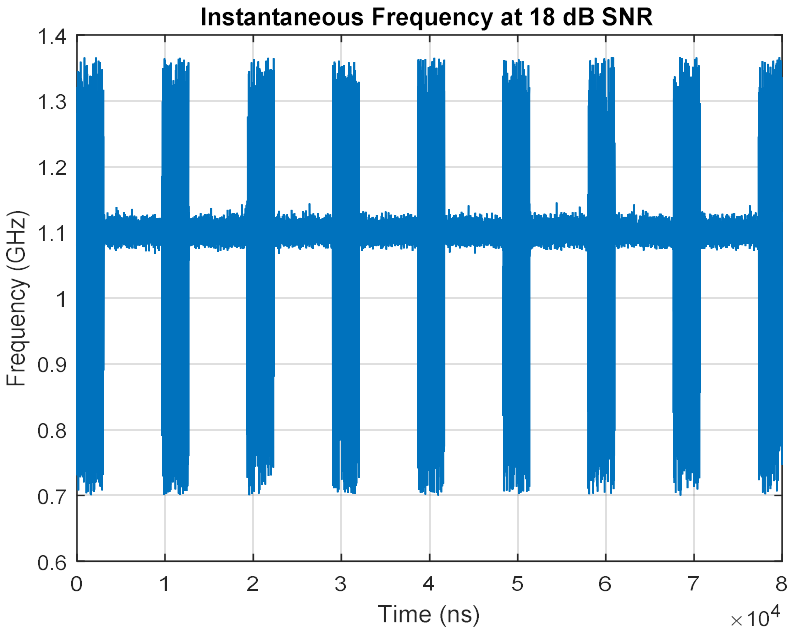

Figure 4.49: Instantaneous frequency profile using DIQ technique without noise cancellation for eight pulses. Simulation parameters: f = 1.1 GHz, η = 18 dB, N = 80,000 samples, and t_s = 1.5 ns.

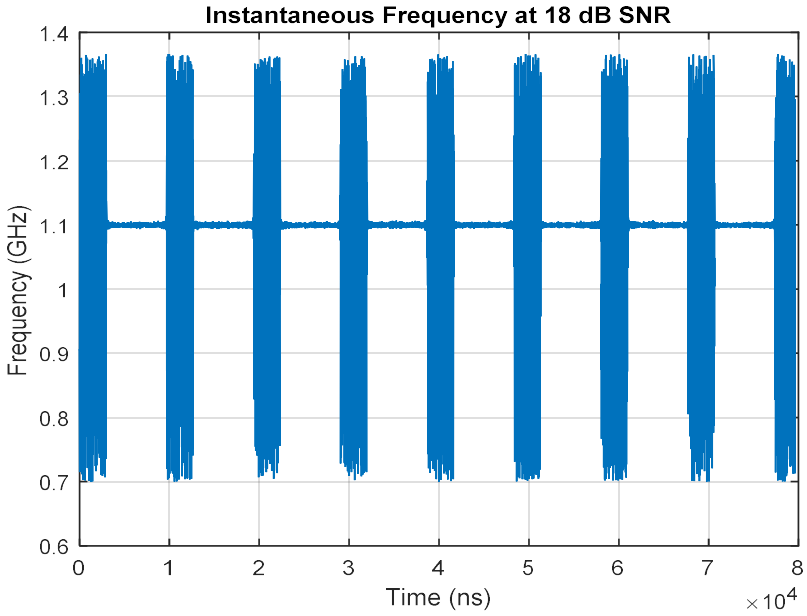

Figure 4.50: Instantaneous frequency profile using DIQ technique with noise cancellation for eight pulses. Simulation parameters: f = 1.1 GHz, η = 18, N = 80,000 samples, and t_s = 1.5 ns.

Instantaneous frequency profile is generated from the multilevel autocorrelation technique without noise cancellation technique as shown in Figure 4.51. Instantaneous frequency profile is generated from the multilevel autocorrelation technique with noise cancellation technique as shown in Figure 4.52. This plot shows frequency measurement is possible at 18 dB SNR using these techniques. It shows that the measured frequency is 1.1 GHz against 1.1 GHz input frequency.

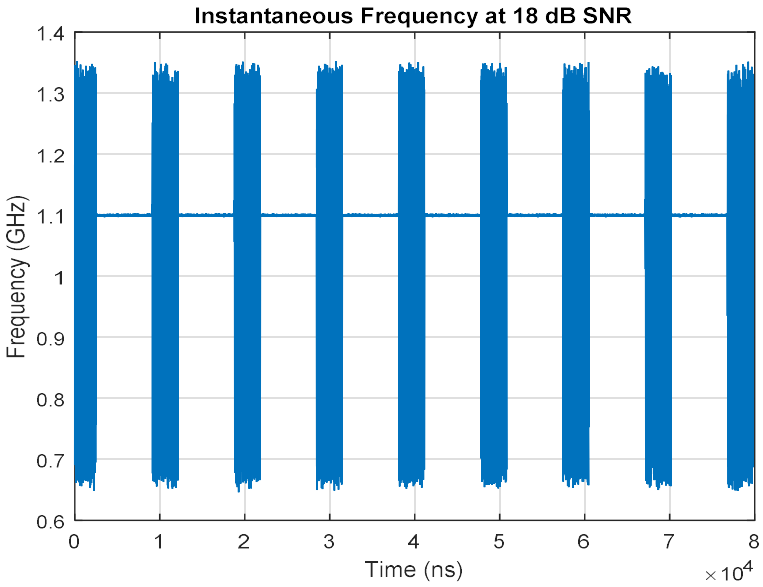

Figure 4.51: Instantaneous frequency profile using moving autocorrelation technique without noise cancellation for eight pulses. Simulation parameters: f = 1.1 GHz, η = 18 dB, N = 80,000 samples, and t_s = 1.5 ns.

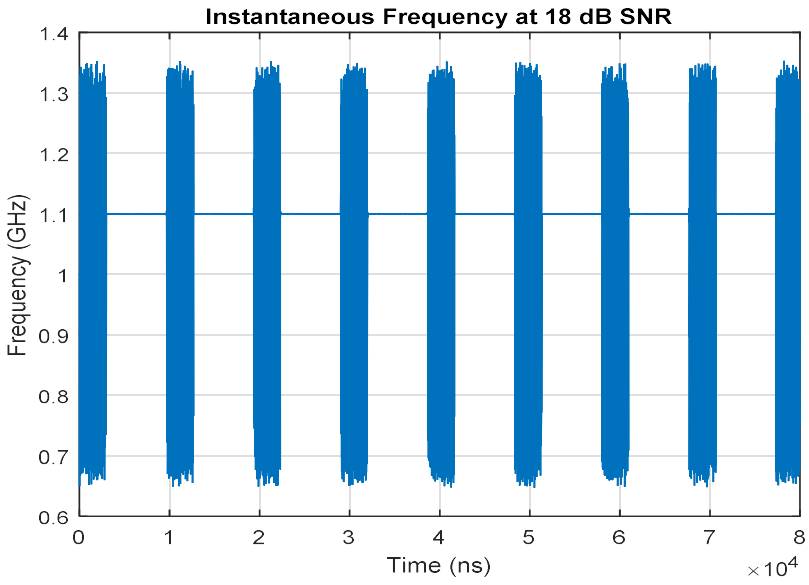

Figure 4.52: Instantaneous frequency profile using moving autocorrelation technique with noise cancellation for eight pulses. Simulation parameters: f = 1.1 GHz, η = 18 dB, N = 80,000 samples, and t_s = 1.5 ns.

The frequency profile results are summarized in Table 4.2 at various SNR. This shows DIQ technique alone can generate the frequency profile upto 18 dB SNR. When the DIQ technique is used with noise cancellation, it is able to generate frequency profile upto 4 dB SNR itself. Similarly, the moving autocorrelation technique alone generates the frequency profile upto 10 dB SNR. When this technique is used with noise cancellation, it generates the correct frequency profile upto -2 dB SNR. The correct frequency profile generation means the mean of frequency should be within 100 kHz within the pulse region.

Table 4.2: Frequency profile generation results suitable for correct reporting for different approaches at various SNR.

Detection Approach	Correct frequency measurement # SNR (η)											
	-4	-2	0	2	4	6	8	10	12	14	16	18
DIQ without Noise Cancellation	N	N	N	N	N	N	N	N	N	N	N	Y
DIQ with Noise Cancellation	N	N	N	N	Y	Y	Y	Y	Y	Y	Y	Y
Autocorrelation without Noise Cancellation	N	N	N	N	N	N	N	Y	Y	Y	Y	Y
Autocorrelation with Noise Cancellation	N	Y	Y	Y	Y	Y	Y	Y	Y	Y	Y	Y

The results from Table 4.1 and Table 4.2 are combined and presented in Table 4.3. This shows the improvement of amplitude and frequency measurement using autocorrelation technique. It shows further improvement, when these techniques are used with noise cancellation technique.

Table 4.3: Amplitude Profile suitable for pulse detection and frequency measurement by different approaches at SNR.

Detection Approach	Correct pulse detection and frequency measurement # SNR (η)												
		-4	-2	0	2	4	6	8	10	12	14	16	18
DIQ without Noise Cancellation	Amplitude	N	N	N	N	N	N	N	N	N	N	N	Y
	Frequency	N	N	N	N	N	N	N	N	N	N	N	Y
DIQ with Noise Cancellation	Amplitude	N	N	N	N	N	N	Y	Y	Y	Y	Y	Y
	Frequency	N	N	N	N	Y	Y	Y	Y	Y	Y	Y	Y
Autocorrelation without Noise Cancellation	Amplitude	N	N	N	N	Y	Y	Y	Y	Y	Y	Y	Y
	Frequency	N	N	N	N	N	N	N	Y	Y	Y	Y	Y
Autocorrelation with Noise Cancellation	Amplitude	N	Y	Y	Y	Y	Y	Y	Y	Y	Y	Y	Y
	Frequency	N	Y	Y	Y	Y	Y	Y	Y	Y	Y	Y	Y

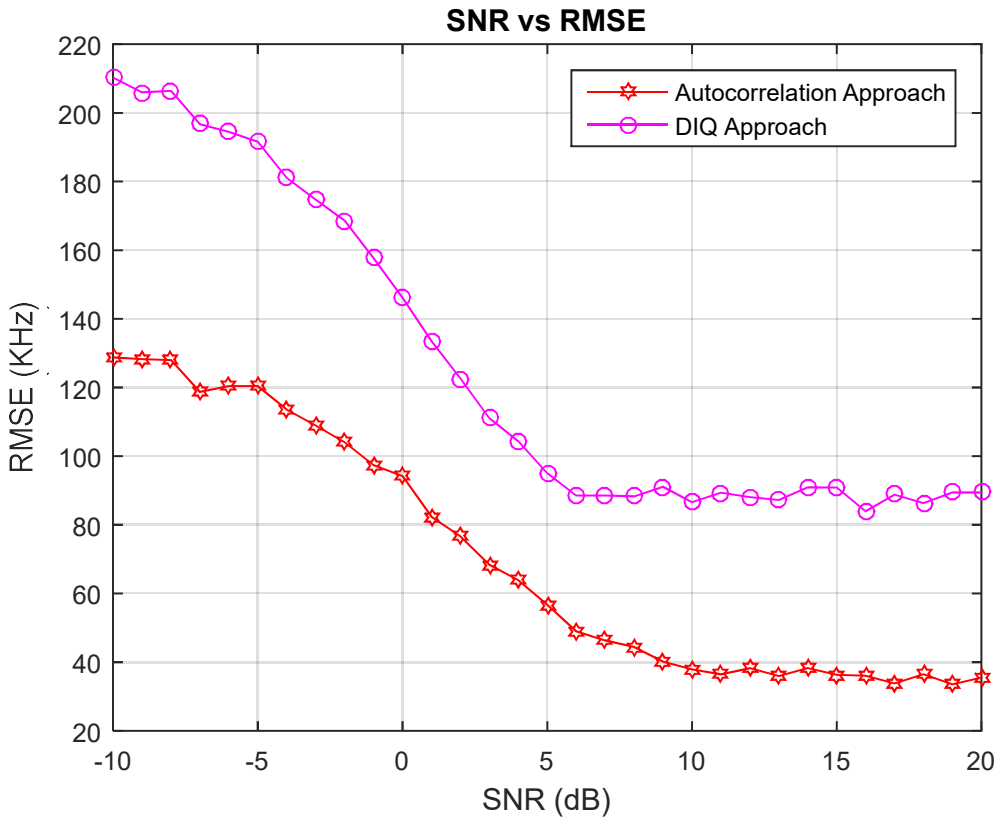

Figure 4.53: Comparison of the RMSE of autocorrelation and DIQ approaches without noise cancellation as a function of SNR. Simulation parameters: f = 1.1 GHz, N = 80,000 samples, and t_s = 1.5 ns.

There is improvement in frequency accuracy with a reduction of SNR requirement at the input in comparison to the DIQ technique as observed through Figure 4.53. This figure is generated without noise cancellation. This shows that the autocorrelation technique is able to process the signal at 10 dB SNR and whereas the DIQ technique fails. The DIQ technique requires an SNR of 18 dB.

Figure 4.54 depicts the frequency accuracy with respect to SNR using both techniques. This figure is generated with noise cancellation. This shows that the autocorrelation technique is able to process the signal at -2 dB SNR and whereas the DIQ technique fails. The DIQ technique requires an SNR of 8 dB.

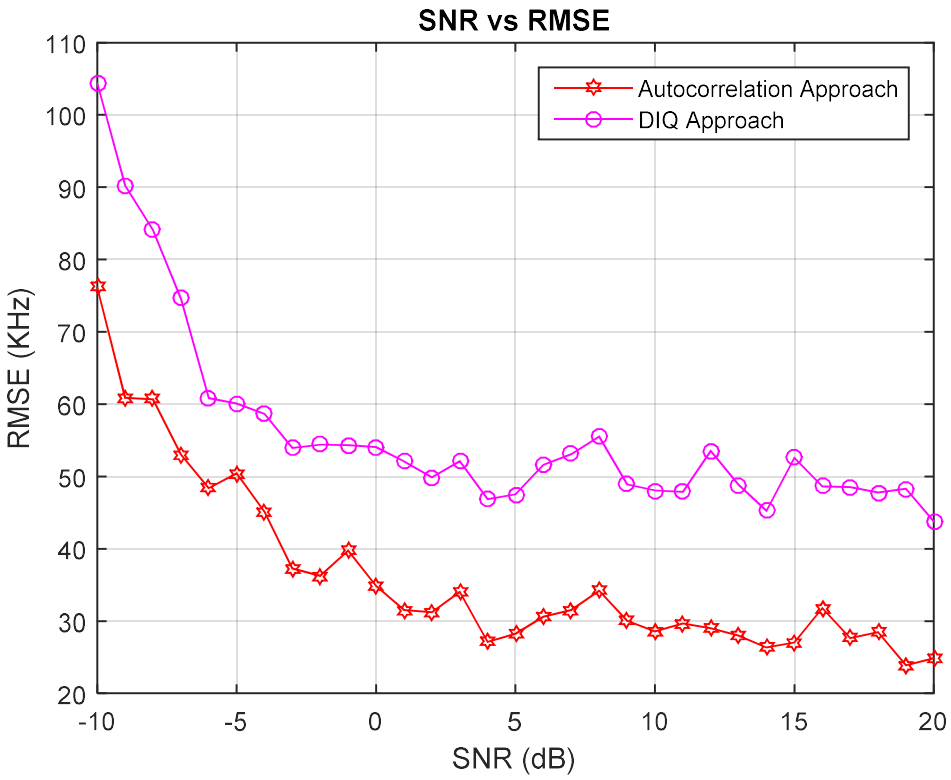

Figure 4.54: Comparison of the RMSE of autocorrelation and DIQ approaches with noise cancellation as a function of SNR. Simulation parameters: f = 1.1 GHz, N = 80,000 samples, and t_s = 1.5 ns.

The field data is also introduced to check the efficacy of the proposed algorithms. Instantaneous amplitude and frequency profiles are depicted in Figure 4.55 and Figure 4.56 using the autocorrelation approach and DIQ approach. These results are generated with the noise cancellation technique. It is evident from instantaneous amplitude and instantaneous frequency profiles generated using autocorrelation approach having better results compared with DIQ approach.

4.3.5 Summary

Amplitude and frequency profiles are generated with autocorrelation technique with noise cancellation technique upto -2 dB SNR. Both autocorrelation and noise cancellation techniques provide SNR advantage as shown in Table 4.3. These techniques are useful for correct signal detection and correct frequency reporting within 100 kHz at -2 dB SNR.

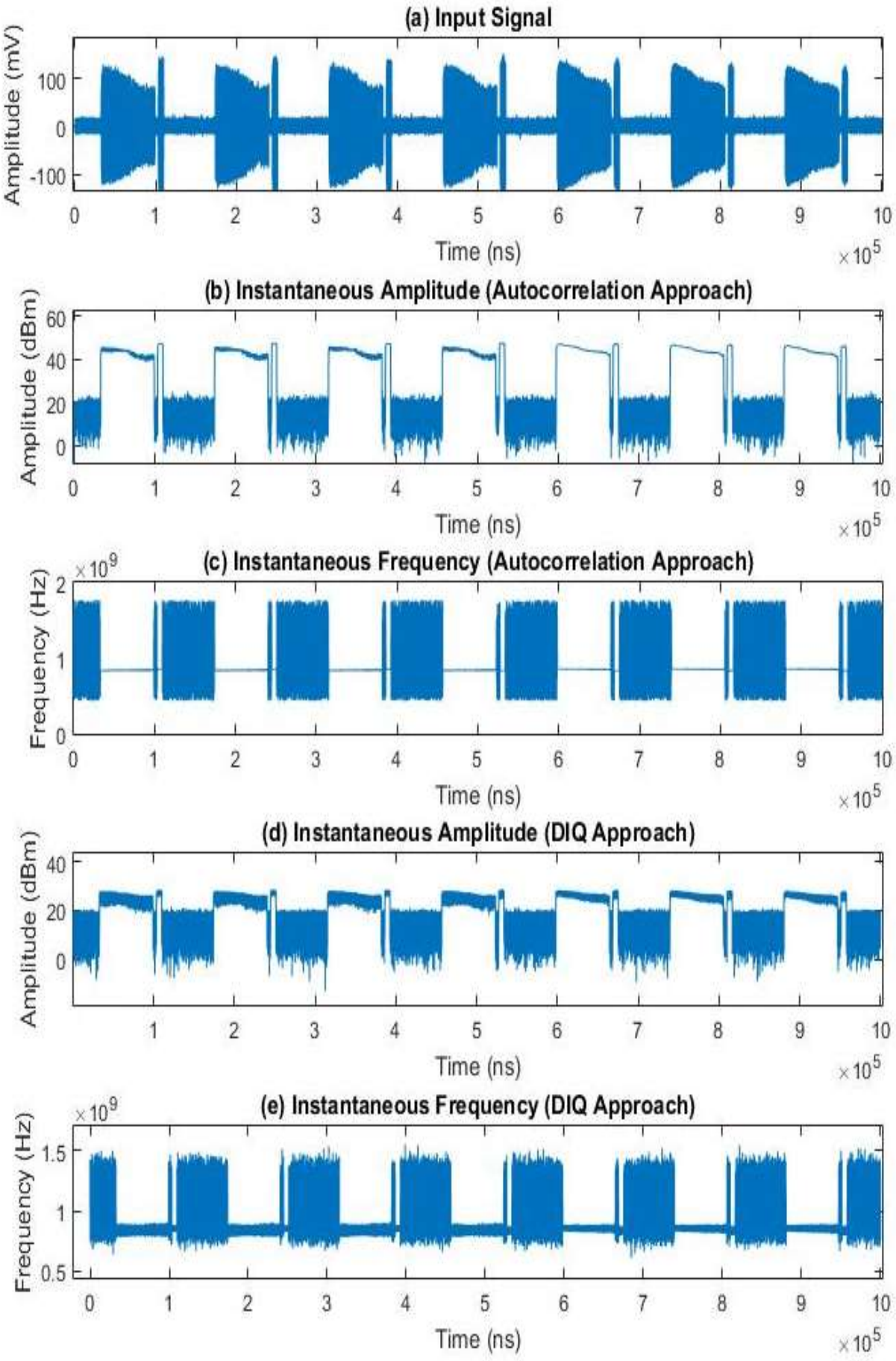

Figure 4.55: Comparison of first field data set result using autocorrelation and DIQ techniques as a function of SNR. Simulation parameters: f = unknown, N = 10,00,000 and t_s = 1.5 ns.

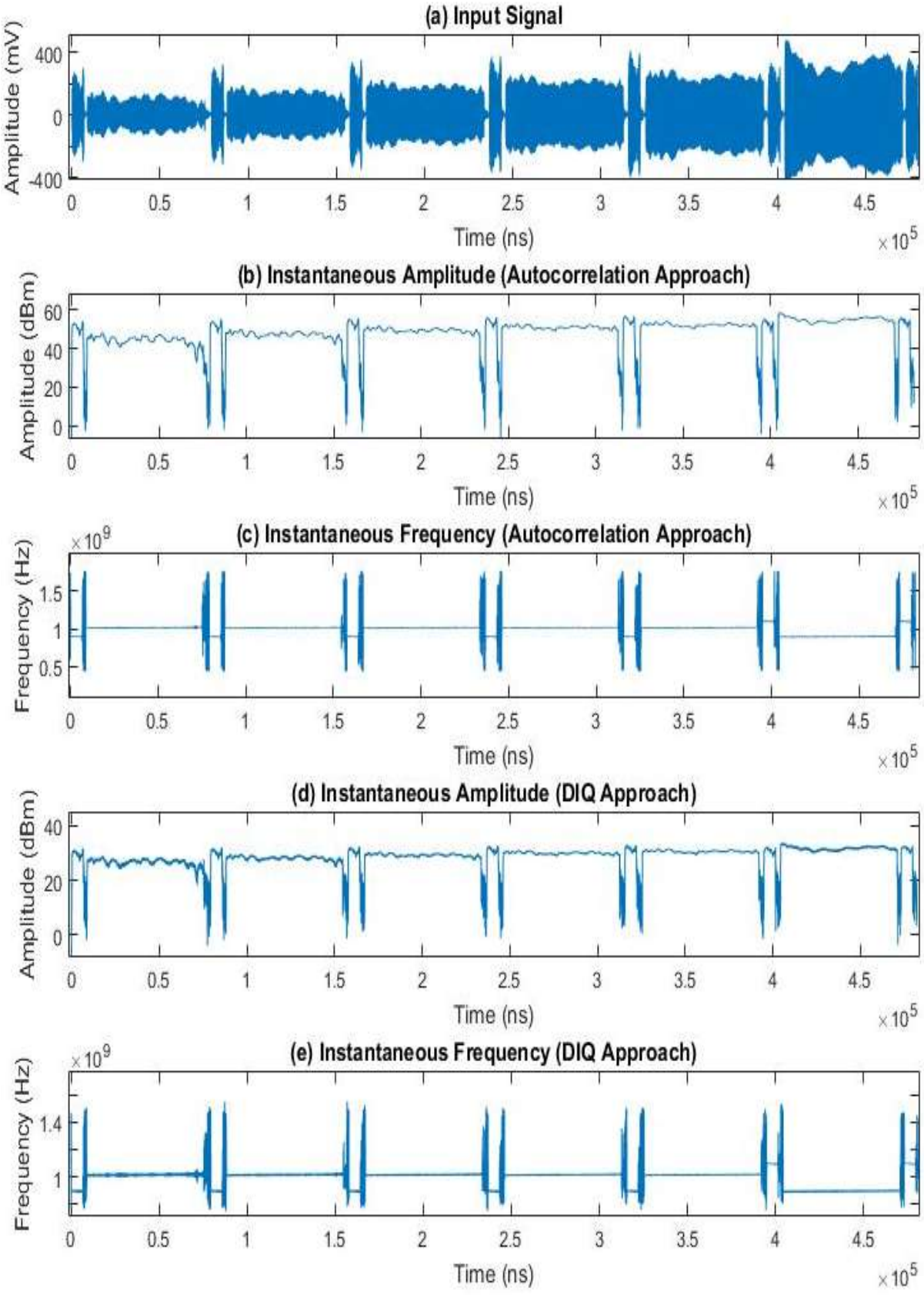

Figure 4.56: Comparison of second field data set result using autocorrelation and DIQ techniques as a function of SNR. Simulation parameters: f = unknown, N = 500,000 and t_s = 1.5 ns.

4.4 Frequency estimation using interpolation

Frequency accuracy can be improved by increasing the FFT number of points. But more FFT number of points requires more multiplications and results in various processing complexities. To avoid this, interpolation is the correct choice to improve the frequency accuracy. This provides the advantage for detecting the radar pulses also.

Discrete spectrum is used to measure the frequency of incoming signal. These measurements are possible after digitizing the IF signal and apply the appropriate windowing operation. Finally compute the spectrum amplitude through FFT analysis. Frequency of the input signal is computed using bin number. This bin number is multiplied by the resolution which depends upon the number of samples considered for FFT computation. Considering higher FFT number of samples is restricted due to computation time and other parameters accuracy. This will restrict the resolution and it affects the frequency accuracy. Curve-fitting or interpolation of inter-bin on FFT output is applied. Both theoretical and practical results are taken and compared. This can be done in real-time as not much hardware resources are required to implement the interpolation.

There are other methods for frequency estimation such as Quinn's methods, Grandke's methods, Gaussian interpolation, parabolic or quadratic interpolation, and many more. So it is required to find out the suitable algorithm which meets the system requirement. In this thesis, a theoretical and experimental work has been carried out and due to its simplicity and accuracy, "Parabolic Interpolation or Quadratic Peak Interpolation" in Fast Fourier Transform (FFT) has been chosen for sinusoidal parameter estimation in communication and non-communication applications.

4.4.1 Interpolation techniques

FFT output is used to implement interpolation technique. The FFT equation is given by

$$S_p = \sum_{n=0}^{N-1} x(n) e^{-j2\pi p \ /N} \tag{4.19}$$

Where p=0,1,2,….,N-1. The limits of p can also be written as -N/2 to N/2. The measured frequency is equivalent to p*f_s/N where the spectrum is having the highest value for that peak p. Figure 4.57 shows the FFT spectrum.

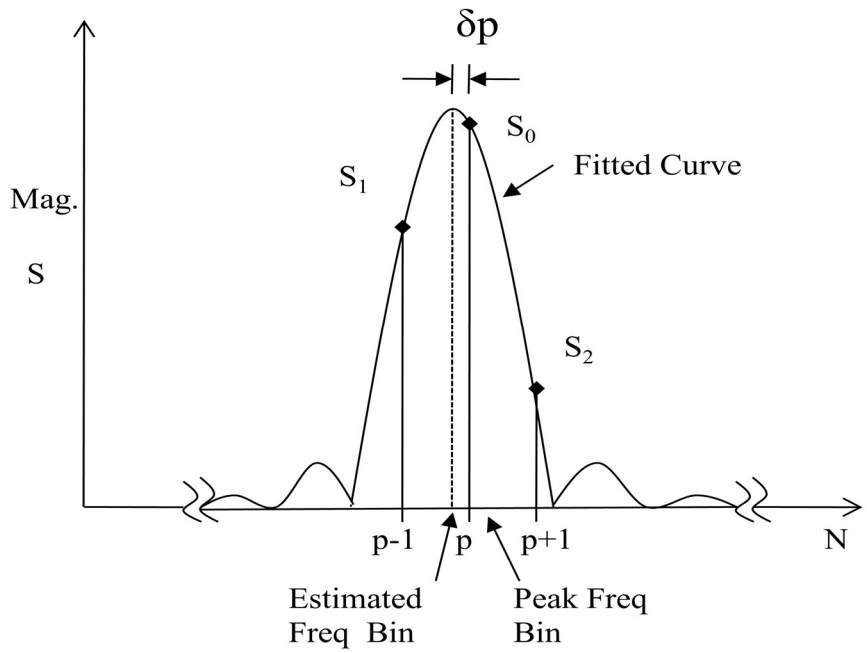

Figure 4.57: FFT spectrum showing three peaks.

The interpolation technique is used to improve the frequency accuracy without increasing the FFT number of points. Different techniques namely Rectangular window-based, Hanning window-based, curve-fitting based, and curve-fitting when FFT is performed with Hanning window are used for this purpose. The frequency is estimated by all four methods. The FFT output spreads across the bins due to the presence of non-coherent signals and white Gaussian noise. Since the input frequency or set frequency is not always the multiple of FFT resolution or least significant bit (LSB) of f_s/N. The spectral component spreads and reported peak frequency will not be the same as the set frequency. Amplitude is extracted from the spectrum at three different bins. The highest-peak (S_0) at bin p, the second highest peak (S_1) at p-1, and the third highest peak (S_2) at p+1 is extracted from the spectrum. The delta bin which is away from the peak by $\pm\delta p$ is computed. The delta bin for the rectangular window is given by [23]

$$\delta p = (S_1 - S_2)/(S_1 + S_2) \tag{4.20}$$

The delta bin for the Hanning window is given by [23]

$$\delta p = (2S_1 - S_0)/(S_0 + S_1) \tag{4.21}$$

These techniques are similar to zero paddings. The windowing methods don't change the shape of the spectrum. But it provides a better estimation of the peak frequency. These

techniques provide an accurate result when only a single frequency is available at the input signal.

When S_0 is very close to the main peak above two techniques are sensitive to noise. Under this situation, S_1 and S_2 are very close to the minima and noise may reverse their amplitudes. The peak will move in the wrong direction using the above equations. When the amplitudes of S_1 and S_2 are reversed then there will be more errors [23].

Curve-fitting is the process of generating a mathematical function which is the best fit to a series of data points. These data points are subjected to constraint. It involves either interpolation, where an exact fit to the data is required, or smoothing, in this the smooth function is constructed that approximately fits the data. Similarly, the delta bin can be written as using the curve fitting technique [32]-[34].

$$\delta p = (S_1 - S_2)/(S_1 - 2S_0 + S_2) \tag{4.22}$$

Finally, the estimated frequency is computed using the delta bin δp as $(p + \delta p)*f_s/\mathrm{N}$. Hanning window is applied on IF data and FFT are performed. The curve-fitting technique is applied to the FFT output to get the delta bin δp from equation 4.22. The modified interpolation technique block diagram is shown in Figure 4.58.

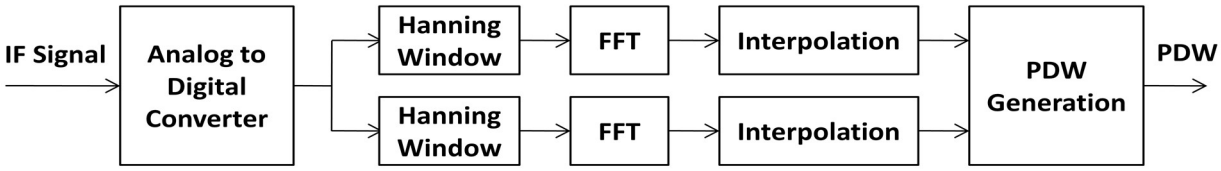

Figure 4.58: Block diagram of modified interpolation technique.

The application of interpolation technique is for real-time systems also. The steps to be followed for interpolation to estimate the frequency is given below:

1) Carry out coarse estimate of the input signal frequency by locating the maximizer of the FFT output magnitude.

2) Isolate the FFT outputs local to the bin determined in step 1.

3) To increase the frequency resolution and magnate estimate on isolated samples apply algorithm.

It is important to observe that decisive success depends on the ability of step (1) to provide the correct FFT output bin number. It is important to consider the limitations of the FFT algorithm itself for this reason.

4.4.2 Simulation results of interpolation

The input signal is generated for the band of input frequencies. The set frequencies are varied from 1100 MHz to 1120 MHz with the step of 0.5 MHz to check the accuracy of algorithms. Figure 4.59 shows the estimated frequency using a Rectangular window, Hanning window, Curve fitting, Curve fitting with Hanning window estimation techniques. All the results are generated using 256 points FFT and compared with set frequency. The result of interpolation techniques is compared with FFT measured frequency alone. Figure 4.60 shows the root mean square error (RMSE) using all frequency estimation techniques versus set frequency.

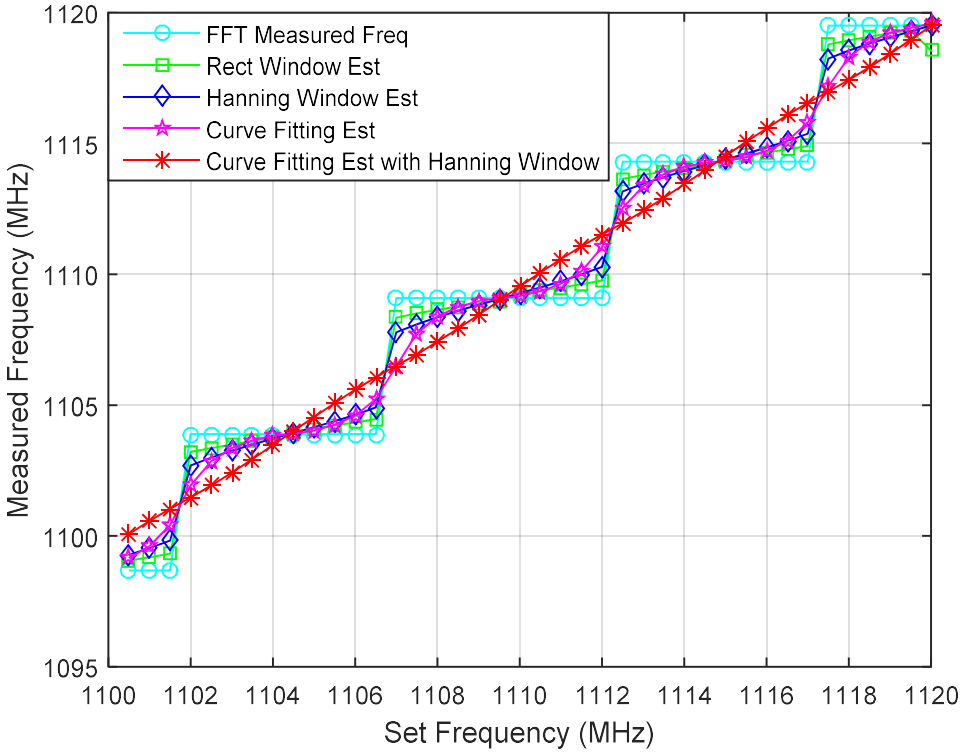

Figure 4.59: Plot of measured frequency versus set frequency using FFT technique, Rectangular window, Hanning window interpolation technique, curve-fitting interpolation technique, and curve-fitting interpolation technique with Hanning window respectively. Simulation parameters: f = 1100 to 1120 MHz, FFT Points = 256, Δf = 0.5 MHz, and t_s = 0.75 ns.

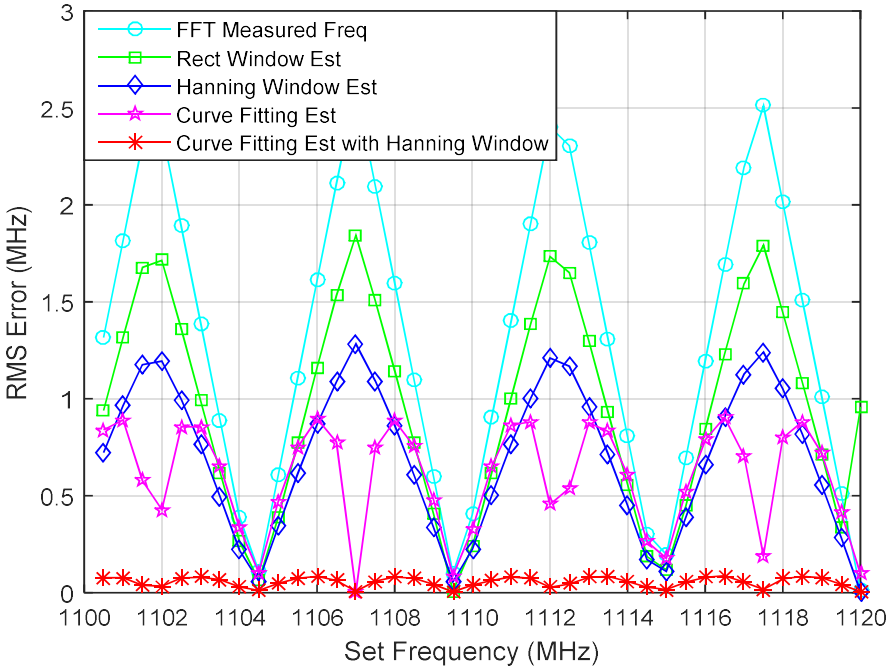

Figure 4.60: RMS Error versus set frequency using FFT technique, Rectangular window, Hanning window interpolation technique, curve-fitting interpolation technique, and curve-fitting interpolation technique with Hanning window respectively. Simulation parameters: f = 1100 to 1120 MHz, FFT Points = 256, $\Delta f = 0.5$ MHz, and $t_s = 0.75$ ns.

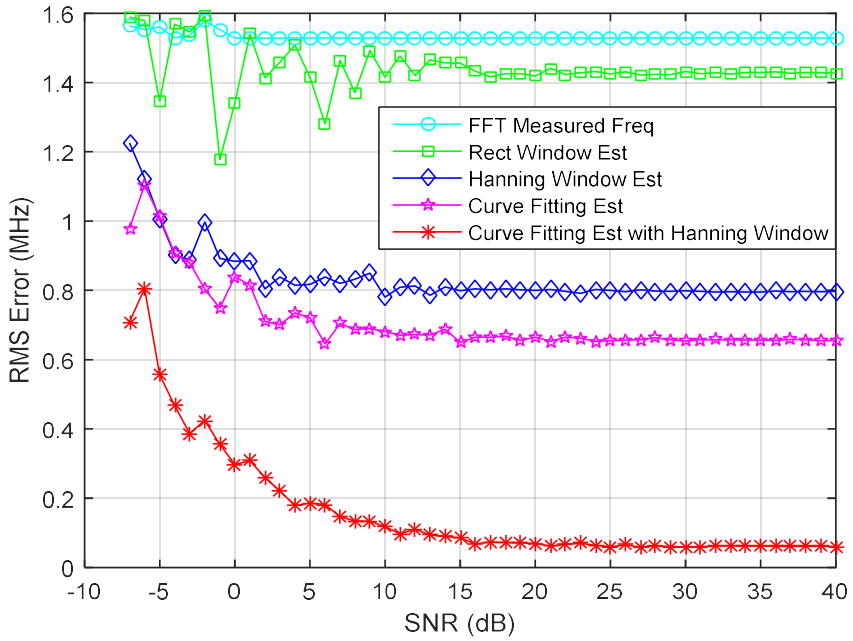

Figure 4.61: Plot of RMS Error versus SNR using FFT technique, Rectangular window, Hanning window interpolation technique, curve-fitting interpolation technique, and curve-fitting interpolation technique with Hanning window respectively. Simulation parameters: f = 1100 to 1120 MHz, FFT Points = 256, $\Delta f = 0.5$ MHz, and $t_s = 0.75$ ns.

The simulation is carried out at different SNRs varying from -2 to 40 dB. Figure 4.61 shows the RMSE versus SNR using all frequency estimation techniques versus set frequency.

Table 4.4: RMSE of estimated frequency for interpolation techniques.

Interpolation Technique	RMSE (MHz) # N Point FFT				
	256	512	1024	2048	4096
FFT Measured Frequency	1.5280	0.7566	0.3702	0.1843	0.0916
Rectangular Window	1.0954	0.5742	0.2929	0.1503	0.0765
Hanning Window	0.7969	0.4584	0.2467	0.1308	0.0681
Curve Fitting Technique (CFT)	0.6561	0.3169	0.1573	0.0787	0.0402
CFT with Hanning window	0.0609	0.0297	0.0148	0.0074	0.0038

Table 4.5: Peak Error of estimated frequency for interpolation techniques.

Interpolation Technique	Peak Error (MHz) # N Point FFT				
	256	512	1024	2048	4096
FFT Measured Frequency	2.5977	1.2988	0.6094	0.3076	0.1567
Rectangular Window	1.8745	0.9872	0.4832	0.2512	0.1309
Hanning Window	1.2722	0.7577	0.3982	0.2149	0.1148
Curve Fitting Technique (CFT)	0.9051	0.4423	0.2197	0.1093	0.0545
CFT with Hanning window	0.0820	0.0418	0.0209	0.0104	0.0052

Based on the frequency accuracy error computed using different interpolation techniques the RMSE and peak error are calculated and tabulated as Table 4.4 and Table 4.5 respectively. It is found from the result that RMSE calculated from measured frequency using 256 points FFT is 1.528 MHz. In the case of the rectangular window interpolation technique, Hanning window interpolation technique, Curve fitting interpolation technique, and Curve fitting interpolation technique with Hanning window the RSME is 1.0954 MHz, 0.7969 MHz, 0.6561 MHz, and 0.0609 MHz respectively. The RMSE is lowest in the case of the curve fitting interpolation technique with the Hanning window. The peak error is also the lowest of

0.0820 MHz in the case of the curve-fitting interpolation technique with the Hanning window. This performs equivalent to multiple times the number of points FFT results without interpolation.

4.4.3 Summary

Discrete spectra can be used to measure frequencies of sinusoidal signal components Such a measurement consists in digitizing a compound signal, performing windowing of the signal samples, and computing their discrete magnitude spectrum, usually utilizing the Fast Fourier Transform algorithm. Frequencies of individual components can be evaluated from their locations in the discrete spectrum with a resolution depending on the number of samples. Computational or other limitations often restrict the number of samples which may be processed, which correspondingly restricts the resolution of the estimate provided by the FFT.

If the actual frequency of a signal does not fall on the centre frequency of an FFT bin several bins near the actual frequency will appear to have a signal component. In that case, use the magnitudes of the nearby bins to determine the actual signal frequency. There are different frequency estimation algorithms from which few are discussed already. Other algorithms are also there and their formulas are written below.

4.5 Direction finding

AOA measurement is carried out using three-antenna based BLI direction-finding techniques. This technique is SWaP optimized as reduction of size, weight, and power compared to four antenna based BLI. There is one advantage of interferometry that it measures the phase accurately using digital hardware even at a reasonable sampling rate. Therefore DOA with high accuracy can be obtained with shorter baselines and without the challenging timing constraints. These interferometers achieve fraction of degree accuracies. Further, preprocessing is used with interferometers and accurately estimates the AOA of multiple signals.

4.5.1 Virtual baseline interferometer using 3 antennas based array

The linear combinations of antennas forms the baseline. Minimum two antennas are sufficient to form the baseline. Two antennas baseline does not provide the sufficient phase measurement accuracy. That is the reason, BLI is used with more than two antennas. Due to the advancement of high density and high speed devices BLI processing capabilities can be

implemented in hardware. Digital interferometers are frequently used in the in the ES and ELINT systems.

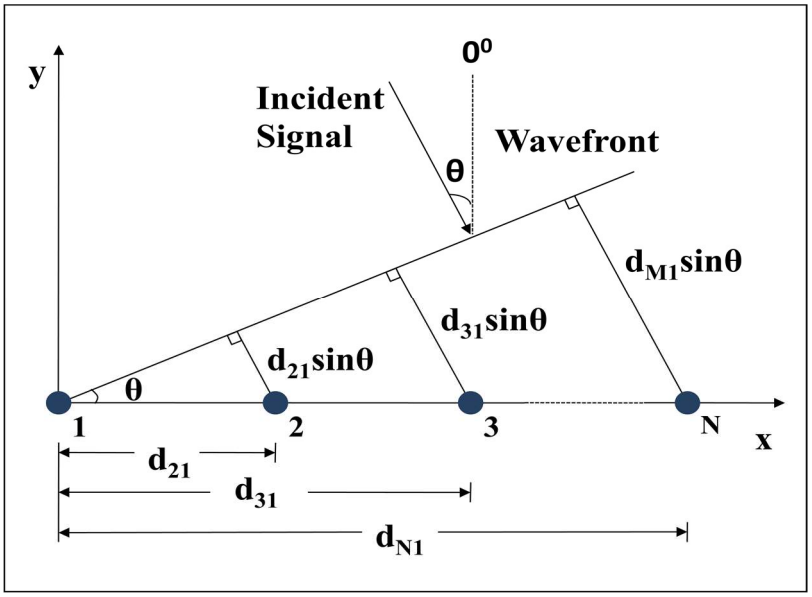

Figure 4.62: Linear array separation of antenna versus propagation phase delay of the incident signal.

In Figure 4.62, a linear array of antennas has been depicted. Since ELINT receivers are used to provide early warning to the presence of emitters, the ELINT receiver usually opted at large distances from the emitter. The radar signal arriving at the ELINT receiver antenna array can therefore be reasonably approximated as a uniform plane wave. Here 1, 2, 3 …, N are the antennas, θ is the intercept angle and d_{N1} are distances between antennas. The DOA of the signal is estimated as below, by estimating the frequency and phase delay of signal between the two antennas outputs.

$$\theta = Sin^{-1}\left(\frac{\lambda\Psi}{2\pi}\right) \tag{4.23}$$

Where wavelength $\lambda = c/f$. The baseline of the interferometer is often referred to as antenna separation 'd'. The accuracy of DOA estimate can be improved by one of the factors such as

- Increasing the SNR of the signal,
- Increasing the signal duration i.e. number of samples,
- Increasing the signal frequency,
- Operating closer to broadside, and
- Increasing the antenna separation.

Since the parameters of the radar are beyond the control of the ELINT receiver, the first three parameters can be changed. Some improvement in DOA estimate accuracy can be gained by actively rotating the interferometer baseline to operate closer to the broadside region. For moving platforms, this can be achieved by changing the trajectory of the platform, while for stationary platforms, this can be achieved by using multiple, short baseline interferometers with different orientations and appropriate switching between the baselines on an intercept-by-intercept basis. However, these methods will only provide a small improvement in the DOA estimation performance and may be impractical to achieve. The most practical method to improve the DOA estimation performance is to utilize long baseline interferometers. While long baseline interferometers offer improved DOA estimation performance, they also introduce an ambiguity issue because the phase delays can only be measured between $[-\pi,\pi]$. This leads to ambiguities as the theoretical phase delay can exceed ±π. This effect is known as phase wrapping. The ambiguity resolution using other independent, non-interferometric DOA estimation methods is generally imposing additional constraints on the design of the direction-finding systems. Also, the accuracy of these algorithms is not being sufficient to resolve the ambiguities of the long baseline interferometers at higher frequencies. The ambiguity resolution using a short baseline interferometer requires that at least one pair of antennas be spaced no more than one half a wavelength apart (at the highest frequency of separation). In practice, these design constraints may not be achievable due to the size of the antenna or mounting characteristics of the platform.

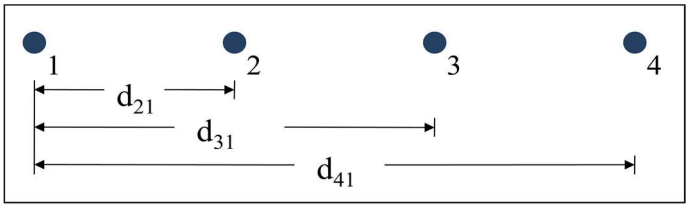

Figure 4.63: Plot of a simple set of interferometer baselines comprising of 4 antennas

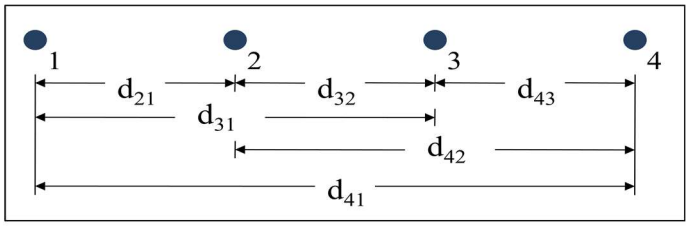

Figure 4.64: Plot of an extended set of interferometer baselines comprising of 4 antennas

Alternative ambiguity resolution methods which make use of multiple long baseline interferometers are based on the Chinese Remainder Theorem (CRT) and require appropriately chosen interferometer baselines. For larger aperture, unambiguous DOA estimates can generally be obtained with fewer intermediate baselines than the short baseline ambiguity resolution method. Figure 4.63 describes a simple set of interferometer baselines comprising 4 antennas whereas Figure 4.64 describes an extended set of interferometer baselines comprising of 4 antennas. The longest baseline d_{41} provide the best DOA estimation.

In order to increase the DOA accuracy further the number of baselines required to be increased and also to process the such number of antenna either more number of switching to be done which decrease the Probability of Intercept (POI) of radar signal or it is required to do the parallel processing that will increase the system hardware, system power. Also, there is space constraint for the space system; it is difficult to increase the number of antennas. For Space ELINT system, instead of increasing the number of antennas, there is a demand to decrease it. So that further SWaP can be reduced for better reliability and better durability. So there is system configuration analysis where 4 antennas configuration has been replaced by 3 antennas system which can provide the same DOA estimation with certain constraints such as the decrease in FOV and little more prone to phase error than earlier configuration.

The first constraint can be possible to resolve by changing the trajectory of the vehicle during the predefined mission. Whereas the later can be resolved by choosing the good hardware component which should be reliable for a particular phase margin of the algorithm so that it could not give wrong DOA estimates.

Based on the above constraint, there is an alternative interferometric algorithm Virtual Baseline Interferometer (VBI) which is based on a second-order difference array. This VBI is computationally as fast as a conventional interferometer and also provides unambiguous DOA estimation using two long baselines.

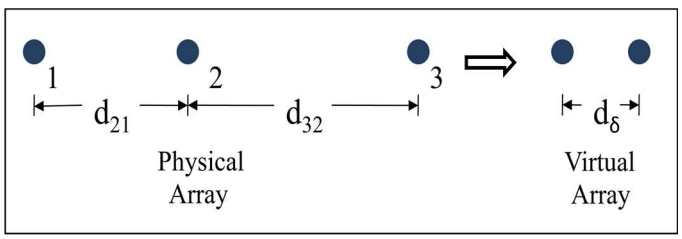

Figure 4.65: Plot of virtual baseline interferometer comprising of 3 antennas

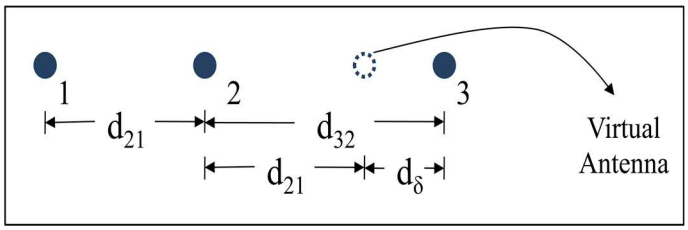

Figure 4.66: Plot of physical interpretation of virtual baseline interferometer

Figure 4.65 describes the concept of a virtual baseline interferometer, where only 3 antennas are required. The unambiguous first-order phase delays for d_{21}, and d_{32} baselines i.e. ψ_{21} and ψ_{32} respectively are derived as below using equation 4.23,

$$\psi_{21} = \left(\frac{2\pi d_{21}}{\lambda}\right) sin\theta \tag{4.24}$$

$$\psi_{32} = \left(\frac{2\pi d_{32}}{\lambda}\right) sin\theta \tag{4.25}$$

Where it is assumed that $d_{21} < d_{32}$, $(\lambda_{\min}/2) << d21$ and $\lambda_{\min}$ corresponds to the wavelength of the highest frequency of interest. The long baselines suggest that the phase delays are highly ambiguous. The second-order phase delay ψ_δ can be calculated as the difference between the first-order delays as follows using equations 4.24 and 4.25,

$$\psi_\delta = \psi_{32} - \psi_{21} = \frac{2\pi(d_{32}-d_{21})}{\lambda} sin\theta = \frac{2\pi d_\delta}{\lambda} sin\theta \tag{4.26}$$

Where $d_\delta = d_{32} - d_{21}$ and this is equivalent to the creation of an antenna virtual pair with a baseline of d_δ as depicted in Figure 4.66.

This virtual baseline phase delay can be unambiguous provided that the baseline is sufficiently short. It means, that it satisfied the following constraint, $0 < d_\delta \leq (\frac{\lambda_{\min}}{2})$ where $\lambda_{\min}$ is the wavelength of the highest frequency of interest. The unambiguous estimate of DOA of the signal using the basic interferometer equation is written as

$$\theta = Sin^{-1}\left(\frac{\lambda\psi}{2\pi d_\delta}\right) \tag{4.27}$$

The RMS error of the virtual baseline interferometer is expected to be degraded compared to first-order interferometer with a physical baseline of d_δ. It is attributed to the fact that three-antenna outputs are used to estimate the phase delay of a virtual two antenna interferometer. The extra antenna output is expected to introduce more noise to the phase delay estimation and hence lead to a reduced DOA estimation performance. This error can be

reduced by using the longest baseline of the antennas array. The equation 4.27 is limited to virtual short baseline, d_δ and does not take advantage of the higher accuracy offered by the longer physical first order baselines i.e. d_{21}, d_{32}, or d_{31}. The longest first-order baseline d_{31} is offered an improvement in the DOA estimation by a factor as below:

$$Improvements = \sqrt{3} * (d_{31}/d_\delta) \tag{4.28}$$

Hence, this method provides better performance with a smaller number of antennas, and hence at a reduced cost, reduced weight, size, and power.

4.5.2 FOV requirement for high altitude ELINT

The field-of-view (FOV) of an interferometer is an important design consideration as it specifies the range of angles that the interferometer can estimate the AOA of a signal with reasonable accuracy. There are two aspects to the FOV consideration, namely the range of angles that can be viewed and the accuracy associated with the FOV.

For a linear array, the range of angles that can be estimated by an interferometer is limited by its AOA estimation performance in the end-fire region. In these regions, the AOA approaches ± 90^0 and so the corresponding phase delay approaches ± π. With the addition of noise errors, the measured phase delay can cross the ± π boundary which results in large AOA estimation errors since a signal arriving from 90^0 may be estimated arriving at – 90^0 and vice-versa. These large AOA estimation errors, therefore, reduce the practical FOV of the interferometer.

By virtue of the lower RMS error performance, long baseline interferometer also has an increased field-of-view (FOV). For a given RMS error tolerances, $\delta\theta_{tol}$, the maximum positive and negative AOA that can be estimated by an interferometer, $\pm\theta_{max}$ can be approximated as below

$$\pm\theta_{\max} \approx \pm\arccos\left(\frac{1}{\sqrt{\eta N}} . \left(\frac{\lambda}{2\pi f d\delta_{\ tol}}\right)\right) \tag{4.29}$$

The FOV then, for an interferometer can therefore be written as

$$\text{FOV} = \theta_{\max} - \theta_{\min} \approx 2.\arccos\left(\frac{1}{\sqrt{\eta N}} . \left(\frac{\lambda}{2\pi f d\delta\theta_{tol}}\right)\right) \tag{4.30}$$

FOV requirement for high altitude is +/-20 degrees. ELINT system at an altitude of approximately 700 km covers almost of approximately 2000 sqkm swath at the ground. The swath means the area covered from high altitude by these systems. Covering this much area is sufficient to capture the radar signals and extract their parameters. Since the FOV requirements

of these systems are less, three antenna BLI techniques become useful. This technique used with noise cancellation provides the advantage equivalent to four antenna BLI arrays.

4.5.3 Phase error margin

It seen that in case of an error occurs in phase measurement, non-integer results being generated for certain computations in the algorithm which ideally should have been integers. Rounding off the results to the nearest integer does not affect the algorithm provided the errors are below a specific value. The phase error margin is defined as the maximum permissible error in the phase measurement below which the algorithm described will not break down. The breakdown of the algorithm is said to take place if rounding off gives a wrong result due to excess phase errors while estimating the modulo integer. This will result in gross errors in DOA computation.

The phase error margin is calculated as below:

The following condition should meet to avoid breakdown in the algorithm,

$$(2\,\delta\Phi_1 - \delta\Phi_2) \,/\, 2\pi \;<\; 0.5 \tag{4.31}$$

Where, $\delta\Phi_1$ is the error in Φ_1 and $\delta\Phi_2$ is the error in Φ_2 i.e.

$$(2\delta\Phi_1 - \delta\Phi_2) \;<\; \pi \tag{4.32}$$

The RF front end following all the antennas in the array are identified and so are the phase measurement and digitization units. Hence, we can assume that the error statistics for phase measurements are independents of the spacing. We can also assume that the error statistics for all the phase measurements are identical. Let the peak error in phase measurement in any channel be δΦ, Hence we get from equation 4.32

$$3\,\delta\Phi \;=\; \pi \tag{4.33}$$

Hence, the available phase error margin in the algorithm is $\pm 60^0$ for the first step in the algorithm. It can be similarly shown that the phase error margin for the second and final steps in the algorithm are $\pm 51^0$ and $\pm 55^0$ respectively. Therefore the system phase error margin is the minimum of all the above, three i.e. $\pm 51^0$. In case higher phase error margins are required the array spacing has to be suitably synthesized.

4.5.4 Accuracy considerations

The theoretical accuracy of the DF system is estimated by differentiating the interference equation i.e.

$$\sigma_\theta = \frac{\sigma_\Phi \lambda}{2\pi D \cos\theta} \tag{4.34}$$

Practically measured values of σ_Φ are around 15^0 RMS for the receiver front end channel including antenna, amplifiers, phase correlators, and phase digitizer. Substituting, this value in equation 4.34 we get a DF accuracy of 1^0 RMS for an IFOV of $\pm 45^0$ even at the lowest frequency i.e. 8 GHz. In general, phase interferometers give better DF accuracy at higher frequencies. The spacing D4 had been considered for calculating the DF accuracy.

The interferometer DF system is generally configured only for FOVs of $\pm 45^0$ since the accuracy will suffer drastically beyond this angle. Four separate sectors each covering $\pm 45^0$ are used to cover the full azimuth of 360^0. The accuracy of the interferometer will also be affected by other parameters like frequency measurement accuracy, phase centre variations in antennas, signal to noise ratio, the elevation of the emitters etc. However, these contribute much less to the overall accuracy compared to the phase measurement errors.

4.5.5 Calibration

Calibration of the system is not required if all the front-end components are perfectly phase matched. In such an ideal situation, when a signal is radiated at bore sight i.e. 0^0. In a practical situation, the RF front end of the DF system will have phase matching of $\pm 30^0$ only. This is due to the practical difficulties in manufacturing the broadband microwave components and the antennas. It is possible to measure the residual phase errors across the channels by calibrating the RF front end components. This data is used to remove the phase errors from the practically measured data. This is done by injecting a signal of known frequency and sorting the residual phase error data in a memory (Look-up table). Whenever signals have intercepted the error for that frequency is algebraically subtracted to give the corresponding phase data. It may be noted that except for the antennas the phase errors in all the other corresponds are only frequency dependents whereas the phase error in the antennas is dependent on both frequency and the DOA of the signal. The phase matching in the antenna array will have a much larger impact on the DF accuracy than the phase matching in the RF front end. The second stage of calibration is done by radiating a signal from 0^0 azimuths so that the phase errors including the error in the antennas are measured at convenient frequency intervals. Calibrations by radiation is generally done only at 0^0 azimuths since the antenna

phase mismatch is most likely to remain static throughout the FOV. The two levels of calibration look-up table (LUT) are required since the antenna being a passive component, is likely to fail and hence has to be replaced. Whenever an RF font-end component is replaced, the LUT corresponding to the injected mode calibration data only needs to be modified.

The phase differences of the outputs of the spiral antennas after the FER are measured with the Quad Digital receiver to give a digital representation of the phase differences of input RF. These phase differences are then processed in the Phase DF processor to extract the DOA of the signal. The processor also takes the amplitude and frequency data for calibration and correction of offset errors (which occur due to phase mismatch in the RF channels over the specified frequency range) and then processed to compute the DOA. High-performance ambiguity resolution algorithms will be implemented in high-speed, high-capacity Xilinx FPGAs to minimize power consumption. Sufficient onboard memory is provided to store the calibration and offset data.

4.5.6 Simulation Results for direction finding

The multi-channel digital receiver configuration block diagram is shown in Figure 4.67. This does the digitization of various intermediate frequencies (IFs) signals which is down-converted by multi-channel superhet receivers. In this various algorithms are applied to extract the pulse descriptor word (PDW) of the signal.

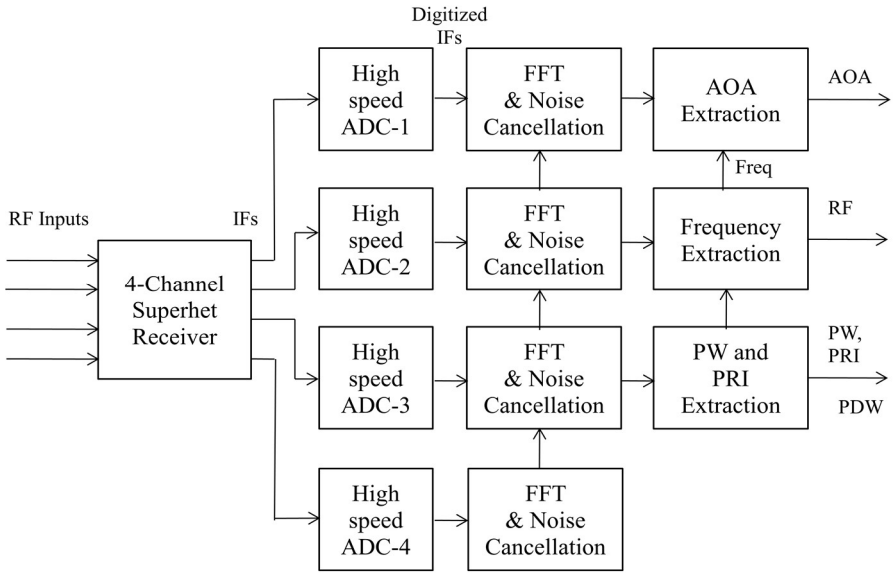

Figure 4.67: Direction finding receiver configuration with noise cancellation.

Virtual antenna based BLI algorithm for AOA extraction, FFT-based interpolation algorithm for frequency extraction, and DDC-based algorithms for PW and PRI extraction are employed. All proposed algorithms are described below.

Four antenna based BLI and three antenna based BLI is considered for simulation. The unambiguous phase is found out for the largest BLI from the ambiguous phase. Finally, the results are compared. The performance of the virtual baseline interferometer algorithm has been simulated for frequency bands 6 - 18 GHz.

(a) Four Antennas BLI: The spacing between the antennas are d_{21} = 45 mm, d_{32} = 52.5 mm. Ambiguous phases d_{32}, d_{31}, and d_{41} for four antennas BLI are plotted in Figure 4.68, Figure 4.69, and Figure 4.70 respectively.

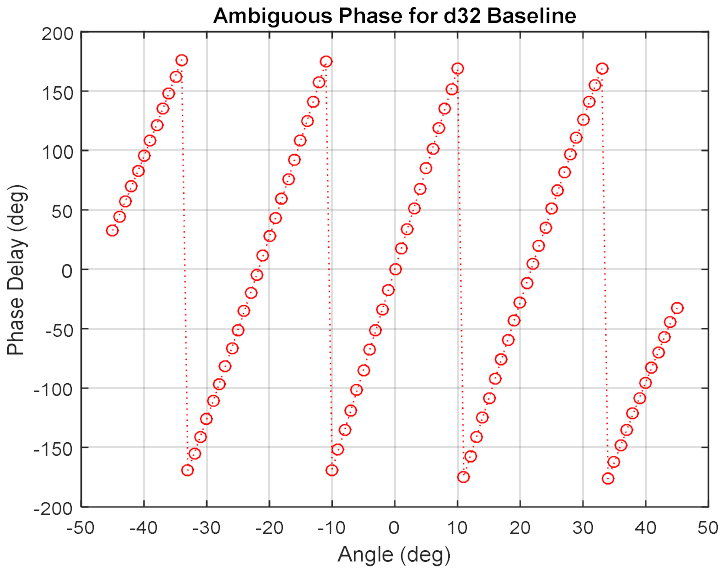

Figure 4.68: Ambiguous phase for d_{32} baseline using four antenna baseline interferometer. Simulation parameters: f = 18 GHz and FOV = ±45°.

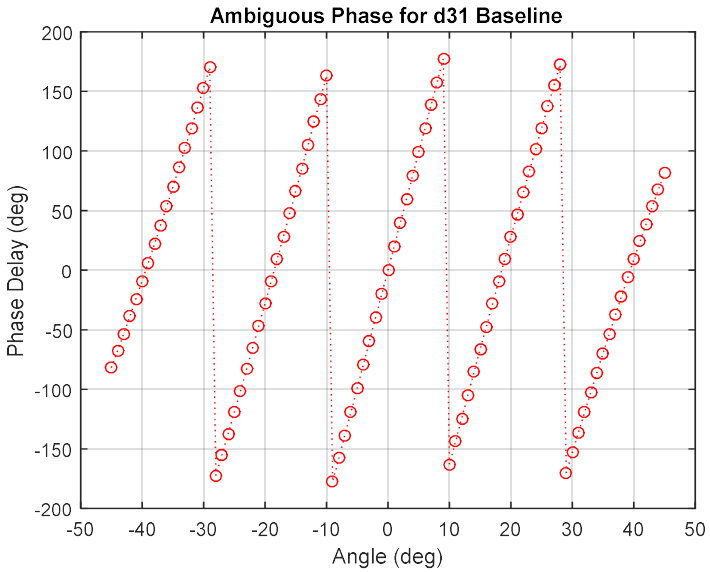

Figure 4.69: Ambiguous phase for d_{31} baseline using four antennas baseline interferometer. Simulation parameters: f = 18 GHz and FOV = ±45°.

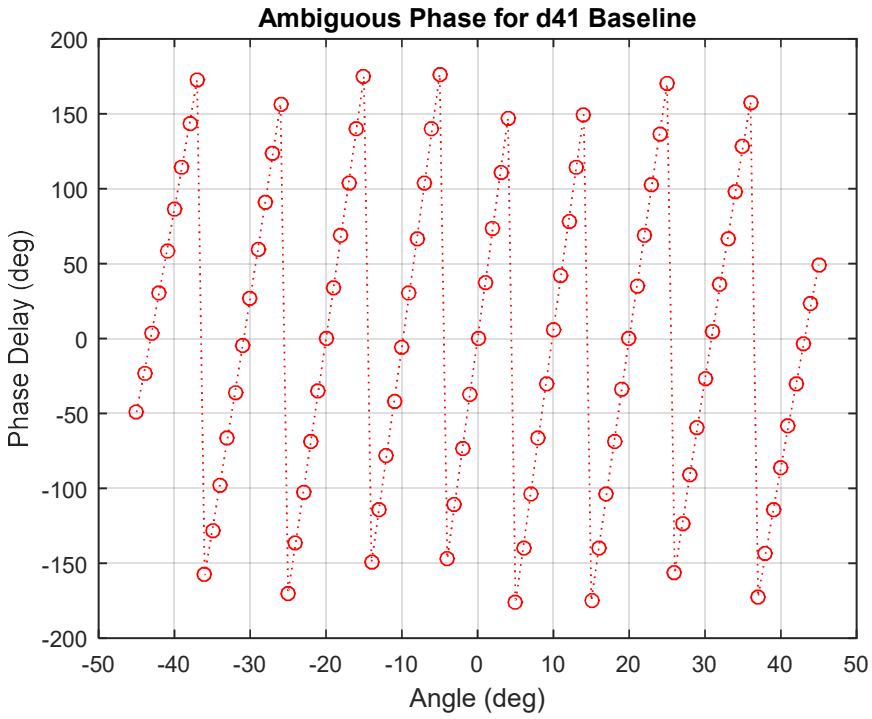

Figure 4.70: Ambiguous phase for d_{41} baseline using four antennas baseline interferometer. Simulation parameters: f = 18 GHz and FOV = ±45°.

The unambiguous phase d_{21} and derived unambiguous phases d_{32}, d_{31}, and d_{41} for four antennas BLI are plotted in Figure 4.71, Figure 4.72, Figure 4.73, and Figure 4.74 respectively.

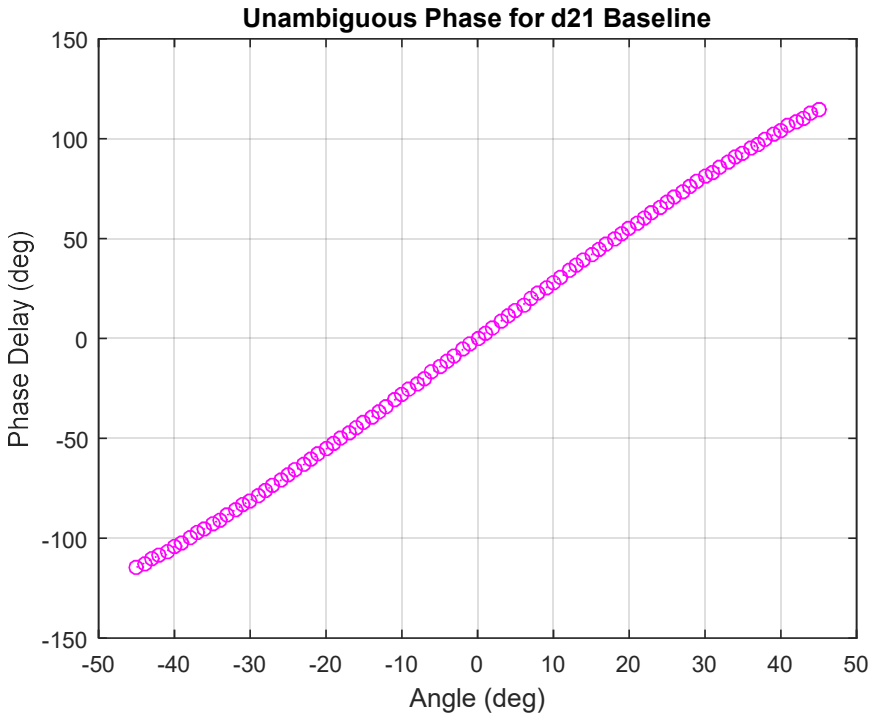

Figure 4.71: Unambiguous phase for d_{21} baseline using four antennas baseline interferometer. Simulation parameters: f = 18 GHz and FOV = ±45°.

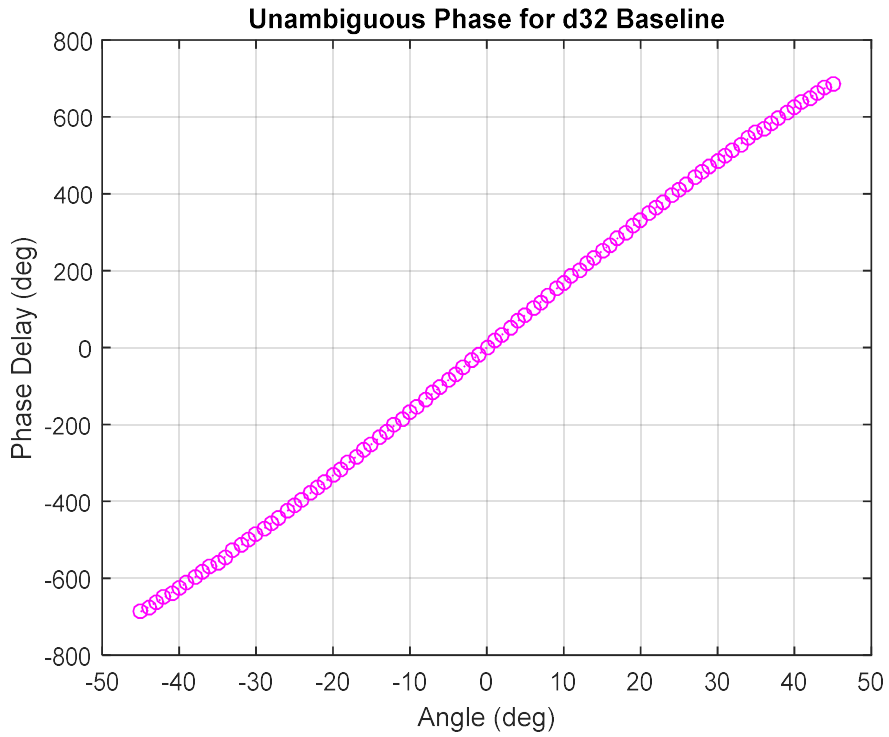

Figure 4.72: Unambiguous Phase for d_{32} baseline using four antennas baseline interferometer. Simulation parameters: f = 18 GHz and FOV = ±45°.

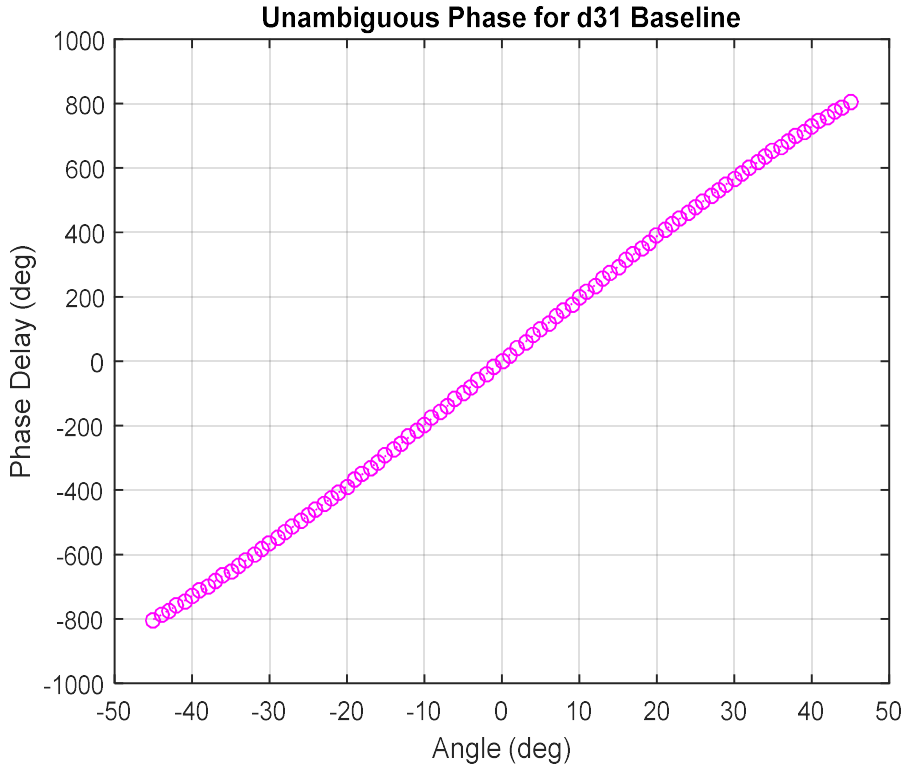

Figure 4.73: Unambiguous phase for d_{31} baseline using four antennas baseline interferometer. Simulation parameters: f = 18 GHz and FOV = ±45°.

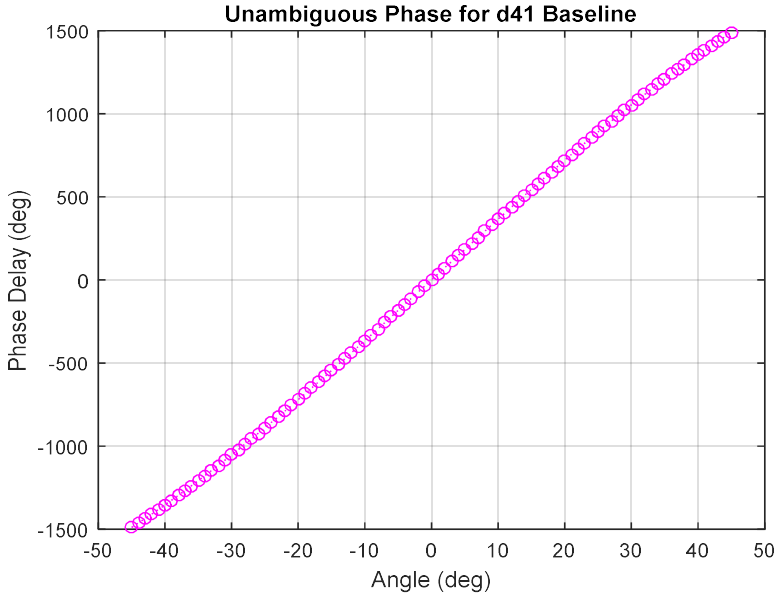

Figure 4.74: Unambiguous phase for d_{41} baseline using four antennas baseline interferometer. Simulation parameters: f = 18 GHz and FOV = ±45°.

(b) Three Antennas BLI: The performance of the virtual baseline interferometer algorithm has been simulated for frequency bands 0.5 - 18 GHz. The spacing between the antennas are d_{21} = 45 mm, d_{32} = 52.5 mm. The d_δ is calculated as $d_\delta = d_{32} - d_{21}$ =7.5 mm. The distance d_{21} and d_{32} are chosen such that $d_\delta < (\lambda_{min}/2)$. The ambiguous phase for the d_{21} baseline and d_{32} baseline is shown in Figure 4.75, and Figure 4.76 respectively. Whereas, d_δ which is derived by virtual baseline interferometer, estimates the unambiguous phase shown in Figure 4.77.

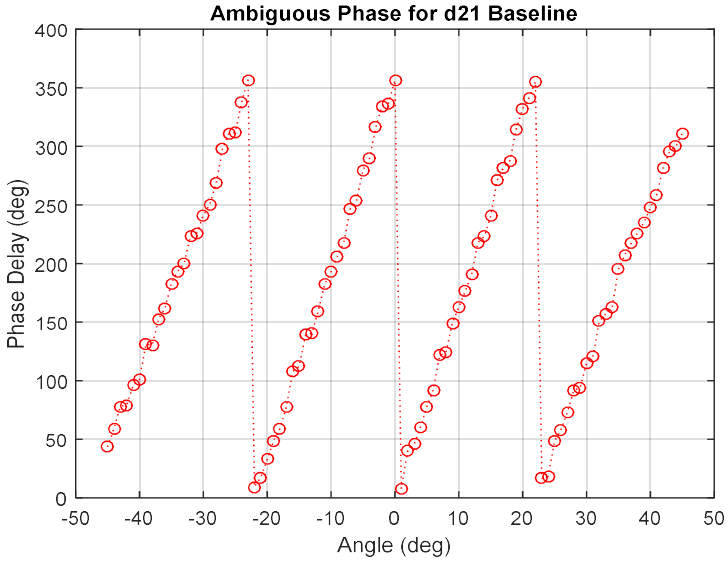

Figure 4.75: Ambiguous phase for d_{21} baseline using three antennas virtual interferometer. Simulation parameters: f = 18 GHz and FOV = ±45°.

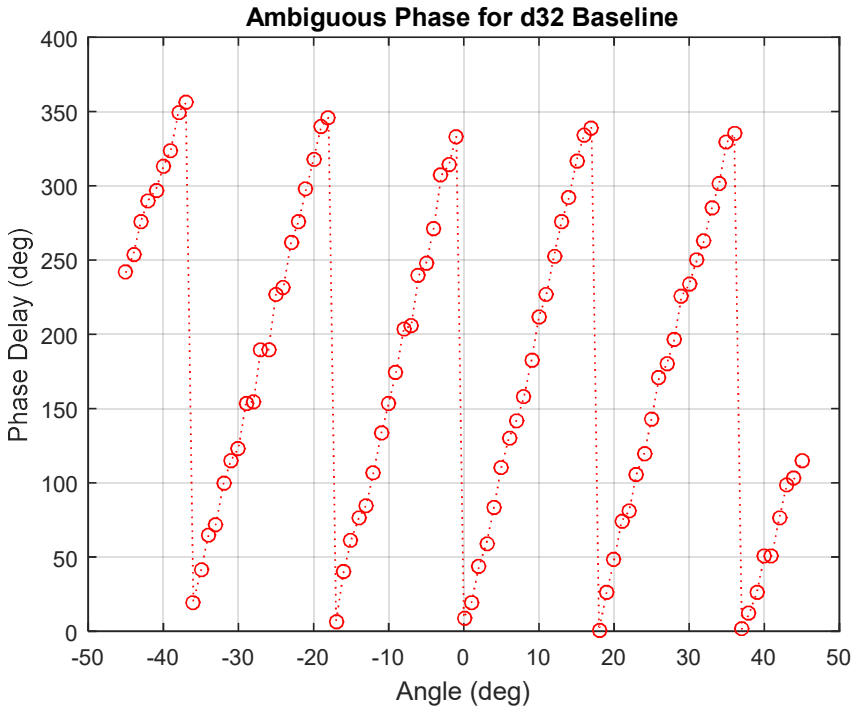

Figure 4.76: Ambiguous phase for d_{32} baseline using three antennas virtual interferometer. Simulation parameters: f = 18 GHz and FOV = ±45°.

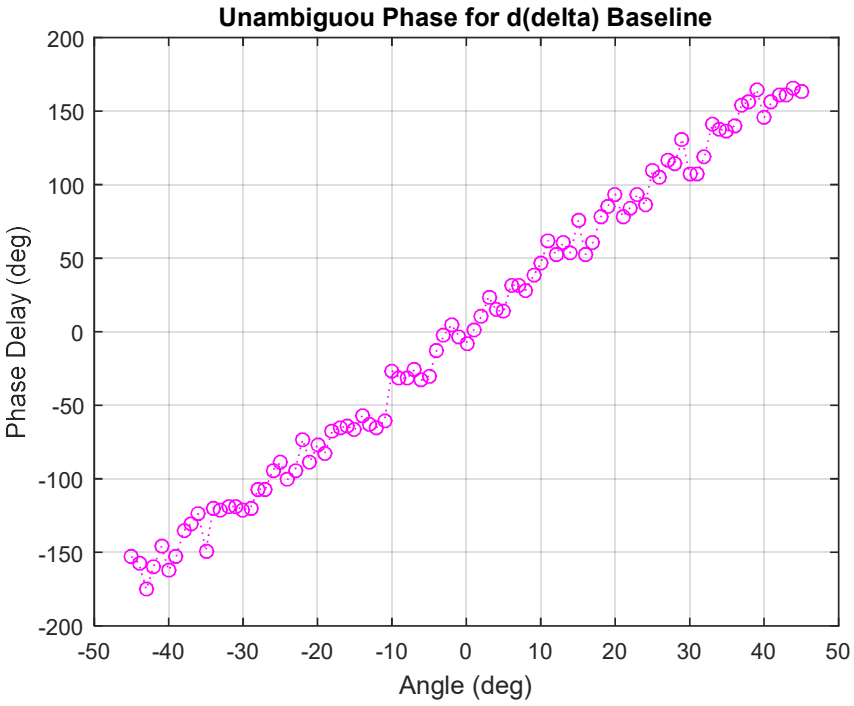

Figure 4.77: Unambiguous phase for d_{δ} baseline using three antennas virtual interferometer. Simulation parameters: f = 18 GHz and FOV = ±45°.

The derived unambiguous phases d_{21}, and d_{32}, and d_{31} for three antenna virtual BLI are plotted in Figure 4.78, Figure 4.79, and Figure 4.80 respectively.

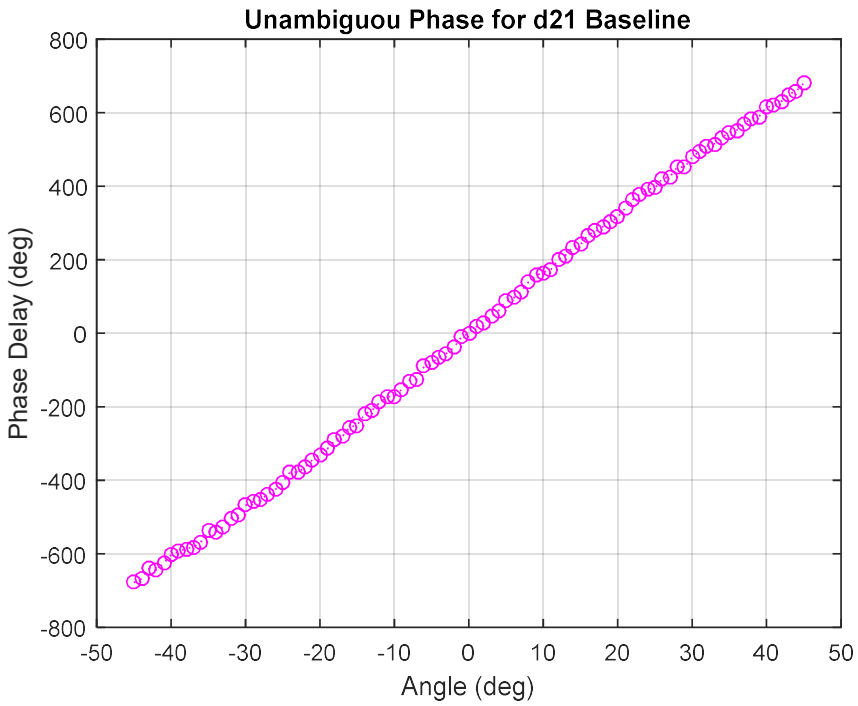

Figure 4.78: Unambiguous Phase for d_{21} baseline using three antennas virtual interferometer. Simulation parameters: f = 18 GHz and FOV = ±45°.

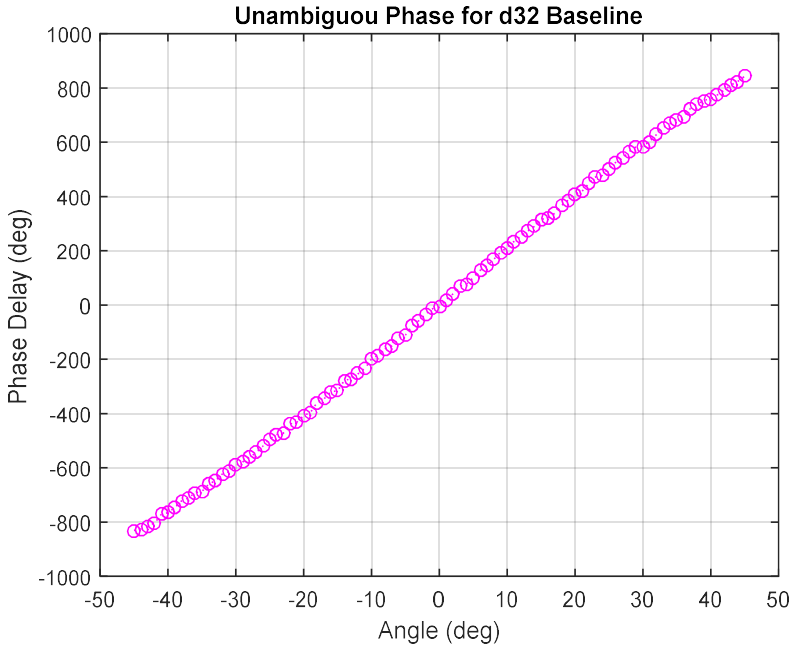

Figure 4.79: Unambiguous phase for d_{32} baseline using three antennas virtual interferometer. Simulation parameters: f = 18 GHz and FOV = ±45°.

Figure 4.81 shows the simulation results for error at 6 GHz between set AOA and measured error and RMSE for 6 to 18 GHz with ±45° FOV. The simulation result of 4 antennas is better compared to 3 antennas interferometers. This is obvious as RMSE measured using the smallest physical antenna gives an advantage of √3 times RMSE for the smallest virtual antenna.

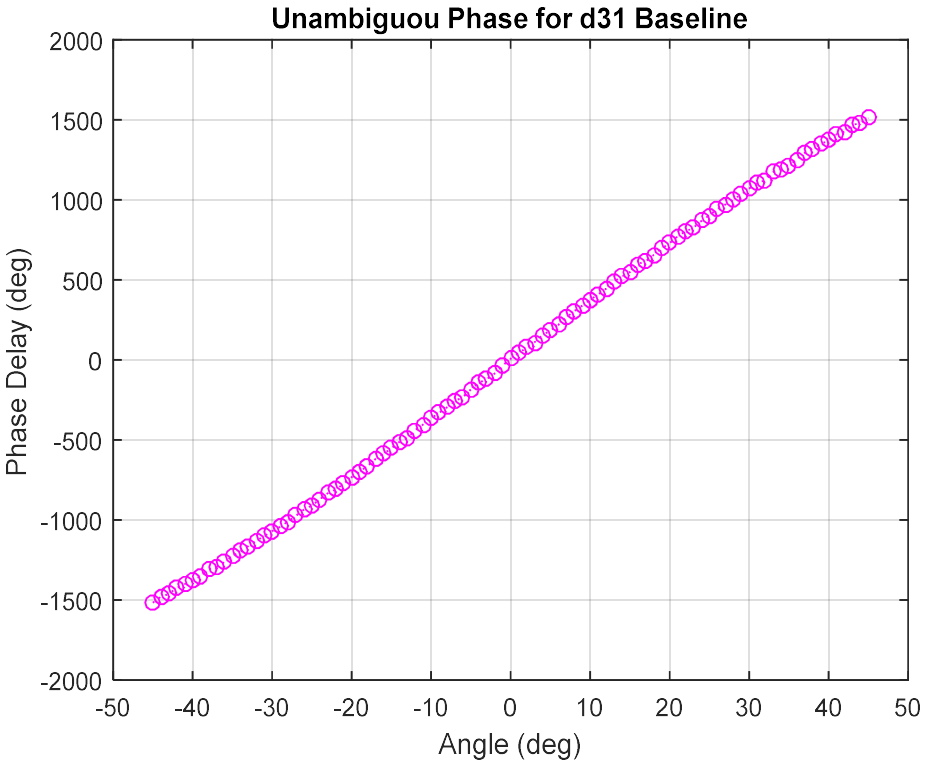

Figure 4.80: Unambiguous Phase for d_{31} baseline using three antennas virtual interferometer. Simulation parameters: f = 18 GHz and FOV = ±45°.

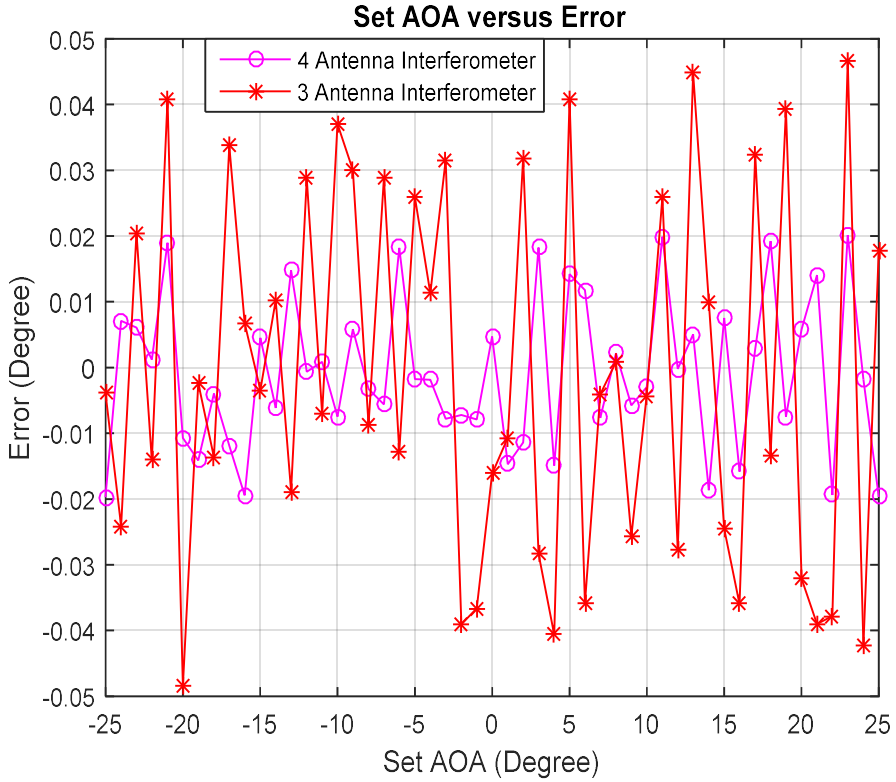

Figure 4.81: Comparison for Set AOA vs Error between four and three antennas interferometers. Simulation parameters: f = 18 GHz and FOV = ±45°.

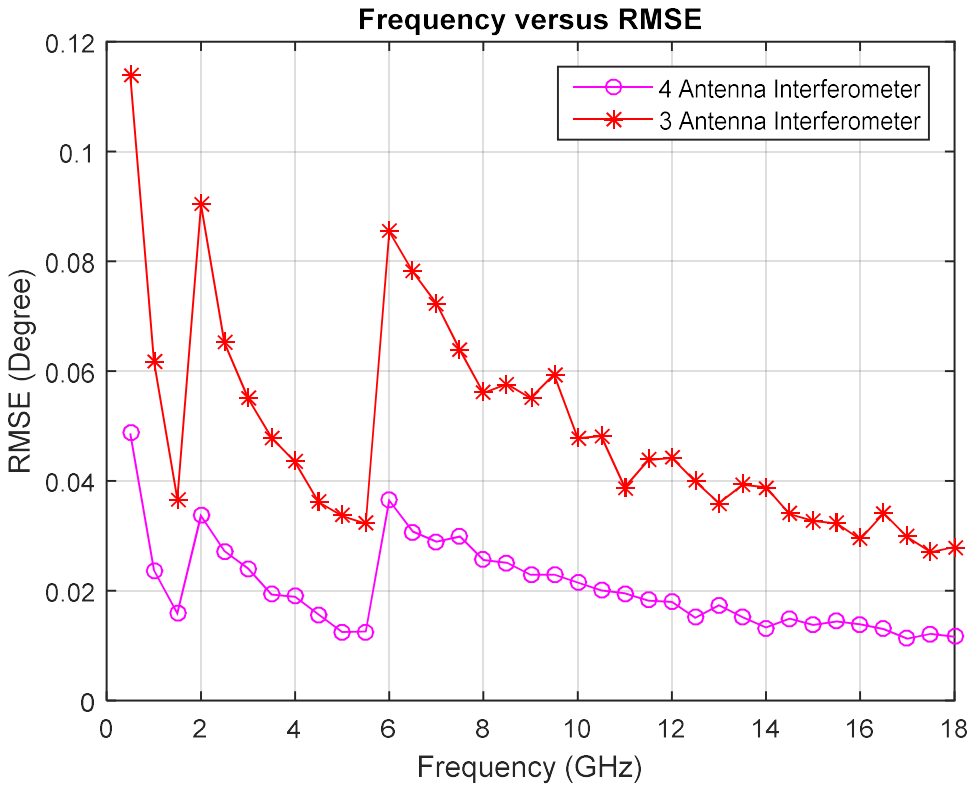

Figure 4.82: Comparison for frequency vs RMSE between four antennas and three antennas interferometers. Simulation parameters: f = 18 GHz and FOV = ±25°.

The comparison of result is generated for ±25° FOV which is sufficient for the ELINT system for space application as shown in Figure 4.82. This result is generated without and with the noise cancellation technique [117]. The system noise of 200 frames is captured and computed 256 points FFT. This is carried out when input is connected to the BITE port and BITE is in signal OFF condition. The estimated average of the noise spectrum is computed for all frames. In system ON condition when input is connected to antenna port and the signal spectrum is computed continuously which is noisy. The estimated noise spectrum is subtracted from the noisy input signal spectrum and an instantaneous magnitude spectrum is computed which is called a restored signal. Again restored time-domain signal is computed by inverse FFT. The SNR of 6 to 8 dB is improved when the signal is passed through this. This result shows that 3 antenna interferometer provides comparable results with 4 antenna interferometer. It shows, on reducing one antenna alone approximately one-fourth of hardware is reduced. Usually, to cover a complete 0.5 to 18 GHz band three different types of antennas are required. With 3 antennas approach, a total of 9 antennas covers the complete band instead of 12 antennas. Hence, further reduction will be there in processing electronics also.

4.5.7 Discussions

The effect of receiver noise is an important consideration in all practical electronic systems. Unlike systematic errors, which can be compensated through calibration, receiver noise errors cannot be eliminated but their effect can be minimized through the careful selection of algorithms. In interferometry, the receiver noise errors affect the AOA estimation by manifesting as random errors in the frequency and phase delay estimation. For estimating the AOA, the frequency error is assumed negligible. This section will, therefore assume that the noise errors are noticeable entirely as phase delay estimation errors.

4.6 Conclusions

Pre-processing of data using noise cancellation will help in moving autocorrelation as well as DIQ approaches. This technique is used for the generation of amplitude profile and frequency profile. This technique has a lot of practical significance in the present scenario. The proposed algorithms are evaluated with the field data to evaluate the efficacy of the technique. Most of the results are generated using AWGN noise data. This technique is tested with uniformly distributed noise.

The proposed technique based on moving autocorrelation and noise estimation has significantly improved the measurement accuracy of instantaneous amplitude and the instantaneous frequency at low SNR conditions. These techniques will help in the measurement of the basic parameters as well as intra-pulse modulation information of radar signals. This will lead to a very efficient and accurate emitter identification. The advancement in signal processing algorithms, coupled with high-performance FPGA has enabled for improvement of the unique emitter identification and also achieves a real-time performance. This is useful for real-time modulation classification based on instantaneous frequency profile.

It is evident from the proposed approaches that there is an improvement in resolution and accuracy of measurement for various parameters direction-of-arrival, frequency, etc. with fewer hardware resources. In case of direction finding, less number of front ends and antennas combinations can be realized in the system that provide RMS DOA error of less than 0.1 degrees with less weight and small size which is the requirement of space platform. The frequency measurement accuracies achieved is less than 0.0609 MHz RMS with this approach against 1.528 MHz RMS with simple FFT spectrum analysis using 256 points FFT. The autocorrelation with the FFT combination approach improves the PW and TOA measurements that can be measured with high accuracy with very few resources. It also helps

to reduce power consumption which is high in today's system. SWaP optimized three antennas based BLI technique for AOA measurement provides results equivalent to four antennas based BLI. These measurement techniques will help to realize a new generation ELINT system based on proposed digital techniques for space applications.

Chapter 5

Signal Detection and Modulation Recognition

In the previous chapter signal estimation techniques are described which include noise cancellation, instantaneous amplitude measurement, instantaneous frequency measurement, FFT-based frequency estimation, and direction-finding techniques. The simulation results are also presented along with the algorithms. In this chapter, noise is estimated on instantaneous amplitude and an adaptive threshold is computed for detection of the signal. SNR and sensitivity are also computed after the detection of the signal. Intra-pulse modulation recognition of radar signals is carried out using instantaneous frequency profiles. These will be supportive parameters for sorting and specific emitter identification.

5.1 Introduction

Modulation in radar signals is one of the important features and modulation recognition is one of the vital problems in the analysis of non-cooperative reception of radar signals. The modulation recognition for communication signals in real-time is quite common due to its lower frequency of operation and less bandwidth. But, in the case of radar signals, the modulation recognition in real-time is being done for limited signals. Whereas the modulation recognition of radar signals is carried out offline by a small number of ELINT systems. These systems can be an add-on to the main systems or they are integrated with the main systems. To meet today's requirement ELINT systems has to classify modulation of radar signals in real-time. This classification helps in the de-interleaving of emitters.

Conventional radars have a simple pulsed waveform or continuous waveform with no modulation. These pulsed radars sometimes have variations in PW or PRI. But complex radars are having various modulations within the pulse alongwith the above variations. The modulation can be linear frequency modulation (LFM), non-linear frequency modulation (NLFM), stepped frequency modulation (SFM), bi-phase modulation (BPM), and hybridization of modulations. These modulations are recognized in real-time using decision-

tree algorithms. The implementation of these signals classification is carried out in FPGA using time-domain techniques for real-time application.

5.2 Signal detection

In this section, noise estimation, pulse detection, sensitivity, and SNR computations are discussed. Noise estimation is carried out on an instantaneous amplitude profiles.

5.2.1 Noise estimation

(i) Approach-1: The standard deviation (σ) of signal $x(n)$ which is obtained by computing the mean of noise is given by equation5.1. To compute the mean, that many samples have to be stored. Finally, summation, squaring and square root functions have to be used to compute the standard deviation. The standard deviation is defined as equation 5.1 and its implementation block diagram is shown in Figure 5.1.

$$\sigma = \sqrt{\sum_{n=0}^{N-1} \frac{(x(n)-x_{avg})^2}{N}} \tag{5.1}$$

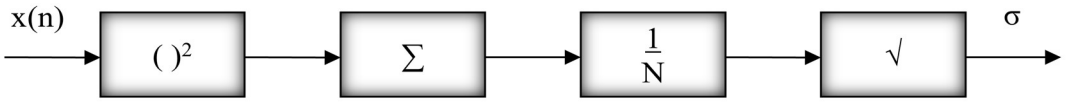

Figure 5.1: Block diagram of standard deviation computation.

Standard deviation gives the actual estimate of the noise present. But this approach requires large computations and takes time to compute the estimate. All samples have to be stored to compute the standard deviation, hence real-time estimate is not done.

(ii) Approach-2: Estimation of noise is carried out using two-point averaging. This reduces the computations required for estimation. Approximated standard deviation (σ_1) is calculated using two-point averaging as given by equation 5.2.

$$\sigma_1 = k_1 * |x(n) + x(n+1)| \tag{5.2}$$

where $k_1$is the constant and set based on minimum error. This approach is faster than the above approach. But the result obtained using this approach is not very close to standard deviation.

(iii) Approach-3: The efficient method of computing standard deviation is discussed in this section. Estimation of noise is done for signal detection which reduces the computation requirement and storage requirement. The mean of the modulus of the noise samples are taken and the approximate standard deviation is computed. The absolute of input signal samples $x(n)$is taken which makes all negative samples positive. The shape of the probability density function (PDF) will be the same but doubles the peak value.

If the input signal is $x(t)$ and absolute of $x(t)$ is $abs(x)$. The absolute value of input samples makes negative samples positive. The shape of the PDF will be the same but doubles the peak value. The mean value of the signal at point c and point b is the same.

$$\mu_c(N) = \mu_b(N) \tag{5.3}$$

$$\mu_c(S+N) = \mu_b(S+N) \tag{5.4}$$

If $x(t)$ is the input signal, B is the bandwidth of the signal and averaged for time T. The variance at point c is $1/(2BT)$ times the variance at point b.

$$\sigma_c^2(N) = \frac{\sigma_b^2(N)}{2BT} \tag{5.5}$$

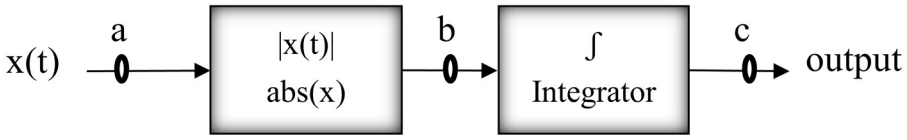

Figure 5.2: Block diagram showing mean and variance at different points.

If 2BT is greater than 20, the central limit theorem allows approximation for a waveform with Gaussian PDF at point c,

$$P_c'(y) = \frac{1}{\sqrt{2\pi\sigma_c^2}} e^{-\frac{(y-\mu_c)^2}{2\sigma_c^2}} \tag{5.6}$$

The Gaussian PDF for waveform at point a with zero mean is given as

$$P_a'(x) = \frac{1}{\sqrt{2\pi(\sigma_x^2+\sigma_e^2)}} e^{-\frac{x^2}{2(\sigma_x^2+\sigma_e^2)}} \tag{5.7}$$

The Gaussian PDF at point b is given as,

$$Q_b'(x) = 2P_a'(x) = \sqrt{\frac{2}{\pi(\sigma_x^2+\sigma_e^2)}} e^{-\frac{x^2}{2(\sigma_x^2+\sigma_e^2)}} \tag{5.8}$$

when both signal and noise is present, the mean at point b is given below

$$\mu_b(S+N) =< x >_b = \int_0^1 x dQ_b'(x) = \sqrt{\frac{2}{\pi(\sigma_x^2+\sigma_e^2)}} \int_0^1 x e^{-\frac{x^2}{2(\sigma_x^2+\sigma_e^2)}} dQ_b'(x) \quad (5.9)$$

This equation is reduced to

$$\mu_b(S+N) = \sqrt{\frac{2}{\pi}} \sqrt{(\sigma_x^2+\sigma_e^2)} \quad (5.10)$$

When only noise is present, the mean at point b is written as

$$\mu_b(N) = \sqrt{\frac{2}{\pi}} \sigma_e \quad (5.11)$$

When only noise is present, the mean of noise will reduce at point c and point b to,

$$\mu_c(N) = \mu_b(N) = \sqrt{\frac{2}{\pi}} \sigma_e \quad (5.12)$$

The standard deviation when only noise is present, is written as below using equation (5.11),

$$\sigma_e = \mu_b(N) \sqrt{\frac{\pi}{2}} \quad (5.13)$$

Considering, $\sigma_2 = \sigma_e$, $k_2 = \frac{1}{N}\sqrt{\frac{\pi}{2}}$ and $\mu_b(N) = \frac{1}{N}\sum_{n=0}^{N-1} |x(n)|$

The above equation shows that by computing the mean of noise and multiply with the multiplication factor, the result will be equivalent to the standard deviation of signal $x(t)$. The efficient digital implementation of noise estimation is proposed. The absolute value of signal $x(n)$ is computed and multiplied with constant (k_2) and is derived as equation 5.14 which is approximately equivalent to the standard deviation of the signal $x(n)$. The block implementation of approximate standard deviation is shown in Figure 5.3.

$$\sigma_2 = k_2 * \sum_{n=0}^{N-1} |x(n)| \quad (5.14)$$

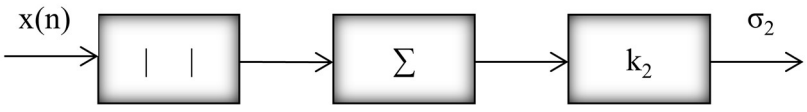

Figure 5.3: Block diagram for approximate standard deviation computation.

The random noise is computed and results are tabulated using both the approaches as shown in Table 5.1. Error is also computed with standard deviation. The error (E_1) computed

is less than 20% using the first approach whereas the error (E_2) is less than 10% using the second approach. Usually, two-level threshold is used which will have a difference of 6 dB. Hence the error computed is less and it is efficient also in hardware implementation. Figure 5.4 shows the comparison of the estimated noise for different approaches as a function of SNR.

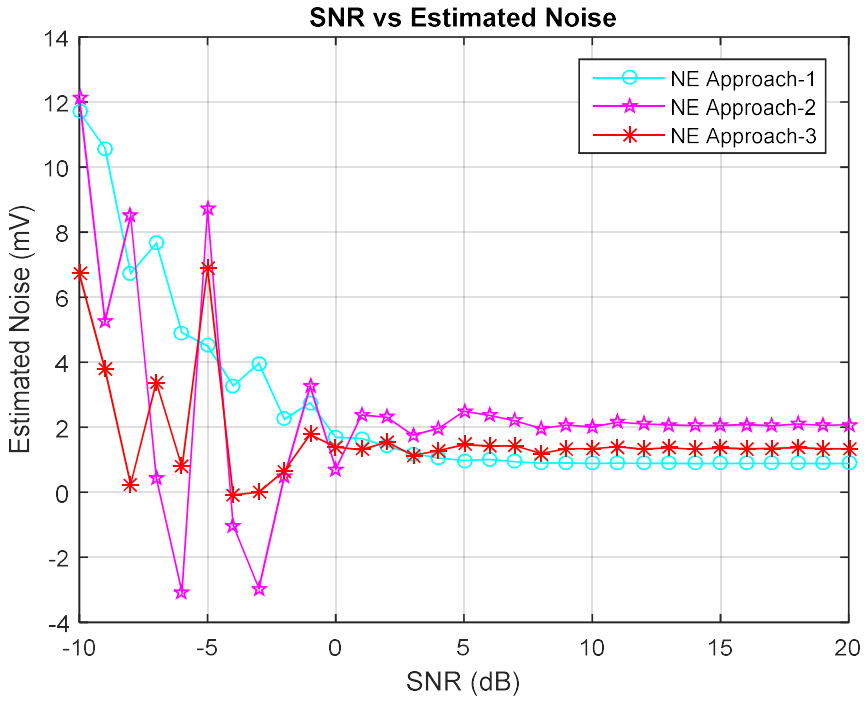

Figure 5.4: Comparison of the estimated noise for different approaches as a function of SNR. Simulation parameters: N = 80,000 samples, and t_s = 1.5 ns.

Table 5.1: Comparison of noise estimation results using a different approach.

Iteration Number	Approach-1 Std. Dev. (σ) A	Approach-2 (σ_1) B	Error-1 E1= A-B	Approach-3 (σ_2) C	Error-2 E2= A-C
1	5.825	5.593	0.232	5.296	0.529
2	5.784	5.339	0.445	5.343	0.441
3	4.852	5.756	-0.904	5.305	-0.453
4	5.567	5.838	-0.271	5.281	0.286
5	4.787	5.598	-0.811	5.256	-0.469
6	5.063	6.008	-0.945	5.323	-0.26
7	5.629	5.663	-0.034	5.324	0.305
8	5.276	5.576	-0.3	5.196	0.08
9	5.091	6.023	-0.932	5.195	-0.104
10	4.466	5.213	-0.747	4.789	-0.323

The noise present in the ELINT system is Gaussian. The standard deviation is computed for the period for which noise is to be estimated. The threshold selected is nothing but, it is the standard deviation of the noise. If the threshold selected is equivalent to standard

deviation. The probability of detection or probability density function (PDF) is 68.27%. If the threshold selected is equivalent to twice the standard deviation. The probability of detection will be 95.45%. If the threshold selected is equivalent to three times the standard deviation. The probability of detection will be 99.73%. Threshold more than three times has not much impact on the probability of detection. But it will limit the receiver sensitivity.

5.2.2 Signal detection using adaptive threshold

The fixed threshold is constant and hence it is not capable to prevent false detection and missed detection. The adaptive threshold has an advantage over the fixed threshold for pulse detection. The noise present in the system varies in the wide frequency band. Therefore, the noise is computed for different time constants, which is selectable. In the case of radar EW, the signal is non-cooperative and pulse width is unknown. Hence lowest time constant is selected, say 1 us. This is useful for all the pulsed signals and continuous wave (CW) signals detection. Hence, the noise estimation is carried out for every 666 samples during pulse-off time.

The adaptive threshold should be higher than the noise estimated to avoid false detection. This threshold correction is applied as a fixed value. The adaptive threshold will keep updating itself at each selected time constant. The conventional and proposed efficient noise estimation is discussed next.

Once the threshold is estimated, it is also important that how this threshold is applied for detection. There are two ways to detect the pulse. One is single-level threshold and the other is two-level threshold. The single-level threshold is suitable when pulse on amplitude variation is more. Pulse on amplitude variation is more at lower SNR. The leading edge is detected with one threshold and the trailing edge is detected with another threshold. Figure 5.5 shows the block diagram of signal detection with two-level threshold.

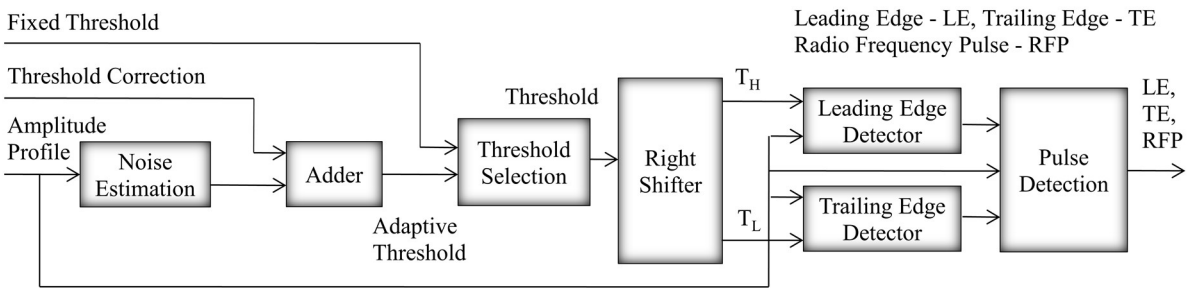

Figure 5.5: Signal detection with two-level adaptive threshold.

Both higher level and lower level thresholds are estimated for detection. High-level threshold (T_H) is computed using estimated noise and accordingly, low-level threshold (T_L) is set as $T_L = (T_H/8)$. T_H is used to detect pulse leading edge (LE) or pulse start and T_L is used for pulse trailing edge (TE) or pulse end. The threshold is adaptive for better detection and analysis of pulses. This is also helpful when noise increases due to system temperature and accordingly noise is estimated and the threshold is set.

5.2.3 Signal flow graph for noise estimation and signal detection

The signal flow graph of noise estimation and signal detection is shown in Figure 5.6. Noise cancellation is performed on the data capture as given in section 4.2. Instantaneous parameter measurement is carried out on restored signal. Further the noise is estimated on the instantaneous amplitude profile. This is carried out during signal-off duration. Signal is detected based on higher (T_H) and lower (T_L) threshold which detects leading and trailing edge of the pulse. Later signal parameters are estimated along with modulation parameters.

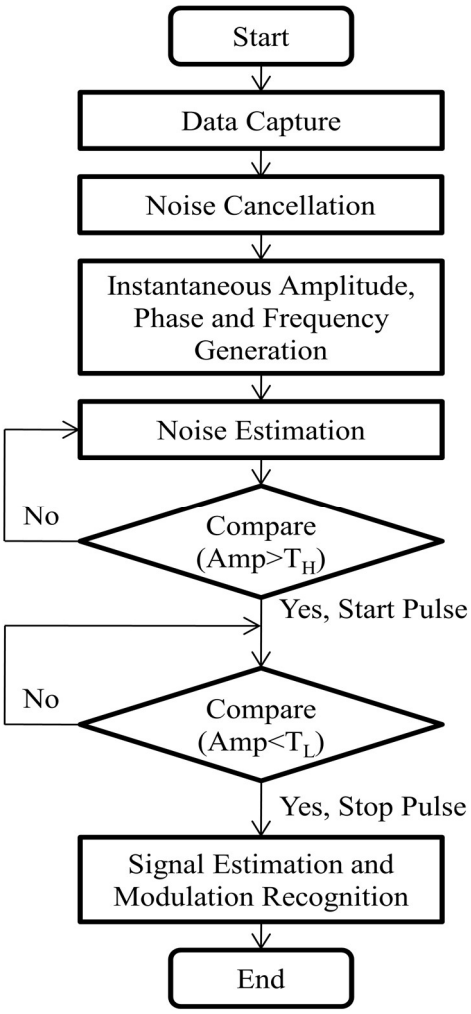

Figure 5.6: Signal Flow graph of noise estimation and signal detection.

5.2.4 SNR and sensitivity computations

In this section, the SNR and sensitivity computations are discussed. The computation of SNR is carried out during signal presence after detection of the signal using instantaneous amplitude profile.

5.2.4.1 SNR Computations

The signal is mixed with noise is written as $x(n) = s(n) + e(n)$. The signal power and noise power are also measured [128]. The P_x is the signal power of x(n) which is tainted by noise when signal is mixed with noise. The P_s is signal power when a signal without noise is measured. Accordingly, signal-to-noise (SNR) is declared.

$$SNR = 10 \log\left(\frac{P_s}{P_x - P_s}\right) = 10 \log\left(\frac{P_s}{P_e}\right) \quad (5.15)$$

Where, P_s and P_x are given by,

$$P_s = \frac{1}{N}\sum_{n=1}^{N} |s(n)|^2 \quad (5.16)$$

$$P_x = \frac{1}{N}\sum_{n=1}^{N} |x(n)|^2 \quad (5.17)$$

The P_x is known and P_s is unknown and has to be computed to declare the SNR. The P_e is the noise power which is computed during noise presence.

5.2.4.2 Sensitivity computations

Sensitivity of the ELINT system using proposed techniques is defined as [116],

$$Sensitivity = -114 + 10\, log_{10}\left(\sqrt{\left(2B_r B_v - B_v^2\right)}\right) + NF + \eta + G_a + G_p \quad (5.18)$$

Where, B_r = Resolution bandwidth (500 MHz)

B_v = Video bandwidth (500 MHz)

NF = Noise Figure (12 dB)

η = SNR (1 dB)

G_a = Horn Antenna Gain (6 dBi Minimum)

G_p = Processing Gain

(i) Sensitivity for IF 1 GHz IF without FFT overlapping:

Sensitivity is computed with above parameters for 1 dB SNR using moving autocorrelation technique with G_p of 7 dB.

$$Sensitivity = -114 + 10\, log_{10}(B_r) + NF + \eta + G_a + G_p$$

$$= -114 + 10 \log_{10}(500) + 12 + 1 - 6 - 7$$

$$= -114 + 26.99 + 12 + 1 - 6 - 7$$
$$= -87.01 \text{ dBm}$$
$$= -87 \text{ dBm (Approx.)}$$

Minimum SNR required using moving autocorrelation algorithm and DIQ algorithm is 1 dB and 8 dB respectively to process all types of modulated signals. Based on this, the summary of sensitivity achieved is given in Table 5.2.

Table 5.2: Sensitivity achieved with different techniques without FFT overlapping.

Proposed technique with	Minimum SNR required without noise cancellation (dB)	Achieved sensitivity without noise cancellation (dBm)	Minimum SNR required with noise cancellation (dB)	Achieved sensitivity with noise cancellation (dBm)
Moving autocorrelation	8	– 80	1	– 87
DIQ	15	– 73	8	– 80

(ii) Sensitivity for IF 1 GHz IF with FFT overlapping of 75%:

Sensitivity is computed with the above parameters for 1 dB SNR using moving autocorrelation technique with G_p of 9 dB for the case with FFT overlapping.

$$Sensitivity = -114 + 10\,log_{10}(B_r) + NF + \eta + G_a + G_p$$
$$= -114 + 10 \log_{10}(500) + 12 + 1 - 6 - 9$$
$$= -114 + 26.99 + 12 + 1 - 6 - 9$$
$$= -89.01 \text{ dBm}$$
$$= -89 \text{ dBm (Approx.)}$$

Table 5.3: Sensitivity achieved with different technique with 75% FFT overlapping.

Proposed technique with	Minimum SNR required without noise cancellation (dB)	Achieved sensitivity without noise cancellation (dBm)	Minimum SNR required with noise cancellation (dB)	Achieved sensitivity with noise cancellation (dBm)
Moving autocorrelation	6	- 82	- 2	- 89
DIQ	13	- 75	6	- 82

Minimum SNR required using moving autocorrelation algorithm and DIQ algorithm is 1 dB and 8 dB respectively to process all types of modulated signals. Based on this, the summary of sensitivity achieved is given in Table 5.3.

5.2.5 Measurement of pulse parameters

The pulse parameters of the radar signals like Pulse Width, Pulse Amplitude, and PRI are also measured using the proposed approaches. The various parameter measurements are discussed below.

SNR Requirement

Proper identification of emitter demands a high signal-to-noise ratio (SNR) for reliable and consistent analysis. For this reason, only those pulses, which have SNR more than 1 dB, will be processed for parameter estimation. SNR of 1 dB is also sufficient for detection purposes for all modulated signals.

Storage Requirement

The digitizer card digitizes the IF for the period of segment length, which is derived from pre-trigger, pulse width, and post-trigger. Pre-trigger and post-trigger are added to measure the pulse width. It saves a huge memory space and reduces transfer time. This data is stored to process it in the future for offline processing. To extract the features offline only raw data and time-of-arrival (TOA) information is sufficient.

Selection of processing hardware

The FPGA based digital processing hardware involves computational intensive operations like moving autocorrelation, digital I-Q method, noise cancellation, etc. It has to perform these operations on large input data. To achieve these computations on large input data with a good reaction time, a state-of-the-art FPGA is required. Computational round-off is an important problem that can limit the accuracy of computations.

Dynamic Range

The dynamic range of ELINT receivers depends on the two factors, the dynamic range of the front-end receiver, and the dynamic range of digital processor hardware. The dynamic range of digital processor hardware further depends on the effective number of bits (ENOB) of ADC used for data acquisition. The digital processor hardware uses 12 bits ADCs and ENOB is approximately 8-bits. Theoretically, a dynamic range can be achieved up to 48 dB.

But due to consideration of practical scenario, the dynamic range has been achieved of 40 dB. Another 7 dB advantage is achieved by the noise cancellation technique. Hence, the practically minimum dynamic range of 47 dB is achieved.

Detection of the Pulse

Detection is carried out on the pulse envelope. Pulse envelope is generated using the moving autocorrelation technique. Detection is done using both a higher threshold and a lower threshold. Higher threshold is used to detect rising edge and lower threshold is used to detect falling threshold. The lower threshold is kept 8 dB lower compared to the higher threshold.

Frequency Measurement

Frequency measurement is carried out during the stable region of the pulse. In case of no modulation on pulse, the average is taken and frequency is reported. In the case of frequency modulation centre frequency, frequency deviation, frequency agility, etc. are reported by measuring frequency at different points during the stable region of the pulse.

Pulse Width measurement

Pulse Width is measured from the detected output from the pulse envelope. The difference between the trailing edge and leading edge is considered the raw pulse width. Further, the 3 dB down from the peak amplitude is considered the practical pulse width. This region is also considered the stable region. The envelope is generated by measuring every 1.5 ns. The measured resolution of pulse width is also 1.5 ns. The counter starts at the leading edge and a trailing edge of this counter value is registered as pulse width and reset after two clocks.

TOA Measurement

TOA measurement is required to get the PRI of the intercepted radar signals. The digitized samples from ADCs are fed to FPGA for implementing the signal processing algorithms. The free-running counter is implemented to register the time of arrival of pulse at the leading edge. The counter value multiplied by the resolution of TOA will yield TOA measurement.

Pulse Amplitude Measurement

Pulse amplitude is measured from the pulse envelope. The peak value of the envelope is registered and converted to dBm and it is reported. Finally, the calibration is done and

amplitude is calibrated at the input of receiving antenna. All components gain and losses are considered in calibration at a few hundred MHz step frequency.

Pulse Descriptor word formation

Pulse descriptor word constitutes the parameters measured by the ELINT receiver. All the parameters allot the definite number of bits and it is used during de-interleaving and emitter identification.

De-interleaving

The ESM processor is required to track up to 1000 emitters simultaneously for pulse density of the order of 1,000,000 pulses per second. In such a dense electromagnetic environment, the large number of independent emitters will cause the ESM system to receive a seemingly random pulse train consisting of interleaved pulse trains. To identify individual emitters, their pulse trains must be de-interleaved. The de-interleaving process is essentially the process of determining whether the newly intercepted radar pulse belongs to one of the already processed emitters or a new emitter. Ideally, there will be a one-to-one correspondence between each pulse train identified by the de-interleaving process and the emitters in the environment. In practice, pulses from several emitters may be combined into one chain, and pulses from one emitter may be split into several chains. The de-interleaving process will take into account the expected characteristics of the radar environment, the known characteristics of the measurement system, and all foreseeable sources of data corruption.

The de-interleaving process is followed by PRI analysis for each pulse chain. This PRI analysis will determine if more than one emitter is mapped to the chain. After PRI analysis, scan analysis and identity search are performed for each emitter pulse chain.

Emitter Identification

These measured parameters which the PDW is useful for de-interleaving because it consists of the AOA and MOP information. The availability of these two parameters in real-time is very important. This will solve the de-interleaving issue in a dense environment signal coming from the same direction within 50 km but having different modulation information.

Finally, the perfect de-interleaving will be helpful for specific emitter identification as the tracks will be formed without any ambiguities in real-time.

5.3 Modulation recognition of radar signal

Conventional radars have a simple pulsed waveform or continuous waveform with no modulation. These pulsed radars sometimes have variations in PW or PRI. But complex radars are having various modulations within the pulse along with the above variations. These intra-pulse modulations can be Linear Frequency Modulation (LFM), Non-Linear Frequency Modulation (NLFM), Stepped Frequency Modulation (SFM), Bi-Phase Modulation (BPM), LFM with BPM, and SFM with BPM. Typically, these modulations are identified by the ELINT system using offline analysis [70]-[99]. Till the earlier generation of Electronic Warfare (EW) systems, these offline analysis tools are either add-on or they are integrated with the main ES systems or ELINT systems. Identification of modulations by the ELINT system in real-time is still a challenge. Various digital methods are discussed for modern digital implementation [60]-[64] and decision-theoretic approaches are mentioned for modulation classification [65]-[69].

Modulations can be identified using frequency domain techniques using offline systems [70]-[71]. Implementation of these techniques in Field Programmable Gate Array (FPGA) for real-time applications is not a viable solution as they consume a lot of hardware resources. Due to this reason, the implementation of signal classification techniques is attempted in FPGA using a time-domain technique for real-time applications. IF signal is digitized in ADC and samples are captured, processed, and further analysed in FPGA. These are possible to implement in FPGA due to parallelism, high density, and high-speed component cores.

The decision-tree based algorithm is proposed to identify the modulation in real-time. The RF pulse (RFP) is generated based on the instantaneous amplitude profile. The complete instantaneous frequency profile data is stored in the Random Access Memory (RAM) during RF pulse. The frequency at different points in the pulse region is fetched from RAM and the algorithm is applied in real-time. The modulation is measured within shadow time based on the frequency parameters.

5.3.1 Modulation types and modulation parameters handling

The following modulations and their parameters are identified using a decision-tree algorithm:

(i) No-Modulation Continuous Wave (NMCW)

(ii) Frequency Modulated Continuous Wave (FMCW)

(iii) No Modulation on Pulse (NMOP)

(iv) Linear Frequency Modulation (LFM)

(a) LFM ascending (LFMa)

(b) LFM descending (LFMd)

(c) LFM ascending - descending (LFMad)

(d) LFM descending - ascending (LFMda)

(v) Non-Linear Frequency Modulation (NLFM)

(a) NLFM forward (NLFMf)

(b) NLFM reverse (NLFMr)

(vi) Stepped Frequency Modulation (SFM) of 2 Level, 4 Level, and 8 Level

(a) SFM ascending (SFMa)

(b) SFM descending (SFMd)

(vii) Phase Modulation (PM)

(a) Bi-Phase Modulation (BPM) of 2-bit, 3-bit, 4-bit, 5-bit, 7 bit, 11 bit, and 13 bit

(viii) Hybridization of LFM and BPM

(a) LFMa with BPM

(b) LFMd with BPM

(ix) Hybridization of SFM and BPM

(a) SFMa with BPM

(b) SFMd with BPM

Total sixteen types of modulations are measured using decision-tree algorithms.

5.3.2 Modelling and characteristics of complex radar signals

Modern radars are exhibiting complex radar waveforms. These waveforms include NMCW, FMCW, NMOP, LFM, NLFM, SFM, BPM, LFM with BPM, and SFM with BPM. The following signal including exotic signals is considered and modelled. They are described as below:

(i) Signal with No Modulation: No-modulation continuous wave (NMCW) and no-modulation on pulse (NMOP) signals does not consist of any modulation. The discrete version of time-domain signal $x(t)$ is given as,

$$x(n) = A.exp[j(2\pi fnt_s + \phi)] \tag{5.19}$$

Where A denotes the carrier amplitude, ϕ denotes the initial phase, f denotes carrier frequency, t_s denotes sampling time, and $n = 1, 2, 3, \ldots N$. for NMOP signals. For simplicity, $\psi(\theta) = 0$, and $\varepsilon(n) = 0$.

When n=1,2,3,…,∞ and signals with T > 1 ms are considered as NMCW and below 1ms, they are considered as pulsed signals, where T denotes the time duration.

(ii) Linear Frequency Modulation (LFM): LFM ascending (LFMa), LFM descending (LFMd), LFM ascending-descending (LFMad), and LFM descending-ascending (LFMda) chirp signals are considered as LFM signals. These signals are also known as Triangular FM.

(a) LFMa: LFMa signal is generated as given by [127],

$$x(n) = A.exp[j(2\pi fnt_s + \phi + \pi\alpha n^2 t^2)] \quad (5.20)$$

for n = (-N/2), (-N/2)+1, ….., -1

Where α is the slope of the LFMa.

(b) LFMd: LFMd signal is generated as given by [127],

$$x(n) = A.exp[j(2\pi fnt_s + \phi + \pi\beta n^2 t^2)] \quad (5.21)$$

for n = 0, 1, 2, …..,, (-N/2)-1.

Where β is the slope of the LFMd. Usually, LFMa and LFMd signals have the same slope, i.e. $\beta = \alpha$.

(c) LFMad and LFMda: LFMad and LFMda signals are generated using a combination of the above two equations. The frequency f is the instantaneous frequency at the peak of the triangular frequency variation, which is the maximum instantaneous frequency within the observation duration in the case of LFMad. The slope α and β are calculated as $2\delta f/\tau$, where δf is the bandwidth with in the time period τ. The parameter τ is a fixed value. The waveform is characterized by f, δf, α, and β.

(iii) Non-Linear Frequency Modulation (NLFM): NLFM signal is represented as given by [127],

$$x(n) = A.exp[j(2\pi fnt_s + \phi + (\delta f/2f_m)\sin(2\pi f_m nt_s))] \quad (5.22)$$

Where the $\delta f/2$ is the peak deviation, f_m is the frequency of the sinusoidal modulating frequency, n = 1, 2, 3,…, N if the signal is narrowband, it means $\frac{\delta f}{2f_m} \ll 1$. It is assumed that only a fraction of the cycle is sampled over an observation time. In the case of the wideband FM signal, $\frac{\delta f}{2f_m} \gg 1$. NLFM forward and NLFM reverse is represented as NLFMf and NLFMr respectively.

(iv) Stepped Frequency Modulation (SFM): SFM signal is generated as below

$$x(n) = A.exp[j(2\pi f_h n t_s + \phi)] \quad (5.23)$$

for n = 1,2,3, ...,N.

Where f_h is the frequency of h^{th} step, and h=1,2,3,…,H. H is the number of steps. Usually, H is in the sequence of 2, 4, 8,…etc. SFM ascending and SFM descending is represented as SFMa and SFMd respectively.

(v) Phase Modulation (PM): Bi-phase Modulation (BPM) is one of the phase modulations and it is generated as given by [127],

$$x(n) = A.exp[j(2\pi f n t_s + \phi + \theta(n))] \quad (5.24)$$

Where $\theta(n) = \pi(1-n)$, when the zero bits of the code sequences are sampled and $\theta(n) = \theta$, when the one bits of the code sequence are sampled. The phase shift θ can be 0^0 and 180^0 in the case of BPM.

(vi) LFM with BPM:

(a) LFMa with BPM: LFM ascending with BPM exotic signal is generated below:

$$x(n) = A.exp[j(2\pi f n t_s + \phi + \pi\alpha n^2 t^2 + \theta(n))] \quad (5.25)$$

(b) LFMd with BPM: LFM descending with BPM exotic signal is generated below:

$$x(n) = A.exp[j(2\pi f n t_s + \phi - \pi\beta n^2 t^2 + \theta(n))] \quad (5.26)$$

(vii) SFM with BPM: SFM with BPM exotic signal is generated below:

$$x(n) = A.exp[j(2\pi f_h n t_s + \phi + \theta(n))] \quad (5.27)$$

5.3.3 Practical significance of modulations

Pulse compression

Pulse compression is one of the popular modulations which is used on radar pulses. The LFM, NLFM, and PM are the type of pulse compression waveforms. Pulse compression permit radars to utilize a long pulse to achieve large radiated energy, but simultaneously to get the range resolution of a short pulse. It realizes this by employing frequency modulation or phase modulation. Pulse compression is very much useful when the peak power required of a short-pulse radar cannot be achieved with practical transmitters.

Comparison of linear FM and phase-coded pulse compression

Both the modulated waveforms have their application, but linear FM pulse compression has probably been more widely used. The time side lobe of the phase-coded pulse is of the order of 1/BT. The peak side lobe of the chirp waveform is generally higher but with low SNR.

Other Pulse compression waveforms

Other pulse-compression methods include nonlinear FM, discrete frequency-shift, poly-phase codes, compound Barker codes, code sequencing, complementary codes, pulse burst, and stretch.

Nonlinear FM

The nonlinear-FM waveform with a constant-amplitude time envelope provides a compressed waveform with low time-side lobes at the output of the receiver. The nonlinear FM is more sensitive to Doppler-frequency shifts and is not Doppler-tolerant.

Discrete frequency-shift or time-frequency coded

The discrete frequency-shift or time-frequency coded waveform is generated by dividing a long pulse into a series of contiguous sub pulses and shifting the carrier frequency from sub pulse to sub pulse. The frequency steps are separated by the reciprocal of the sub pulse width. This provides a less range resolution.

Application of short pulse to radar

Conventionally short-pulse is used by radar for the following purposes:

(i) Range resolution
(ii) Range accuracy
(iii) Clutter reduction
(iv) Clint reduction
(v) Multipath resolution
(vi) Minimum range
(vii) Target classification
(viii) ECCM
(ix) Doppler tolerance

A short-pulse radar is also having some disadvantages. It requires more bandwidth with the possibility for interference to other users of the band. Pulse compression is a method for achieving most of the benefits of a short pulse while keeping within the practical constraints of the peak power limitation.

5.3.4 Decision-tree modulation recognition algorithm

The IF signal is a down-converted signal of RF signal digitized at the sampling frequency f_s which is equivalent to $f_s = 4f_c/3$, where f_c is the center frequency of the IF signal[48]. Four samples are latched into FPGA coming from ADC at the clock rate of $f_s/4$. The samples are latched at both the clock edges. All eight samples are processed in parallel at $f_s/8$ clock rate and results are combined at the output.

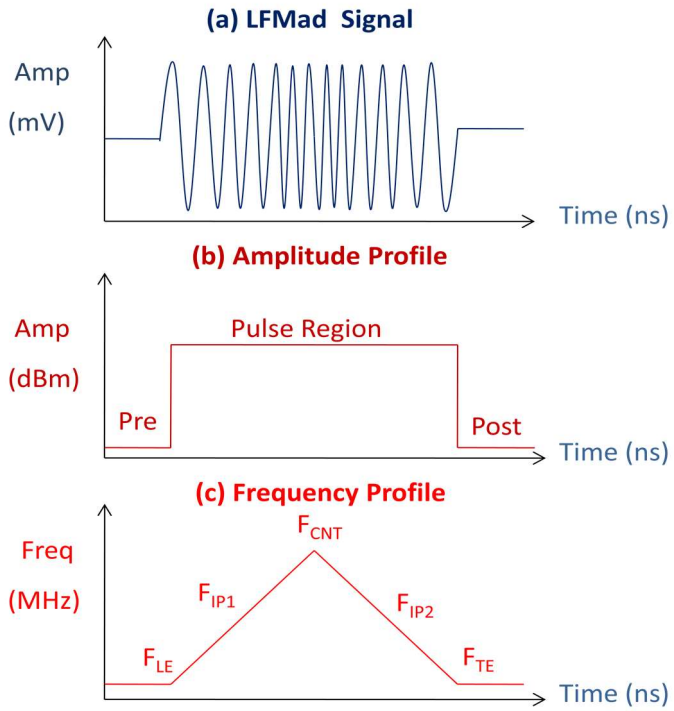

Figure 5.7: LFMad signal and their amplitude and frequency profiles.

The instantaneous amplitude and instantaneous frequency profiles are generated using the moving autocorrelation approach. LFMad and FMCW signals frequency profiles are shown in Figure 5.7 and Figure 5.8 respectively for presentation purposes. In the case of pulsed signals, the pre-trigger and post-trigger region of the pulse is also captured to get the complete intra-pulse information including rise-time and fall-time. The pre-trigger region is captured based on the circular buffer memory concept which is implemented in first-in-first-out (FIFO) memory. The instantaneous frequency profile is used to extract frequency at various points. The frequency is extracted at an equal time interval at five different points

from the stored instantaneous frequency profiles as shown in Figure 5.5. These frequencies are known as leading edge frequency (F_{LE}), trailing edge frequency (F_{TE}), center frequency during the pulse (F_{CNT}), the frequency at the first intermediate pint (F_{IP1}), and the frequency at the second intermediate point (F_{IP}). The F_{LE} and F_{TE} are latched at the leading edge (LE) and trailing edge (TE) of the RFP pulse. The RFP is generated using an instantaneous amplitude profile. Whereas to extract frequency at other three points the frequency data is stored during the pulse region in RAM which is generated using block RAM resource of FPGA. The frequency at these three points i.e. F_{IP1}, F_{CNT}, and F_{IP} are fetched from RAM based on the address calculated from the pulse region.

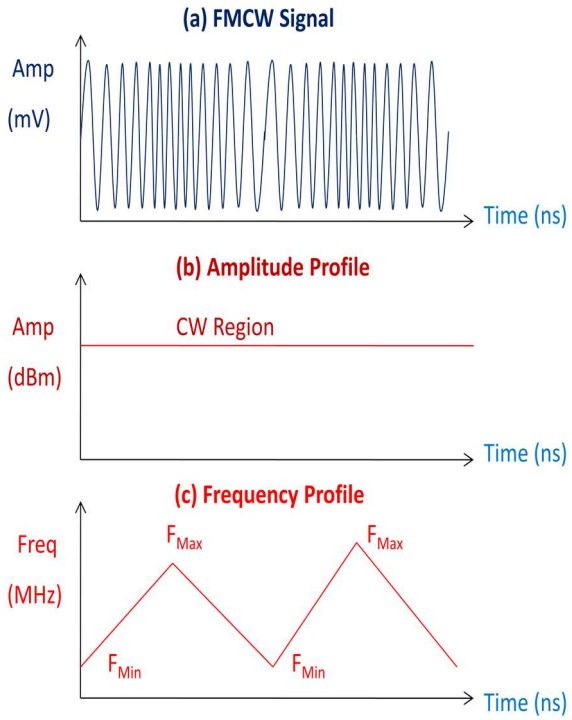

Figure 5.8: FMCW signal and their amplitude and frequency profiles.

In the case of the FMCW signal, the maximum frequency (F_{max}) and minimum frequency (F_{min}) are computed in real-time and stored. The frequency tolerance limit (Δf) and phase tolerance limit ($\Delta \phi$) are used during comparisons and windows are fixed.

The flow chart for the proposed decision-tree modulation recognition algorithm is shown in Figure 5.9. First, the IF signal is captured and amplitude and frequency profiles are computed. The pulse start and pulse end are detected based on high and low-level thresholds respectively. As per the flow chart initially, the signal is distinguished between pulsed and CW signals. If PW is greater than the predefined time limit T, it is declared as MMCW, otherwise, this is considered as a pulsed signal. The frequency profile of the NMCW signal is

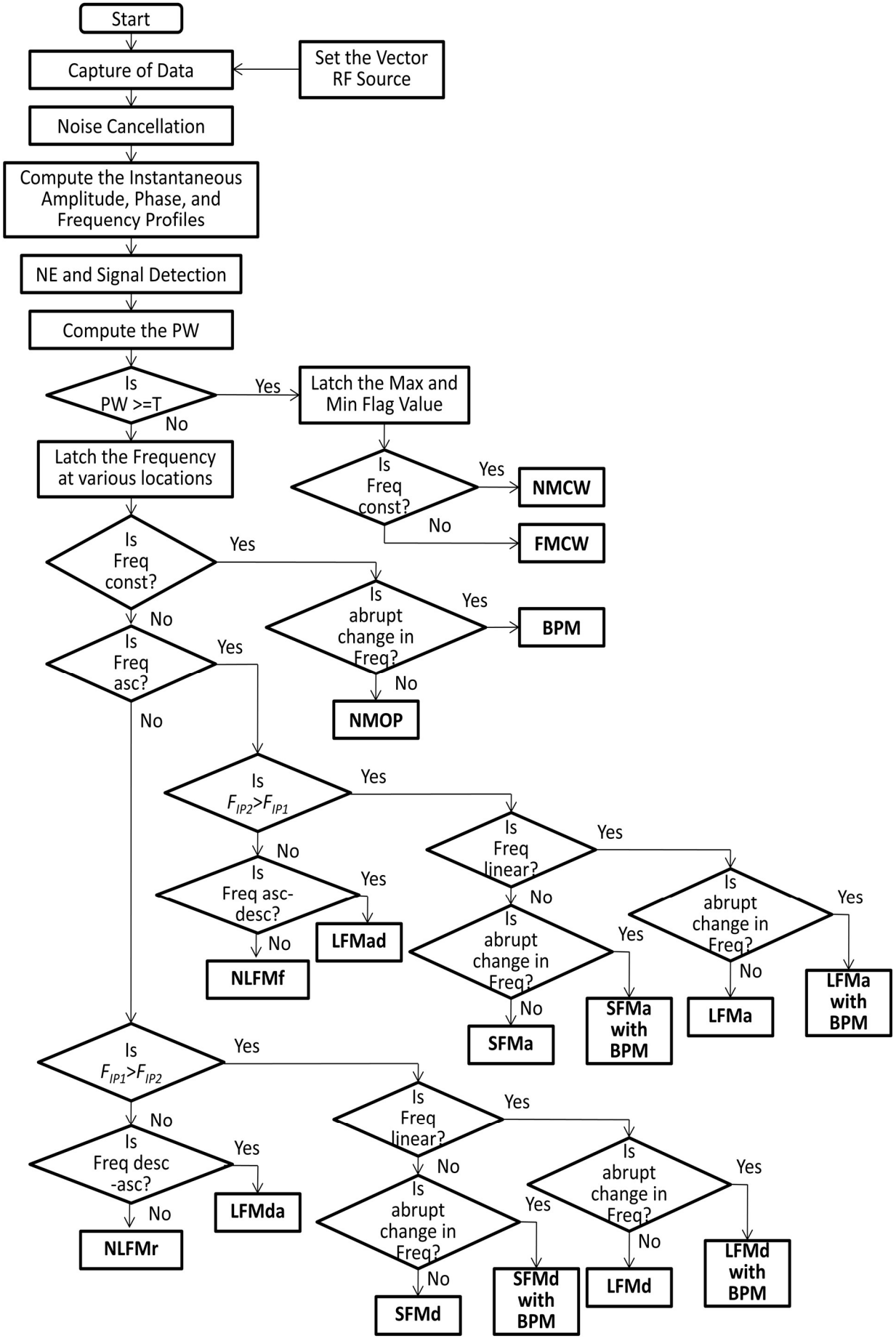

Figure 5.9: Decision-tree algorithm flow chart for modulation recognition.

shown in Figure 5.10. If the signal is CW, the algorithm will look for frequency variations within that period. If F_{max} and F_{min} are within the set tolerance limit (Δf) i.e. frequency is constant, it will be declared as NMCW signal. Whereas, if the difference of F_{max} and F_{min} is more than the Δf, it will be declared as an FMCW signal. The frequency profile of the FMCW signal is shown in Figure 5.11.

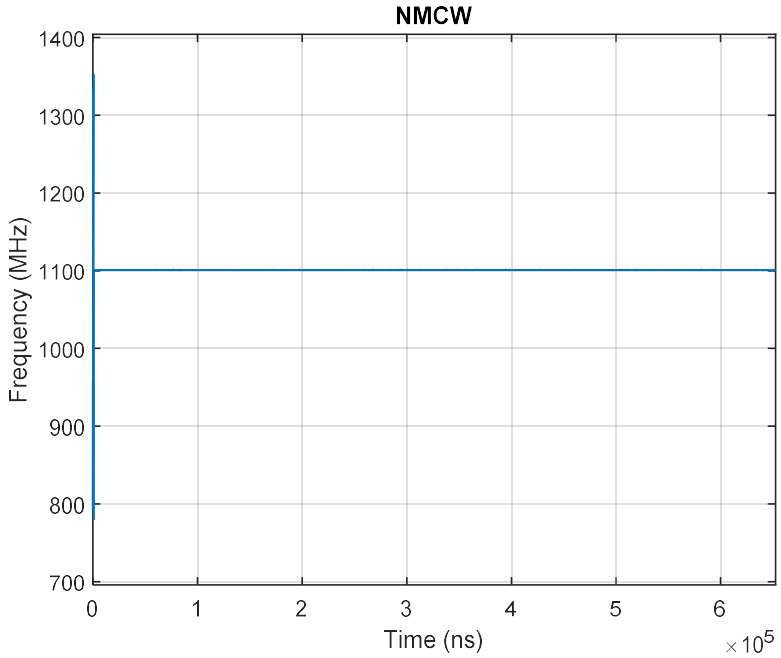

Figure 5.10: NMCW signal frequency profile. Simulation parameters: f = 1.1 GHz, N = 7,00,000 samples, and t_s = 1.5 ns.

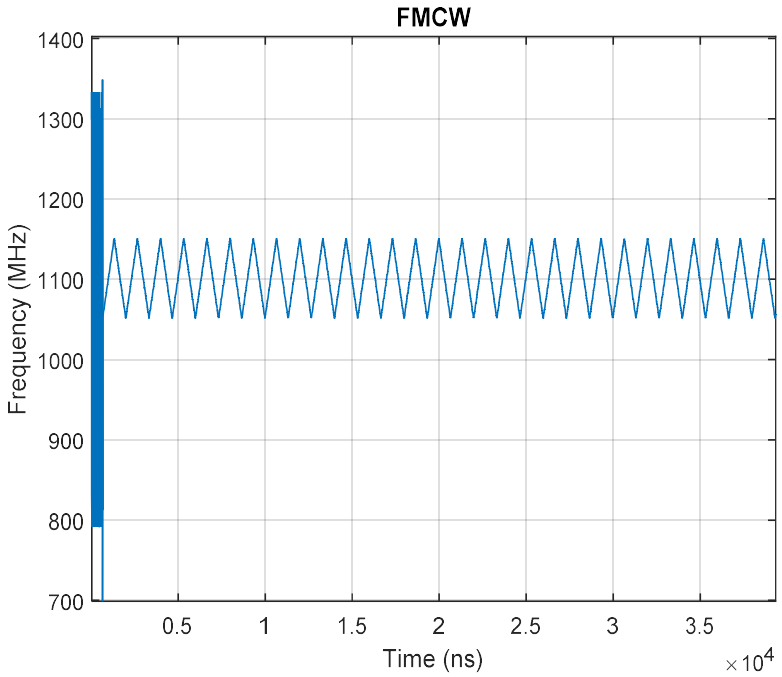

Figure 5.11: FMCW signal frequency profile and zoomed portion only due to visibility, Simulation parameters: f = 1.1 GHz, FD= ±50 MHz, N = 7,00,000 samples, and t_s = 1.5 ns.

If the signal is below predefined time limit T, and if the frequency is constant in the pulse region and there is no frequency discontinuity it is declared as No modulation on pulse (NMOP). The frequency profile of the NMOP signal is shown in Figure 5.12.

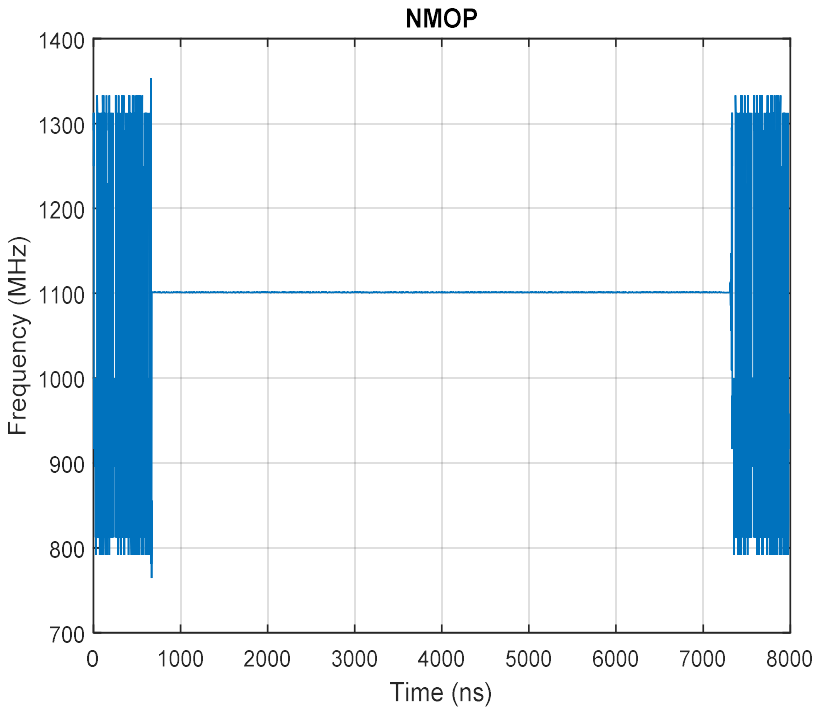

Figure 5.12: NMOP signal frequency profile. Simulation parameters: f = 1.1 GHz, N = 8,000 samples, and t_s = 1.5 ns.

When there is an abrupt change in frequency profile due to a sudden change in phase, it will be declared as BPM in which phase changes occur closed to pi. The number of phase changes and minimum duration is stored. The total width of the signal is divided by the minimum duration and the BPM pattern is identified. BPM pattern starts with 1's and each phase change is represented by 0's from 1's and 1's from 0's and when there is no phase change it will continue with the same 1's or 0's.

There are different lengths of phase modulation that exists and their bit pattern will be different. Table 5.4 shows the different lengths of phase modulation [126]:

Table 5.4: BPM codes with side lobe level

S. No.	Code length	Bi-phase code	Side lobe level (dB)
1	2-bit	10	-6.0
2	3-bit	110	-9.5
3	4-bit	1101, 1110	-12.0
4	5-bit	11101	-14.0
5	7-bit	1110010	-16.9
6	11-bit	11100010010	-20.8
7	13-bit	1111100110101	-22.3

If there is a sudden change in frequency, this change is recognized and noted. If there is only one change, both the portion before and after the change are equal. The bit-pattern is identified as {10} which is 2-bit BPM. If there is only one change but the first half bit time is double than the second half. The bit-pattern is identified as {110} which is 3-bit BPM. The 2-bit and 3-bit BPM signal frequency profiles are shown in Figure 5.13 and Figure 5.14 respectively.

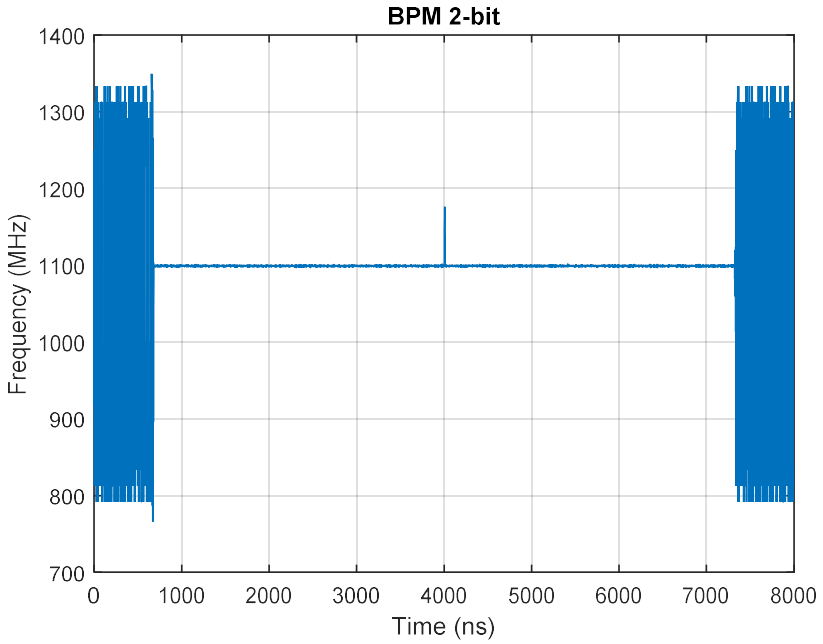

Figure 5.13: BPM 2-bit signal frequency profile. Simulation parameters: f = 1.1 GHz, N = 8,000 samples, and t_s = 1.5 ns.

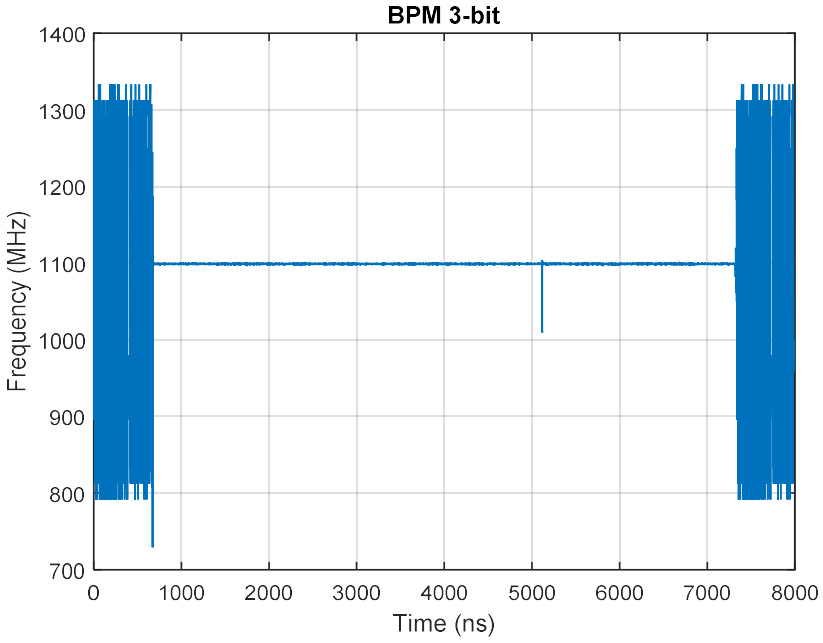

Figure 5.14: BPM 3-bit signal frequency profile. Simulation parameters: f = 1.1 GHz, N = 8,000 samples, and t_s = 1.5 ns.

If there are two changes in frequency profile, and the first portion consists of the two-bit widths. Accordingly, the bit pattern is identified as {1101} which is 4-bit BPM. If there are two changes in frequency profile, and the first portion consists of three-bit widths. The bit-pattern is identified as {11101} which is 5-bit BPM. The 4-bit and 5-bit BPM signal frequency profiles are shown in Figure 5.15 and Figure 5.16 respectively.

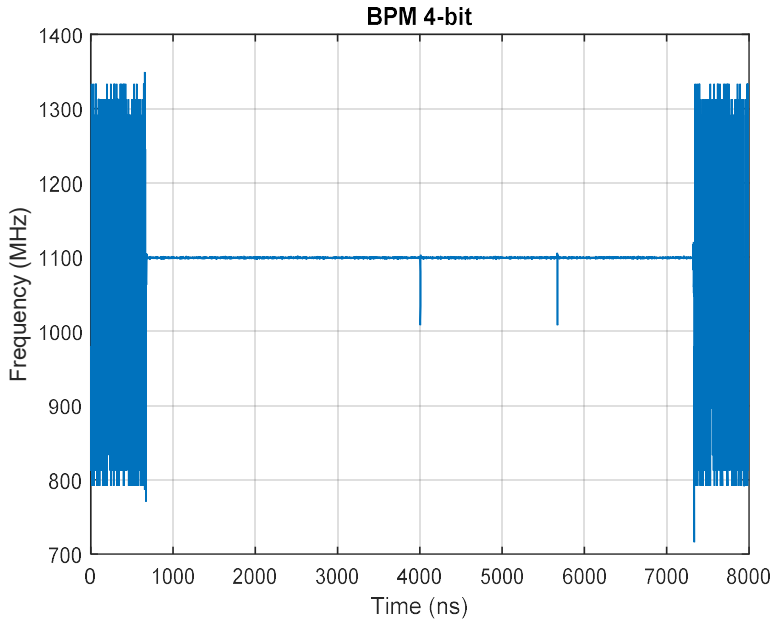

Figure 5.15: BPM 4-bit signal frequency profile. Simulation parameters: f = 1.1 GHz, N = 8,000 samples, and t_s = 1.5 ns.

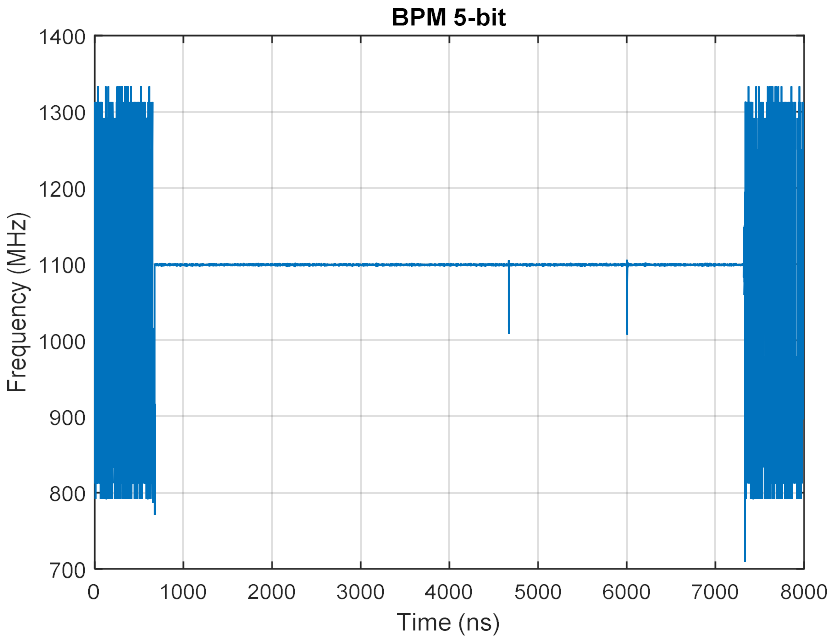

Figure 5.16: BPM 5-bit signal frequency profile. Simulation parameters: f = 1.1 GHz, N = 8,000 samples, and t_s = 1.5 ns.

If there are three changes in frequency profile and based on phase changes the bit-pattern is identified as {1110010} which is 7-bit BPM. If there are five changes in frequency profile and based on phase changes the bit-pattern is identified as {11100010010} which is 11-bit BPM. The 7-bit and 11-bit BPM signal frequency profiles are shown in Figure 5.17 and Figure 5.18 respectively.

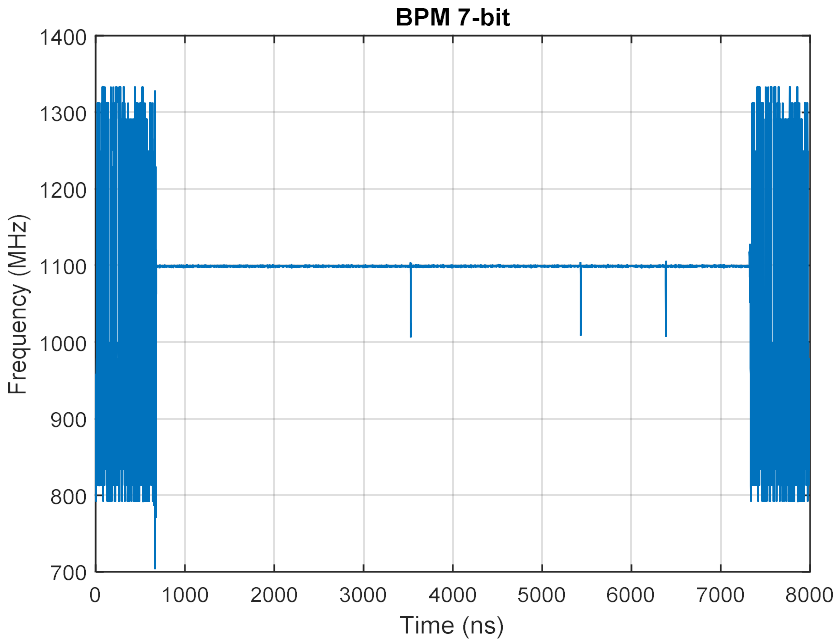

Figure 5.17: BPM 7-bit signal frequency profile. Simulation parameters: f = 1.1 GHz, N = 8,000 samples, and t_s = 1.5 ns.

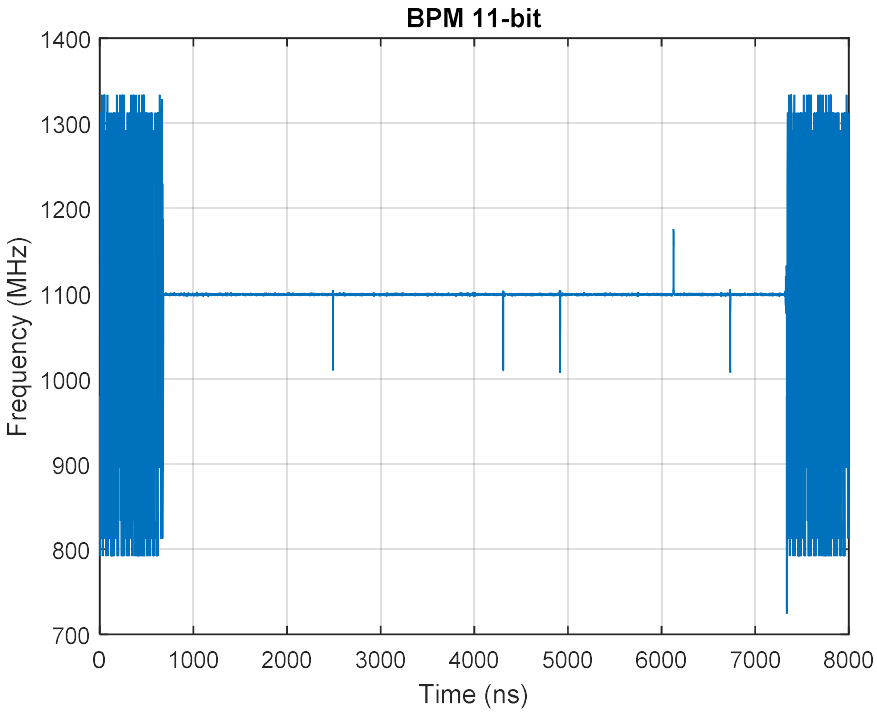

Figure 5.18: BPM 11-bit signal frequency profile. Simulation parameters: f = 1.1 GHz, N = 8,000 samples, and t_s = 1.5 ns.

The bit-pattern for 13-bit BPM code is represented as {1111100110101} based on total of six phase changes. The frequency profile of 13-bits BPM is represented in Figure 5.19. Practically, 13-bit BPM is frequently used in radar systems as it gives a minimum side lobe level of -22.3 dB.

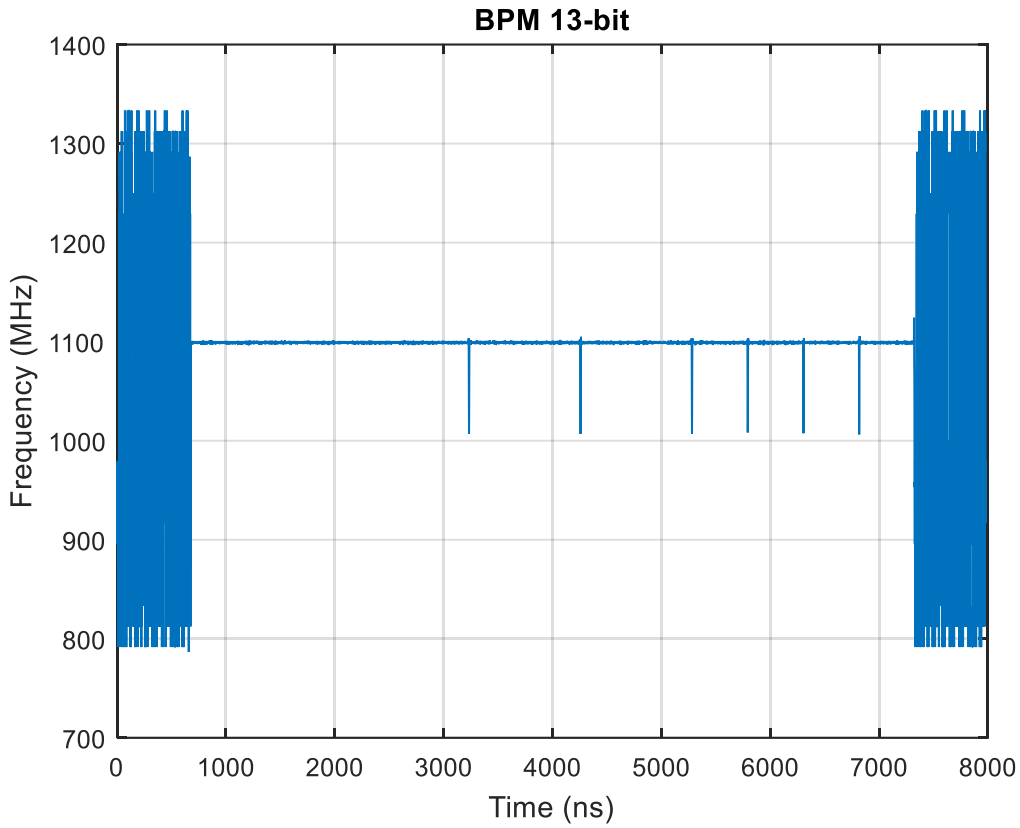

Figure 5.19: BPM 13-bit signal frequency profile. Simulation parameters: f = 1.1 GHz, N = 8,000 samples, and t_s = 1.5 ns.

The signal is declared as NLFMf when F_{IP2} is less than F_{IP1} as well as frequency is sinusoidal. Whereas, if F_{IP1} is greater than F_{IP2} as well as frequency is sinusoidal, the signal is declared as NLFMr. SFMa is declared when F_{IP2} is greater than F_{IP1} as well as frequency changes in steps. If F_{IP1} is greater than F_{IP2} as well as frequency changes in steps, the signal is declared as SFMd. In SFM signals, there will be a step-change in the frequency. NLFM signals are generated based on the approximation of SFM signals. The frequency profiles of NLFM and SFM signals are represented in Figure 5.20 to Figure 5.27. More than two steps are identified when the frequency is latched with more number of intermediate points on the frequency profile.

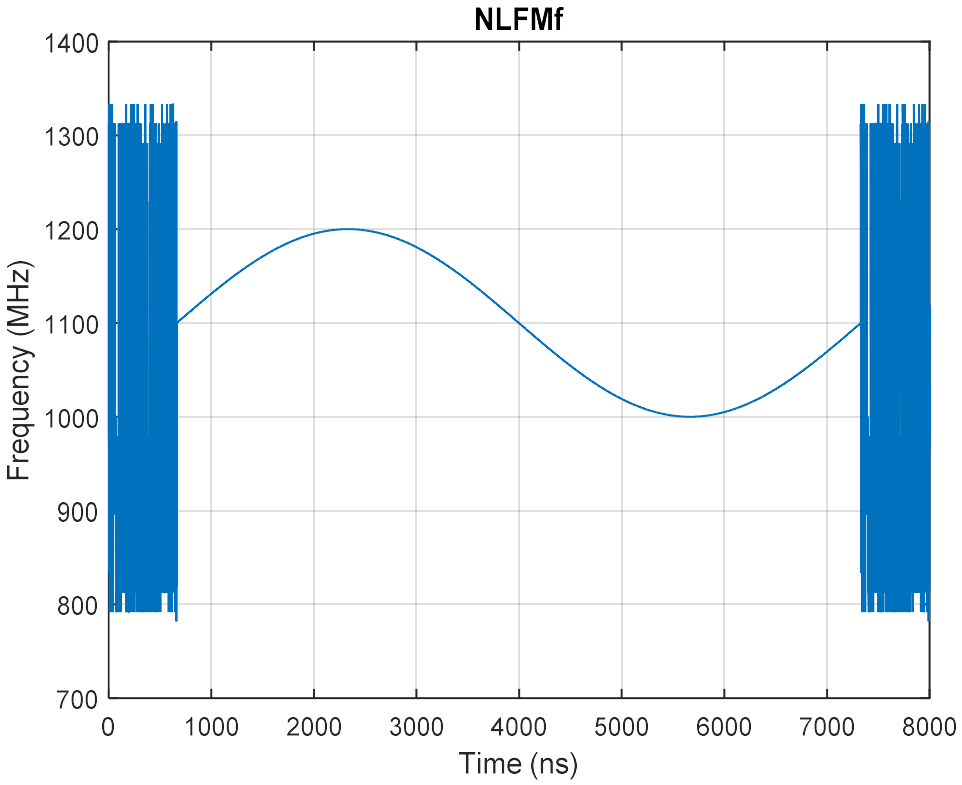

Figure 5.20: NLFM forward signal frequency profile, Simulation parameters: f = 1.1 GHz, N = 8,000 samples, and t_s = 1.5 ns.

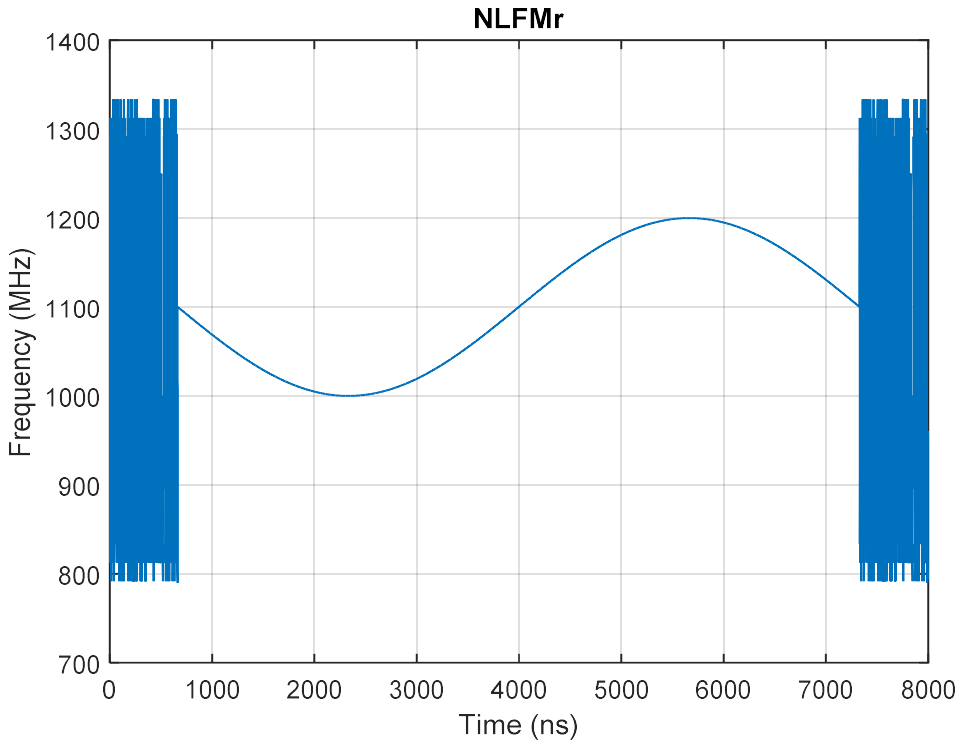

Figure 5.21: NLFM reverse signal frequency profile, Simulation parameters: f = 1.1 GHz, N = 8,000 samples, and t_s = 1.5 ns.

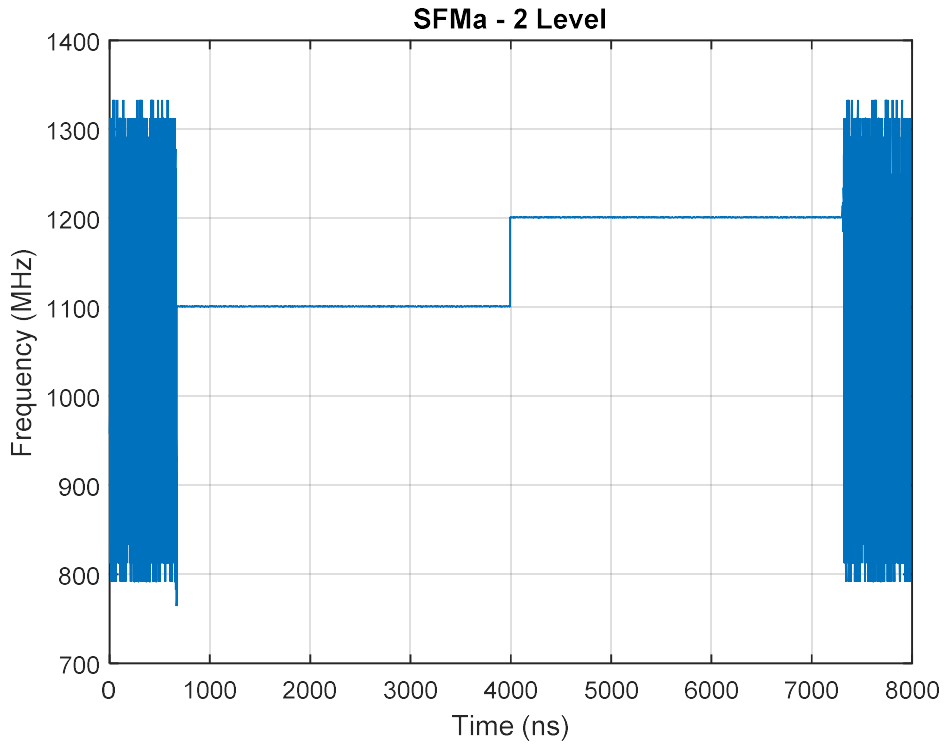

Figure 5.22: SFMa - 2 level signal frequency profile. Simulation parameters: f = 1.1 GHz, N = 8,000 samples, and t_s = 1.5 ns.

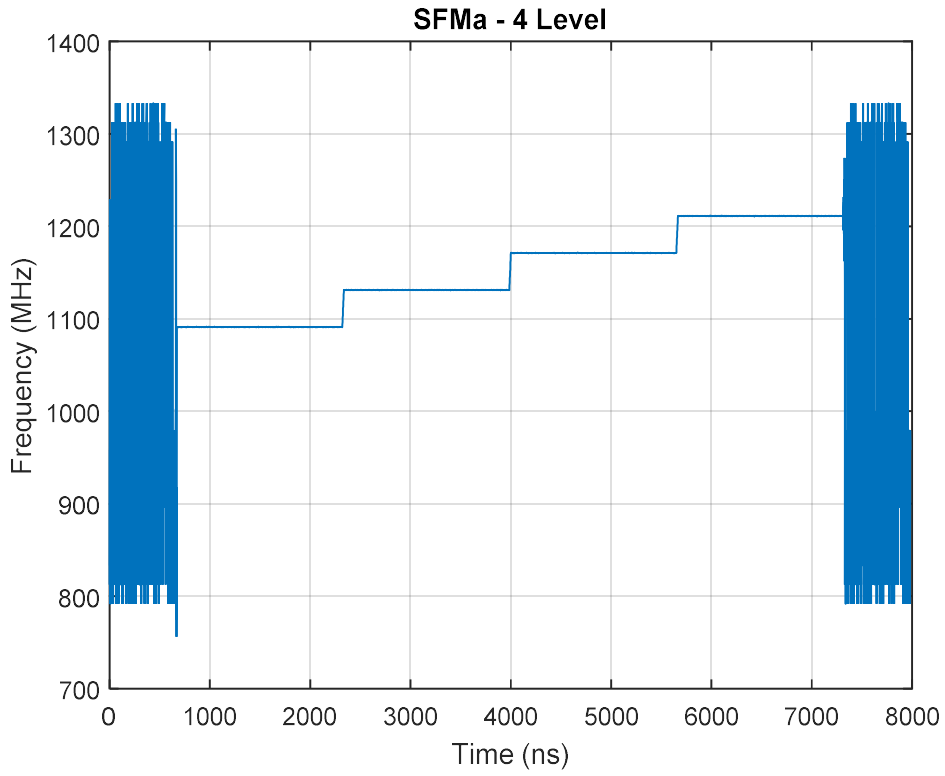

Figure 5.23: SFMa - 4 level signal frequency profile. Simulation parameters: f = 1.1 GHz, N = 8,000 samples, and t_s = 1.5 ns.

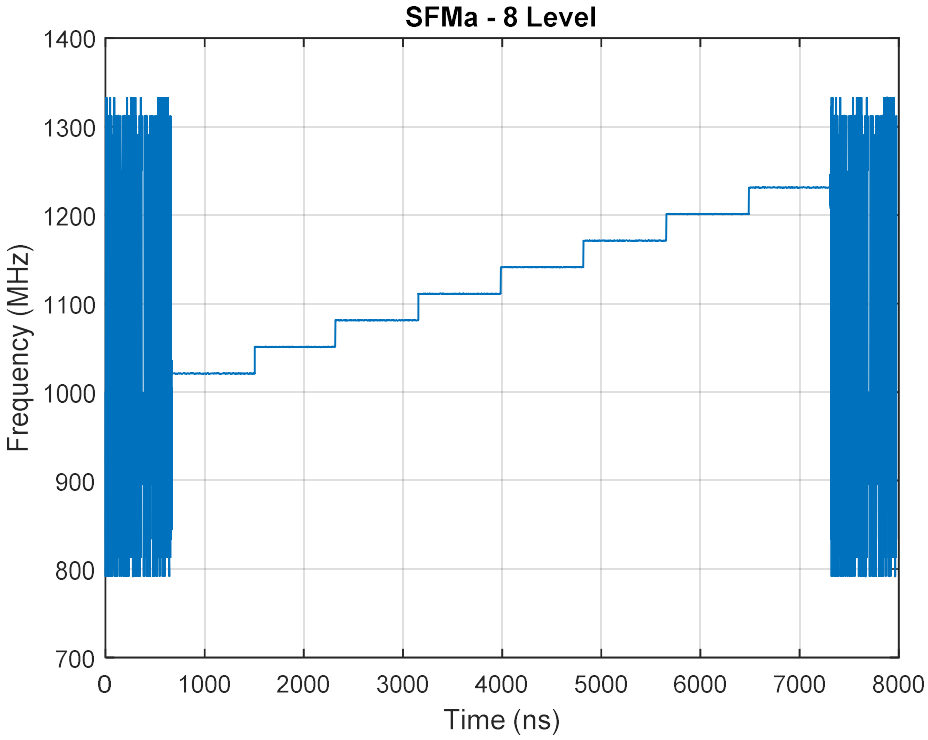

Figure 5.24: SFMa - 8 level signal frequency profile. Simulation parameters: f = 1.1 GHz, N = 8,000 samples, and t_s = 1.5 ns.

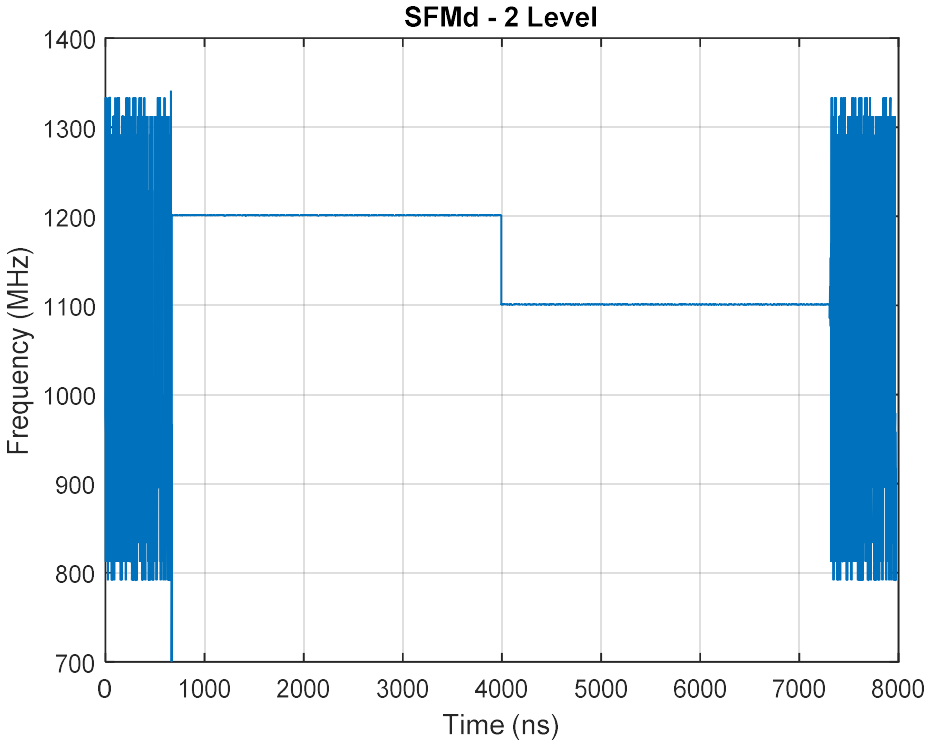

Figure 5.25: SFMd - 2 level signal frequency profile. Simulation parameters: f = 1.1 GHz, N = 8,000 samples, and t_s = 1.5 ns.

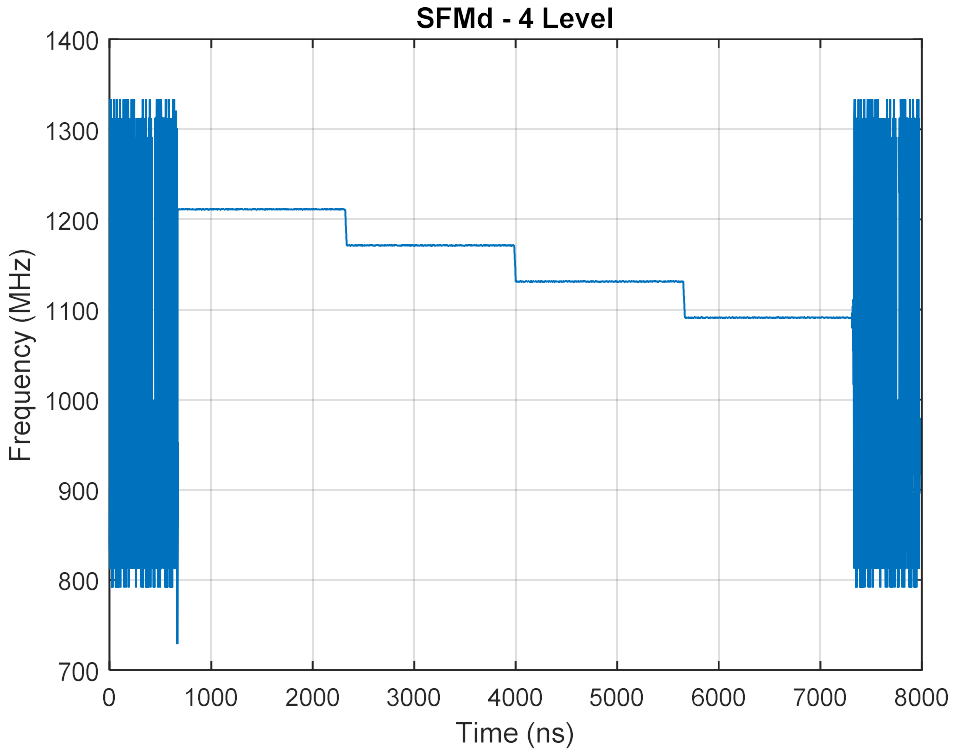

Figure 5.26: SFMd - 4 level signal frequency profile. Simulation parameters: f = 1.1 GHz, N = 8,000 samples, and t_s = 1.5 ns.

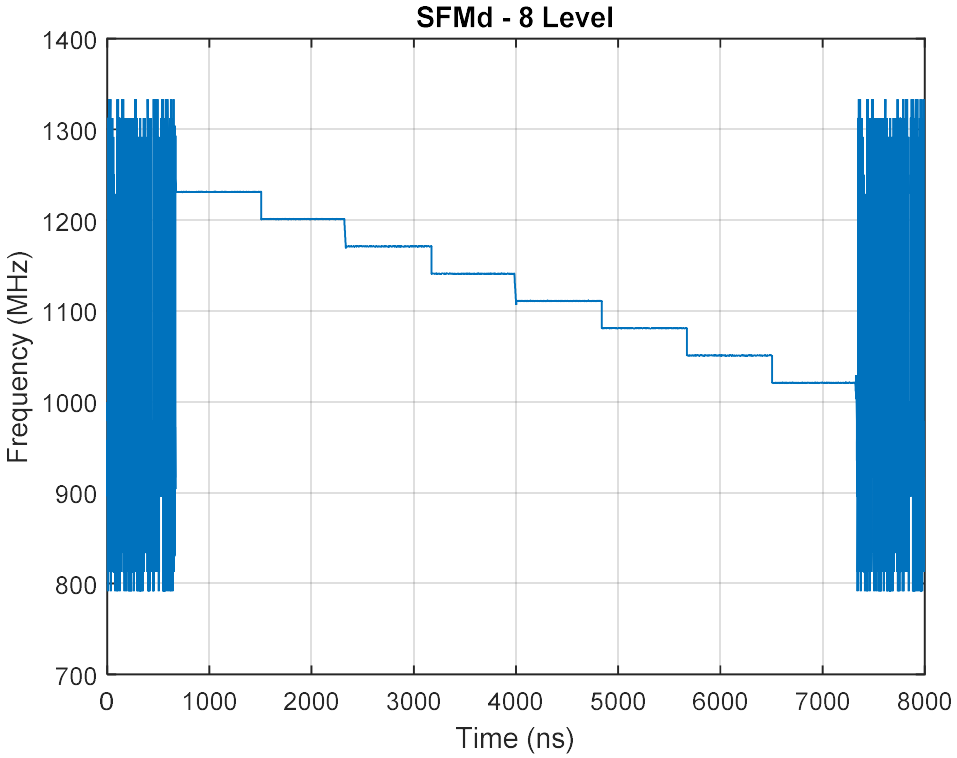

Figure 5.27: SFMd - 8 level signal frequency profile. Simulation parameters: f = 1.1 GHz, N = 8,000 samples, and t_s = 1.5 ns.

When the linear change of frequency trend is ascending, descending or both in the pulse region the modulation present is known as LFM. Modulation is declared as LFMa when F_{IP2} is greater than F_{IP1} as well as frequency changes linearly. Whereas, if F_{IP2} is less than F_{IP1} and frequency changes in ascending-descending order, the signal modulation is declared as LFMad. When F_{IP1} is greater than F_{IP2} and frequency changes linearly, the signal modulation is declared as LFMd. If F_{IP1} is less than F_{IP2} and frequency changes in descending-ascending order, the signal is declared as LFMda. Above mentioned LFM signals frequency profile is illustrated in Figure 5.28 to Figure 5.32.

The frequency profile shown in Figure 5.28, is generated for frequency deviation of 500 MHz i.e. ±250 MHz. This shows that the multilevel autocorrelation algorithm used to identify LFM signals will work well as this algorithm is not breaking anywhere in the band of interest of 750 MHz to 1250 MHz.

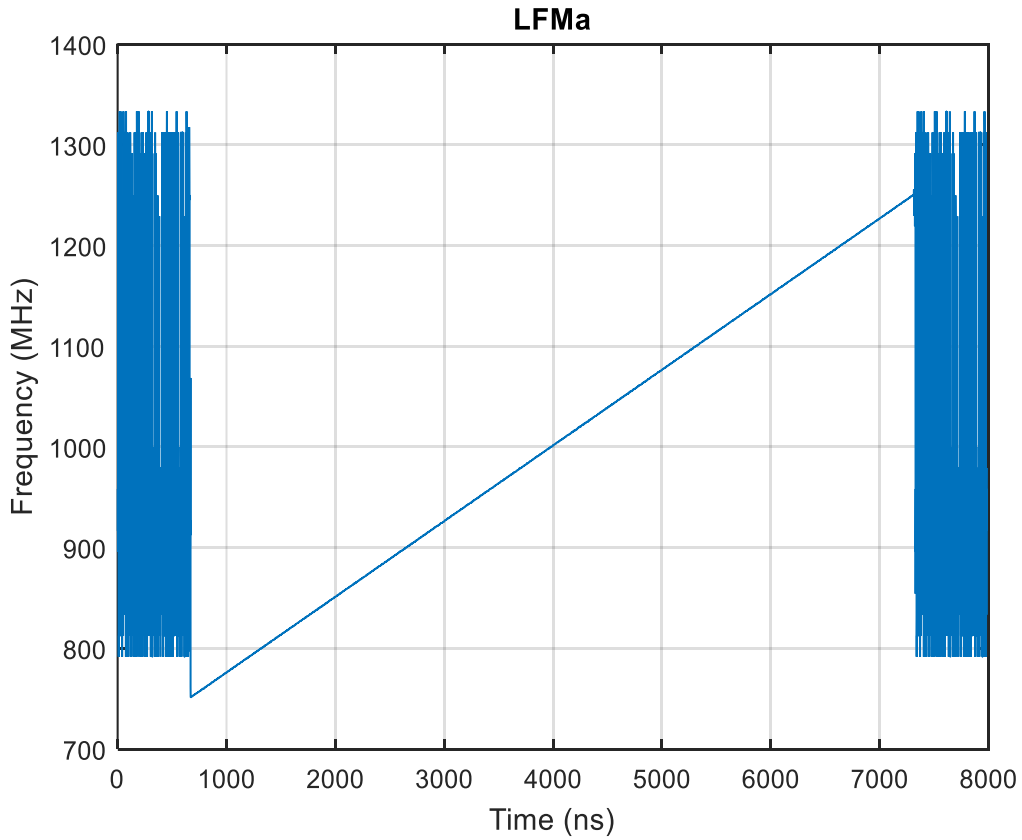

Figure 5.28: LFMa signal frequency profile. Simulation parameters: fc = 1 GHz, FD = ±250 MHz, N = 8,000 samples, and t_s = 1.5 ns.

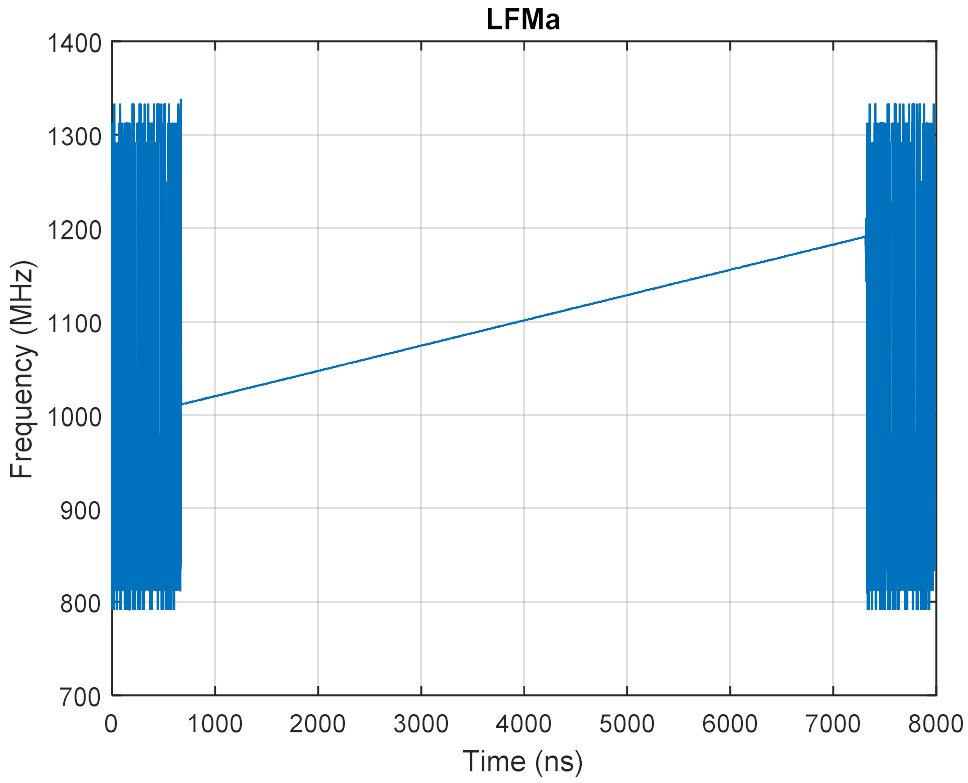

Figure 5.29: LFMa signal frequency profile. Simulation parameters: fc = 1.1 GHz, FD = ±100 MHz, N = 8,000 samples, and t_s = 1.5 ns.

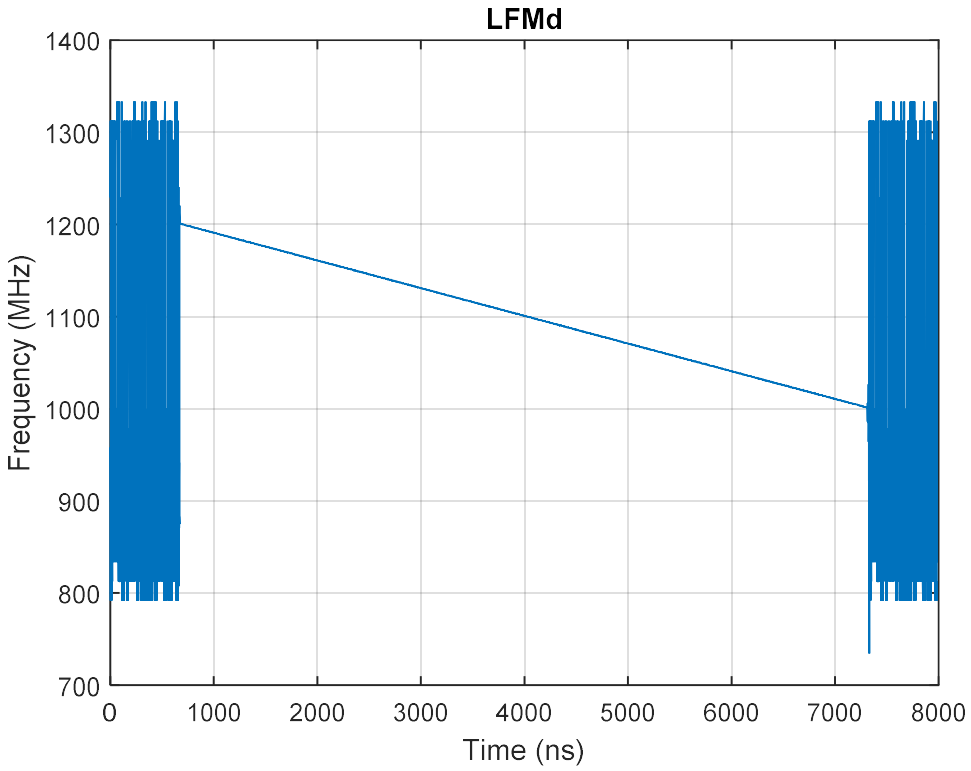

Figure 5.30: LFMd signal frequency profile. Simulation parameters: fc = 1.1 GHz, FD = ±100 MHz, N = 8,000 samples, and t_s = 1.5 ns.

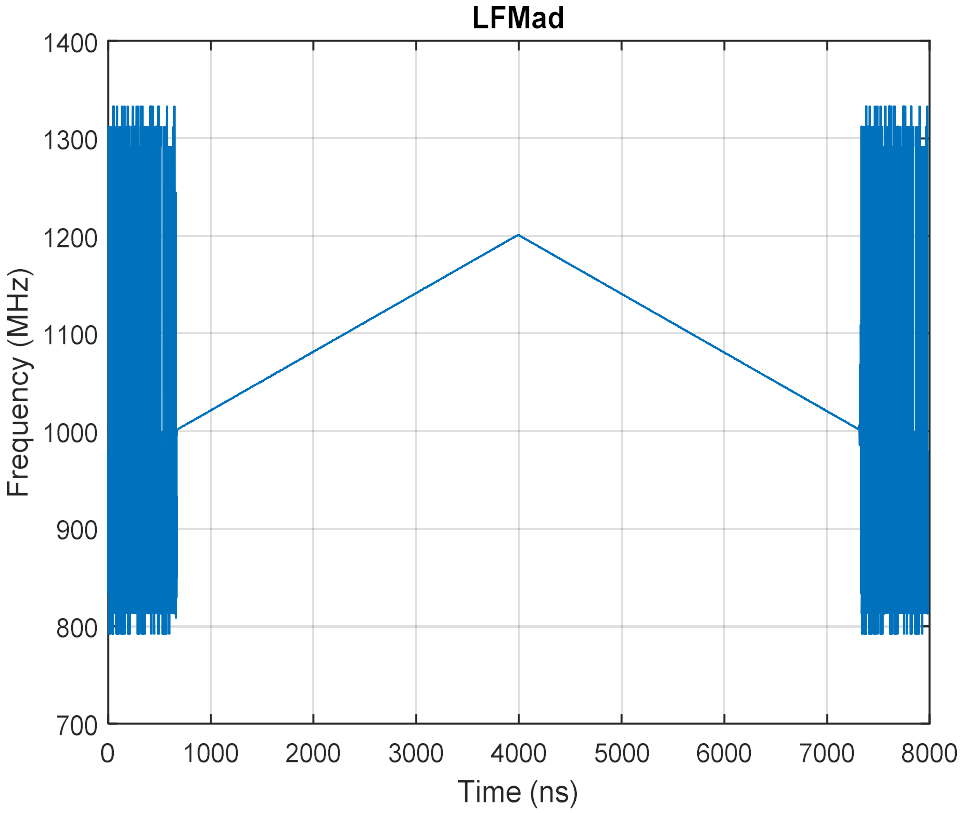

Figure 5.31: LFMad signal frequency profile. Simulation parameters: fc = 1.1 GHz, FD = ±100 MHz, N = 8,000 samples, and t_s = 1.5 ns.

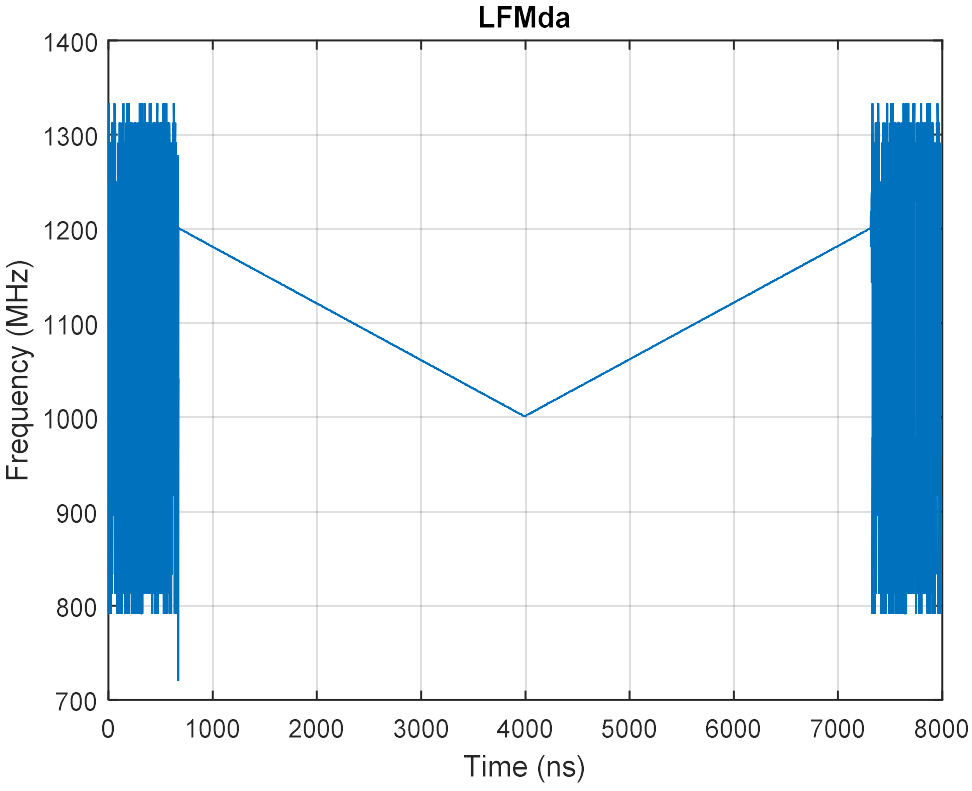

Figure 5.32: LFMda signal frequency profile. Simulation parameters: fc = 1.1 GHz, FD = ±100 MHz, N = 8,000 samples, and t_s = 1.5 ns.

When a pulsed signal is detected and frequency modulation exists. If the frequency is linear with an ascending trend and there is an abrupt change in frequency, the modulation will be declared as LFMa with BPM. The frequency profile of LFMa with 13-bit BPM is shown in Figure 5.33. Otherwise, it will be declared as LFMa itself. Similarly, if the frequency is linear with a descending trend and there is an abrupt change in frequency, the modulation will be declared as LFMd with BPM. The frequency profile of LFMd with 13-bit BPM is shown in Figure 5.34. Otherwise, it will be declared as LFMd alone.

If there is stepped frequency in pulsed waveform exists. If the frequency is stepped with an ascending trend and there is an abrupt change in frequency within each step. It will be declared as SFMa with BPM. The frequency profile of SFMa with 13-bit BPM is shown in Figure 5.35. Steps with ascending trend and without abrupt change in frequency will be declared as SFMa. If it is found that frequency is stepped with the descending trend and there is an abrupt change in frequency within each step. It will be declared as SFMd with BPM. The frequency profile of SFMd with 13-bit BPM is shown in Figure 5.36. Steps with the descending trend and without an abrupt change in the frequency will be declared as SFMd.

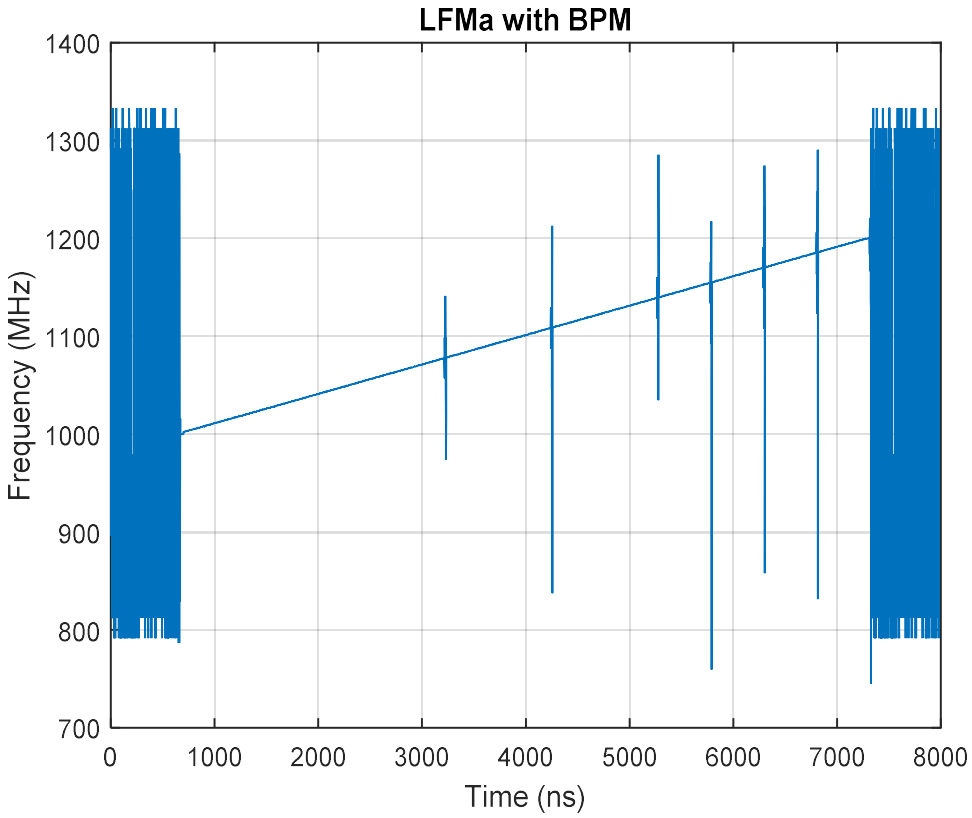

Figure 5.33: Signal frequency profile of LFMa with BPM 13-bit. Simulation parameters: fc = 1.1 GHz, FD = ±100 MHz, N = 8,000 samples, and t_s = 1.5 ns.

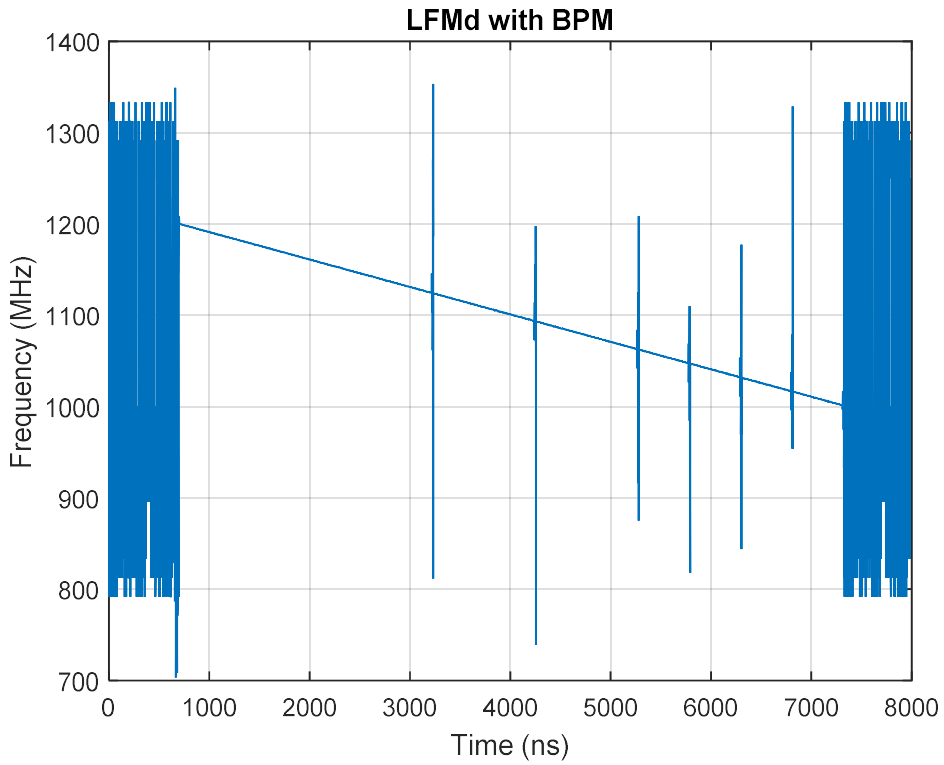

Figure 5.34: Signal frequency profile of LFMd with BPM 13-bit. Simulation parameters: fc = 1.1 GHz, FD = ±100 MHz, N = 8,000 samples, and t_s = 1.5 ns.

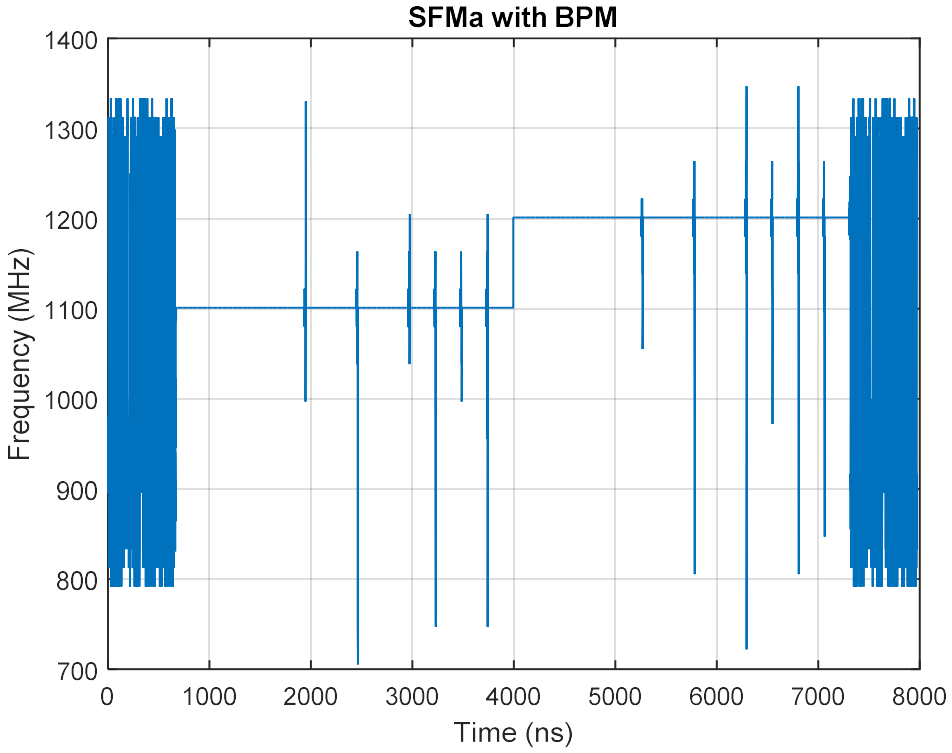

Figure 5.35: Signal frequency profile of SFMa with BPM 13-bit. Simulation parameters: fc = 1.1 GHz, FD = ±100 MHz, N = 8,000 samples, and t_s = 1.5 ns.

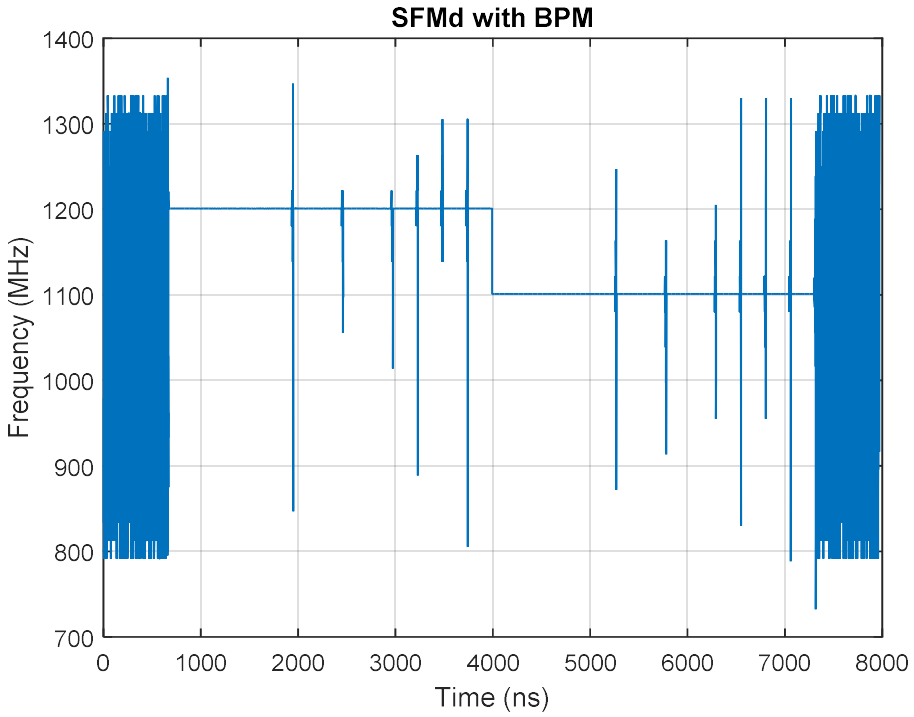

Figure 5.36: Signal frequency profile of SFMd with BPM 13-bit. Simulation parameters: fc = 1.1 GHz, FD = ±100 MHz, N = 8,000 samples, and t_s = 1.5 ns.

Once the type of modulation is found out, their parameter is also estimated like slope in the case of LFM, which is known as chirp rate in MHz/us. Similarly, a number of steps, BPM code is the parameters in case of SFM and BPM signals respectively. Both modulation type (MT) and modulation parameter (MP) are represented using four bytes in Table 5.5 and Table 5.6 respectively.

Table 5.5: Representation of bit-pattern for modulation type (MT)

Modulation Type (MT)	Bit-pattern for MT			
	B[15:12]	B[11:8]	B[7:4]	B[3:0]
NMCW	0000	0000	0000	0001
FMCW	0000	0000	0000	0010
NMOP	0000	0000	0000	0100
LFMa	0000	0000	0000	1000
LFMad	0000	0000	0001	0000
LFMd	0000	0000	0010	0000
LFMda	0000	0000	0100	0000
NLFMf	0000	0000	1000	0000
NLFMr	0000	0001	0000	0000
SFMa	0000	0010	0000	0000
SFMd	0000	0100	0000	0000
BPM	0000	1000	0000	0000
LFMa with BPM	0000	1000	0000	1000
LFMd with BPM	0000	1000	0010	0000
SFMa with BPM	0000	1010	0000	0000
SFMd with BPM	0000	1100	0000	0000

Table 5.6: Representation of bit-pattern for modulation parameter (MP)

Modulation Type (MT)	Bit-pattern for MP			
	B[15:12]	B[11:8]	B[7:4]	B[3:0]
NMCW	0000	0000	0000	0000
FMCW	DF (kHz)		FD (MHz)	
NMOP	0000	0000	0000	0000
LFMa	0000	0000	UCR (MHz/us)	
LFMad	DCR (MHz/us)		UCR (MHz/us)	
LFMd	DCR (MHz/us)		0000	0000
LFMda	DCR (MHz/us)		UCR (MHz/us)	
NLFMf	0000	0000	0000	0000
NLFMr	0000	0000	0000	0000
SFMa	0000	0000	No. of Steps	
SFMd	0000	0000	No. of Steps	
BPM	0000	0000	BPM Code	
LFMa with BPM	UCR (MHz/us)		BPM Code	
LFMd with BPM	DCR (MHz/us)		BPM Code	
SFMa with BPM	No. of Steps		BPM Code	
SFMd with BPM	No. of Steps		BPM Code	

Minimum SNR required using moving autocorrelation technique and DIQ technique is 1 dB and 8 dB respectively to process all types of modulated signals. Based on this, the sensitivity achieved is -87 dBm and -80 dBm using the proposed algorithm with moving autocorrelation technique and DIQ technique respectively.

The comparison of this work with other similar works is not reasonable because the frequency domain techniques get the inherent processing gain. But they suffer from PW and PRI measurement accuracies. The minimum PW measurement is restricted to the number of FFT points and its percentage of overlapping. Whereas, the proposed time-domain technique measures the minimum PW of the order of 50 ns. The fact of the matter is that lower PW does not have the modulation but still, any processing method should meet all basic system requirements along with critical requirements.

Classification of modulation presented are based on the frequency domain processing and they are implemented on DSP processors for ELINT applications [70]-[71]. Due to the limitations of the number of MACs in the DSP processor these techniques are not suitable for tactical operations. The proposed decision-tree algorithm is implemented on FPGA hardware which provides real-time performance.

5.3.5 Matlab results using field data

Field data is generated using the system front-end. This field data is used to demonstrate the effectiveness and performance of the proposed decision-tree algorithm for modulation recognition.

(i) Field data #1: The field data shown in Figure 5.37 is used as input signal generated using vector signal generator which is contaminated with widely used additive white Gaussian noise (AWGN) and SNR is measured of -2 dB SNR. The same signal is used in the simulation for generating instantaneous amplitude and frequency profile using the autocorrelation technique which is shown in Figure 5.38 and Figure 5.39 respectively.

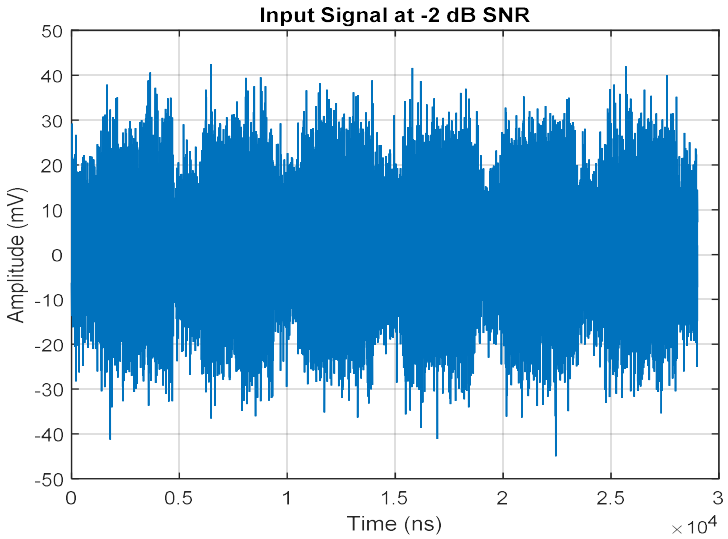

Figure 5.37: Captured signal. Vector signal generator parameters: f = 9.1 GHz, PW = 7 us, PRI = 10 us, fc = 1.1 GHz, samples captured N = 28800 samples, η = -2 dB, and t_s = 1.5 ns.

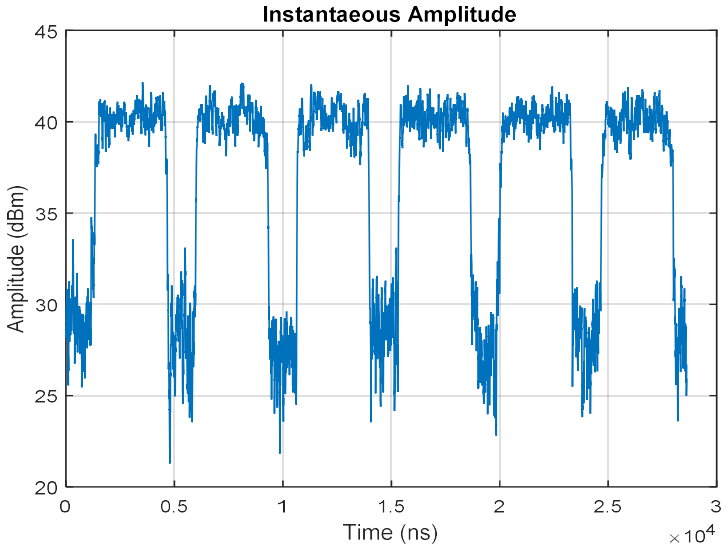

Figure 5.38: Instantaneous amplitude profile. Vector signal generator parameters: f = 9.1 GHz, PW = 7 us, PRI = 10 us, fc = 1.1 GHz, samples captured N = 28800 samples, η = -2 dB, and t_s = 1.5 ns.

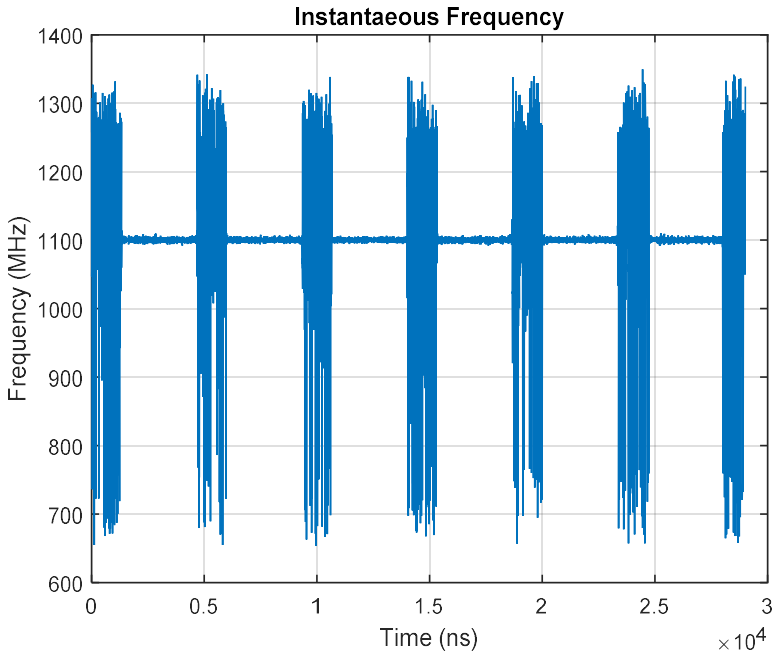

Figure 5.39: Instantaneous frequency profile. Vector signal generator parameters: f = 9.1 GHz, PW = 7 us, PRI = 10 us, fc = 1.1 GHz, samples captured N = 28800 samples, η = -2 dB, and t_s = 1.5 ns.

(i) Field data #2: This field data is captured in the field with the system front end. Data is sampled at 666 MSPS and stored in the system. Only initial pulses of data are shown in Figure 5.40.

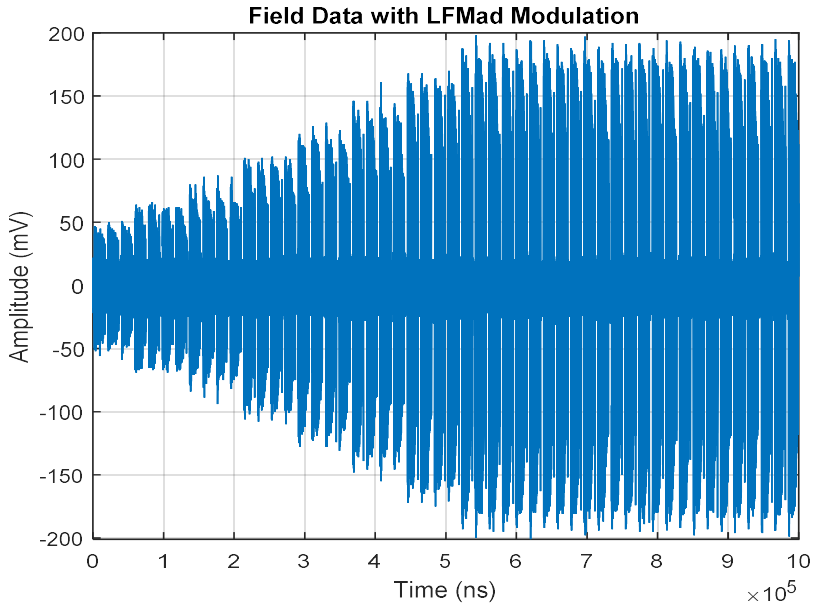

Figure 5.40: Field data with LFMad modulation. Parameters: f = X-band, PW = 19 us, PRI = 100 of us, f_c = 1.0 GHz (±250 MHz), samples captured N = 10,00,000 samples, η = variable, and t_s = 1.5 ns.

Initial 13 pulses are zoomed and shown in Figure 5.41. These samples are considered for noise cancellation and the signal is restored after spectral subtraction. Noise samples are taken from the pre and post samples of the pulses. Restored field data is shown in Figure 5.42.

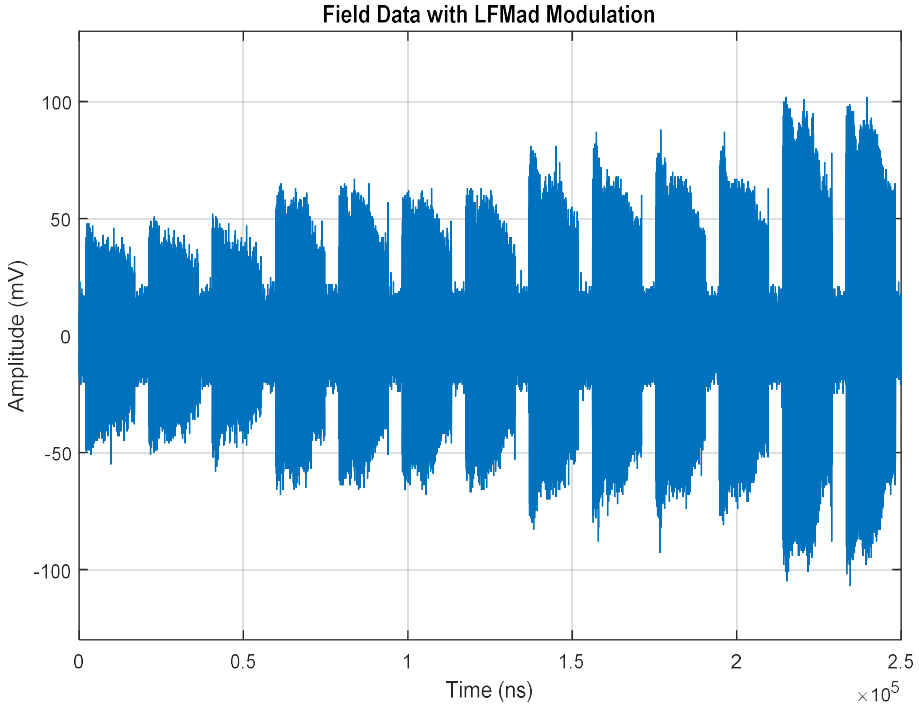

Figure 5.41: Field data with LFMad modulation. Parameters: f = X-band, PW = 19 us, PRI = 100 of us, No. of Pulses = 13, f_c = 1.0 GHz (±250 MHz), samples captured N = 2,50,000 samples, η = variable, and t_s = 1.5 ns.

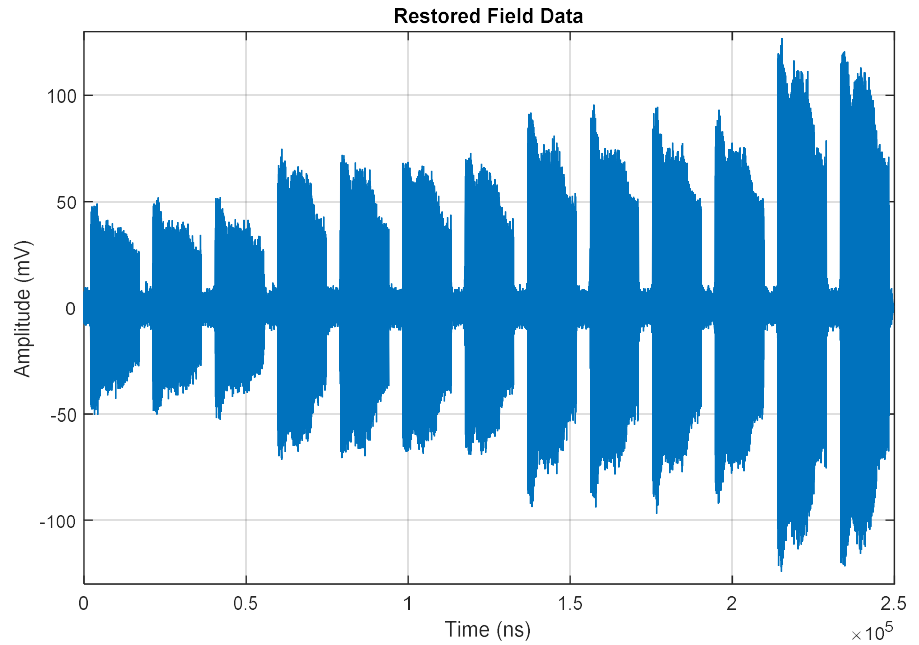

Figure 5.42: Restored field data with LFMad modulation. Parameters: f = X-band, PW = 19 us, PRI = 100 of us, No. of Pulses = 13, f_c = 1.0 GHz (±250 MHz), samples captured N = 2,50,000 samples, η = variable, and t_s = 1.5 ns.

Figure 5.43 shows the first pulse to show the simulation results. This pulse data is used to generate an instantaneous amplitude profiles using the DIQ technique as shown in Figure 5.44.

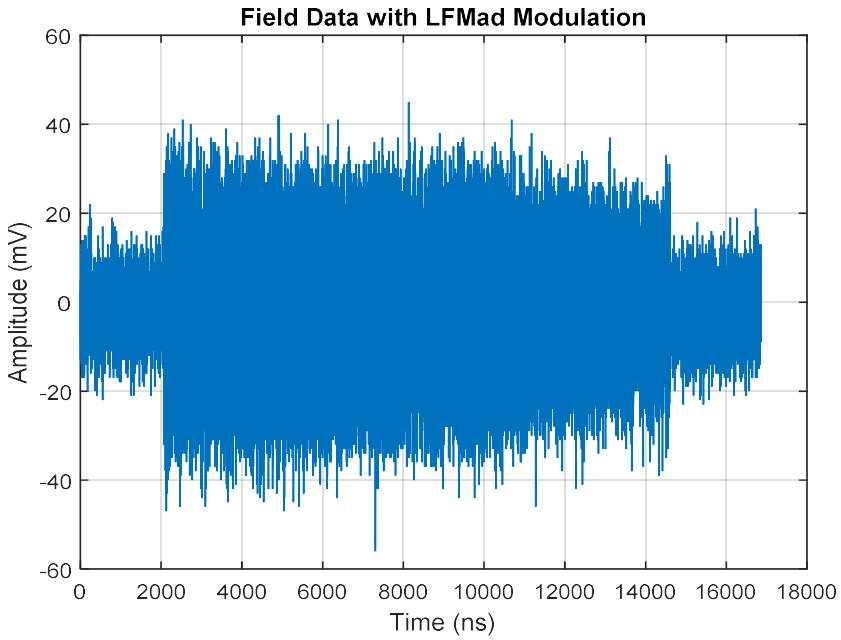

Figure 5.43: Field data with LFMad modulation (first pulse). Parameters: f = X-band, PW = 19 us, PRI = 100 of us, No. of Pulses = 1, f_c = 1.0 GHz (±250 MHz), samples captured N = 16,400 samples, η = variable, and t_s = 1.5 ns.

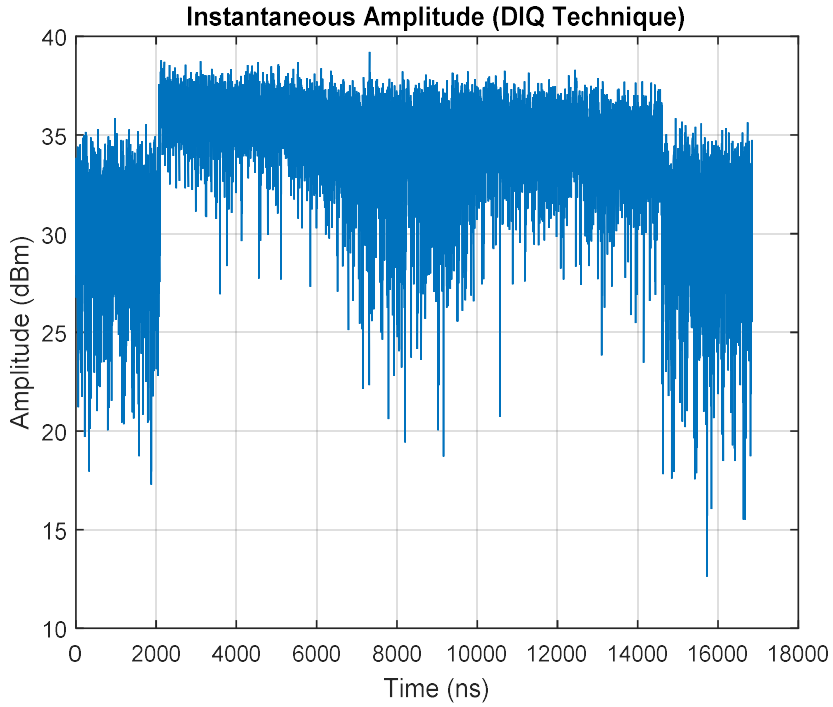

Figure 5.44: Instantaneous amplitude profile using DIQ technique without noise cancellation (fourth pulse). Parameters: f = X-band, PW = 19 us, PRI = 100 of us, No. of Pulses = 1, f_c = 1.0 GHz (±250 MHz), samples captured N = 16,400 samples, η = variable, and t_s = 1.5 ns.

Instantaneous frequency profile is generated using the DIQ technique as shown in Figure 5.45. Both amplitude and frequency profiles are generated using the DIQ technique without noise cancellation shows this algorithm is failed as the received signal SNR is less. The instantaneous amplitude profile generated using the autocorrelation technique is shown in Figure 5.46.

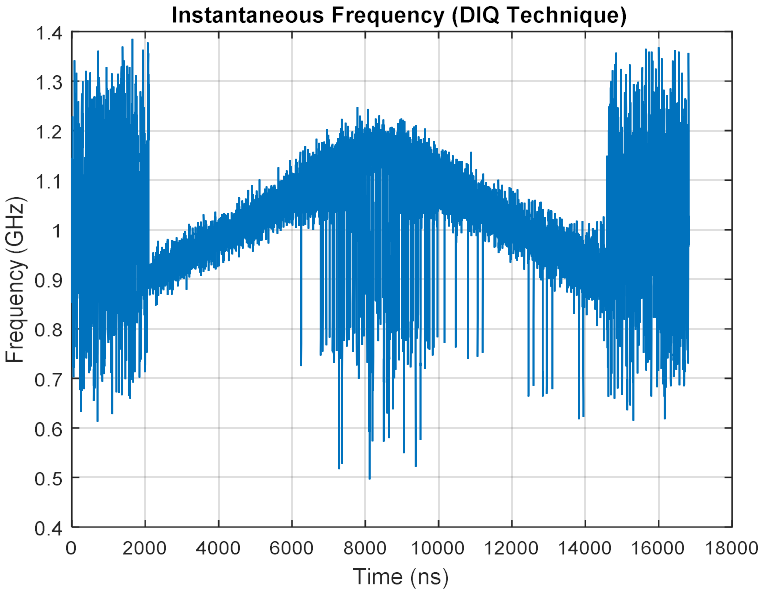

Figure 5.45: Instantaneous frequency profile using DIQ technique without noise cancellation (first pulse). Parameters: f = X-band, PW = 19 us, PRI = 100 of us, No. of Pulses = 1, f_c = 1.0 GHz (±250 MHz), samples captured N = 16,400 samples, η = variable, and t_s = 1.5 ns.

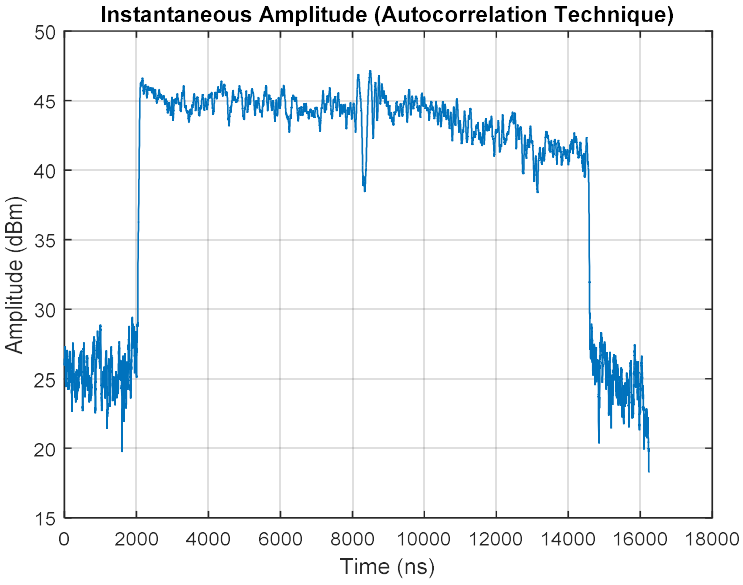

Figure 5.46: Instantaneous amplitude profile using Autocorrelation Technique without noise cancellation (first pulse). Parameters: f = X-band, PW = 19 us, PRI = 100 of us, No. of Pulses = 1, f_c = 1.0 GHz (±250 MHz), samples captured N = 16,400 samples, η = variable, and t_s = 1.5 ns.

Instantaneous frequency profile is generated using the autocorrelation technique as shown in Figure 5.47. Both amplitude and frequency profiles are generated using the autocorrelation technique without noise cancellation shows this algorithm is failed as the received signal SNR is less. Further, these techniques are used after noise cancellation. The restored signal obtained after noise cancellation is shown in Figure 5.48.

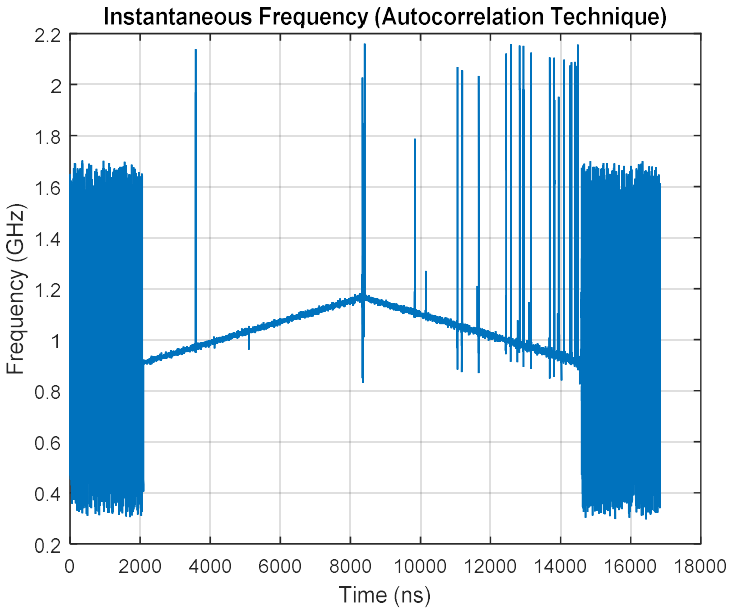

Figure 5.47: Instantaneous frequency profile using autocorrelation technique without noise cancellation (first pulse). Parameters: f = X-band, PW = 19 us, PRI = 100 of us, No. of Pulses = 1, f_c = 1.0 GHz (±250 MHz), samples captured N = 16,400 samples, η = variable, and t_s = 1.5 ns.

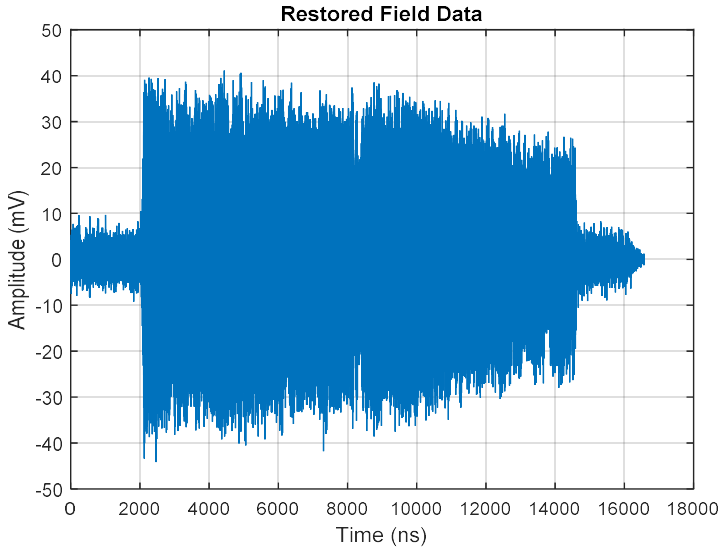

Figure 5.48: Restored field data with LFMad modulation with noise cancellation (first pulse). Parameters: f = X-band, PW = 19 us, PRI = 100 of us, No. of Pulses = 1, f_c = 1.0 GHz (±250 MHz), samples captured N = 16,400 samples, η = variable, and t_s = 1.5 ns.

The instantaneous amplitude profile generated using the DIQ technique with noise cancellation is shown in Figure 5.49. Instantaneous frequency profile is generated using the DIQ technique with noise cancellation as shown in Figure 5.50. Both amplitude and frequency profiles are generated using the DIQ technique with noise cancellation show this algorithm is still failing as signal SNR is less.

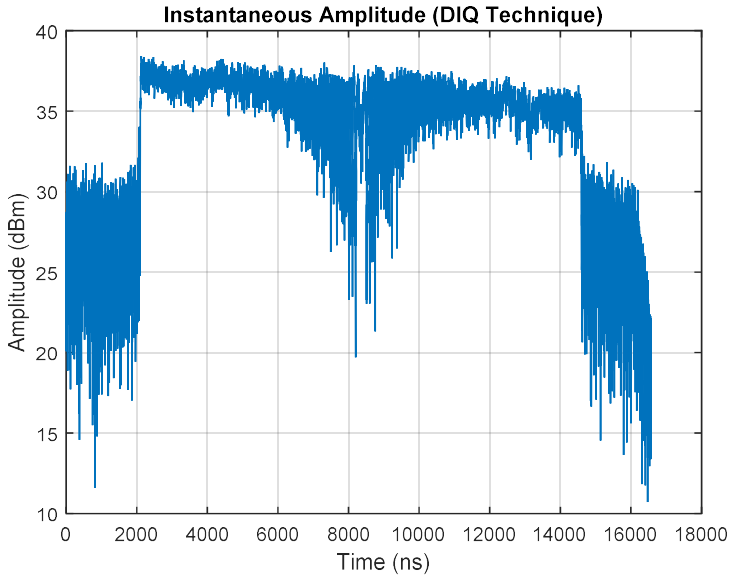

Figure 5.49: Instantaneous amplitude profile using DIQ technique with noise cancellation (first pulse). Parameters: f = X-band, PW = 19 us, PRI = 100 of us, No. of Pulses = 1, f_c = 1.0 GHz (±250 MHz), samples captured N = 16,400 samples, η = variable, and t_s = 1.5 ns.

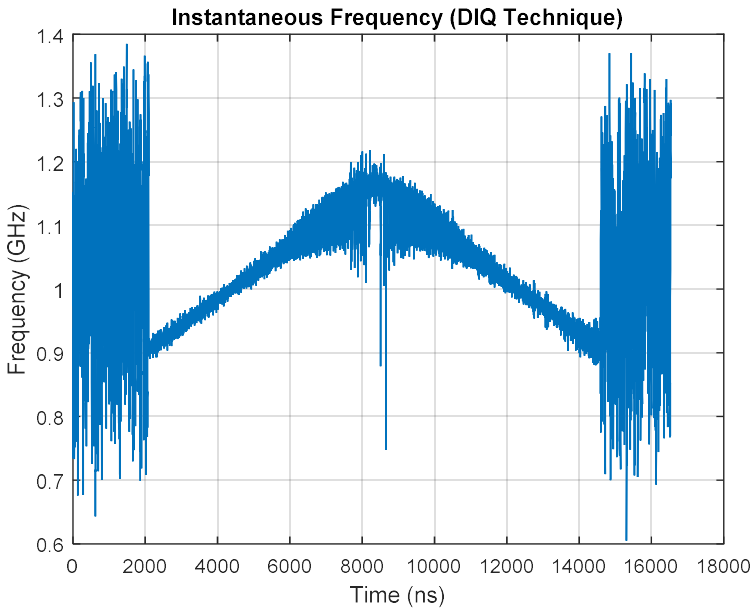

Figure 5.50: Instantaneous frequency profile using DIQ technique with noise cancellation (first pulse). Parameters: f = X-band, PW = 19 us, PRI = 100 of us, No. of Pulses = 1, f_c = 1.0 GHz (±250 MHz), samples captured N = 16,400 samples, η = variable, and t_s = 1.5 ns.

The instantaneous amplitude profile generated using the autocorrelation technique with noise cancellation is shown in Figure 5.51. Instantaneous frequency profile is generated using autocorrelation technique with noise cancellation as shown in Figure 5.52. Both amplitude and frequency profiles are generated using the autocorrelation technique with noise cancellation shows this algorithm is able to generate the profiles correctly at lower signal SNR itself.

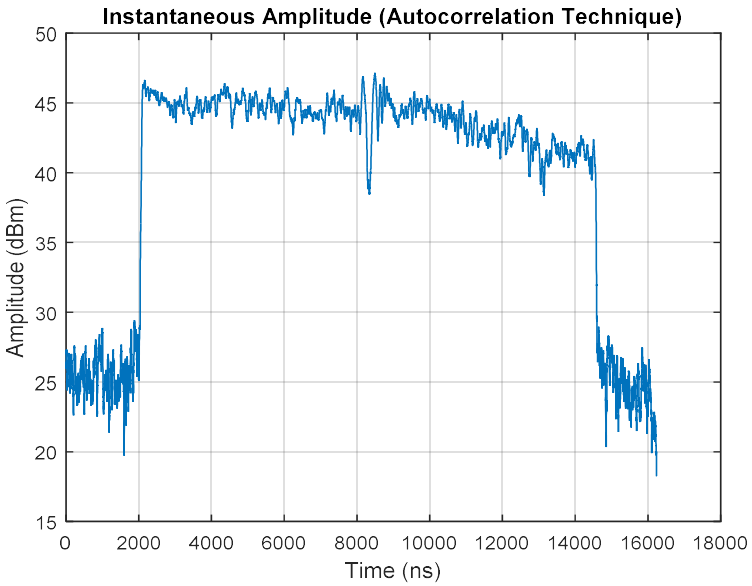

Figure 5.51: Instantaneous amplitude profile using autocorrelation technique with noise cancellation (first pulse). Parameters: f = X-band, PW = 19 us, PRI = 100 of us, No. of Pulses = 1, f_c = 1.0 GHz (±250 MHz), samples captured N = 16,400 samples, η = variable, and t_s = 1.5 ns.

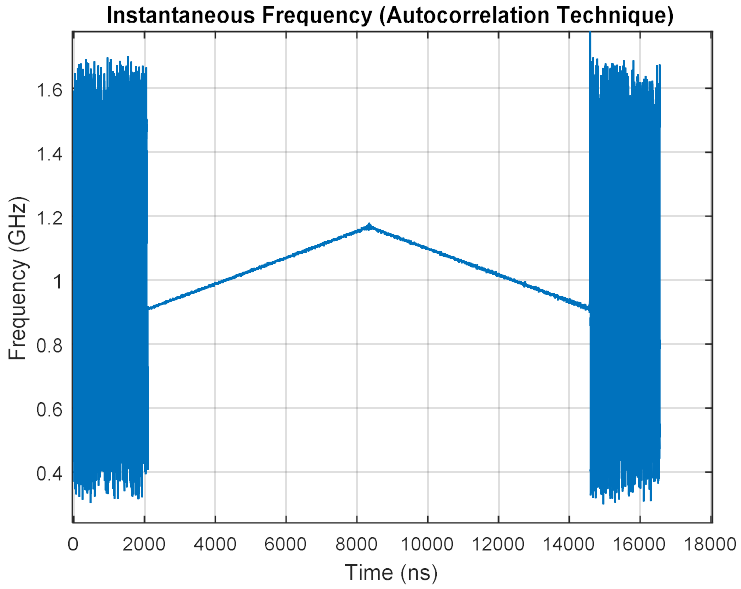

Figure 5.52: Instantaneous frequency profile using autocorrelation technique with noise cancellation (first pulse). Parameters: f = X-band, PW = 19 us, PRI = 100 of us, No. of Pulses = 1, f_c = 1.0 GHz (±250 MHz), samples captured N = 16,400 samples, η = variable, and t_s = 1.5 ns.

Figure 5.53 shows the fourth pulse to show the simulation results. This pulse data is used to generate an instantaneous amplitude profiles using the DIQ technique as shown in Figure 5.54.

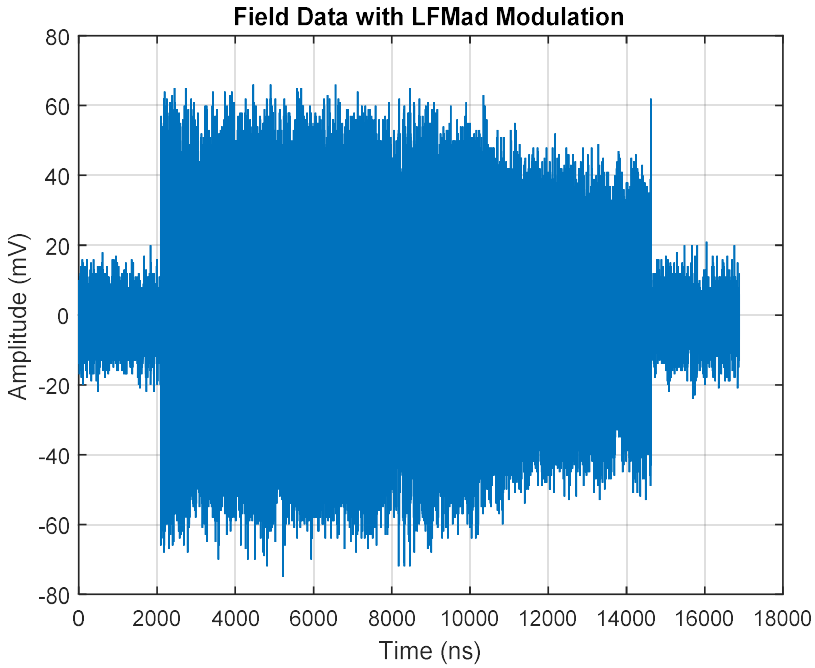

Figure 5.53: Field data with LFMad modulation (fourth pulse). Parameters: f = X-band, PW = 19 us, PRI = 100 of us, No. of Pulses = 1, f_c = 1.0 GHz (±250 MHz), samples captured N = 16,400 samples, η = variable, and t_s = 1.5 ns.

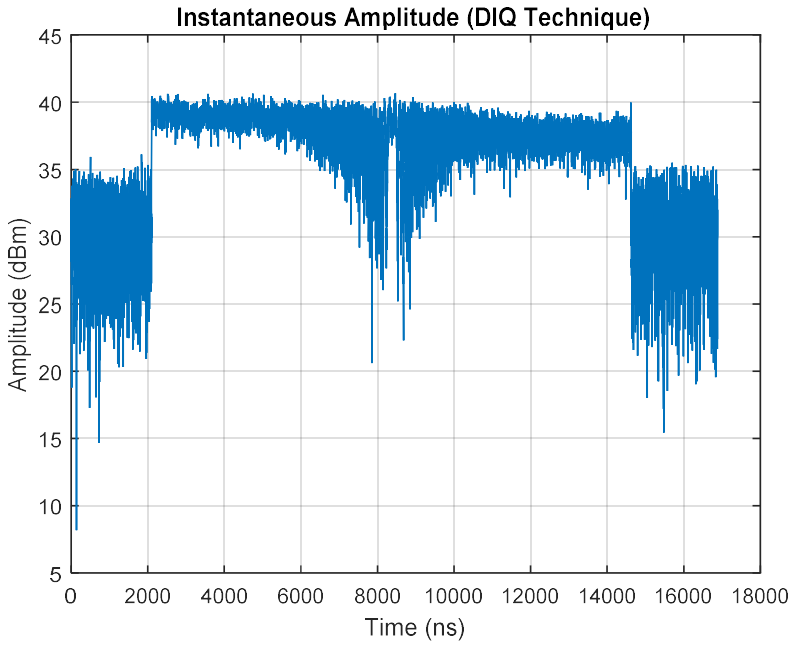

Figure 5.54: Instantaneous amplitude profile using DIQ technique without noise cancellation (fourth pulse). Parameters: f = X-band, PW = 19 us, PRI = 100 of us, No. of Pulses = 1, f_c = 1.0 GHz (±250 MHz), samples captured N = 16,400 samples, η = variable, and t_s = 1.5 ns.

Instantaneous frequency profile is generated for the fourth pulse using the DIQ technique as shown in Figure 5.55. Both amplitude and frequency profiles are generated using the DIQ technique without noise cancellation shows this algorithm is failed as the received signal SNR is less. The instantaneous amplitude profile generated using the autocorrelation technique is shown in Figure 5.56.

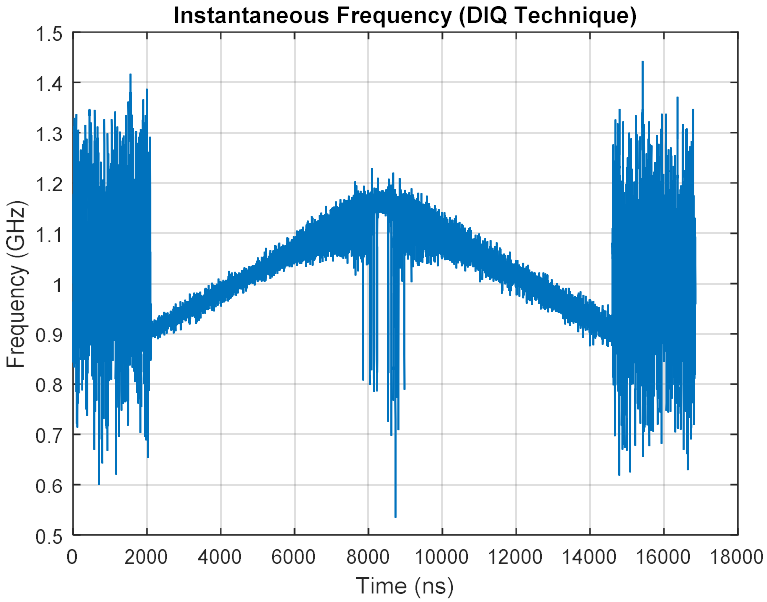

Figure 5.55: Instantaneous frequency profile using DIQ technique without noise cancellation (fourth pulse). Parameters: f = X-band, PW = 19 us, PRI = 100 of us, No. of Pulses = 1, f_c = 1.0 GHz (±250 MHz), samples captured N = 16,400 samples, η = variable, and t_s = 1.5 ns.

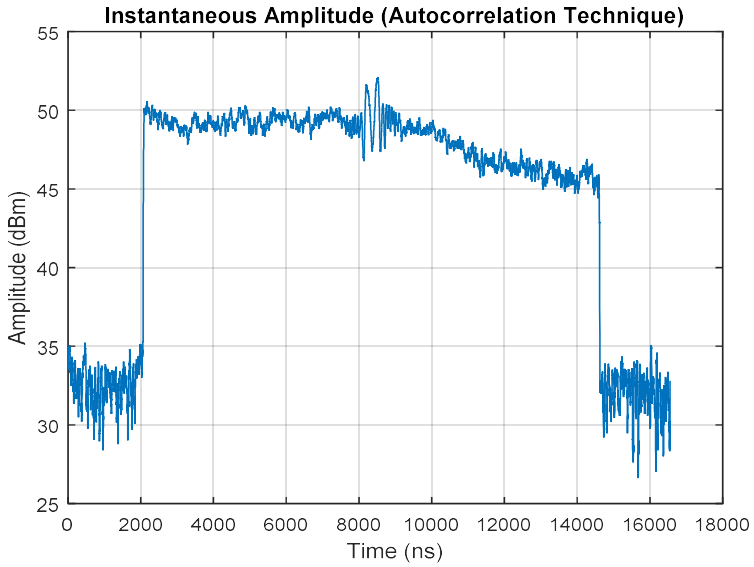

Figure 5.56: Instantaneous amplitude profile using Autocorrelation Technique without noise cancellation (fourth pulse). Parameters: f = X-band, PW = 19 us, PRI = 100 of us, No. of Pulses = 1, f_c = 1.0 GHz (±250 MHz), samples captured N = 16,400 samples, η = variable, and t_s = 1.5 ns.

Instantaneous frequency profile is generated using the autocorrelation technique as shown in Figure 5.57. Both amplitude and frequency profiles are generated correctly using the autocorrelation technique without noise cancellation shows this algorithm is working at lower SNR also. Further, these techniques are used after noise cancellation. The restored signal of the fourth pulse obtained after noise cancellation is shown in Figure 5.58.

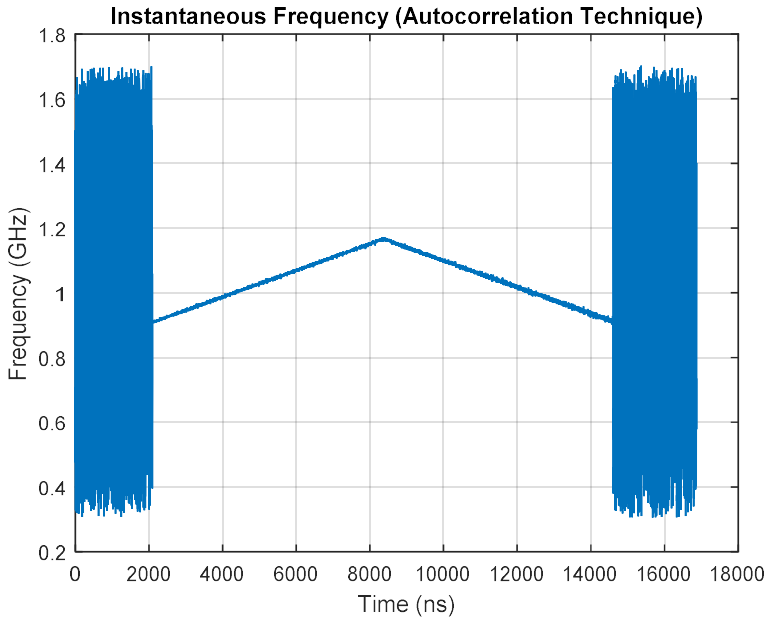

Figure 5.57: Instantaneous frequency profile using autocorrelation technique without noise cancellation (fourth pulse). Parameters: f = X-band, PW = 19 us, PRI = 100 of us, No. of Pulses = 1, f_c = 1.0 GHz (±250 MHz), samples captured N = 16,400 samples, η = variable, and t_s = 1.5 ns.

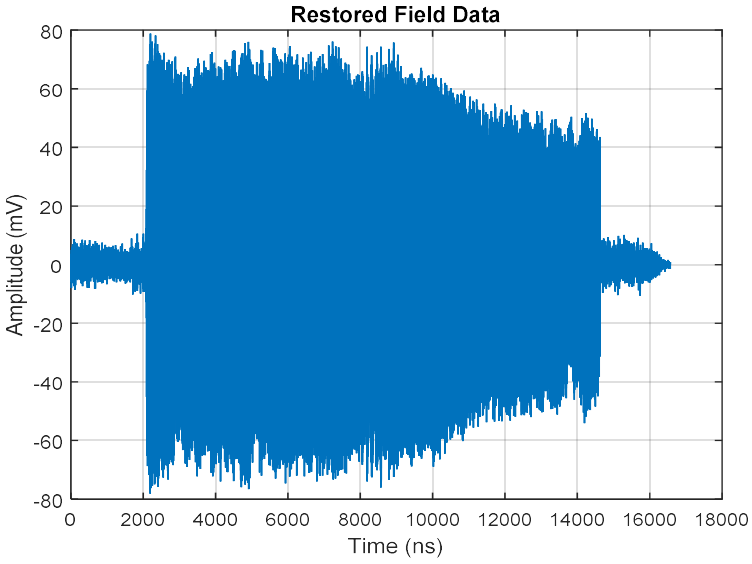

Figure 5.58: Restored field data with LFMad modulation with noise cancellation (first pulse). Parameters: f = X-band, PW = 19 us, PRI = 100 of us, No. of Pulses = 1, f_c = 1.0 GHz (±250 MHz), samples captured N = 16,400 samples, η = variable, and t_s = 1.5 ns.

The instantaneous amplitude profile generated using the DIQ technique with noise cancellation is shown in Figure 5.59. Instantaneous frequency profile is generated using the DIQ technique with noise cancellation as shown in Figure 5.60. Both amplitude and frequency profiles are generated using the DIQ technique with noise cancellation show this algorithm is still failing as signal SNR is less.

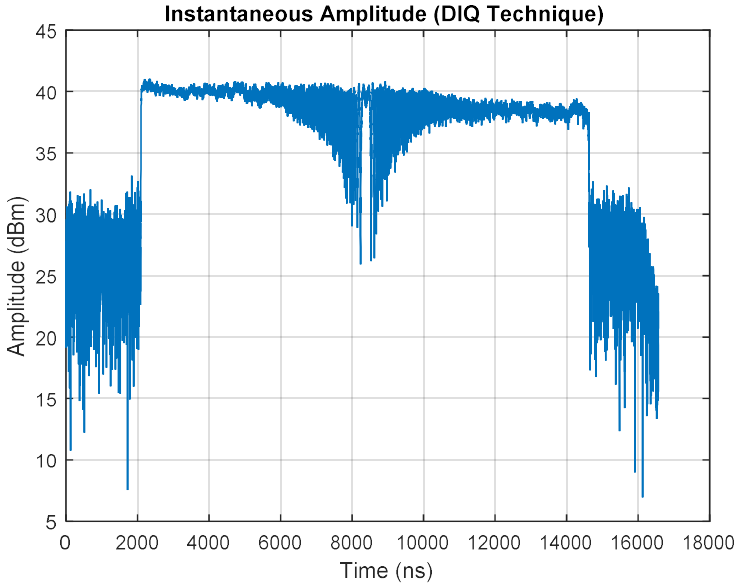

Figure 5.59: Instantaneous amplitude profile using DIQ technique with noise cancellation (fourth pulse). Parameters: f = X-band, PW = 19 us, PRI = 100 of us, No. of Pulses = 1, f_c = 1.0 GHz (±250 MHz), samples captured N = 16,400 samples, η = variable, and t_s = 1.5 ns.

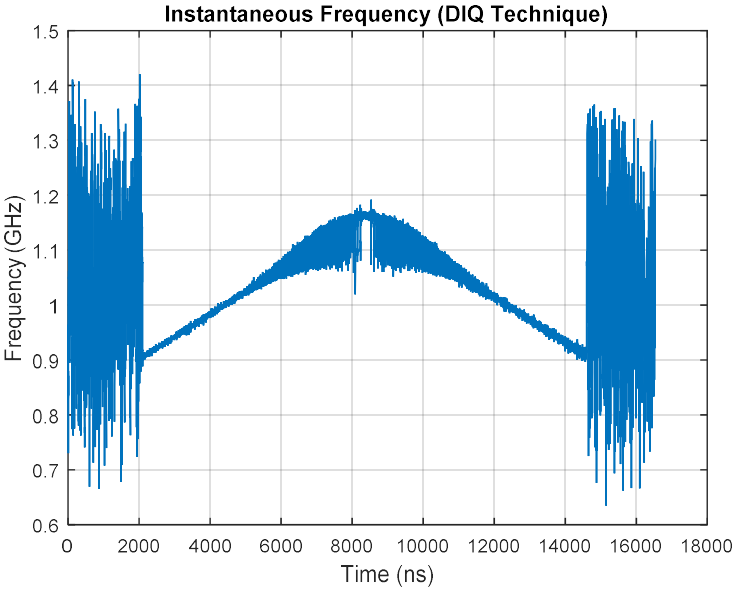

Figure 5.60: Instantaneous frequency profile using DIQ technique with noise cancellation (fourth pulse). Parameters: f = X-band, PW = 19 us, PRI = 100 of us, No. of Pulses = 1, f_c = 1.0 GHz (±250 MHz), samples captured N = 16,400 samples, η = variable, and t_s = 1.5 ns.

The instantaneous amplitude profile generated using autocorrelation technique with noise cancellation is shown in Figure 5.61. Instantaneous frequency profile is generated using autocorrelation technique with noise cancellation as shown in Figure 5.62. Both amplitude and frequency profiles are generated using the autocorrelation technique with noise cancellation shows this algorithm is able to generate the profiles correctly at this SNR as expected.

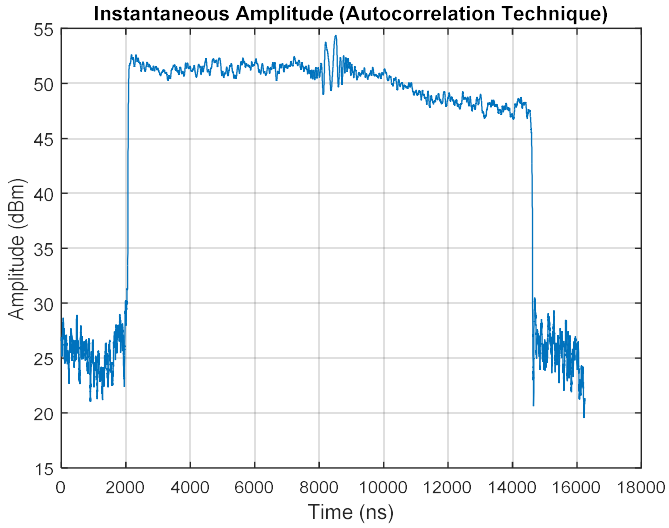

Figure 5.61: Instantaneous amplitude profile using autocorrelation technique with noise cancellation (fourth pulse). Parameters: f = X-band, PW = 19 us, PRI = 100 of us, No. of Pulses = 1, f_c = 1.0 GHz (±250 MHz), samples captured N = 16,400 samples, η = variable, and t_s = 1.5 ns.

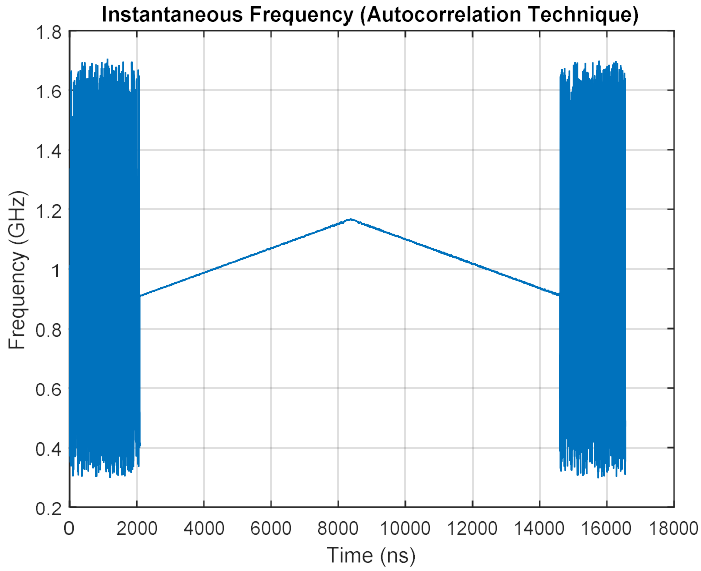

Figure 5.62: Instantaneous frequency profile using autocorrelation technique with noise cancellation (fourth pulse). Parameters: f = X-band, PW = 19 us, PRI = 100 of us, No. of Pulses = 1, f_c = 1.0 GHz (±250 MHz), samples captured N = 16,400 samples, η = variable, and t_s = 1.5 ns.

The detection performance of modulation recognition is given in Table 5.7. Extensive simulation is carried out to test the performance. Total 1000 different signal sequences are generated to test each modulation. All sixteen types of modulation have been verified and the result is tabulated. The detection performance of all modulations is given in Table 5.8.

Table 5.7: Success rate for modulation recognition.

Modulation Type	SNR of Input Signal								
	-4	-3	-2	-1	0	1	2	3	4
NMCW	98	99	100	100	100	100	100	100	100
FMCW	-	-	-	-	-	99	100	100	100
NMOP	-	-	98	100	100	100	100	100	100
LFM	-	-	-	-	99.9	100	100	100	100
NLFM	-	-	-	-	-	97.9	100	100	100
SFM	-	-	97.5	100	100	100	100	100	100
BPM	-	-	-	-	-	-	99.2	100	100
LFM with BPM	-	-	-	-	-	97.2	98.0	99.2	100
SFM with BPM	-	-	-	-	-	97.0	98.4	99.0	100

Table 5.8: Detection Performance of Modulation Recognition.

Modulation Type	Proposed Technique	Existing Technique	Correct Classification
NMCW	-2	5	99
FMCW	-1	7	98
NMOP	-2	6	99
LFM	0	7	98
NLFM	1	8	98
SFM	-2	5	99
BPM	1	8	97
LFM with BPM	1	8	97
SFM with BPM	1	8	97

The confusion matrix is extracted from the detection performance at SNR of -2 dB for the proposed algorithm with moving autocorrelation as shown in Table 5.9. The result shows the detection performance with 99% accuracy at -2 dB SNR for NMCW, NMOP, and SFM signals. The probability of correct identification is dropped below the respective SNR of all modulations. The different modulations are compared for the SNR required for set modulation and declared modulation.

Minimum SNR required using moving autocorrelation technique and DIQ technique is 1 dB and 8 dB respectively to process all types of modulated signals. Based on this, the sensitivity achieved is -87 dBm and -80 dBm using the proposed algorithm with moving autocorrelation technique and DIQ technique respectively.

Table 5.9: Confusion Matrix of modulation identification at SNR of -2 dB.

Declared MT -> Set MT (Below)	NMCW	FMCW	NMOP	LFM	NLFM	SFM	BPM	LFM with BPM	SFM with BPM
NMCW	99%	1%	-	-	-	-	-	-	-
FMCW	5%	95%	-	-	-	-	-	-	-
NMOP	-	-	99%	-	-	-	1%	-	-
LFM	-	-	-	94%	4.5%	1.5%	-	-	-
NLFM	-	-	-	3.5%	95%	1.5%	-	-	-
SFM	-	-	-	0.5%	0.5%	99%	-	-	-
BPM	-	-	4%	2.5%	1.5%	1%	91%	-	-
LFM with BPM	-	-	2.5%	1.5%	1.5%	1%	2.5%	91%	-
SFM with BPM	-	-	2.5%	1.5%	1.5%	1%	2.5%	-	91%

5.3.6 Discussions

In this work, NMCW, FMCW, NMOP LFM, NLFM, SFM, BPM, LFM with BPM, and SFM with BPM modulations have been identified using the decision-tree algorithm. This decision-tree algorithm, hence a unique method for modulation identification has been proposed. The length of the input signal is assumed constant to generate a particular type of modulated signal. The advancement in signal processing algorithms, tied with high-performance hardware has enabled the improvement of emitter identification and also achieved a real-time performance. It will meet the 1 million pulses per second (MSPS) requirement of ELINT system which has the PRI of 1 us. It will measure all the parameters within 300 ns of TE of pulse. Hence all the parameter measurements are in real-time. The real-time measurement of parameters is shown in Figure 5.63.

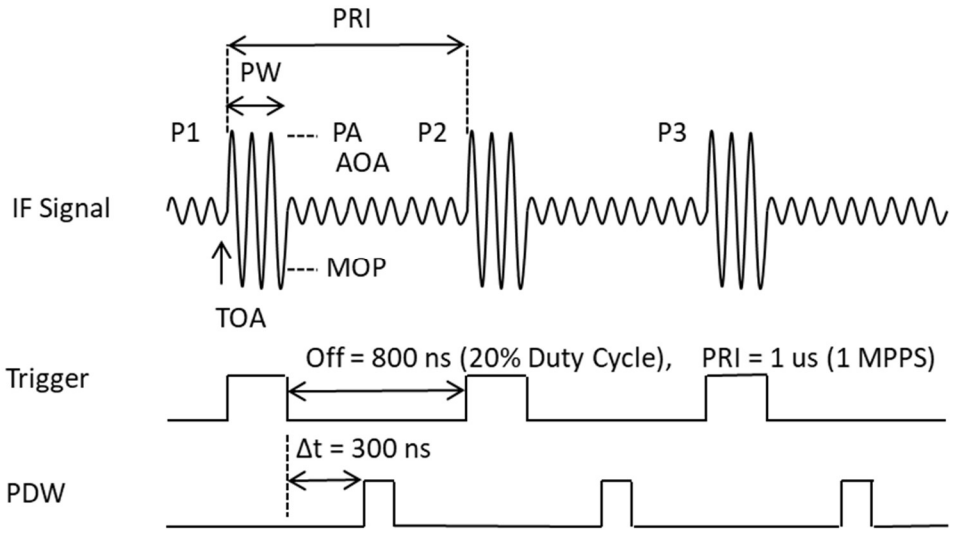

Figure 5.63: Real-time measurement of parameters.

5.4 Significance of angle-of-arrival and modulation parameters chosen for Specific Emitter Identification (SEI)

In the modern battlefield, due to proliferation of the similar radars growing demand for specific emitter identification. Identifying these radars uniquely in real-time is a challenge to understand the deployment pattern. Present ELINT systems are required to decipher the exotic modulations on a pulse to pulse basis to achieve specific emitter identification of military radars. Measured modulations contribute to the de-interleaving of signals.

Various fire control and weapon locating radars operate nearby which makes the electronic environment very dense, especially in L and S bands. Measuring conventional parameters are not sufficient to distinguish them. Intra-pulse measurement with exotic modulation measurement is the requirement in the present scenario [59]. Electronic intelligence (ELINT) systems that are capable to measure this information will have an edge in the field.

ELINT systems estimated many parameters which together are called pulse descriptor word (PDW) includes direction-of-arrival (DOA), radio-frequency (RF), pulse-width (PW), time-of-arrival (TOA), etc. [3]. These systems do the intra-pulse analysis including modulation measurement of radar signals on a pulse-by-pulse basis using stored data to match the speed of processing hardware. Measurement of exotic modulation in real-time is a challenge along with other parameter measurements.

The following process is adopted for emitter identification. In which matching is carried in three levels.

Level 1: The level 1 matching is carried out based on AOA parameter matching

(i) AOA parameter with $\pm 10^0$ window

Level 2: The level 2 matching is carried out based on attribute matching and basic parameter window matching

(i) Type of emitter - Pulsed/CW

(ii) Modulation - modulation type

(iii) Basic parameters with course windows

RF - 10 MHz, PW - 200 ns, PRI - 100 ns

Level 3: The level 3 matching is carried out with the following parameters

(i) Basic parameters with fine windows

RF - 2 MHz , PW - 20 ns, PRI - 10 ns

(ii) Intrapulse parameters matching -

Rise Time - 10 ns, Fall Time - 10 ns

(iii) Parameters of Freq. Agility, PW Agility, PRI Agility

(iv) Modulation Parameters with tolerance window

Accurate identification of radar and its platform is possible as Angle-of-arrival (AOA) parameter will be used for matching as present radar waveform generation is based on DDS-based technology and not much variation is found in Rise Time, Fall Time, overshoot, and Undershoot. To overcome this issue, the AOA parameter has to be used for matching. It will also help for nearby frequency radars coming from different directions.

Conventionally, de-interleaving is performed based on the DOA, RF, and PW. On arrival of the first PDW, one bucket is created with PDW parameter (DOA, RF, and PW). If the next PDW parameters (DOA, RF, and PW) falls within the tolerance limit, they will be stored in the same bucket. If all three parameter (i.e. DOA, RF, and PW) are not falling within the tolerance limit, another bucket will be created. Pulse repetition interval (PRI) is the derived parameter that is computed from the time-of-arrival (TOA) of each successive pulse. This is estimated after all the buckets are created for a time slice.

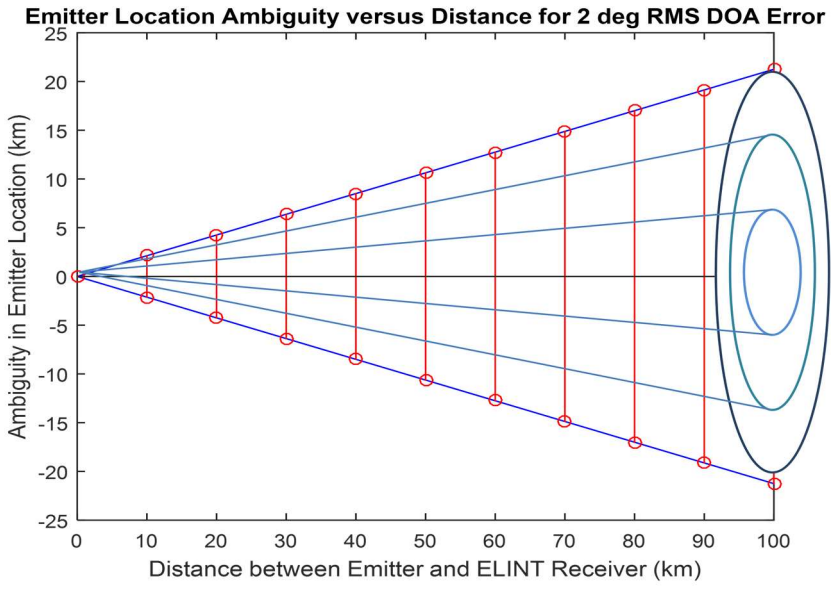

Figure 5.64: Plot of distance versus emitter location

Considering, the DOA RMS value of approximately 2 degrees in L and S bands. The tolerance of DOA will be ± 3 times of RMS value. The total error will be 12 degrees. This total DOA error will translate into a 21 Km error in azimuth from a 100 Km distance. It means a target located at 21 Km apart, will be considered for the same basket. Figure 5.64

shows the DOA error versus emitter location in azimuth. Similarly, the RF of 500 kHz and PW of 20 ns RMS value will translate into 3 MHz and 120 ns tolerance windows respectively.

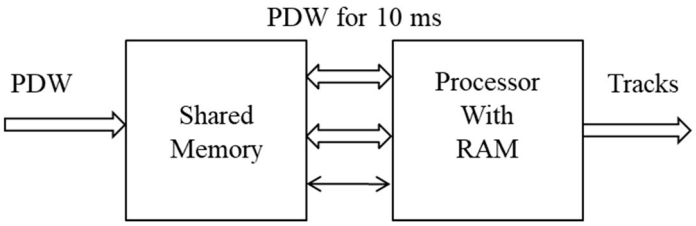

Figure 5.65: Block diagram of the de-interleaving process.

The other parameters are the modulation type and modulation parameter, which is used here for de-interleaving. This helps to improve the de-interleaving and reduces the effect of DOA inaccuracies. If signals are coming from identical DOA within tolerance, having the modulation parameter for de-interleaving is precious. Figure 5.65 shows the block diagram of the de-interleaving process.

Accuracy of parameters

The accuracy with which the parameters are measured determines the ability to differentiate one emitter from the other. Therefore in an ideal scenario, it is better to have as much accuracy as possible. The two most important factors that determine the accuracy in measurement of various parameters like amplitude, frequency, and phase are the number of bits of A/D and the sampling frequency. The selection of the high sampling frequency is a necessity to cover the required bandwidth of interest without aliasing. Due to the technological limitation at the high sampling frequency, the maximum resolution available for an A/D is 12 bits. These two constraints put a limit on the accuracy of the parameters that can be obtained. However, based on the scenario, better accuracy can be obtained by using improved techniques and algorithms with the existing limitations. The parameters whose accuracy can be improved this way are the resolution of frequency in the STFT method, wherein based on the bandwidth, the sampling frequency is reduced by decimating in the DSP. Similarly in the DIQ method, the frequency accuracy is improved whenever there is no ambiguity with the bandwidth of the signal.

Since the extraction of all the parameters is done in software, computational noise due to finite word lengths can limit the accuracy of parameters. To reduce these errors, the processing is done using a floating-point DSP processor.

5.5 Conclusions

The modulation identification is based on a time-domain technique which identifies the complex modulated signals i.e. NMCW, FMCW, NMOP, LFM, NLFM, SFM, LFM with BPM, and SFM with BPM. This technique is also implementable on FPGA as this technique consumes limited hardware resources. Even if the radar signal is coming from the same direction but having a different modulation within the pulse identifies as a different emitter. Such an idea to utilize modulation information will become a crucial parameter for PDW for better de-interleaving of specific emitter identification having a group of similar radars operating in the proximity.

The ability to specific emitter identification from a class of emitters would be of strategic advantage to the ELINT activity. The task of specific emitter identification becomes even more challenging in dense environments consisting of a wide variety of agile emitters. But due to the availability of the AOA parameter, the process of identification can be simplified if a specific characteristic can be ascribed to each emitter. This specific characteristic is the 'Specific Identification' of the emitter.

Identification refers to the specific identification of emitters among the same model of radars. The specific identification is based on intra-pulse analysis of radar waveforms and measures the frequency, phase, and amplitude variations within the pulse of that radar. These variations may be intentional and/or unintentional. The intentional modulations on pulse (IMOP) are well known, the simplest being linear chirp and Barker code phase modulation. The unintentional modulations on pulse (UMOP) are due to the inherent characteristics of all high-powered radar transmitters. The amount and type of modulation vary with the transmitter type. These modulations are present in the output of high power transmitting tubes and are due to pushing, pulling, and other effects such as temperature, aging, and poor maintenance. The modulations - IMOP and/or UMOP generate minute variations in the signal characteristics of every emitting system creating a specific signature for the emitter.

To capture the minute variations, which may be due to intentional and/or unintentional modulation, an intra-pulse analysis is needed. Such an intra-pulse analysis, extracts as many parameters (features) of radar pulses as possible with fine grain accuracy. With these extracted features the unique emitter identification attempted will be highly effective.

Chapter 6

ELINT Operation Methodology

In the previous chapter, noise estimation, adaptive threshold, radar signal detection, sensitivity computation, and SNR computation are described. Various radar signal modulation recognition using the decision-tree algorithms are also elaborated. In this chapter, details on ELINT operation methodology which includes frequency scan operation, experimental setups, setup hardware, and test conditions are discussed. Various levels of test setups are also considered. The FPGA implementation results obtained using System Generator and Vivado simulation tool. The discussion on the results is also presented in the later part of the chapter.

6.1 Introduction

The ELINT operation methodology is developed for frequency scan operation, experimental test setup, and hardware used. Defence Electronics Research Laboratory (DLRL) of India is located in Hyderabad, India. The ELINT test setup exists in the single-channel and multichannel configurations. Single-channel configuration is used to demonstrate and evaluate signal processing algorithms, such as noise cancellation, signal estimation, and modulation estimation for ELINT applications. The four-channel configuration of the ELINT test setup was used to evaluate the AOA estimation algorithms proposed in the thesis. The following hardware is used for ELINT test setup for single-channel configuration

(a) Vector signal generator

(b) RF front end

(c) Data acquisition board

(d) Xtreme DSP development kit

Whereas for multi-channel configuration the following hardware is used

(e) RFSoC evaluation board

The high-speed data acquisition board is designed to digitize the IF signal of 1 GHz and 160 MHz. The author contribution to the development of the ELINT setup is as follows:

- designing of high-speed data acquisition board used for digitizing the IF signal

- developing the software front-end for data collection and analysis, and
- used the single-channel front end as per thesis requirement
- validating the performance of the ELINT setup through experimentation by the organization and actively participating in several data collection field trials and through extensive analysis of the trial data.

A total of five different types of ELINT Test setups are used for modelling, simulation, validation, and testing for the thesis work. The following software tools are also used for the testing of the algorithms.

(a) Matlab 2015
(b) Xilinx Vivado 2016.4
(c) Xilinx System Generator 2016.4
(d) Xilinx Simulator 2016.4

RF front end is used for down-conversion in both fixed frequency and scan operation. Whereas the high-speed data acquisition board is used to digitize the IF signal. The following test graphic user interfaces (GUI) is used for tuning the RF front-end and data acquisition.

(a) RF front-end test GUI
(b) Data acquisition test GUI

While the development of signal processing theory is important, the practical value of any algorithm can only be realized if it can be successfully transitioned into hardware. In this chapter, the parameter estimation algorithms including the real-time modulation measurement technique (Chapter 4-5), will be experimentally validated using data collected from the ELINT setup (Chapter 6).

During the course of this Ph.D. research, a total of five separate modulation recognition experiments, or “field trials”, were conducted between the years 2017 to 2020. The initial experiment, were conducted to test and debug the ELINT setup and so the collected data was saved in the data files. This experiment was specifically conducted to capture data to experimentally validate the algorithms discussed in this thesis using the latest and most stable iteration of the ELINT setup. This chapter will therefore focus on the results obtained from the Field Trial and results obtained after implementation on FPGA hardware.

6.2 Experimental test setups

The various experimental test setups are used during the collection of data and validation of results. The first test setup TS-1 considered is shown in Figure 6.1 used for

modulated signal generation, instantaneous amplitude and frequency measurements, noise cancellation, noise estimation and pulse detection using amplitude profile, extraction of frequencies at various points in pulse region, and validation of results using decision-tree algorithms in Matlab. In this setup, all modulation signal is generated using Matlab itself with different SNR. This setup is used to generate most of the results mentioned in chapter-4 and chapter-5. The design and modelling of algorithms are carried out using the Matlab in the initial stages and these algorithms validation is also carried out using Matlab itself with the generated data.

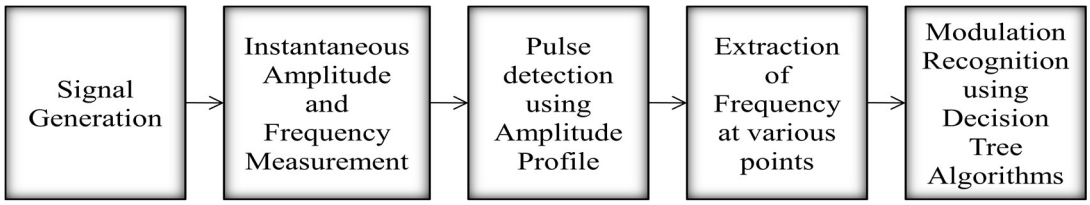

Figure 6.1: Test setup TS-1 modulated signal generation, instantaneous measurements, pulse detection, extraction of frequencies, and validation of results using decision-tree algorithms in Matlab.

The test setup TS-2 is shown in Figure 6.2. In this vector signal generator (VSG) is used to generate various complex modulated radar signals, single-channel front end is used for down-conversion of RF signal to IF signal, and high-speed analog to digital converter board is used for collection of data. The data collected is saved into the data file and this data file is used as an input data file in Matlab for validation of algorithms. In this setup following algorithms are validated i.e. noise cancellation, instantaneous amplitude profile and instantaneous frequency profile generation using autocorrelation technique and DIQ technique, noise estimation for pulse detection, extraction of frequency at various points, and decision-tree algorithm for modulation measurement. All these algorithms are the part of the last block i.e. Matlab algorithms. This setup is used to generate few results mentioned in chapter-5.

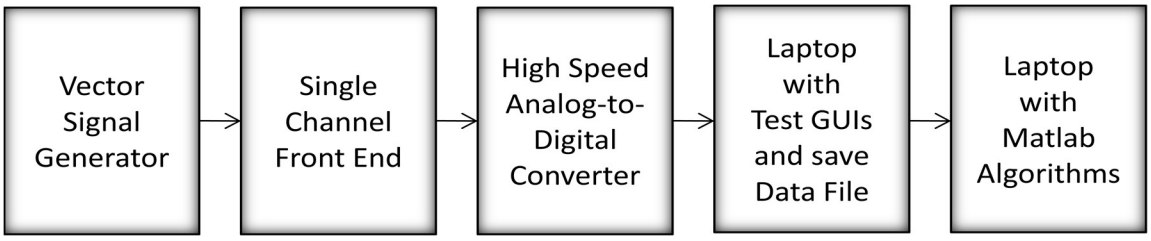

Figure 6.2: Test setup TS-2 for generation of modulated signals, down-conversion, collection of data, and measurements using Matlab.

The test setup TS-3 is shown in Figure 6.3. In this vector signal generator (VSG) is used to generate various complex signals. Single-channel front-end is used for down-conversion of RF signal to IF signal and high-speed analog to digital converter board is used for capturing, collection and storing of data. The data collected is saved into the data file and this data file is used as input for the Xilinx FPGA hardware for the validation of results. In this setup these algorithms noise cancellation, instantaneous amplitude profile and instantaneous frequency profile generation using autocorrelation technique and DIQ technique, noise estimation for pulse detection, extraction of frequency at various points, and decision-tree algorithm for modulation measurement are implemented in FPGA using system generator. Data collected for complex signals are used to validate the algorithms implemented in FPGA hardware. This setup is used to generate few results mentioned in chapter-6. In this FPGA hardware results were checked using the Xilinx Vivado simulation tool. The simulation results are matched with the input data file and verified.

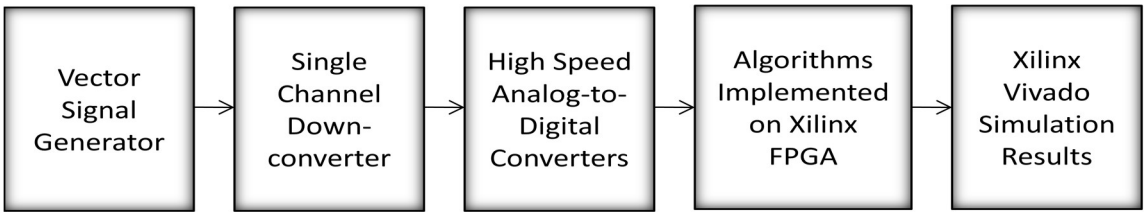

Figure 6.3: Test setup TS-3 for generation of modulated signals, collection of data, implementation of Xilinx FPGA platform, and validation of results with Xilinx Vivado tool.

The setup TS-4 is shown in Figure 6.4 with the RFSoC evaluation board. In this setup vector signal generator (VSG) is used to generate various complex signals and other stages are implemented in the RFSoC evaluation board. AOA algorithms are implemented in the RFSoC evaluation board and results are obtained. RFSoC devices consist the high-speed analog to digital converter to sample the IF signal of 750 MHz to 1250 MHz at high speed. The design is carried out using a system generator to generate the phase-shift between various channels. Both four antenna and three antenna based BLI algorithms are verified using TS-4 as mentioned in chapter-4. The results are generated at each 500 MHz steps and comparison is carried out.

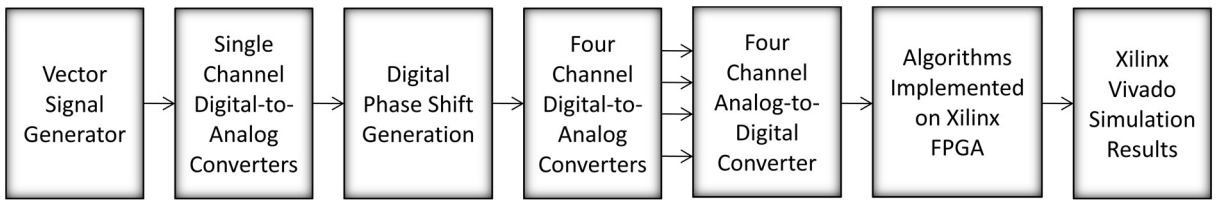

Figure 6.4: Test setup TS-4 for RFSoC hardware implementation of algorithms and simulation.

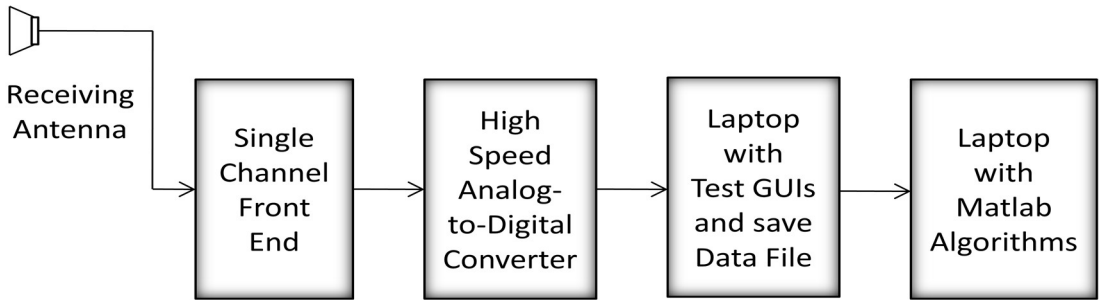

Figure 6.5: Test setup TS-5 for receiving a signal with an antenna to capture radar signals in the field.

The test setup TS-5 is shown in Figure 6.5 along with the radiation setup. The antenna is used to receive the electromagnetic signals in the form of radar signals. Antenna output is used by single-channel front-end for down-conversion of RF signal to IF signal. High-speed ADC board is used to digitize the IF signal. This setup is used to capture the radar signals including hostile radars in the field. This setup is also used to generate various results mentioned in chapter-5.

6.3 Frequency scan operation

The four-channel front end provides four IF outputs on four channels. Either 1 GHz IF or 160 MHz IF can be selected independently from the IF output. IF of 1 GHz is selected to carry out this work. In place of four-channel front-end, the RFSoC evaluation board is used for this purpose.

A total of 0.5 to 18 GHz frequency band is considered for the thesis work. The front-end receiver (or down-converters) down-converts the RF signal into an IF signal. The front end tuned for the RF frequency is mapped to the 750 to 1250 MHz band. This is for the case of fixed frequency. Scan operation is required to cover complete frequency band coverage to enhance the POI.

In the case of scan, the front-end scans the entire band of 0.5 - 18 GHz. The scan band is defined based on sub-band or spot frequencies. At the start of a scan, the front-end will tune at F-1, then it will tune to F-2, …., and finally, it will tune at F-N, where F-1 is the first frequency of the given band, F-2 is the second frequency of the given band, and F-N is the Nth frequency of the given band. Figure 6.6 shows the ELINT operation in the case of scan mode of operation. The first signal is Start of Scan (SS), this will be high for few micro seconds and indicates the scan start. After reaching at end of the scan, again SS signal will go high for few micro seconds. The second signal is Lock Signal (LS). This signal shows the tuning of the front-end for a scan frequency. It will toggle multiple times based on a number

of tuning frequencies given in a scan band. Instead of scan band spot frequencies also possible to select for scan operation. Under the lock signal, the available IF signal is detected, captured, and parameters will be measured. All three signals SS, LS and IF are available from the front end.

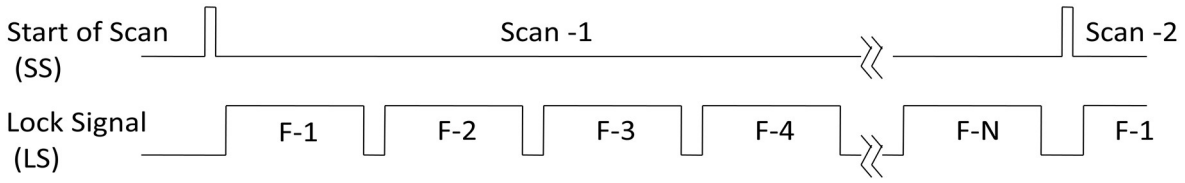

Figure 6.6: ELINT operation for scan mode of operation.

ELINT operation from 8.5 GHz to 9.5 GHz scan band is shown in Figure 6.7. Total five LS will be generated in one scan. The length of LS depends upon the set dwell time. The front end will dwell sequentially to all frequencies of the scan band for a given dwell time with 250 MHz steps. In this case, the signal frequency set is 9.0 GHz. The corresponding IF signal will appear at 750 MHz, 1000 MHz, and 1250 MHz for the tuning frequency 8.75 GHz, 9 GHz, and 9.25 GHz respectively.

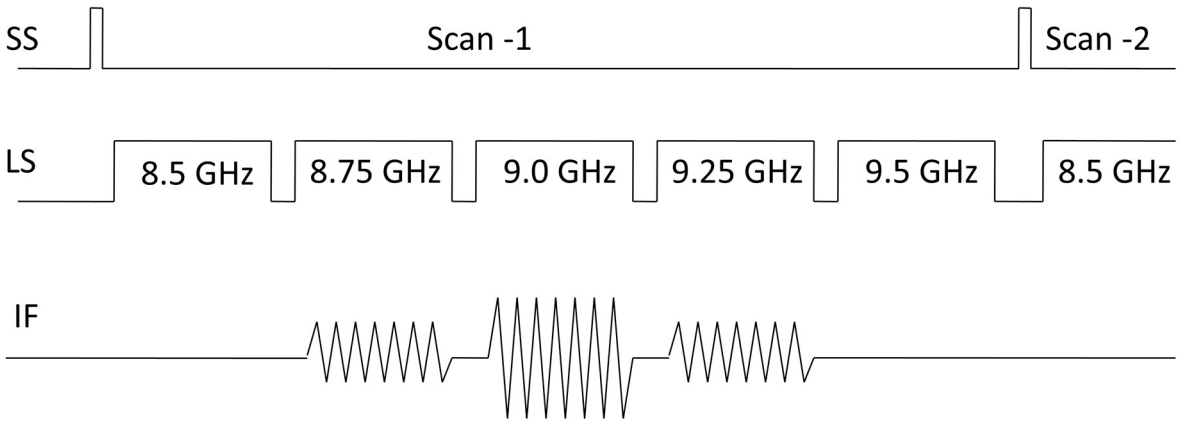

Figure 6.7: ELINT scan operation from 8.5 GHz to 9.5 GHz scan band.

The power level of the IF signal is depends upon the 500 MHz band pass filter (BPF). Usually, lower side and upper side power levels will be less compared to center frequency. This happens as 3 dB bandwidth is considered for the BPF bandwidth. This variation of power is shown in the IF signal power level at 8.75 GHz and 9.25 GHz frequencies which corresponds to 750 MHz and 1250 MHz IFs.

Test GUI for RF front-end tuning is shown in Figure 6.8. This GUI is used to keep the front end in scan mode of operation. In this RF attenuation, RF Chain mode, Scan dwell-time, and No. of Scan Freq can be set. Depending upon these parameters the front-end will be tuned to each frequency and data capture will be carried out by data acquisition card.

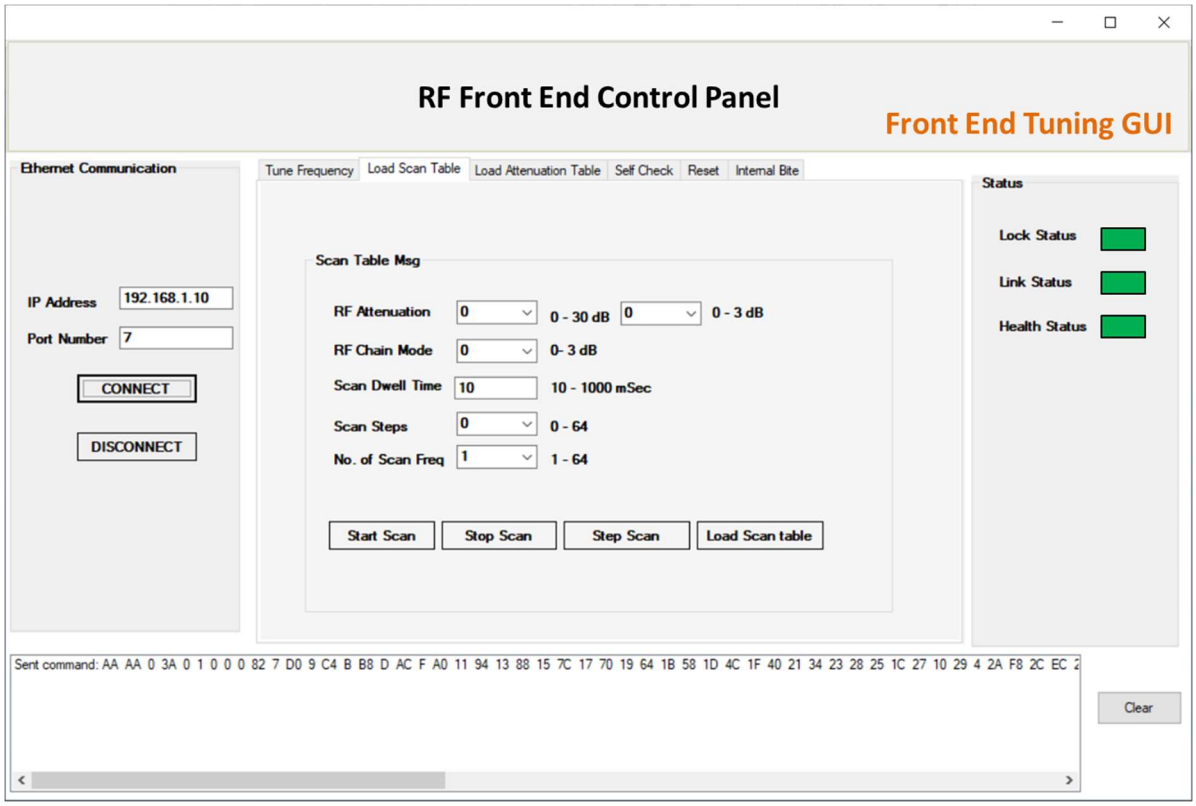

Figure 6.8: RF front-end control panel for tuning the 0.5 to 18 GHz RF tuner.

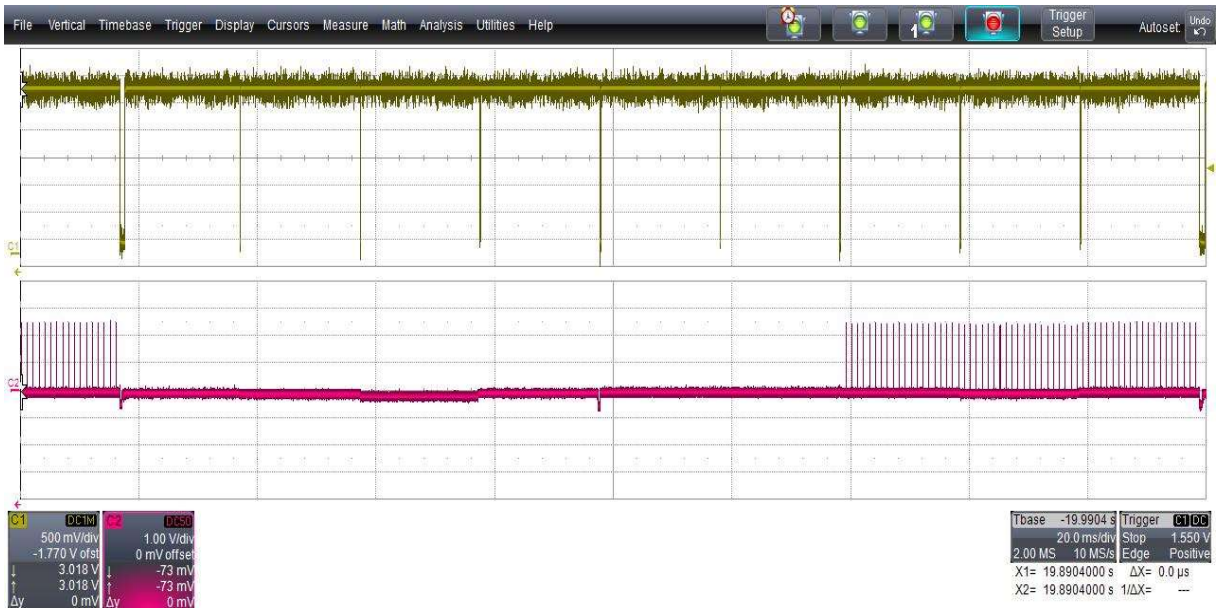

Figure 6.9: Lock signal and video signal captured on an oscilloscope in scan mode of operation.

The lock signal and video signal captured on an oscilloscope in scan mode of operation are shown in Figure 6.9. In this dwell-time of 20 ms is selected, hence about 20 pulses are being captured in each lock signal where pulsed signal with 1 us PW and 1 ms PRI is selected.

6.4 Data collection hardware

6.4.1 Design objectives

The objective of the ELINT Setup is to provide a research and development platform to implement and evaluate new algorithms and architectures for next generation electronic intelligence receivers. The current implementation of the ELINT Setup is designed to meet the specifications described in Section 1.4.1 as follows:

- be able to monitor signals in the frequency range of 0.5-18 GHz
- be able to operate in simultaneous wide bandwidth of 500 MHz
- be able to operate in a narrow band (bandwidth 40 MHz) and wide band (500 MHz or more) simultaneously
- be able to exploit multiple simultaneously instructive signals
- maintain in real-time operation in a high signal density environment,
- maintain a high POI at all times,
- be cost-effective

The ELINT Setup is implemented in a modular fashion using commercial off-the-shelf (COTS) components and indigenous components. A modular architecture was intentionally chosen to allow the system to be added for different operations. The use of COTS components and proven indigenous components reduces the risk, cost, and development time of the system compared to the development of custom hardware.

6.4.2 Sampling architecture

The signal models and associated parameters estimation theory discussed in this thesis have assumed a complex signal model. In practice, the digital representation of the complex signal consists of in-phase (real) and quadrature-phase (imaginary) components. Both components must be available before the application of the parameter estimation algorithms. While the reception of the in-phase component is straight forward, reception of quadrature-phase component can either be explicitly performed using quadrature sampling techniques or generated from the in-phase component using real-signal sampling or band pass sampling

techniques. The sampling architecture of the ELINT setup was chosen to implement a band pass sampling architecture to achieve the computational efficiencies in quadrature generation, filter design, and base banding. Both low pass and band pass sampling are used to sample the signal. Band pass sampling is suitable as it reduces the data load and hence helps the signal processing in real-time.

6.4.3 Sampling band pass signals

Band pass sampling is used to sample a continuous band pass signal that is centred about some frequency other than 0 Hz. Band pass sampling

- reduces the speed requirement of ADC below that necessary with traditional low pass sampling,
- reduces the amount of digital memory necessary to capture a given time interval of a continuous signal.

Consider sampling the band limited signal shown in Figure 6.8 centred at f_c = 1000 MHz, with bandwidth B = 500 MHz (i.e. ± 250 MHz) signal. Band pass sampling is used for the process of sampling continuous signals whose centre frequency has been translated up from zero hertz, it is also called IF sampling, harmonic sampling, sub-Nyquist sampling, and under sampling. It is more concerned with a signal's bandwidth than its highest frequency component in band pass sampling.

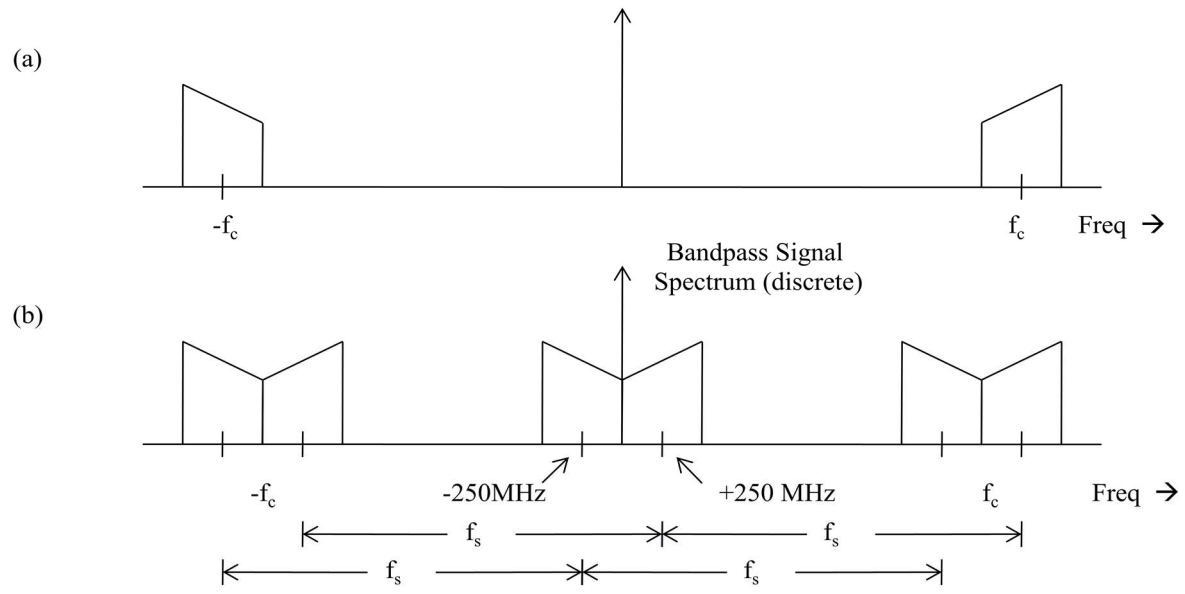

Figure 6.10: Bandpass sampling (a) original continuous signal spectrum (b) sampled signal spectrum replications.

In this example, highest frequency component is 1250 MHz. Confirming the Nyquist criteria (sampling at twice the highest frequency content of the signal) implies that the sampling frequency must be a minimum of 2500 MHz. Consider the effect of the sampling rate is 1333 MHz as shown in Figure 6.10. Note that the original spectral components remain located at $\pm f_c$, and spectral replications are located exactly at the base band. Instead, the spectral replication effect is used. It should satisfy the following relation

$$\left(\frac{2f_s-B}{m}\right) \geq f_s \geq \left(\frac{2f_s+B}{m+1}\right), \text{ and} \tag{6.1}$$

$$f_s \geq 2B \tag{6.2}$$

Greater computational efficiencies can be obtained in the signal processing that typically occurs immediately after digitization, such as quadrature generation, filtering and base banding, when the signal of the interest is centred at $f_s/4$. An efficient signal processing "trick" that can be used to shift a signal centred at f_c to $f_s/4$ is to specifically choose a sample rate that satisfies the following,

$$f_s = \frac{4f_c}{m_{odd}} \tag{6.3}$$

Where f_s is the sample rate, f_c is the centre frequency of the signal and m_{odd} is an odd integer. At this specific sample rate, aliasing effects are intentionally exploited to shift the signal from f_c to $f_s/4$ without any explicit frequency translation operation. Note that the choice of m_{odd} must be still ensured that the Nyquist criterion is satisfied, i.e. $f_s \geq 2B$ MSPS. While the chosen sample rate as equation 6.1 is often faster than the minimum necessary by the Nyquist criteria, the computational advantages offered by this choice of sample rate are often a good trade-off against the cost of a faster ADC as will be discussed below.

Figure 6.10, illustrates the frequency spectrum of a typical real signal at various stages of the band pass sampling process. In this figure, the signal is assumed to be centred at f_c with bandwidth B MHz. The sample rate is chosen to be $f_s = 4f_c/3$. i.e. $m_{odd} = 3$. Figure 6.10(a) depicts the frequency spectrum of the real signal prior to sampling. The trapezoid centred at f_c represents the signal energy at the positive frequency component and the trapezoid centred at $-f_c$ represents the signal energy at the negative frequency component. Note that the negative frequency component is spectrally inverted. After sampling at a rate of $f_s = 4f_c/3$, aliasing causes the positive frequency component to be "copied" to -$f_s/4$ and the negative frequency component to be copied to $f_s/4$. In signal processing, base banding of a signal (i.e. frequency

translation to 0 MHz) is a commonly operation. Another advantage of centring the signal at $f_s/4$ is that base banding can also be performed without the use of any multiplications [48].

Finally, filtering is a common operation that is performed in digital signal processing. The digital filters instead to allow frequencies within the pass band of the filter to pass through the system while rejecting all frequencies outside the pass band (i.e. the stop band). In practice, all digital filters designs require some transition bandwidth between the pass band and the stop band [23], [48]. The sample rate of practical digital receivers will therefore need to be faster than the Nyquist rate to provide a buffer in the frequency spectrum to allow for the transition bandwidth of digital filters. Another advantage of centring the signal at $f_s/4$ is that the maximum transition bandwidth is available for the digital filters for a given sample rate. In general, a wider transition bandwidth allows simpler digital filters to be used.

6.4.4 Selection of sampling rate

The sampling architecture of the ELINT Setup was chosen to implement band pass sampling of the signal centred at $f_s/4$ due to the computational efficiencies it offers in quadrature generation, filter design, and base banding. Currently, many commercially available, microwave (super-heterodyne) tuners exist which are designed to operate between 2-18 GHz. These quad superhet receivers commonly down-converts the radio frequency (RF) to intermediate frequency (IF) of 1 GHz and provide an instantaneous bandwidth of 500 MHz. Using these specifications with equation 6.3, the sample rate of the ELINT setup was chosen to be

$$f_s = \frac{4x1GH}{3} = 1333.33 \text{ MSPS} \tag{6.4}$$

Where the centre frequency is set to the IF of 1 GHz and $m_{odd} = 3$. For a signal with a 500 MHz instantaneous bandwidth, the Nyquist criteria requires that the sample rate be at least 1000 MSPS, and so the above sample rate satisfies the Nyquist criteria. The sample interval of the ELINT Setup will therefore be $t_s = 1/f_s$ =0.75 ns.

The above sampling rate is alright for the DIQ technique where I and Q signal conversion will be carried out based on translation and the real signal itself. But for the autocorrelation technique where I and Q signals are readily required for the algorithms. So, data sampled at 1333.33 MSPS is converted to I and Q signals using the Hilbert transform. Further, these signals can be decimated by 2 as the sampling rate of 666.66 MSPS is sufficient. Both I and Q signals can be directly sampled at 666.66 MSPS if they are available in analog form.

Note that the down-conversion of the radar signal from RF to IF changes the measured carrier frequency of the signal, however, the signal's original RF can still be determined since the local oscillator frequency is known. The phase of the signal remains unchanged after down-conversion and so the phase delays will still be directly related to the signals original RF.

6.4.5 Data capture hardware

The ELINT Setup follows a conventional digital receiver design with a band pass sampling architecture and is illustrated in Figure 6.10. Microwave radars signals are received at the antennas and down-converted from RF to IF using single-channel, wideband microwave tuners. Signal conditioning (i.e. amplification and filtering) is performed at both RF and IF to improve the fidelity of the down-conversion. The IF is digitized using parallel high-speed ADCs and then transferred to a laptop and stored in a data file named adc_data.dat. All components of the ELINT Testbed are discrete, commercially available components that are connected using RF and IF cables with SMA connectors.

Figure 6.11: VPX based high-speed data acquisition card.

VPX based high-speed data acquisition card is shown in Figure 6.11. The researcher has designed this board with two input channels, one external trigger input, one external clock input, and one signal monitoring output. Channel-1 is having a 10 dB higher gain compared to channel-2 which is used for data collection. The data acquisition hardware is designed with the ADC (P/N: ADC12D1800RF) to sample IF signal at 1333 MSPS. Only pulse data is captured along with pre-trigger and post-trigger portions to measure rise-time and fall-time. Off-time between the pulses is not captured which saves a lot of memory space and reduces the power consumption. It also enhances the maximum pulses storing capability. This card

has the PCIe and Ethernet interfaces with the controller. Ethernet interface is used to capture the data on the laptop directly.

Test GUI shown in Figure 6.12 is used to control the data acquisition cards and capture the IF signal based on the settings. The captured data is stored in the trig_data.dat file along with the time-of-arrival (TOA) of each pulse, reported frequency, etc. in trig_info.txt file. This digitized IF data is used to validate the algorithms at various levels. This hardware is used to capture the radar signals in the field along with the front-end.

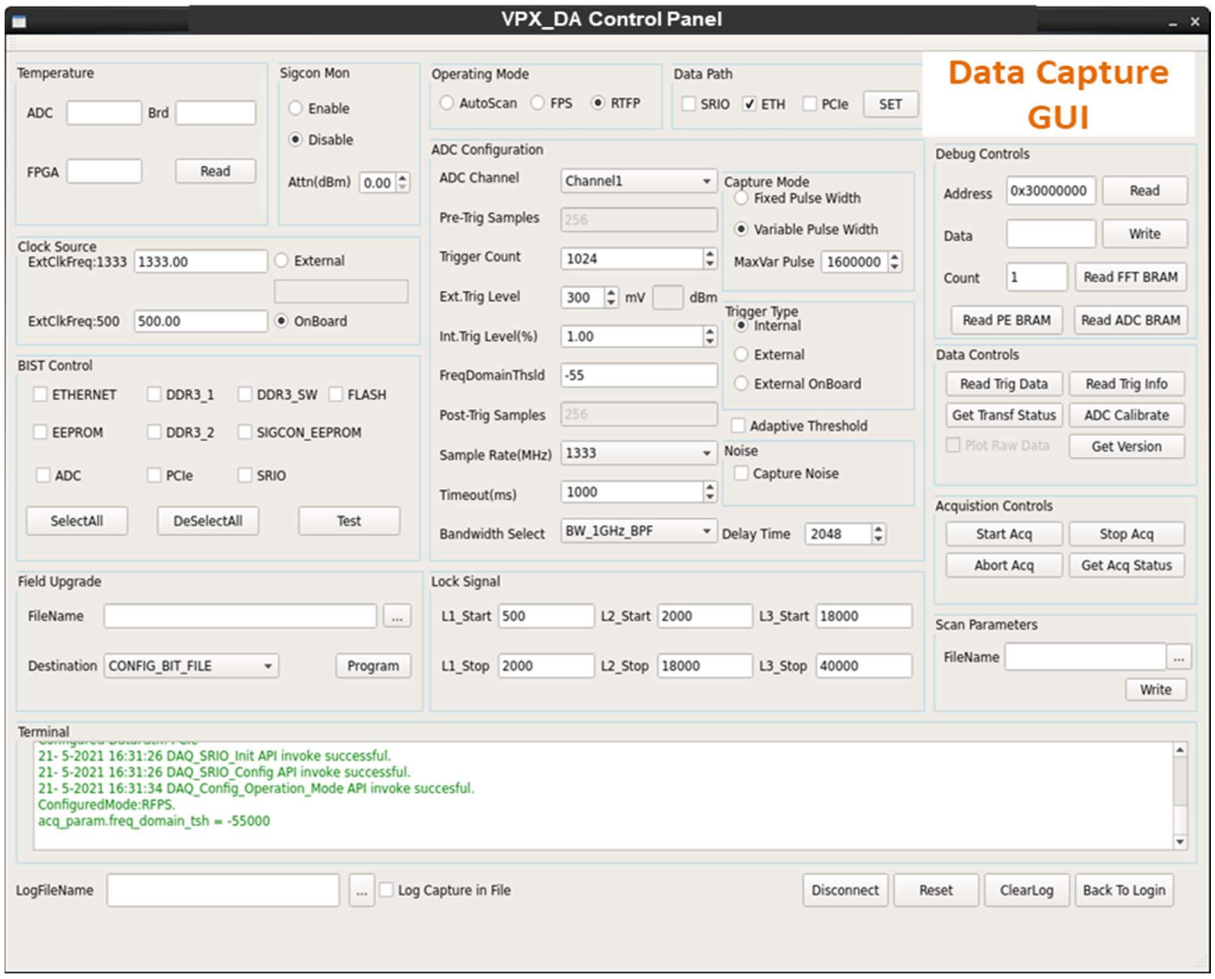

Figure 6.12: VPX acquisition card control panel.

The sample rate of the 12-bit high-speed ADC was set to 1333 MSPS and was specifically chosen to produce an intentionally aliased digital IF recording centred 1000 MHz. The process of capturing data is as follows:

- Turn off the ELINT Setup and vector signal generator
- Ensure that the RF switch is set to direct injection from the signal generator. (i.e. Ensure no signal enters the system through the antennas)
- Power-up the ELINT Setup

- wait a few seconds to ensure that all components have fully powered-up

- Turn on the vector signal generator
- Capture 10-100 pulses and readout trig_data.dat file
- Use this file as input data in Matlab and apply the following algorithms
- Perform noise cancellation in each channel using spectral subtraction
- Estimate instantaneous amplitude and frequency profiles
- Estimate the noise in one channel using instantaneous amplitude profile
- Detection of pulse using adaptive threshold on same channel
- Estimate the other parameters using amplitude and frequency profiles.
- Estimate the modulation and their parameters using instantaneous frequency profile

6.4.6 Data collection methodology

The data was recorded using a time-domain and frequency-based triggering system with a set pulse width. This is a spectrum-based triggering system that activates a data recording when the signal energy in one or more chosen frequency bins of an FFT spectrum exceeds a specified threshold. When a trigger signal is detected, a set number of pulses data is collected with the pre-trigger and post-trigger data. This pre-trigger and post-trigger data is collected based on the pulse width. Pre-trigger data is collected based on the circular memory concept and this facilitates to measure of the rise-time. The pulse data is recorded adaptively based on the pulse region. It will also continue to record beyond falling edge equivalent to the pre-trigger region.

This data was also captured with continuous mode for low SNR conditions. The VSG was set with pulsed width of 5 us and pulse repetition interval of 7 us. The data is collected in this manner to obtain more information in less time duration as the simulation tools also having the limit, in which more data loading consumes more time. Instead of that pulsed data is fed in the form of CW collected data and used for simulation as well as for FPGA simulation. When a trigger signal is detected, a burst of 100 us of continuous data is recorded. For this particular collection, each trigger is expected to capture approximately 14 pulses.

6.5 Test setup hardware

Two different types of Xilinx FPGA hardware are used to test the algorithms i.e. XtreamDSP development kit and RFSoC evaluation kit. Both the boards consist ADCs to digitize the signals and DACs to convert the digital words into analog signals.

6.5.1 XtremeDSP development kit

The XtremeDSP development kit-4 is used as a development platform with Virtex-4 FPGA technology which is used to design scalable systems based on signal processing algorithms available from M/s Nallatech. This board has dual-channel high-speed ADCs and DACs, as well as the programmable Virtex-4 device which is used to implement signal processing algorithms for software defined radio, radar, and EW applications. The block diagram of the Nallatek development kit is shown in Figure 6.13.

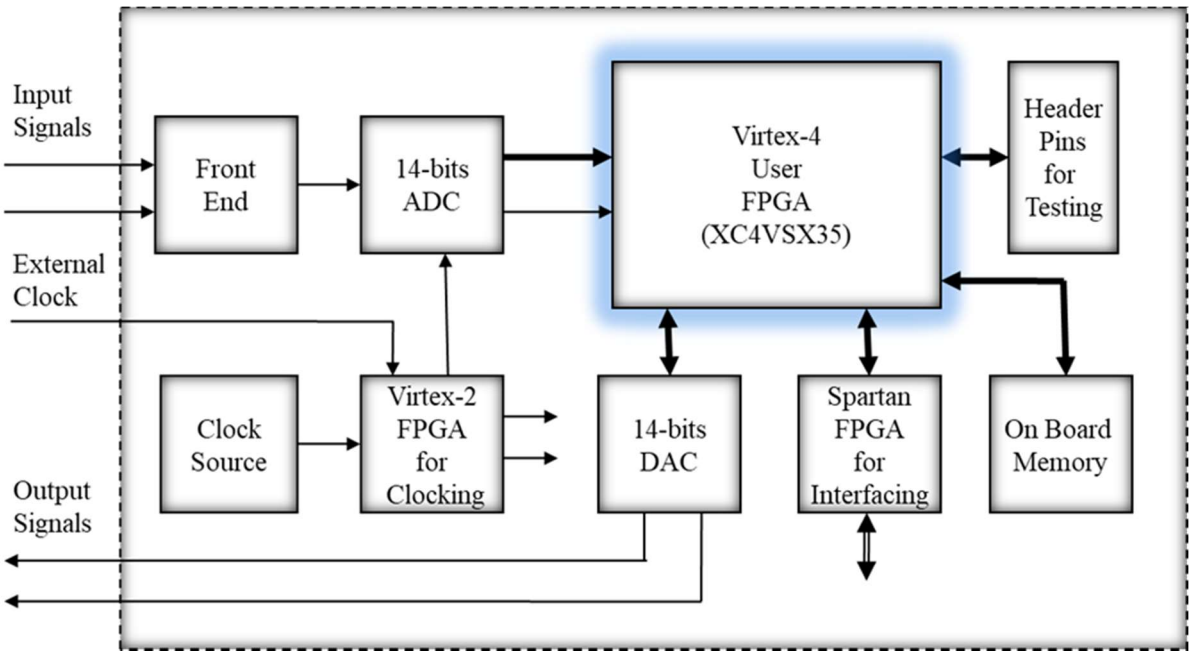

Figure 6.13: Block diagram of Nallatek development kit.

Figure 6.14: Nallatek Xilinx Virtex-4 FPGA development kit.

The photograph of Nallatek Xilinx Virtex-4 FPGA development kit is shown in Figure 6.14. The development kit consists of three Xilinx FPGAs namely a Virtex-4 User FPGA, a Virtex-II FPGA for clock management, and a Spartan-II FPGA for interfaces. The Virtex-4 device is available exclusively for User designs while the Spartan-II is used for pre-configured firmware for peripheral component interface (PCI). The PCI interfacing firmware can be used for user designs or applications. The Interface FPGA also communicates directly with the User FPGA. The Virtex-4 XC4VSX35-10FF668 device is intended to be used for the main part of a User's design. The Virtex-II XC2V80-4CS144 is used for clock configuration in a design. The clock generated by this FPGA is used for User designs.

USB JTAG Downloading Cable

Figure 6.15 shows the JTAG USB downloading cable. The .bit file is generated using the Xilinx ISE tool is downloaded into the FPGA using this cable, The iMPACT tool is used to download the bit file into Xilinx FPGA. The ChipScope Pro Analyzer tool also can be used to download the .bit file.

Figure 6.15: Xilinx USB Jtag cable.

ADC Clocking

The clock is generated by Virtex-II XC2V80-4CS144 FPGA is called clock FPGA. This clock is used for ADC clocking also. This signal is differential LVPCL. The same FPGA is used for DAC clocking. Based on bit files ADCs can be clocked in different ways. The following various clocks can be used through clock FPGA:

- Onboard clock of 105 MHz generated using a crystal oscillator.
- External clock input is given through the middle MCX connector.
- Various programmable oscillators clock are available in the kit.

The onboard clock of 105 MHz is used to drive the FPGA logic.

Synthesis and Implementation Settings

This synthesis and implementation settings are given in this section, which are used for the development and implementation of FPGA designs to run on the Nallatech board.

Synthesis Options

To synthesize HDL code for user designs no specific settings are required for Nallatek hardware. But the synthesis tool is required to synthesize the FPGA code.

Implementation Options

To develop, synthesize and implement user design, the Xilinx implementation tool is required. The synthesis tool which is part of Xilinx Implementation tools is used to synthesize the user design to the target device. Now, these tools are part of Xilinx Vivado tools.

Necessary Settings

The following mandatory settings are required which need to mention for the user design to configure and run on Nallatek hardware.

1. Select Enable Readback and Reconfiguration
2. Select the JTAG Startup Clock in the bit file generation properties.

Downloading the .bit File

The Xilinx iMPACT tool is used to configure the User FPGAs in the XtremeDSP development kit-IV. This section details how the iMPACT tool is used with the kit.

Connect a JTAG Download Cable

The JTAG download cable is required to configure Xilinx Virtex-IV User FPGA. Parallel-IV cable is supported which is connected to FPGA with the header and the other side is connected to the laptop with a USB interface.

Detect the Card and Enable Power Supplies

The power supply is to be switched on to detect all the three FPGAs on the board through JTAG. All power good LEDs will become green after red immediately.

If using the Kit standalone with the external power supply

Board can be used in PCI slot of the personal computer and it can be also used with their standalone power supply. Once the power supply module is connected to the supply and it starts power to the board.

The sampling rate of this board is limited to 105 MSPS which can be enhanced to 250 MSPS with the external clock. This sampling rate is sufficient for 160 MHz IF signal but it is not sufficient for the sampling of 1000 MHz IF signal at 1333 MSPS. Due to this reason, the digitized IF data trig_data.dat file is used in this board to validate the algorithms. This board is used for test setup TS-3 in section 6.3.

6.5.2 RFSoC evaluation kit

Zync Kintex UltraScale plus RFSoC ZCU111 is the high density, high speed, RFSoC evaluation board. ZCU111 is used for high-performance RF applications. This kit features a Zynq UltraScale plus RFSoC supporting eight 12-bit, 4.096GSPS ADCs, and eight 14-bit 6.554GSPS DACs. This kit provides a rapid, comprehensive RF Analog-to-Digital signal chain prototyping platform

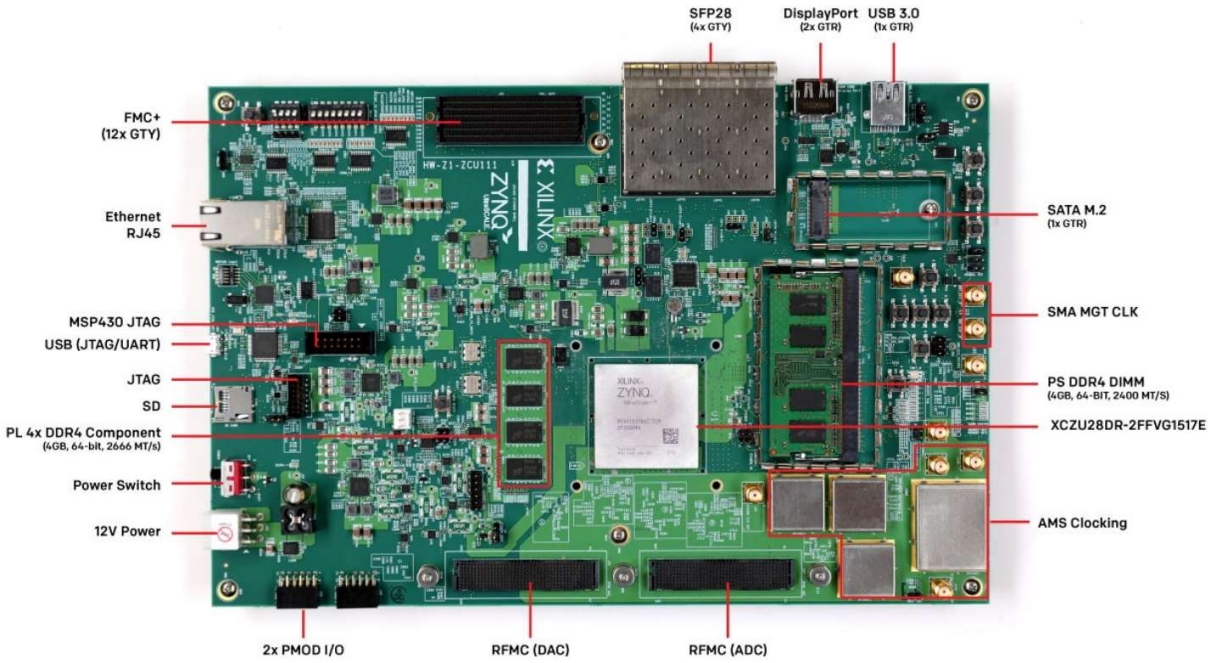

Figure 6.16: ZCU111 RFSoC evaluation kit.

The kit is equipped with the industry's only single-chip adaptable radio device. The Zync UltraScale plus RFSoC ZCU111 evaluation kit is the ideal platform for both rapid

prototyping and high-performance RF application development. The included ZU28DR is Xilinx's highest ADC sample rate RFSoC device, designed for applications requiring wide instantaneous bandwidth. Eight integrated SD-FEC cores provide forward error correction at 80% lower power consumption than soft implementations, making the ZU28DR ideal for microwave backhaul, and small cell applications. References add-on cards and connectivity options make the ZCU111 kit suitable for developing complexity and improving time to market. Figure 6.17 shows the mezzanine card to connect the ADC and DAC ports.

The algorithms are tested with four channel hardware with four Analog-to-digital converters (ADCs) and four Digital-to-analog converters DACs). It consists of Zync Ultra Scale Plus RFSoC ZU24DR FPGA which consists of the following:

Zync UltraScale plus RFSoC ZCU111 XCZU28DR-2FFVG1517E RFSoC:	
System Logic Cell	930K
Memory	60.5 Mb
DSP Slices	4,272
Transceivers	16

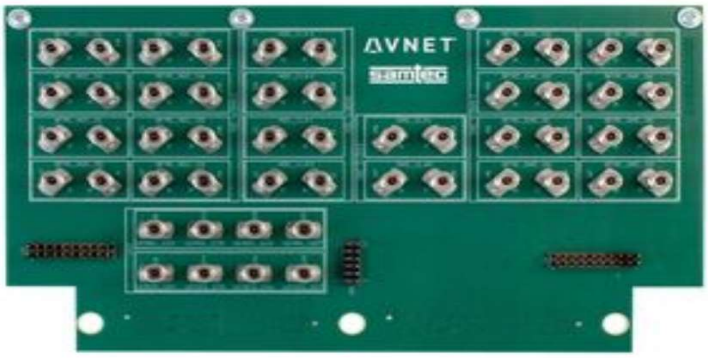

Figure 6.17: ZCU111 RF mezzanine board for ADC and DAC.

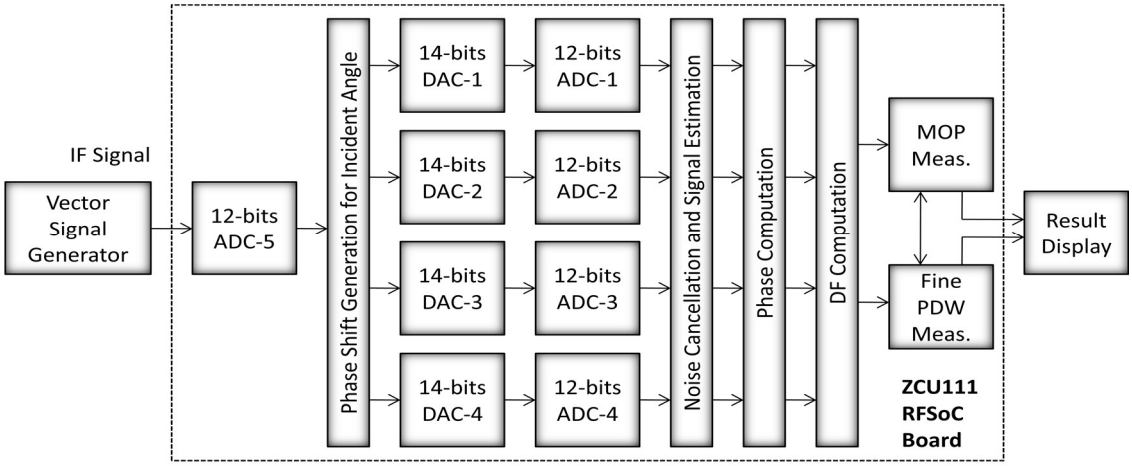

Figure 6.18: AOA algorithms testing setup using ZCU111 RFSoC evaluation kit.

The AOA algorithms are verified in the detailed setup as shown in Figure 6.18. In this, a single IF input goes to one of the ADC channels. Phase shift is provided to this channel according to the angle of incident of electromagnetic waves to four or three antennas. The digital data with a phase shift to all channels is diverted to DAC for conversion to the analog signal. These analog signals are taken out and again connected to four or three ADC inputs from the mezzanine card to digitize these signals. AOA algorithms are applied to these digitized data and verified the measured AOA.

6.6 System generator models

All algorithms are implemented with a system generator using Xilinx Vivado 2016.4 tool. The Xilinx device selected is Virtex-7 XC7VX415T FPGA. The synthesis is carried out for netlist generation, mapping for exact mapping of components, and place & route is carried out.

6.6.1 Amplitude and frequency measurement models

The following models are generated as part of the amplitude and frequency measurement as shown in Figure 6.19 to Figure 6.21. Their performance is verified first in simulation using the system generator itself. The autocorrelation approach is implemented for amplitude and the multilevel autocorrelation approach is used for frequency generation block.

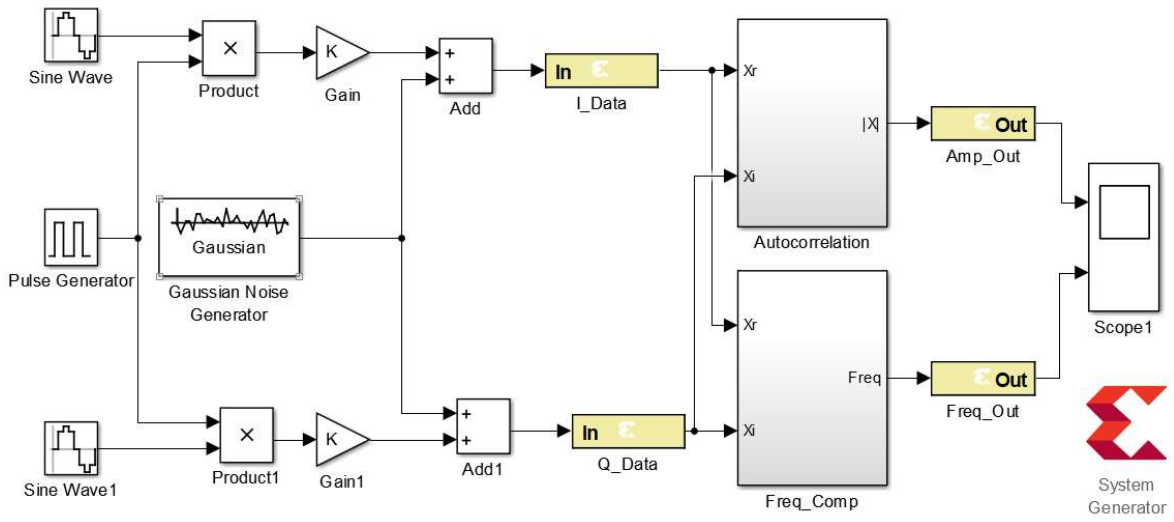

Figure 6.19: Instantaneous amplitude and frequency measurement system generator models.

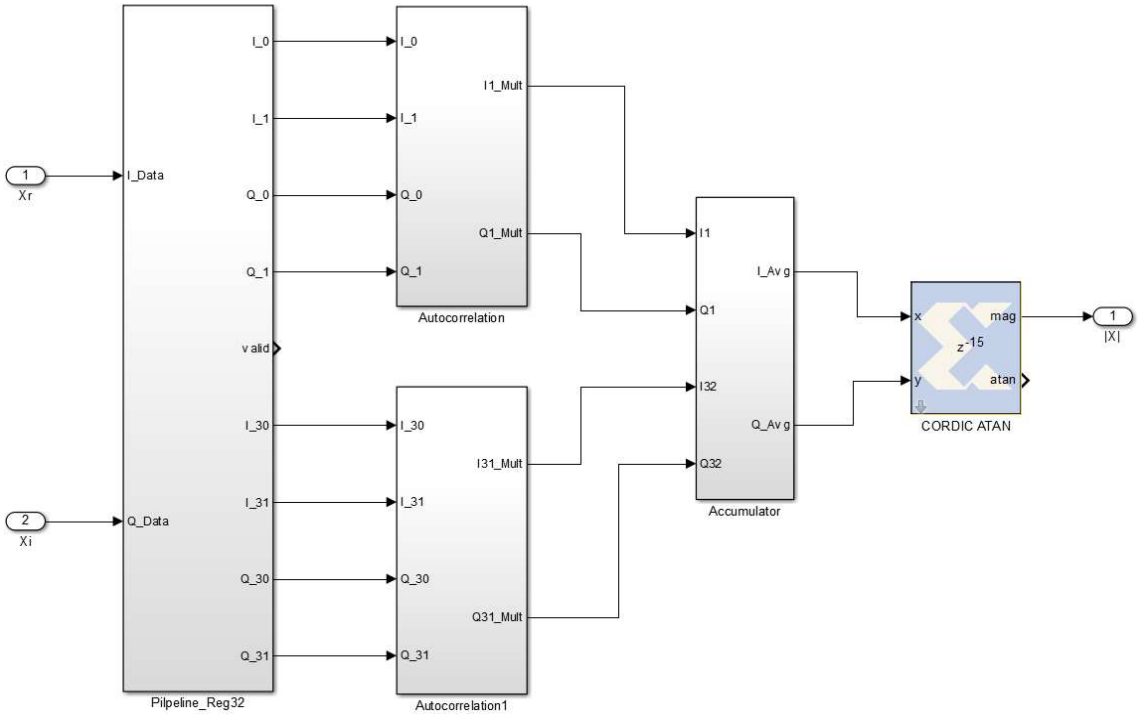

Figure 6.20: Detailed instantaneous amplitude measurement system generator model.

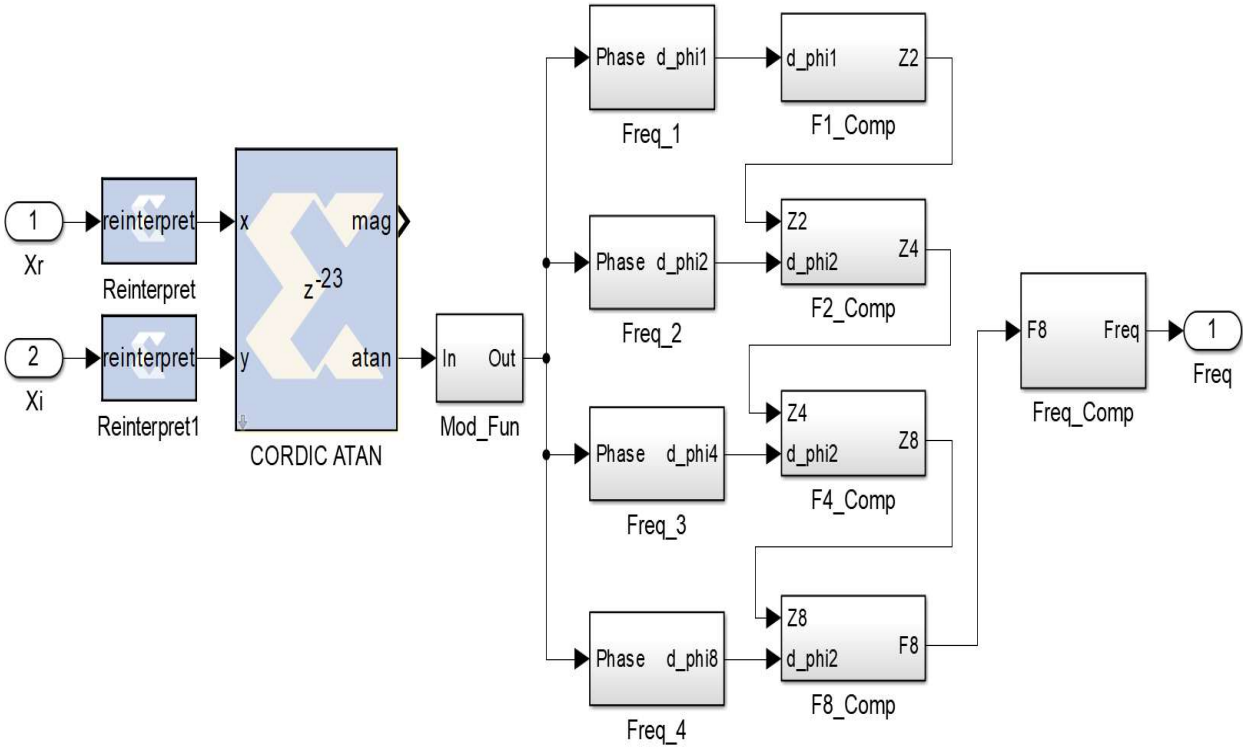

Figure 6.21: Detailed instantaneous frequency measurement system generator model.

6.6.2 AOA measurement model

The angle-of-arrival measurement model is generated using a system generator as shown in Figure 6.22. The frequency measurement is carried out using FFT based technique. The frequency is estimated using FFT based interpolation techniques which are used to an estimate the AOA.

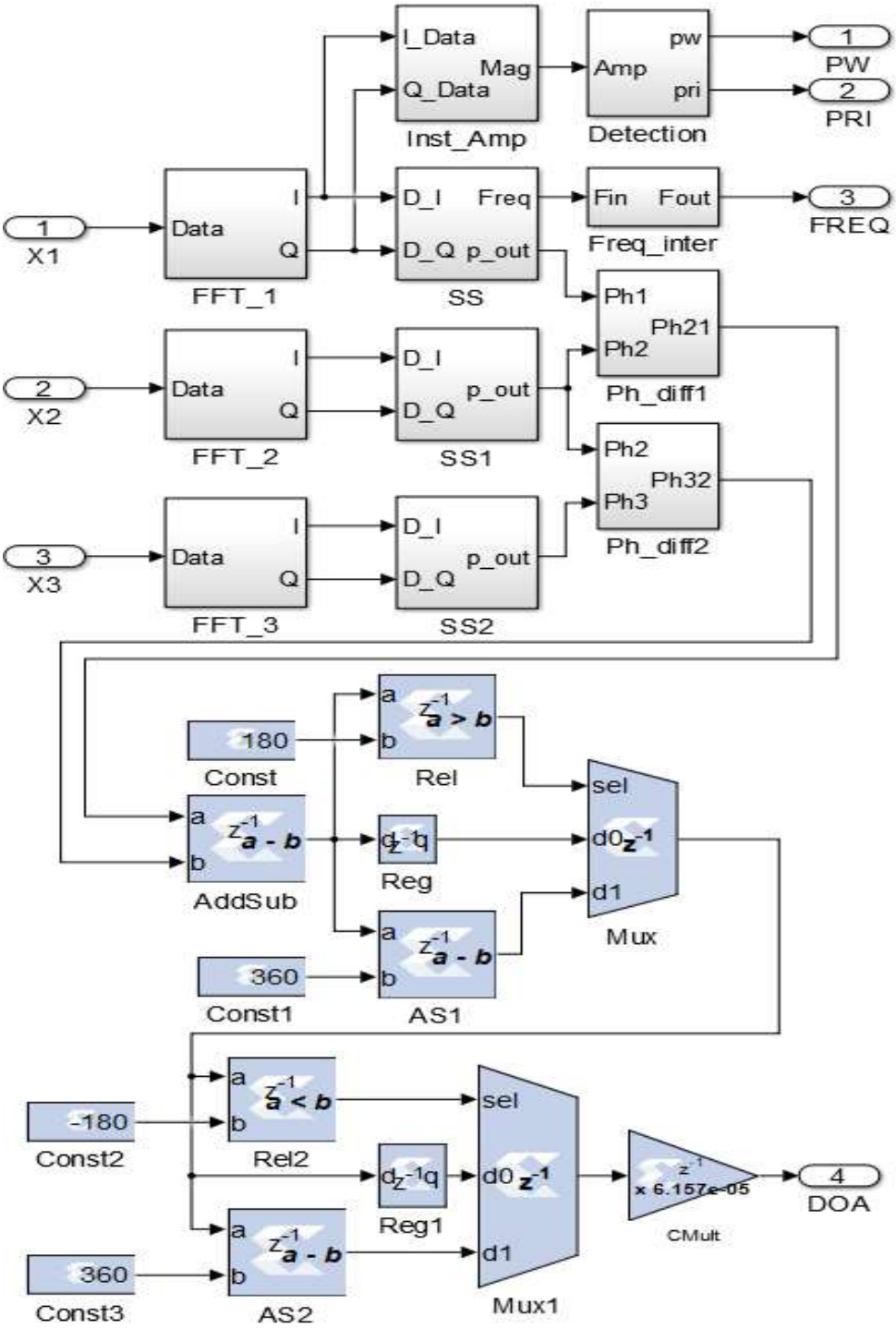

Figure 6.22: Detailed AOA Measurement system generator model.

6.6.3 Modulation measurement model

The modulation recognition system generator model is shown in Figure 6.23. In this amplitude and frequency profiles are generated using the autocorrelation technique. Modulation recognition is carried out using decision-tree algorithms using frequency profiles.

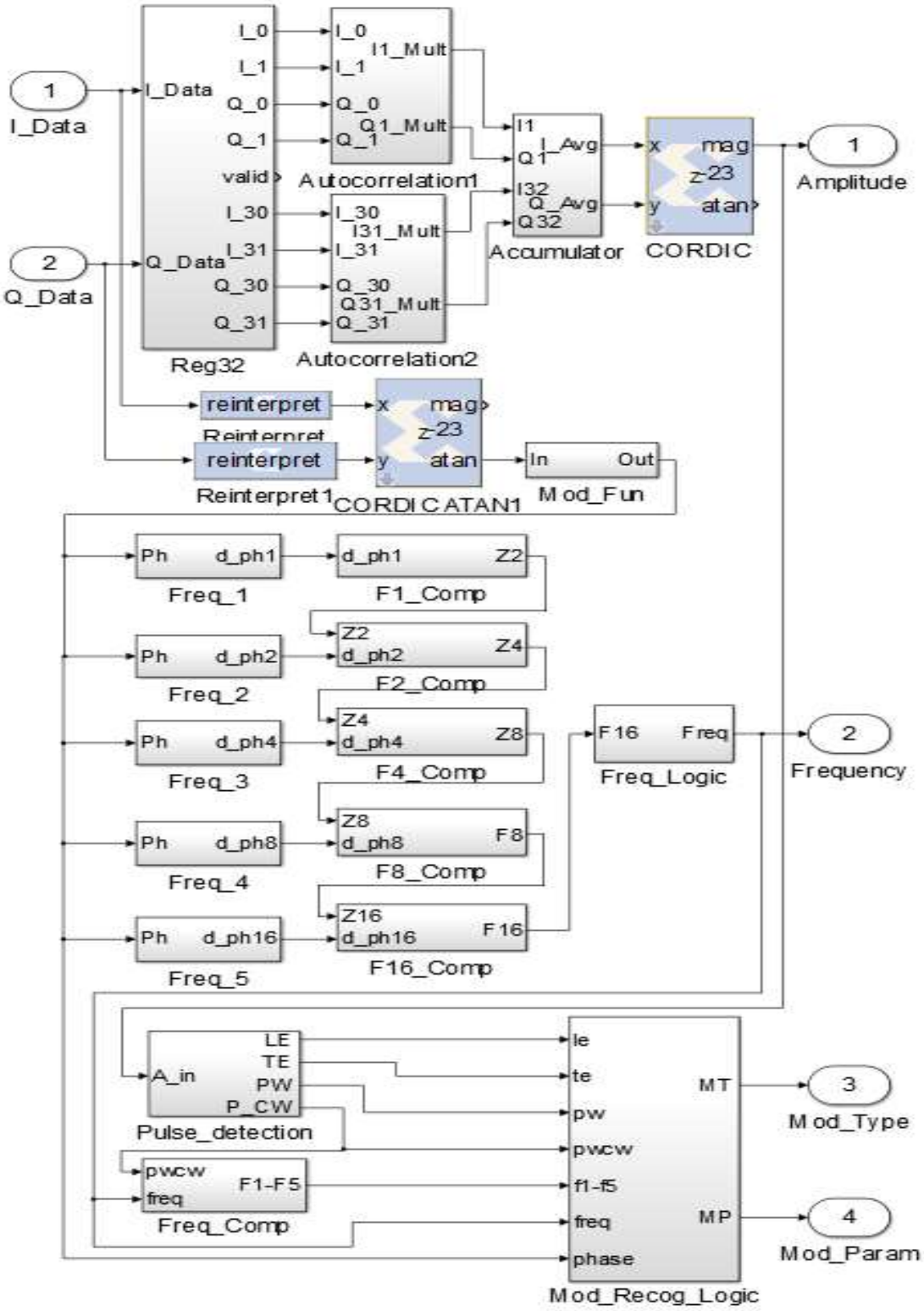

Figure 6.23: Modulation recognition system generator model.

6.7 Implementation Results

6.7.1 Instantaneous amplitude and frequency results

The instantaneous amplitude and frequency profiles results are generated using a system generator model for different frequencies 750 MHz, 1000 MHz, and 1250 MHz as shown in Figures 6.24, 6.25, and 6.26 respectively.

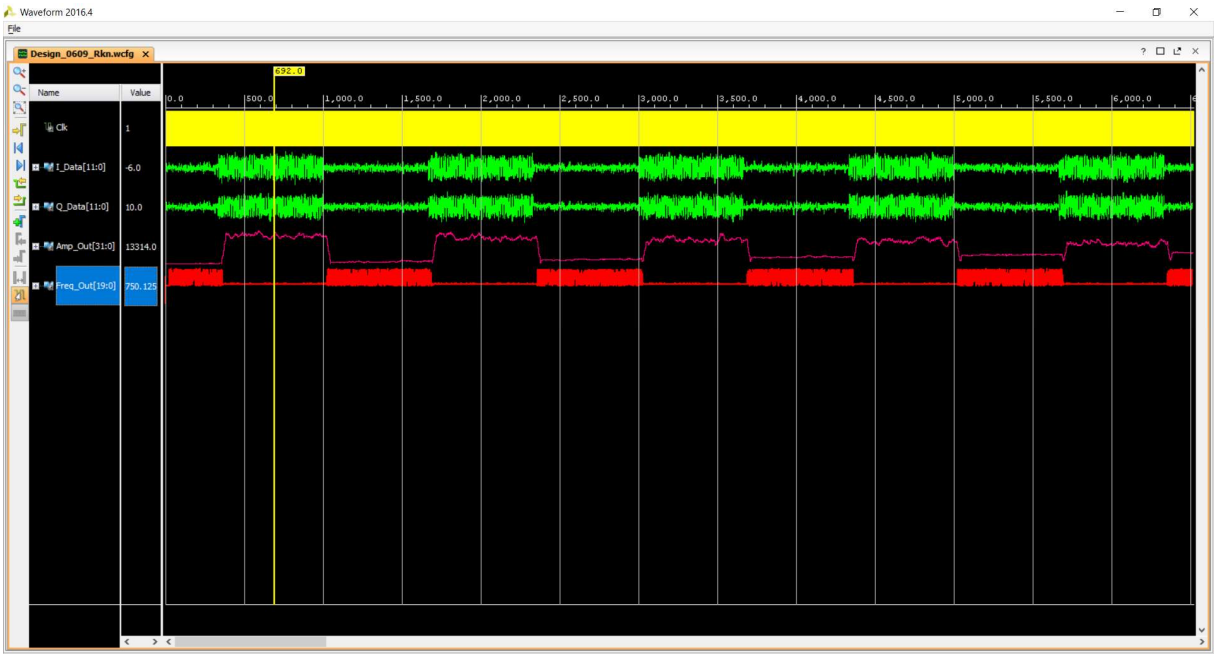

Figure 6.24: System generator simulation result for frequency 750 MHz.

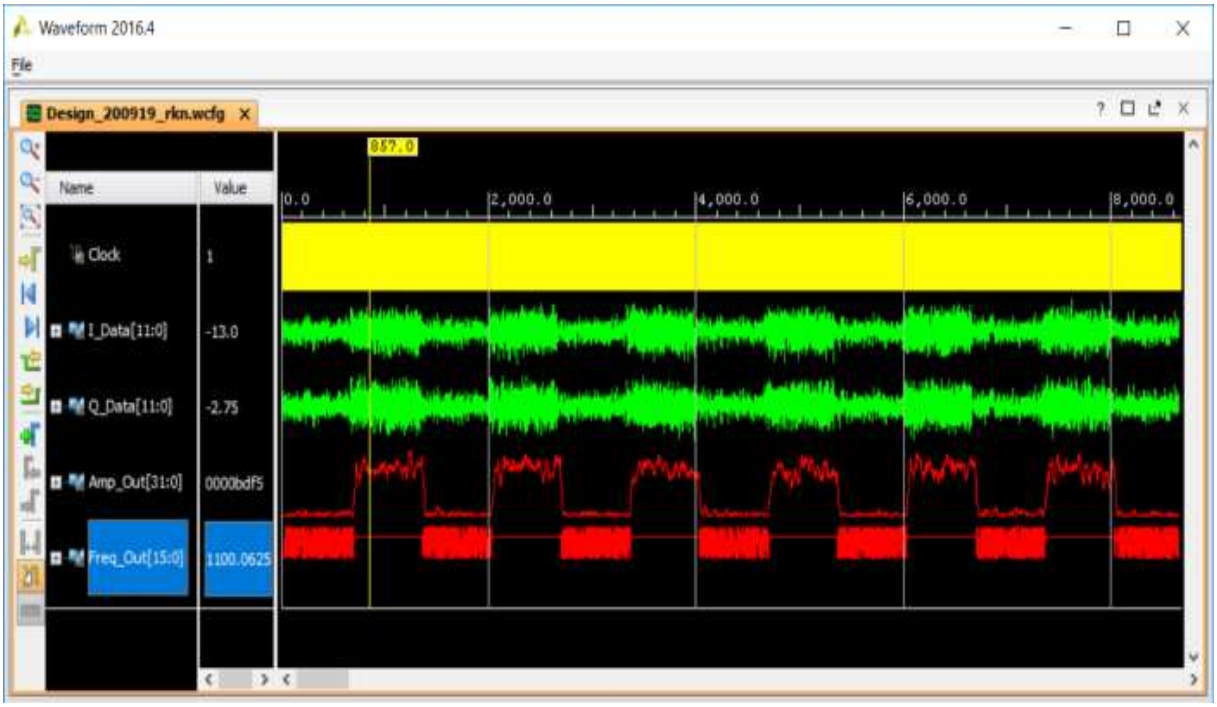

Figure 6.25: System generator simulation result for frequency 1000 MHz.

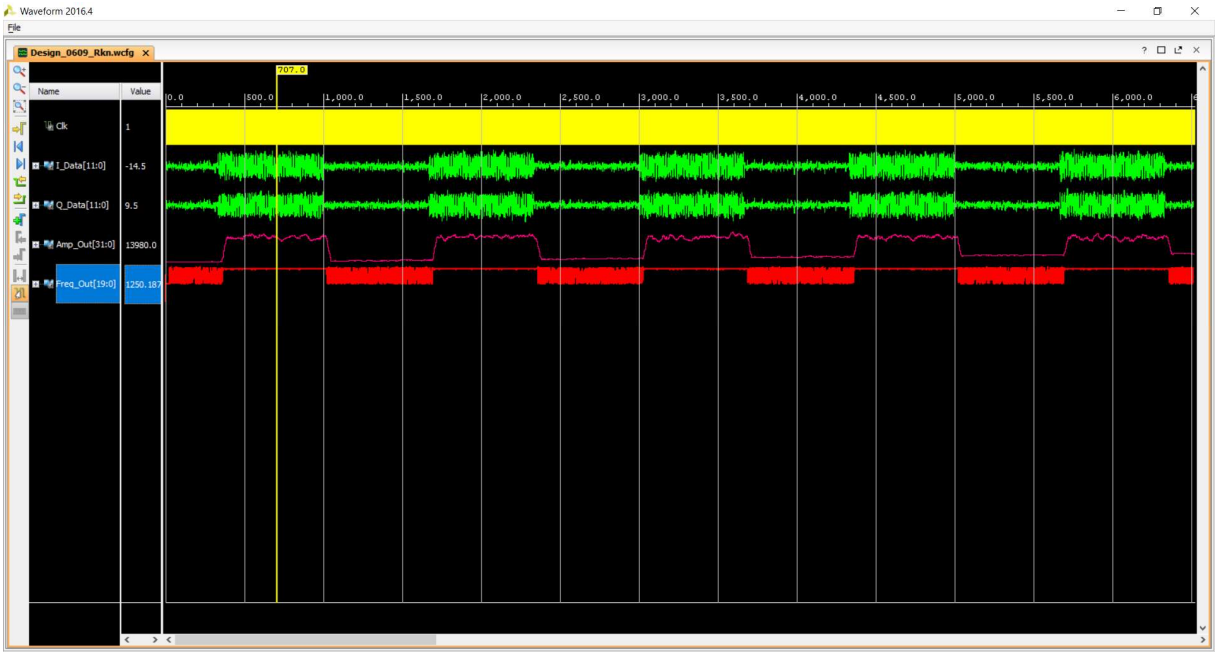

Figure 6.26: System generator simulation result for frequency 1250 MHz.

6.7.2 Modulation recognition results

Figure 6.27 shows the system generator result for LFMad modulation. In this first half of pulse frequency increases and the second half frequency decreases. LFMa modulation type is measured 0x5 and modulation parameter is ascending and descending chirp rate which is measured as 0xc8c8. The minimum frequency measured is 1000 MHz and the maximum frequency is measured as 1200 MHz.

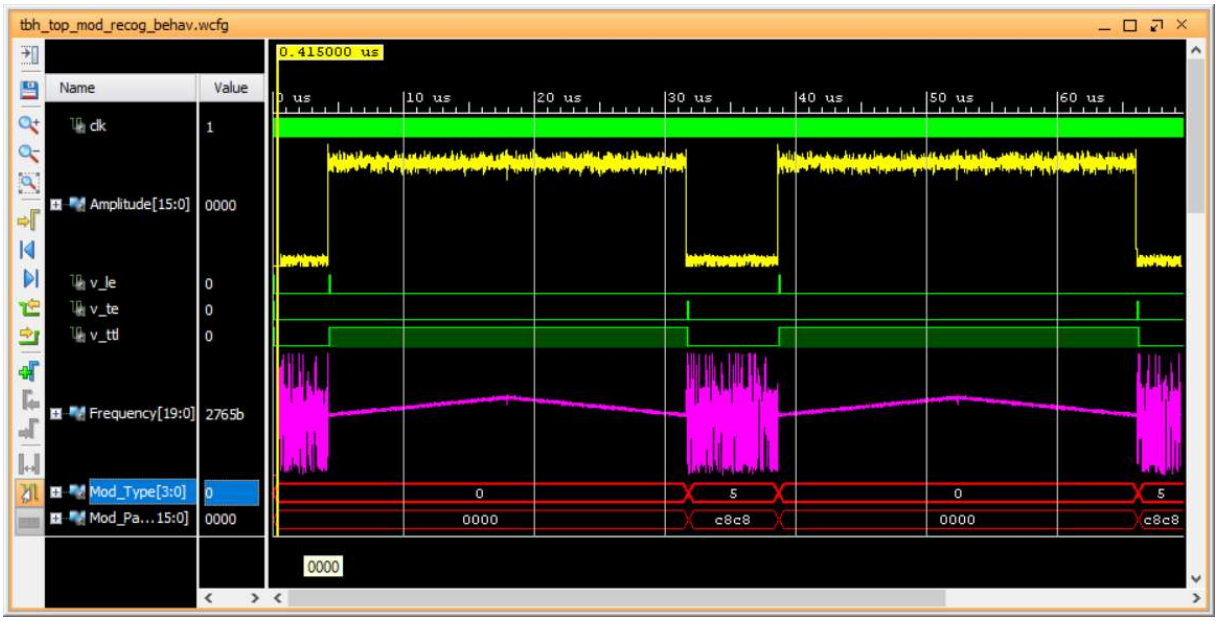

Figure 6.27: Simulation result for LFMad modulation recognition feature at 0 dB SNR.

The system generator result for SFMa - 2 level modulation is shown in Figure 6.28. In this, the first half of pulse and the second half of pulse there is a step change in the frequency. The modulation type is declared as 0xa and the modulation parameter as 0x0002 which shows the number of steps in the pulse. Figure 6.29 shows the BPM modulation. In BPM modulation, the phase is changed by 180^0. Due to this reason sudden change occurs in the frequency. The modulation type is declared as 0xc and modulation parameter as 0x1f35 which is equivalent to the 13-bit BPM.

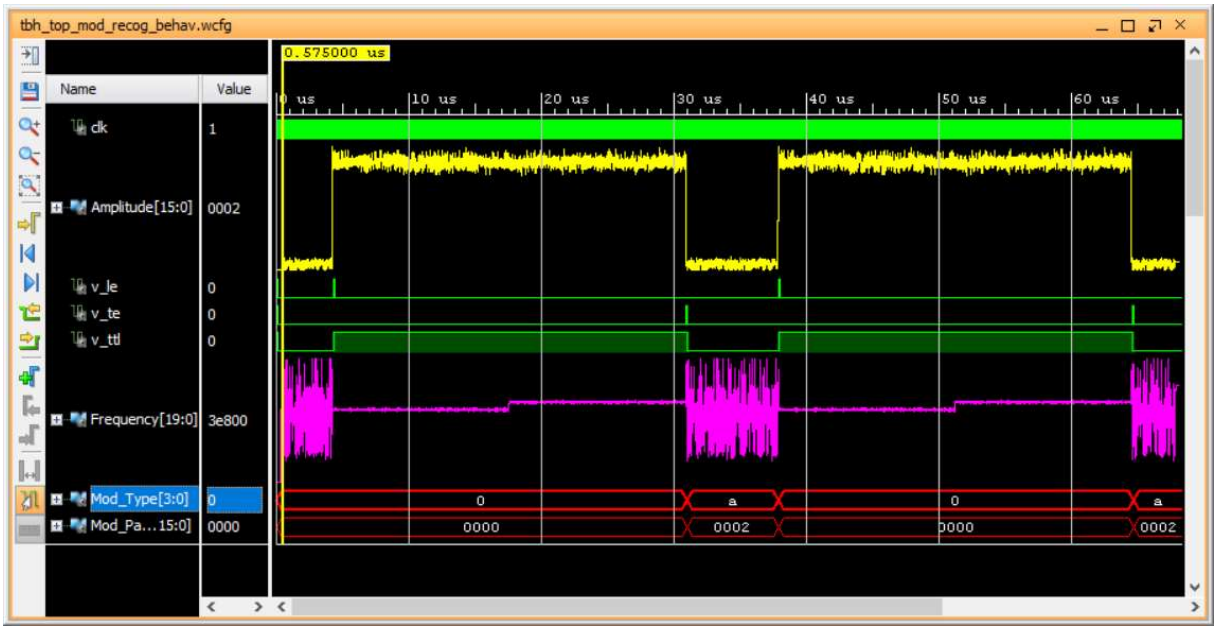

Figure 6.28: Simulation result for SFMa modulation recognition feature at 0 dB SNR.

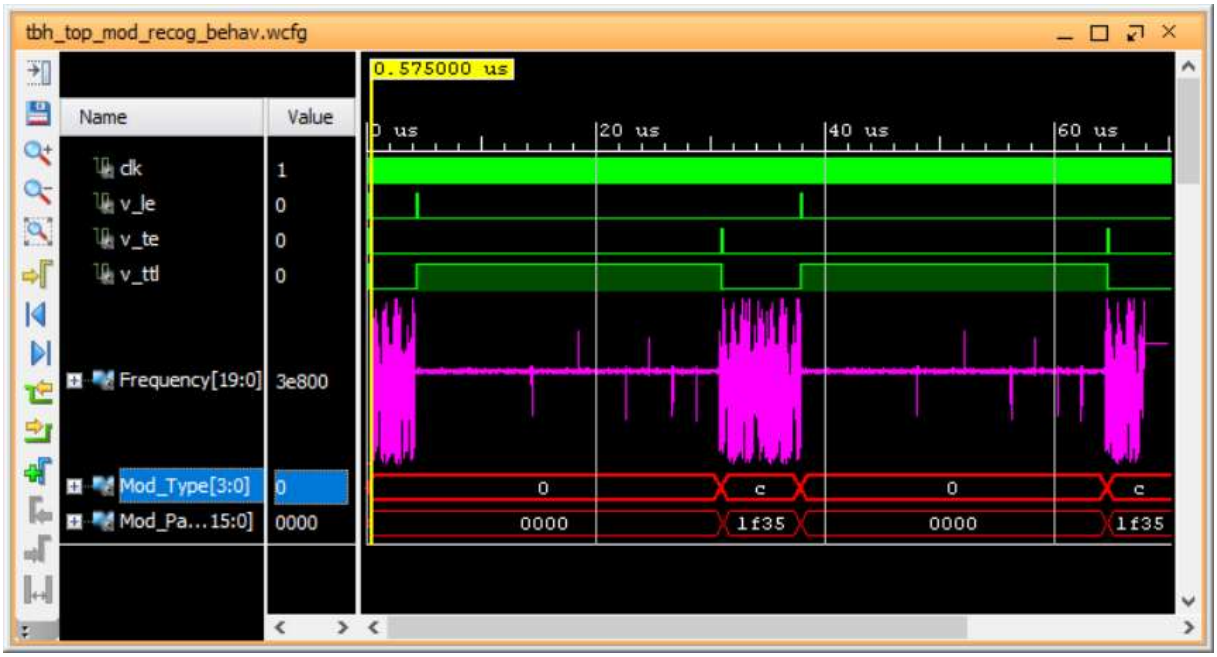

Figure 6.29: Simulation result for BPM modulation recognition feature at 0 dB SNR.

Resource Utilization Summary

The proposed autocorrelation algorithm is implemented with a system generator using Xilinx Vivado 2016.4 tool. The Xilinx device selected is Virtex-4 XC4VSX35-10FF668 FPGA. The synthesis is carried out for netlist generation, mapping for exact mapping of components, place, and route is carried out. The utilization summary is compared for various FPGA resources with the existing DIQ technique and is shown in Table 6.1. Mainly, consumption of DSP resources are very less using proposed algorithm with moving autocorrelation technique compared to the proposed algorithm with DIQ technique. This is possible as no filter implementation is required in autocorrelation approach.

Table 6.1: FPGA resource utilization summary for modulation measurement with amplitude and frequency measurement (Device: XC4VSX35)

FPGA Resource Utilization with Max Operating Freq.	Proposed algorithm with autocorrelation technique	Proposed algorithm with DIQ technique	Savings in %
Maximum Clock Frequency (MHz)	238.6	231.9	2.89
Slice F/Fs	2334	4353	46.38
LUT (4 Inputs)	2883	4136	30.29
DSP Slices	12	42	71.43
Block RAM (FIFO)	15	15	-
Total Power (mW)	546	782	30.18

The AOA estimation is implemented on the Xilinx Kintex Ultra Scale FPGA XCKU060-FFVA1517 which is footprint compatible with radiation tolerant device XQRKU060-CNA1509 for AOA estimation. The resources are compared with the four antennas and three antenna based BLI approaches and mentioned in Table 6.2. BLI algorithms are also implemented in ZCU111 kit and similar results are obtained.

Table 6.2: Resource comparison AOA estimation (Xilinx FPGA: XCKU060-FFVA1517)

FPGA Resource Utilization	3 Antenna Based Proposed Approach	4 Antenna Based Approach	Savings in %
Registers	16567	21355	22.4
LUTs	12893	16283	20.81
36 Kb Block RAM	757	1026	26.21
18 Kb Block RAM	1532	2042	25.02
DSP48 Slices	40	50	20.0
Total Power (mW)	16464	21152	22.16

6.8 Summary

A significant part of this Ph.D. research is concerned with the experimental validation of the algorithms discussed in this thesis. In this chapter, the hardware architecture of the single-channel and multi-channel ELINT Setup that was used to collect the data for experimental validation was presented. A significant portion of the author's time during this Ph.D. candidature was spent in testing, debugging, and calibrating the ELINT setup to allow single-channel and multi-channel data to be collected. In particular, data collected with different SNR conditions and different modulations for single-channel was a critical contribution to the development of real-time modulation measurement for functional ELINT systems.

This chapter has experimentally validated that the real-time modulation identification of signals is performed well when instantaneous amplitude and frequency measurements are carried out using the autocorrelation based techniques compared to the DIQ technique. This is verified till -2 dB of SNR and above 1 dB of SNR for targeted all 16 types of modulations are recognized correctly. These modulations are identified after the signal is preprocessed with a noise cancellation algorithm and SNR advantage has been achieved. This restored signal is used for instantaneous measurements and modulation measurements. To check the efficacy of algorithms, these algorithms are implemented in FPGA based hardware and results are verified. These results are matching with Matlab performance. The error introduced by converting floating point numbers into fixed point numbers has not impacted as a sufficient fractional portion in terms of bits has been chosen.

Similarly, the virtual BLI based AOA estimation algorithms have been chosen compared to four channel BLI estimation algorithms. As the FOV requirement is limited to ±25 degree, the virtual BLI based AOA estimation along with noise cancellation technique is performed similarly to four channel BLI based algorithms. This configuration becomes the size, weight, and power (SWaP) optimized as one-fourth of saving will be there compared to other configurations. The performance of these algorithms was quantified at 4 dB SNR with a 3-antenna and 4-antenna array geometry and their experimental performance was compared.

ELINT systems come under the category of hard real-time as they are used for tactical missions and missing the deadline may cause serious consequences. These systems complete the critical tasks within a response time. This requires that all the delays in the system be bounded from the falling edge of the pulse. These timelines should be met for the formation of PDW. The formation of track based on de-interleaving using the required number of pulses should also be bounded to meet the real-time requirement.

Chapter 7

Conclusions and Future Scope

In the previous chapter ELINT operation methodology is discussed. This includes scan strategy, experimental setups, the hardware used, and various test conditions along with FPGA implementation results. This chapter presents the summary, and conclusions of the thesis. The future scope of the work is also given in the later part of the chapter.

7.1 Conclusions

This thesis is considered the problem of estimating the signal estimation, angle-of-arrival (AOA) estimation, and modulation measurement of intercepted radar signals using ELINT receiver for real-time surveillance (Chapter 1). Due to the tactical and operational requirements of ELINT receivers, especially estimation algorithms need to be computationally fast and highly accurate. Wide frequency surveillance from a large distance requires identifying emitters accurately.

Many contemporary intercept receivers are described. All the receiver advantages and disadvantages are also discussed. It is found that a single channel or multi-channel superhet or a channelized receiver is the best choice for the electronic intelligence receiver. The prime requirement of an electronic intelligence receivers is sensitivity. Simultaneously achieving high sensitivity and large bandwidth is not possible. This will impact on the probability of intercept (POI). When radar transmitter antenna and ELINT receiver antenna are looking at each other within the antenna beam width. In this condition, ELINT receiver will receive the radar pulses. The POI problem is reduced by scanning fast for the complete coverage of the frequency band of 0.5 to 18 GHz. The scanning is controlled by dwell time. If prior knowledge is available of radars and their frequency coverage. The scanning can be planned for those bands only.

A novel technique based on noise cancellation has been developed the first time for electronic intelligence receivers to overcome the effect of noise at low SNR conditions. So far it was used for communication receivers. In this noise spectrum of fixed time duration during

noise region is computed. Noise average is obtained from all FFT outputs. The spectrum of the incoming signal is also obtained and it is subtracted from the noise average. Inverse FFT is computed on subtracted output and restored signal is obtained. The phase of the incoming signal is combined with the restored signal. This technique of noise cancellation enhances the SNR of the incoming signal by 6 to 14 dB (Refer Table 4.3).

A novel technique based on optimized autocorrelation has been developed to calculate accurate instantaneous amplitude profile till 4 dB SNR for pulse detection and other pulse parameter measurements. The autocorrelation technique result is compared with the DIQ technique and found advantages of about 6 to 14 dB (Refer Table 4.3). Instantaneous frequency profile is also computed using the multilevel autocorrelation technique. This technique enables the measurement of intra-pulse parameters. It can be utilized for feature extraction and identification of modulated signals also. Using this technique the instantaneous amplitude and frequency parameters of a pulse can be measured to -2 dB SNR. The total advantage of about 20 dB is achieved if autocorrelation techniques are used after the noise cancellation technique compared with DIQ technique without noise cancellation technique.

Time-domain techniques have limited use due to their less sensitivity compared to frequency domain techniques. But these techniques are capable of instantaneous measurements of frequency and amplitude which gives certain advantages of modulation measurement. But frequency domain techniques provide processing gain advantage inherently. If hardware is capable, this gain can be further improved by increasing the FFT number of points. Fast Fourier Transform (FFT) is used to detect the activity, measurement of frequency, pulse width, and pulse repetition interval. FFT with interpolation technique is proposed to get the frequency accuracy advantage without increasing the FFT number of points. The advantage in detection is also achieved as FFT output itself is used for detection.

In chapter 4, the noise cancellation technique based on spectral subtraction is used which provides a significant SNR advantage. The SNR advantage is also achieved when the autocorrelation technique is used for computing instantaneous amplitude profile and instantaneous frequency profile. These advantages are not possible with the contemporary DIQ technique. Contemporary phase-based interferometric algorithms are computationally fast and offer high accuracy AOA estimation using a less number of antennas. However, the requirement to use physically large wideband antennas for electronic surveillance applications introduces a significant ambiguity problem to the AOA estimation. To perform unambiguous AOA estimation, the antenna positions must be carefully chosen and coupled with ambiguity

resolution algorithms. Further, three antennas based AOA estimation technique provides SWaP advantage for high altitude applications.

It was shown that the ambiguity problem can be completely avoided by using a virtual array to create a virtual short-baseline interferometer. This algorithm was shown to be computationally efficient and operated effectively over the entire microwave frequency range between 0.5 - 18 GHz. The performance of this algorithm was also shown to be limited to the smaller aperture but it is also independent of the physical antenna spacing. Accurate frequency estimation is shown using FFT based technique with interpolation. This accurate measurement of frequency is used for estimating the AOA using the interferometry technique. Both four antenna and three antenna based baseline interferometry are described. Virtual interferometry using three antenna based provides better results when it is used with noise cancellation.

In chapter 5, it was shown that the noise estimation is carried out efficiently for selectable time duration on instantaneous amplitude profiles. The estimated noise is used for computing the adaptive threshold which is used for the detection of the radar signals. The detection of the radar signals is carried out using an amplitude profile. The instantaneous frequency profile generated using the multilevel autocorrelation approach is used for estimating the modulations using the decision-tee algorithm. This algorithm is based on the time-domain based which estimates the modulation in real-time.

In chapter 6, the ELINT receiver methodology is discussed. In this chapter, different level of testing is explained. The data capture is generated using Matlab initially with different SNR and with various modulations and algorithms are verified. This signal is generated with a vector signal generator and captured using a VPX data acquisition card and the digitized IF data is stored in the file. This file is used to validate the algorithms. Later this file is used to verify hardware implementation using FPGA boards. The performance of signal estimation and modulation estimation methods were experimentally validated using the hardware developed.

In chapter 7, a summary of the thesis, overall conclusions, and future scope are given.

7.2 Future scope

This thesis was presented several computationally fast modulation recognition algorithm including signal estimation and evaluated their theoretical and experimental

performance. However, many areas of this work may warrant further investigation. These areas will be briefly discussed below:

Experimental Validation of Other Frequencies - Due to the time constraints and the safety and licensing of transmitting RF signals, the experimental validation of the algorithms in this was only performed for 0.5-18 GHz. Since the objective is to have a radar intercept receiver that can operate between 0.175-40 GHz, it would be desirable to experimentally validate the performance of algorithms at other frequencies.

Experimental Validation Using Different Transmitters - Due to time constraints, the experimentally validation of AOA estimation could not complete with antenna array hardware. This was done using an RFSoC board where three-antenna delay was manually generated instead of between three-antenna output and work was completed. In order to fully validate the experimental performance of the algorithms, it would be desirable to use one transmitter for the calibration signal and a different transmitter for the AOA estimation.

LPI signal - Few low probability intercept (LPI) signals are already attempted in this thesis. But due to the availability of resource-intensive FPGAs the identification of LPI signals may be extended in real-time for polyphase and polytime signals also. But this work requires lot of resources because processing algorithms are frequency domain based which needs to be implemented in processing hardware. But initially, simple LPI signals detection may be tried.

In the future, the modulation identification will be extended for additional signals and other practical combinations of signals. Artificial Intelligence (AI) based algorithms to be developed for the specific emitter identification. This will be an unconventional way of matching. Conventionally, the matching is carried out based on the parameter matching within their window. AI based matching will be helpful to train the algorithm for all available emitters. But implementation feasibility for real-time application will have to be verified.

Third-order spectra (Bispectra) are used to get the high accuracy in amplitude and frequency measurements. But their processing time is large as N (FFT length) is considered the highest possible. Hence, it is difficult to use for real-time ELINT systems where accuracy is achieved in hundreds of kHz. It is used where accuracy is more important i.e. instrument identification where the data rate is comparatively slow. It is useful in analysis based ELINT systems also. In the future, this may be possible to use for real-time systems also.

Appendix - A

Modelling of signal

Conventional narrowband radar signal can be modelled as a single tone and as a function of time as below:

$$s(t) = Ae^{j(2\pi ft+\ )} \tag{A.1}$$

Where A is the amplitude, f is the carrier frequency, t is time and φ is the initial phase. The variation in frequency will be visible. Practically, the ideal signal is corrupted by additive noise component $\epsilon(t)$. For a multi-channel system with K antennas, the signal of the kth antenna with respect to 1th antenna is represented as:

$$x_{kl}(t) = s(t + \tau_{kl}) + \epsilon_k(t) = Ae^{j(2\pi ft+\ )} + \epsilon_k(t) \tag{A.2}$$

Where, k=1,2,3,….K and τ_{kl} is the time taken from kth antenna to 1th antenna. The τ_{kl} is given as

$$\tau_{kl} = \frac{d_{kl}}{c}\ sin\ \theta \cos \phi \tag{A.3}$$

Assuming only incident wave azimuth angle is θ and elevation angle is ϕ=0^0. The above equation is reduced to,

$$\tau_{kl} = \frac{d_{kl}}{c}\ sin\ \theta \tag{A.4}$$

The receiver noise in the kth channel is modelled as an independent and ideally distributed with zero mean and Gaussian random noise with $\sigma^2_{\epsilon_k}$ variance. The receiver noise is assumed to be independent for each receiver. The real and imaginary component of $\epsilon_k(t)$ has an equal variance that is equal to $\sigma^2_k = \sigma^2_{\epsilon_k}/2$. It is generally assumed that each receiver channel having the same noise power and the complex receiver noise power is written as $\sigma^2_\epsilon = \sigma^2_{\epsilon 1} = \sigma^2_{\epsilon 2} = \ldots\ldots = \sigma^2_{\epsilon K}$, and the corresponding real and imaginary noise power can be written as $\sigma^2 = \sigma^2_1 = \sigma^2_2 = \cdots\ldots\ldots = \sigma^2_K$. The signal-to-noise ratio (SNR) of the signal η, can be defined as below:

$$\eta = \frac{A^2}{\sigma^2_\epsilon} = \frac{A^2}{2\sigma^2} \tag{A.5}$$

For a narrowband signal and a linear array geometry, propagation time can be converted into a phase as below:

$$\psi_{kl} = 2\pi f \tau_{kl} = 2\pi f \frac{d_{kl}}{c} \sin\theta \tag{A.6}$$

For a multi-channel digital receiver, the digital sampling of signal occurs at a regular, discrete-time intervals, t_s. For a collection of nt_s samples, the nth sample of digital sample of a narrowband signal model can be re-written as below:

$$x_{kl}(nt_s) = Ae^{j(2\pi f nt_s + \varphi + \psi_{kl})} + \epsilon_k(nt_s) \tag{A.7}$$

The nt_s sample is commonly written as n and the above equation is modified as below:

$$x_{kl}(n) = Ae^{j(2\pi f n + \varphi + \psi_{kl})} + \epsilon_k(n) \tag{A.8}$$

which corresponds to the time instant $t = nt_s = n$, and n = 0, 1, 2….., (N-1).

It should be noted that the time propagation τ_{kl}, is actually the time advances for positive θ and time delay for negative θ. Similarly, the propagation phase ψ_{kl}, is a phase advance for positive θ and phase delay for negative θ. However, for notation conciseness, this thesis will generally refer to τ_{kl} and ψ_{kl} propagation delay and phase delay respectively.

Appendix - B

Fixed Point Presentation of Numbers

The implementation of signal processing algorithms with fixed point numbers (or integer numbers) provides a considerable enhancement in speed. The reason behind is the fixed point numbers support for field programmable gate array or processors. This will also reduce the complexity of software to follow multiplication and division operations. This enhancement of speed achieves with the cost of reduced range and accuracy of the signal processing algorithms variables. If sufficient numbers of bits are chosen for the required range and accuracy, then true speed is achieved.

To further improve the execution speed or throughput the calculations are carried out with two's complement signed fixed-point representations. This requires the virtual decimal placed in between given bits of data. Q-point is the notation used for representing fixed point numbers. This is represented below

$$Q[QI].[QF]$$

Where QI = Number of integer bits, and QF = Number of fractional bits

The number of integer bits (QI) plus the number of fractional bits (QF) yields the total number of bits used to represent the number. The sum $QI + QF$ is known as the word length (WL). For example, a $Q8.8$ number would be a 16-bit value with eight integer bits and eight fractional bits.

B.1 Fixed point range – integer portion

The range of floating point variable (i.e. Min to Max range) in an algorithm sets the number of bits (QI) required to represent the integer portion of the number. This is defined for unsigned numbers as below:

$$QI = Ceil\left(\log_2\left(abs(\alpha)\right)\right) \tag{B.1}$$

Where α is the floating point variable and $0 \leq \alpha \leq 2^{QI}$.

For signed numbers ($\pm\alpha$), the relationship is defined as:

$$QI - 1 = Ceil\left(\log_2(\max(abs[\alpha_{max}, \alpha_{min}]))\right) \quad \text{(B.2)}$$

Where α is the floating point variable, and $-2^{QI-1} \leq \alpha < 2^{QI-1}$.

For example when input frequency varies from 140 to 180 MHz. Integer portion 8 bits are enough because it can cover from 0 to 255 MHz. If the input frequency is varied from 750 to 1250 MHz, the integer portion is chosen 11 bits. Whereas for amplitude number of the integer portion chosen is 8-bits.

B.2 Fixed point resolution – fractional portion

The resolution is limited for a given word length (WL). Since the integer portion is already fixed based on the range and dynamic range of the number the remaining bits will be used for the fractional portion (QF) of the number. In case, where required resolution of a number is high, the world length has to be increased to accommodate the required resolution. The resolution ε , of a fixed point number is defined by the following equation:

$$\varepsilon = \frac{1}{2^{QF}} \quad \text{(B.3)}$$

However, since QF is an integer value only. Therefore, the number of fractional bits (QF) required for a particular resolution is defined by the equation:

$$QF = ceiling\left(\log_2\left(\frac{1}{\varepsilon}\right)\right) \quad \text{(B.4)}$$

The fractional number of bits is chosen for amplitude and frequency of #B-bits for this requirement.

References

[1] Adamy, D.L., “EW 101: A First Course in Electronic Warfare”, Boston, MA, USA: Artech House, pp. 83, 2001.

[2] Adamy, D.L.” EW 102: A Second Course in Electronic Warfare”, Boston, MA, USA: Artech House, pp. 67-72, 2004.

[3] Richard, G.W., “ELINT, the Interception and Analysis of Radar Signals”, Boston, MA, USA: Artech House, 2006.

[4] Ramachandran, R., Sharma, R., & Varughese, S., “Graceful degradation: An airborne surveillance radar perspective”, *Def. Sci. J.*, vol. 69, no. 4, pp. 389-395, 2019. DOI:10.14429/dsj.69.12135.

[5] Aly, O.A.M., Omar, A.S., & Elsherbeni, A.Z., “Detection and localization of rf radar pulses in noise environments using wavelet packet transform and higher order statistics”, *Progress in Electromagnetics Research*, vol. 58, pp. 301–317, 2006, DOI:10.2528/pier05070204.

[6] Aceros-Moreno, C.A., & Rodriguez, D., "Fast discrete chirp Fourier transforms for radar signal detection systems using cluster computer implementations", 48th Midwest Symposium on Circuits and Systems, vol. 2, pp. 1047-1050 2005, doi: 10.1109/MWSCAS.2005.1594284.

[7] Shin, J., Song, K., Yoon, K., & Kim, H., "Weak radar signal detection based on variable band selection," *IEEE Transactions on Aerospace and Electronic Systems*, vol. 52, no. 4, pp. 1743-1755, 2016, DOI: 10.1109/TAES.2016.150121.

[8] Moghaddam, M.H., & Masoumi, N., "Real-time adaptive threshold adjustment method for pulse detection in IFM receiver", *Iranian Conference on Electrical Engineering (ICEE)*, 2018, pp. 244-249, DOI: 10.1109/ICEE.2018.8472596.

[9] Carpentieri, E., & Cuomo, S., "An adaptive threshold algorithm for detection of pulse radar signals," *In Proceedings of the IEEE Radar Conference*, pp. 1-5, 2008, doi: 10.1109/RADAR.2008.4720754.

[10] Gross, F.B., & Chen, K., "Comparison of detectability of traditional pulsed and spread spectrum radar waveforms in classic passive receivers," *IEEE Transactions on Aerospace and Electronic Systems*, vol. 41, no. 2, pp. 746-751, 2005, DOI: 10.1109/TAES.2005.1468765.

[11] Pace, P. E., “Detecting and classifying low probability of intercept radar” 2nd Ed, Boston, London, Artech House, pp. 41-63, 2008.

[12] Conning, M., & Potgieter, F., “Analysis of measured radar data for specific emitter identification”, *In Proceedings of the IEEE Radar Conference*, Washington DC, 2010. DOI: 10.1109/RADAR.2010.5494658.

[13] Szhong, W., “Study on the feature extraction method of radar pulse”, [J]. *Ship Electronic Warfare*, vol. 25, no. 1, pp. 25-28, 2002.

[14] Gupta, M., Hareesh, G., & Mahla, A.K., “Electronic warfare: Issues and challenges for emitter classification”, *Def. Sci. J.*, vol. 61, no. 3, pp. 228-234, 2011. DOI:10.14429/dsj.61.529.

[15] Dudczyk, J., & Kawalec, A., “Identification of emitter sources in the aspect of their fractal features”, *Bull. Pol. Ac.: Tech.*, vol. 61, no. 3, pp. 623–628, 2013. DOI:10.2478/bpasts-2013-0065.

[16] Dudczyk, J., & Kawalec, A., “Specific emitter identification based on graphical representation of the distribution of radar signal parameters”, *Bulletin of the Polish Academy of Sciences: Technical Sciences*, vol. 63, no. 2, pp. 391-396, 2015, DOI:10.1515/bpasts-2015-0044.

[17] Kawalec, A., & Owczarek, R., “Radar emitter recognition using intrapulse data”, *In Proceedings of the MICON*, *Microwave & Radar Week In Poland*, Warsaw, vol. 2, pp. 435-438, 2004. DOI: 10.1109/MIKON.2004.1357059.

[18] Deng, S., Huang, Z., & Wang, X., “A novel specific emitter identification method based on radio frequency fingerprints”, *In Proceedings of the IEEE ICCIA-2017*, Beijing, pp. 368-371, 2017. DOI: 10.1109/CIAPP.2017.8167241.

[19] Pan, Y., Peng, H., Li, T., & Wang, W., “High-fidelity symbol synchronization for specific emitter identification”, *In Proceedings of the IEEE ITNEC-2019***,** Chengdu, pp. 393-398, 2019. DOI: 10.1109/ITNEC.2019.8729181.

[20] Michel, K., & Adams, K., “Matched filter module as an application of modern FPGA in radar systems”, *In Proceedings of the SPIE*, vol. 107150, 2018, DOI: 10.1117/12.2317907.

[21] Niranjan, R.K., & Bhukya, R.N., “Approach of pulse parameters measurement using digital IQ method”, IJIEE, vol. 4, no. 1, pp. 31-35, 2014. DOI: 10.7763/IJIEE.2014.V4.403.

[22] Simin, Z., Deguo, Z., & Bin, T. A., “Wideband pulse detection algorithm based on autocorrelation”. *In Proceedings of the IEEE ICEMI-2009*, Beijing, China, Vol. 4, pp. 287-289, 2009. DOI: 10.1109/ICEMI.2009.5274088.

[23] Tsui, J.B.Y., “Digital Techniques for Wideband Receivers”, 2nd Ed, Norwood, MA Artech House, 2004.

[24] Mahlooji, S., & Mohammadi, K. “Very high resolution digital instantaneous frequency measurement receiver”, *In Proceedings of the IEEE International Conference on Signal Processing and Systems*, ICSPS-2009, 2009. DOI:10.1109/ICSPS.2009.43.

[25] Helton, J., Henry, C.I., David, M.L., & Tsui, J.B.Y., “FPGA - based 1.2 GHz bandwidth digital instantaneous frequency measurement receiver”, *In Proceedings of the ISQED*-2008, San Jose, CA, USA, pp. 265-270, 2008. DOI:10.1109/ISQED.2008.4479798.

[26] Pandolfi, C., Fitini, E., Gabrielli, G., Megna, & E., Zaccaron, A., “Comparison of analog IFM and digital frequency measurement receivers for electronic warfare”, *In Proceedings of the IEEE European Radar Conference*, 2010. ISBN:978-2-87487-019-4.

[27] Pekau, H., & Haslen, J.W., “A comparison of analog front end architectures for digital receivers”, CCECE/CCGEI, Saskatoon, May 2005, IEEE.

[28] Kaiser, S.G., "Digital receiver technology, architecture, and application", *IEEE MTT-S International Microwave Symposium Digest*, pp. 1331-1334 vol. 3, 1996, DOI:10.1109/MWSYM.1996.512181.

[29] Sanchez, M.A., Garrido, M., Lopez-Vallejo, M., & Grajal, J., "Implementing FFT-based digital channelized receivers on FPGA platforms," *IEEE Transactions on Aerospace and Electronic Systems*, vol. 44, no. 4, pp. 1567-1585, 2008, DOI:10.1109/TAES.2008.4667732.

[30] Singh, A.K., & Rao, S.K., “Digital Receiver-based electronic intelligence system configuration for the detection and identification of intrapulse modulated radar signals”, *Def. Sci. J.*, vol. 64, no. 2, pp. 152-158, 2014. DOI:10.14429/dsj.64.5091.

[31] Niranjan, R.K., & Bhukya, R.N., “FPGA based implementation of pulse parameters measurement”, *In Proceedings of IEEE* Science and Information Conference, London, pp. 862-867, 2014.

[32] Akima, H., “A method of smooth curve fitting”, ESSA Tech, ERL 101-ITS 73 US Government Printing Office, Washington D.C., 1969.

[33] Quinn, B.G., “Estimating frequency by interpolation using Fourier coefficients”, *IEEE Trans. Signal Processing*, 2014, vol. 42, no. 5, pp. 1264-1268, 2014. DOI: 10.1109/78.295186

[34] Voglewede, P., “Parabola approximation for peak determination”, *Global DSP Magazine*, vol. 3, no. 5, pp. 13-17, 2004.

[35] Djukanovi, S., “An accurate method for frequency estimation of a real sinusoid”, *In Proceedings of the IEEE Signal Processing Letters*, vol. 23, no. 7, 2016. DOI:10.1109/LSP.2016.2564102.

[36] Upperman, G.J., Upperman, T.L.O., Fouts, D.J., & Pace, P.E., “Efficient time-frequency and bi-frequency signal processing on a reconfigurable computer”, *In Proceedings of the IEEE 42nd Asilomar Conference on Signals, Systems and Computers*, Pacific Grove, pp. 176-180, 2008, DOI: 10.1109/ACSSC.2008.5074386.

[37] Dan, S., Yaqing, T., Ming, L., & Jianyuan, L.U.O., "Comparative analysis of frequency estimation methods," *In Proceedings of the 31st Chinese Control Conference*, pp. 5442-5447, 2012, ISBN:978-1-4673-2581-3.

[38] Sajedian, I., & Rho, J., “Accurate and instant frequency estimation from noisy sinusoidal waves by deep learning”, *Springer*, *Nano Convergence*, 2019, DOI:10.1186/s40580-019-0197-y.

[39] So, H.C., & Chan, K.W., "Reformulation of pisarenko harmonic decomposition method for single-tone frequency estimation," *IEEE Transactions on Signal Processing*, vol. 52, no. 4, pp. 1128-1135, 2004, DOI: 10.1109/TSP.2004.823473.

[40] So, H.C., Chan, K.W., Chan, Y.T., & Ho, K.C., "Linear prediction approach for efficient frequency estimation of multiple real sinusoids: algorithms and analyses," *IEEE Transactions on Signal Processing*, vol. 53, no. 7, pp. 2290-2305, 2005, DOI:10.1109/TSP.2005.849154.

[41] So, H.C., & Chan, K.W., "A generalized weighted linear predictor frequency estimation approach for a complex sinusoid," *IEEE Transactions on Signal Processing*, vol. 54, no. 4, pp. 1304-1315, April 2006, DOI: 10.1109/TSP.2005.863119.

[42] So, H.C., Chan, F.K.W., Lau, W.H., & Chan, C., "An efficient approach for two-dimensional parameter estimation of a single-tone," *IEEE Transactions on Signal Processing*, vol. 58, no. 4, pp. 1999-2009, 2010, DOI: 10.1109/TSP.2009.2038962.

[43] Liu, L., Liu, X., & Ma, X., "First-order perturbation analysis of singular vectors in singular value decomposition," *IEEE Transactions on Signal Processing*, vol. 56, no. 7, pp. 3044-3049, 2008, DOI: 10.1109/TSP.2007.916137.

[44] Chan, F.K.W., So, H.C., & Sun, W., “Subspace approach for two-dimensional parameter estimation of multiple damped sinusoids,” *Elsevier Signal Processing*, vol. 92, no. 9, pp. 2172-2179, 2012, DOI:10.1016/j.sigpro.2012.02.003.

[45] Kay, S.M., “Modern Spectral Estimation: Theory and Applications”, Prentice-Hall, 1988.

[46] Stoica, P., & Moses, R., “Spectral Analysis of Signals”, Prentice Hall, 2005.

[47] Zeng, B., Teng, Z., Cai, Y., Guo, S., & Qing, B., “Harmonic phasor analysis based on improved FFT algorithm,” *IEEE Transactions on Smart Grid*, vol.2, no.1, pp. 51-59, 2011, DOI: 10.1109/TSG.2010.2078841.

[48] Lyons, R.G., “Understanding Digital Signal Processing”, Boston, Addison Wesley Longman, Inc., 1997.

[49] Lipsky, S.E., “Microwave Passive Direction Finding”, SciTech Publishing, Inc., 2004.

[50] Sundaram, K.R., Mallik, R.K., & Murthy, U.M.S.. “Modulo conversion method for estimating the direction of arrival”, *IEEE Transactions on Aerospace and Electronic Systems*, vol. 36, no. 4, pp. 1391-1396, 2000. DOI: 10.1109/7.892687

[51] Orduyilmaz, A., Kara, G., Gürel, A.E., Serin, M., Yildirim, A., & Soysal, G., “Real time four channel phase comparison direction finding method”, *In Proceedings of the Signal Processing and Communications Applications Conference (SIU)*, Izmir, Turkey, 2018. DOI: 10.1109/SIU.2018.8404590.

[52] Gurel, A.E., Orduyilmaz, A., Yıldırım, S.A., Kara, G., Serin, M., Ortatatlı, I.E., & Yildirim, A., “Real time passive direction finding In FPGA environment”, *In Proceedings of the IEEE Signal Processing and Telecommunication Applications*, Antalya, 2017. DOI: 10.1109/SIU.2017.7960593.

[53] Ata, S.O., & Isik, C., “High-resolution direction-of-arrival estimation via concentric circular arrays”, *Hindawi Publishing Corporation ISRN, Signal Processing Volume*, 2013, DOI: 10.1155/2013/859590.

[54] Yuan, Q., Chen, Q., & Sawaya, K., "Accurate DOA estimation using array antenna with arbitrary geometry," *IEEE Transactions on Antennas and Propagation*, vol. 53, no. 4, pp. 1352-1357, 2005, DOI: 10.1109/TAP.2005.844409.

[55] Sakai, H., Nishiyama, E., & Toyoda, I., "Direction of arrival estimating array antenna," *International Symposium on Antennas and Propagation (ISAP)*, 2012, pp. 1124-1127. ISBN: 978-1-4673-1001-7.

[56] Osman, L., Sfar, I., & Gharsallah, A., “An overview of direction-of-arrival estimation using an antenna array with four elements“, *American Journal of Applied Sciences*, *Science Publication*, vol. 9, no. 12, pp. 1979-1984, 2012, DOI:10.3844/ajassp.2012.1979.1984.

[57] Gross, F.B., & Chen, K., “Comparison of detectability of traditional pulsed and spread spectrum radar waveforms in classic passive receivers”, *IEEE Transactions on Aerospace and Electronic Systems*, vol. 41, no. 2, pp. 746-751, 2005. DOI**:** 10.1109/TAES.2005.1468765.

[58] Fan, X., Li, L., Li, T., & Chen, T., "A new method for polyphase pulse compression codes modulation recognition based on IQPF and FRFT", *In Proceedings of the* Advanced Information Technology, Electronic and Automatio*n Control Conference (IAEAC)*, IEEE, pp. 1172-1176, 2017. DOI**:** 10.1109/IAEAC.2017.8054198.

[59] Nadav, L., & Eli, M., "Radar Signals", Wiley–Interscience, New York, 2004.

[60] Azzouz, E.E., & Nandi, A.K., "Automatic Modulation Recognition of Communication Signals", Kluwer Academic Publishers. Boston, MA, 1996.

[61] Yun, L., & Chunguang, M., "Automatic modulation recognition of communication signals", IJFGCN, vol. 10, no. 1, pp. 83-96, 2017. DOI:10.14257/ijfgcn.2017.10.1.08.

[62] Park, B., & Ahn, J.M., "Intra-pulse modulation recognition using pulse description words and complex waveforms", *International Conference on Information and Communication Technology Convergence (ICTC)*, Jeju, pp. 555-560, 2017. DOI:10.1109/ICTC.2017.8191039.

[63] Yar, E., Kocamis, M.B., Orduyilmaz, A., Serin, M., & Efe, M., "A complete framework of radar pulse detection and modulation classification for cognitive EW", *In Proceedings of the European Signal Processing Conference (EUSIPCO)*, pp. 1-5, 2019. DOI: 10.23919/EUSIPCO.2019.8903045.

[64] Zhang, J., Li, Y., & Yin, J., "Modulation classification method for frequency modulation signals based on the time–frequency distribution and CNN", *In IET Radar, Sonar, Navigation*, vol. 12, no. 2, pp. 244-249, 2018. DOI: 10.1049/iet-rsn.2017.0265.

[65] Azzouz, E.E., & Nandi, AK., "Automatic identification of digital modulation types", *Elsevier, Signal Processing*, vol. 47, no. 1, pp. 55-69, 1995. DOI:10.1016/0165-1684(95)00099-2.

[66] Nandi, A.K., & Azzouz, E.E., "Automatic analogue modulation recognition", *Elsevier,* Signal Processing, vol. 46, no. 2, pp. 211-222. 1995. DOI: 10.1016/0165-1684(95)00083-P.

[67] Nandi, A.K., & Azzouz, E.E., "Algorithms for automatic modulation recognition of Communication signals", *IEEE Trans. on Communications*, vol. 46, no. 4, pp. 431-436, 1998, DOI: 10.1109/26.664294.

[68] Dubuc, C., Boudreau D., Patenaude F., & Inkol R., "An automatic modulation recognition algorithm for spectrum monitoring applications", *In Proceedings of the International Conference on Communications*, IEEE, Vancouver, BC., pp. 570-574, 1999. DOI: 10.1109/ICC.1999.768003.

[69] Chan, Y.T., & Gadbois, L.G., “Identification of the modulation type of a signal”, *In Proceedings of the Signal Processing*, vol. 16, no. 2, pp. 149-154, 1989. DOI:10.1109/ICASSP.1985.1168289.

[70] You, H., Su. F., & Qu, K., “A novel multiple LFM signals detection method”, *In Proceedings of the International Conference on Microwave and Millimeter Wave Technology (ICMMT)*, pp. 818-821, 2004. DOI:10.1109/ICMMT.2004.1411655.

[71] Xu S.W., & Shui, P.L., “Nonparametric detection of frequency modulated signals using fractional Fourier transform”, *Electronics Letters*, vol. 46, no. 9, pp. 649-650, 2010. DOI: 10.1049/el.2010.0569.

[72] Qun, Y. , Heng, C., & Moyun, G., “Radar specific emitter identification using carrier frequency feature”, *In Proceedings of the IEEE International Conference on Signal, Information and Data Processing, ICSIDP-2019*, pp. 1-4, 2019.

[73] Dudczyk, J., & Kawalec, A., “Fast-decision identification algorithm of emission source pattern in database”, *Bulletin of the Polish Academy of Sciences Technical Sciences*, vol. 63, no. 2, 2015, DOI: 10.1515/bpasts-2015-0043.

[74] Wong, L.J., Headley, W.C., & Michaels, A.J., "Specific emitter identification using convolutional neural network-based IQ imbalance estimators," *in IEEE Access*, vol. 7, pp. 33544-33555, 2019, DOI: 10.1109/ACCESS.2019.2903444.

[75] Matuszewski, J., "The analysis of modern radar signals parameters in electronic intelligence system," *In Proceedings of the IEEE 13th International Conference on Modern Problems of Radio Engineering, Telecommunications and Computer Science (TCSET)*, 2016, pp. 298-302, DOI: 10.1109/TCSET.2016.7452040.

[76] Zanga, H., & Li, Y., “Overview of radar intra-pulse modulation recognition”, *In Proceedings of the International Conference on Computer-Aided Design, Manufacturing, Modeling and Simulation (CDMMS)*, 2018, DOI: 10.1063/1.5039020.

[77] Qu, Z., Hou, C., Hou, C., & Wang, W., "Radar signal intra-pulse modulation recognition based on convolutional neural network and deep Q-learning network," *In IEEE Access*, vol. 8, pp. 49125-49136, 2020, DOI: 10.1109/ACCESS.2020.2980363.

[78] Chilukuri, R.K., Kakarla, H.K., Subbarao, K., “Estimation of modulation parameters of LPI radar using Cyclostationary method”, *Springer, Sensing and Imaging*, 2020, DOI: 10.1007/s11220-020-00313-3.

[79] Kawalec, A., & Owczarek, R., "Radar emitter recognition using intrapulse data," *In Proceedings of the International Conference on Microwaves, Radar and Wireless Communications* (IEEE Cat. No.04EX824), Warsaw, Poland, 2004, pp. 435-438, vol. 2, DOI:10.1109/MIKON.2004.1357059.

[80] Guo, S., White, R.E., & Low, M., "A comparison study of radar emitter identification based on signal transients," *In Proceedings of the IEEE Radar Conference (RadarConf18)*, 2018, pp. 0286-0291, DOI: 10.1109/RADAR.2018.8378572.

[81] Erdem, C., and Kara, A., "Specific emitter identification using video signals," *In Proceedings of the Signal Processing and Communications Applications Conference (SIU)*, Mugla, Turkey, 2012, pp. 1-4, DOI: 10.1109/SIU.2012.6204738.

[82] H. Jiang, W. Guan and L. Ai, "Specific radar emitter identification based on a digital channelized receiver," *In Proceedings of the International Congress on Image and Signal Processing*, 2012, pp. 1855-1860, DOI: 10.1109/CISP.2012.6469940.

[83] Gillespie, B.W., & Atlas, L.E., "Optimizing time-frequency kernels for classification", *In Proceedings of the IEEE Transactions on Signal Processing*, vol. 49, no. 3, pp. 485-496, 2001, DOI: 10.1109/78.905863.

[84] Xi, T., Yishan, L., Xianyue, P., & Wentao, C., "Intra-pulse intentional modulation recognition of radar signals at low SNR," *In Proceedings of the IEEE International Conference on Circuits, System and Simulation (ICCSS)*, 2018, pp. 66-70, DOI: 10.1109/CIRSYSSIM.2018.8525907.

[85] W. Fenghua, H. Zhitao, Z. Yiyu and J. Wenli, "A new approach for intra-pulse modulation recognition", *In Proceedings of the International Conference on Radar (CIE)*. pp. 1-5, 2006, DOI:10.1109/ICR.2006.343571.

[86] Ho, K.C., Prokopiw, W., & Chan, Y.T., "Modulation identification by the wavelet transform", *In Proceedings of the Military Communications Conference (MILCOM)*, IEEE, vo. 2, pp. 886 -890, 1995, DOI: 10.1109/MILCOM.1995.483654.

[87] Shi, Q. & Karasawa, Y., "Automatic modulation identification based on the probability density function of signal phase", *IEEE Transactions on Communications*, vol. 60, no. 4, pp. 1033-1044, 2012, DOI: 10.1109/TCOMM.2012.021712.100638.

[88] Mingquan, L., Xianci, X., & Lemin, L., "Cyclic spectral features based modulation recognition", *Communications Technology Proceedings*, *International Conference (IICT)*, vol. 2, pp: 792-795, 1996, DOI: 10.1109/icct.1996.545000.

[89] Haderer, H., Feger, R., & Stelzer, A., "A comparison of phase-coded CW radar modulation schemes for integrated radar sensors," *In Proceeding of 11th European Radar Conference*, pp. 593-596, 2014, DOI: 10.1109/EuRAD.2014.6991340.

[90] Zhou, Y., Wang, X., Tian, Y., & Zhou, D., "A novel time-frequency atomic dictionary for radar intra-pulse modulation signal sparse representation", *In Proceeding of the Asia-Pacific Microwave Conference (APMC)*, 2015, DOI:10.1109/apmc.2015. 7411680.

[91] Fan, X., Li, L., Li, T., & Chen, Z., "A new method for polyphase pulse compression codes modulation recognition based on IQPF and FRFT," *IEEE 2nd Advanced Information Technology, Electronic and Automation Control Conference (IAEAC)*, 2017, pp. 1172-1176, DOI: 10.1109/IAEAC.2017.8054198.

[92] Wang, P., Qiu, Z., Zhu, J., & Tang, B., "Autonomous radar pulse modulation classification using modulation components analysis", *EURASIP Journal on Advances in Signal Processing*, 2016, DOI:10.1186/s13634-016-0394-3

[93] Lunden, J., & Koivunen, V., "Automatic radar waveform recognition," *IEEE Journal of Selected Topics in Signal Processing*, vol. 1, no. 1, pp. 124-136, 2007, DOI:10.1109/JSTSP.2007.897055.

[94] Selim, A., Paisana, F., Arokkiam, J.A., Zhang, Y., Doyle, L., & Dasilva, L.A., "Spectrum monitoring for radar bands using deep convolutional neural networks," *In Proceeding of IEEE Global Communications Conference*, 2017, pp. 1-6, DOI:10.1109/GLOCOM.2017.8254105.

[95] Shun, Z., "A radar signal intra-pulse modulation characteristic analysis method" *[J]. Space Electron Countermeasure*, vol. 22, no. 1, pp. 52-54, 2006.

[96] Fenghua, W., Zhitao, H., & Wenli, J. "An effective method for intra-pulse modulation" *Signal Identification Journal*, *Signal Processing*, vol. 23, no. 5, pp. 686-689. 020048-5, 2007.

[97] Germany, Z., Hui, X., Keyu, L., et al., "Identification of intra-pulse modulated signal types based on phase difference", *Journal of Electronics & Measurements*, vol. 10, no. 10, pp. 85-90, 2009.

[98] Wang, H.W., Zhao, G.Q., & Wang, Y.J., "Identification of radar emitter based on pulse envelope", *Leading Waveform Journal*, *Automated Space Electronics*, vol. 25, no. 2, pp. 35-38, 2009.

[99] Zheng, L., Wenli, J., et al., "Signal recognition of radiation source based on wavelet transform", *[J]. Signal Processing*, vol. 21, no. 5, pp. 460-464, 2005.

[100] Ge, Z., Sun, X., Ren, W., Chen, W., & Xu, G. "Improved algorithm of radar pulse repetition interval deinterleaving based on pulse correlation", *IEEE Access*, vol. 7, pp. 30126-30134, 2019. DOI:10.1109/ACCESS.2019.2901013.

[101] Iglesias, V., Grajal, J., Yeste-Ojeda, O., Garrido, M., Sánchez, M.A., & López-Vallejo, M., "Real-time radar pulse parameter extractor", *In Proceedings of the IEEE Radar Conference*, pp. 371-375, 2014. DOI:10.1109/RADAR.2014.6875617.

[102] Bagheri, M., & Sedaaghi, M.H., “A new approach to pulse deinterleaving based on adaptive thresholding”, *Turk. J. Elec. Eng. & Comp. Sci.*, vol. 25, pp. 3827-3838, 2017. DOI:10.3906/elk-1606-415.

[103] Zhang-Meng, L., “Online pulse deinterleaving with finite automata”, *IEEE Transactions on Aerospace and Electronic Systems*, vol. 56, no. 2, pp. 1139-1147, 2020. DOI:10.1109/TAES.2019.2925447.

[104] Fuhua, F., & Xuezhong, Y., “Improved method for deinterleaving radar pulse trains with stagger PRI from dense pulse series”, *International Conference on Signal Processing Systems (ICSPS), IEEE.*, vol. 3, pp. 250-253, 2010, DOI: 10.1109/ICSPS.2010.5555655.

[105] Barnwal, P., Upadhyay, D., & Bera, S.C., "A novel approach for radar PRI classification based on features estimation," *In Proceedings of the IEEE URSI Asia-Pacific Radio Science Conference (AP-RASC)*, 2019, pp. 1-1, DOI: 10.23919/URSIAP-RASC.2019.8738194.

[106] Li, H., Zhao, J., & Zhang, Y., "Signals deinterleaving for es systems using improved CFSFDP algorithm," *IEEE Radar Conference (RadarConf)*, 2019, pp. 1-5, DOI:10.1109/RADAR.2019.8835717.

[107] Noone, G., "Radar pulse train parameter estimation and tracking using neural networks," *In Proceedings of the International Two-Stream Conference on Artificial Neural Networks and Expert Systems*, pp. 95-98, 1995, DOI:10.1109/ANNES.1995.499448.

[108] Wei, S., Qu, Q., Wu, Y., Wang, M. & Shi, J., "PRI modulation recognition based on squeeze-and-excitation networks," *In IEEE Communications Letters*, vol. 24, no. 5, pp. 1047-1051, 2020, DOI: 10.1109/LCOMM.2020.2970397.

[109] Xi, Y., Wu, X., Wu, Y. Cai, Y., & Zhao, Y., "A novel algorithm for multi-signals deinterleaving and two-dimensional imaging recognition based on short-time PRI transform," *Chinese Automation Congress (CAC)*, pp. 4727-4732, 2019, DOI:10.1109/CAC48633.2019.8996290.

[110] Jawad, M., Iqbal, Y., & Sarwar, N., "PRI characteristics analysis under complex environment of spurious and missing observations," *In Proceedings of the IEEE 17th International Bhurban Conference on Applied Sciences and Technology (IBCAST)*, pp. 617-621, 2020, DOI: 10.1109/IBCAST47879.2020.9044592.

[111] X. Li, Z. Liu and Z. Huang, "Attention-based radar PRI modulation recognition with recurrent neural networks," in IEEE Access, vol. 8, pp. 57426-57436, 2020, DOI:10.1109/ACCESS.2020.2982654.

[112] Ahmed, U.I., Aziz, I., & Rehman, T.U., "Comprehensive Review of Pulse Repetitions Interval (PRI) Classification Schemes," *In Proceedings of the IEEE International Conference on Aerospace Science and Engineering (ICASE)*, pp. 1-6, 2019, DOI: 10.1109/ICASE48783.2019.9059170.

[113] Li, X., Liu, Z., & Huang, Z., "Deinterleaving of pulse streams with denoising autoencoders," *IEEE Transactions on Aerospace and Electronic Systems*, vol. 56, no. 6, pp. 4767-4778, 2020, DOI: 10.1109/TAES.2020.3004208.

[114] Shi, Z., Wu, H., Shen, W., Cheng, S., & Chen, Y., "Feature extraction for complicated radar PRI modulation modes based on auto-correlation function," *In Proceedings of the IEEE Advanced Information Management, Communicates, Electronic and Automation Control Conference (IMCEC)*, pp. 1617-1620, 2016, DOI: 10.1109/IMCEC.2016.7867491.

[115] Lbpez-Risuefio, G., Grajal, J., Yeste-Ojeda, O.A., Sanz-Osorio, A., & Moreno, J.A., "Two digital receivers based on time-frequency analysis for signal interception", *In Proceedings of the International Conference on Radar,* IEEE, pp. 394-399, 2003. DOI:10.1109/RADAR.2003.1278774.

[116] Tsui, J.B.Y., "Microwave Receivers with Electronic Warfare Applications", SciTech Publishing, Inc, Raleigh, NC.

[117] Saeed, V.V., "Advanced Digital Signal Processing and Noise Reduction", 4th Ed, John Wiley, Sons, pp. 321-323, 2008.

[118] Kay, S.M., "Fundamentals of Statistical Signal Processing: Estimation Theory", Prentice-Hall, 1993.

[119] "IEEE standard for digitizing waveform recorders," *In IEEE Std* 1057-1994, 1994, DOI:10.1109/IEEESTD.1994.122649.

[120] Wu, Y.W., Rhodes, S., & Satorius, E.H., "Direction of arrival estimation via extended phase interferometry", *IEEE Transactions on Aerospace and Electronic Systems*, vol. 31, no. 1, pp. 375-381, 1995. DOI: 10.1109/7.366318.

[121] Peter, Q.C., Ly, Stephen, D.E., Douglas, A. G., & Joy, Li., "Unambiguous AOA estimation using SODA interferometry for electronic surveillance", *In Proceedings of the IEEE Sensor Array and Multichannel Signal Processing Workshop (SAM)*, Hoboken, NJ, USA, 2012. DOI: 10.1109/SAM.2012.6250488.

[122] Xia, X.G., & Wang, G., "Phase unwrapping and a robust Chinese remainder theorem", *IEEE Signal Processing Letters*, vol. 14, pp. 247-250, 2007.

[123] Hyun, e., et al., "FPGA based signal processing module design and implementation for FMCW vehicle radar systems," *In Proceedings of IEEE CIE International Conference on Radar*, pp. 273-275, 2011, DOI: 10.1109/CIE-Radar.2011.6159531.

[124] Ishwerya, P., Geethu, S., & Lakshminarayanan, G., "Autocorrelation based spectrum sensing architecture on FPGA with dynamic offset compensation," *IEEE Distributed Computing, VLSI, Electrical Circuits and Robotics (DISCOVER)*, pp. 153-157, 2016, DOI: 10.1109/DISCOVER.2016.7806250.

[125] Lopez-Risueno, G., Grajal, J., Yeste-Jeda, O.A. Sanz-Osorio, A., & Moreno, J.A., "Two digital receivers based on time-frequency analysis for signal interception," *In Proceedings of the IEEE International Conference on Radar*, pp. 394-399, 2003, DOI:10.1109/RADAR.2003.1278774.

[126] Skolnik, M.I., “Introduction to Radar Systems”, Tata McGraw Hill, First Edition, pp. 376-382, 1980.

[127] Stephen, S., & Yifeng., Z., “Modulation recognition algorithms for Intentional Modulation on Pulse (IMOP) applications”, *Defence R&D Canada*, Patent no. CA020899.

[128] Han, J., He, M., Tang, Z., & Hao, Y., “A novel method for estimating the SNR of unknown emitter signal”, *J. Electron, China*, vol. 27, no, 1, pp. 134-138, 2010. DOI:10.1007/s11767-009-0031-5.

Publications by the Candidate

Journal Publications

Some part of this thesis is published for journal. The following is the list pertaining to the publications:

- Niranjan, R.K., Rama Rao, C.B., & Singh, A.K., "FPGA based Identification of Frequency and Phase Modulated Signals by Time Domain Digital Techniques for ELINT Systems", *Def. Sci. J.*, vol. 71, no. 1**,** pp. 79-86, Jan 2021, DOI:10.14429/dsj.71.15705.
- Niranjan, R.K., Singh, A.K., & Rama Rao, C.B., "SWaP Optimized Parameter Extraction of Radar Signals for Space Electronic Intelligence Application", *Def. Sci. J.*, vol. 70, no. 6**,** pp. 642-649, Nov 2020, DOI:10.14429/dsj.70.15619.
- Niranjan, R.K., Singh, A.K., & Rama Rao, C.B., "High Accuracy Parameter Estimation for Advanced Radar Identification of Electronic Intelligence system", *Def. Sci. J.*, vol. 70, no. 3**,** pp. 278-284, May 2020, DOI: 10.14429/dsj.70.15105.

Conference Publications

Some part of this thesis is published for conference proceedings. The following is the list pertaining to the publications:

- Niranjan, R.K., Rama Rao, C.B., & Singh, A.K., "Real-Time Identification of Exotic Modulated Radar Signals for Electronic Intelligence Systems", 2021 International Conference on Emerging Trends in Industry 4.0 (ETI 4.0), 19-21 May 2021. (Presented)
- Niranjan, R.K., Rama Rao, C.B., & Singh, A.K., "Performance Comparison of FFT based Frequency Estimation using different Interpolation Techniques for ELINT Systems", *International Conference on Advances in Electrical, Computing, Communications and Sustainable Technologies, Proceedings of ICAECT-2021*, pp. 1-4, 19-20 Feb 2021. DOI: 10.1109/ICAECT49130.2021.9392605 (IEEE Xplorer)
- Niranjan, R.K., Rama Rao, C.B., & Singh, A.K., "Improved Parameters Estimation of Radar Pulses using Autocorrelation", *International Conference on Advances in Electrical, Computing, Communications and Sustainable Technologies, Proceedings of ICAECT-2021*, pp. 1-4, 19-20 Feb 2021. DOI: 10.1109/ICAECT49130.2021.9392569 (IEEE Xplorer)

Defence Science Journal, Vol. 71, No. 1, January 2021, pp. 79-86, DOI : 10.14429/dsj.71.15705

FPGA based Identification of Frequency and Phase Modulated Signals by Time Domain Digital Techniques for ELINT Systems

R.K. Niranjan[#,@,*], C.B. Rama Rao[#], and A.K. Singh[@]

[#]*Department of ECE, National Institute of Technology, Warangal - 506 004, India*
[@]*DRDO-Defence Electronics Research Laboratory, Hyderabad - 500 005, India*
[*]*E-mail: niranjanrk2004@gmail.com*

ABSTRACT

In this paper, a decision tree algorithm based on time-domain digital technique is developed for the identification and classification of diverse radar intra-pulse modulated signals for the electronic intelligence system in real-time. This includes linear frequency modulation, non-linear frequency modulation, stepped frequency modulation and bi-phase modulation. The received signal is digitised and the instantaneous phase and high accuracy instantaneous frequency are estimated. The instantaneous amplitude is also estimated to get the start and stop of the pulse. Instantaneous parameters are estimated using a moving autocorrelation technique. The proposed algorithm is employed on the instantaneous frequency and the modulation is identified. The modulation type and modulation parameter are important for unique radar identification when similar radars are operating in a dense environment. Simulations are carried out at various SNR conditions and results are presented. The model for algorithm is developed using a system generator and implemented in FPGA. These results are compared when the proposed algorithm is used with the existing digital in-phase and quadrature-phase (DIQ) technique of instantaneous frequency and amplitude estimation.

Keywords: Complex radar signals; Instantaneous frequency profile; Intra-pulse modulation; moving autocorrelation technique; Digital in-phase and quadrature-phase technique

NOMENCLATURE

$x(t)$	Continuous-time signal
$x(n)$	Discrete-time signal
t_s	Sampling time
f_s	Sampling frequency
ϕ	Initial phase of the signal
τ	Fixed time period
α	Ascending chirp rate
β	Descending chirp rate
T	Time duration
f_c	Centre frequency of IF signal
$F_{\max}$	Maximum frequency of FMCW signal
$F_{\min}$	Minimum frequency of FMCW signal
F_{LE}	Leading edge frequency
F_{TE}	Trailing edge frequency
F_{CNT}	Center frequency during the pulse
F_{IP1}	Frequency at the first intermediate point
F_{IP2}	Frequency at the second intermediate point
δf	Frequency deviation
f_m	Sinusoidal modulating frequency
Δf	Frequency tolerance limit
$\Delta\phi$	Phase tolerance limit

1. INTRODUCTION

Modulation on radar pulse is one of the most important features and one of the vital problems in the analysis of non-cooperative radar signals is modulation classification for emitter identification[1-2]. The modulation classification plays a very important role in electronic intelligence (ELINT) systems[4-5]. Firstly, the modulation type of a signal is important to identify the radar type. Second, on identifying the correct modulation type the carrier frequency is re-estimated. Third, it helps to distinguish similar radars deployed in proximity. But for radar signals, the modulation classification in real-time is very challenging due to the possibility of various modulations within a very short pulse.

An earlier generation of electronic support (ES) systems was based on instantaneous frequency measurement (IFM) receiver and pulse measurement using log video. The time-domain technique was used for noise estimation and signal detection[6] and frequency were measured using time-frequency analysis[7-9]. But during conversion from radio frequency (RF) or intermediate frequency (IF) to log video, the phase and hence the modulation information is lost. Due to this reason these systems measure only basic parameters like RF, Pulse width (PW), pulse repetition interval (PRI) and pulse amplitude (PA). These parameters broadly are called inter-pulse parameters. But the measurement of these parameters alone is not sufficient against modern RADARs.

Conventional radars have simple pulsed waveform or continuous waveform with no modulation. These pulsed radars sometimes have the variations in PW or PRI. But complex radars are having various modulations within the pulse along with the above variations. These intra-pulse modulations can be linear frequency modulation (LFM), non-linear frequency

Received : 14 May 2020, Revised : 28 August 2020
Accepted : 09 October 2020, Online published : 01 February 2021

modulation (NLFM), stepped frequency modulation (SFM) and bi-phase modulation (BPM). Typically, these modulations are identified by the ELINT system using offline analysis[10-15]. Till the earlier generation of electronic warfare (EW) systems, these offline analysis tools are either add-on or they are integrated with the main ES systems or ELINT systems. Identification of modulations by the ELINT system in real-time is still a challenge. Various digital methods are discussed for modern digital implementation[16-21] and decision-theoretic approaches are mentioned for modulation classification[22-26].

Modulations can be identified using frequency domain techniques using offline systems[27-28]. Implementation of these techniques in Field Programmable Gate Array (FPGA) for real-time applications is not a viable solution as they consume a lot of hardware resources. Due to this reason, the implementation of signal classification techniques is attempted in FPGA using time-domain technique for real-time applications. IF signal is digitised in ADC and samples are captured, processed and further analysed in FPGA. These are possible to implement in FPGA due to parallelism, high density and high-speed component cores.

In this paper, an algorithm to identify modulation in real-time has been discussed and elaborated. The decision-tree based algorithm is proposed to identify the modulation. The RF pulse (RFP) is generated based on the instantaneous amplitude profile. The complete instantaneous frequency profile data is stored in the random access memory (RAM) during RF pulse. The frequency at different points in the pulse region is fetched from RAM and the algorithm is applied in real-time. The modulation is measured within shadow time based on the frequency parameters.

The validity of the algorithm has been tested with various modulated signals at different SNR conditions. In section-2, modelling and characteristics of various radar signals are given. The proposed modulation recognition algorithm is discussed in section-3. The performance and effectiveness of the algorithm are presented in section-4 through simulations and implementation on FPGA hardware is given in section-5.

2. MODELLING AND CHARACTERISTICS OF VARIOUS RADAR SIGNALS

The RF signal is down-converted to the IF signal using a superhet receiver and it is digitised. The instantaneous amplitude, phase and frequency are estimated. Pulse is detected using amplitude and modulation is identified using phase and frequency. The block diagram of FPGA based modulation identification is shown in Fig. 1.

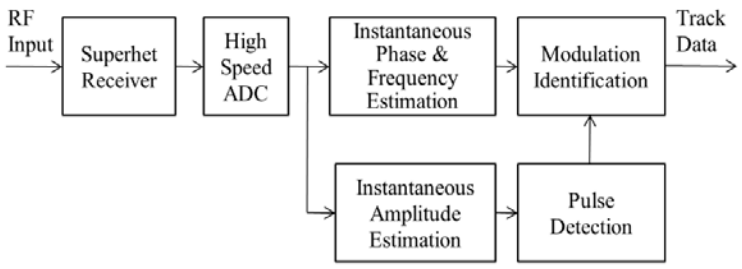

Figure 1. FPGA based modulation identification.

Modern radars are exhibiting complex radar waveforms. These waveforms include No-Modulation Continuous Wave (NMCW), Frequency Modulated Continuous Wave (FMCW), No-Modulation On Pulse (NMOP), LFM, NLFM, SFM and BPM. The following signals are considered and modelled. They are described as below:

(i) *Signal with No Modulation*: NMCW and NMOP signals do not consist of any modulation. The discrete version of the time-domain signal $x(t)$ is given as[29],

$$x(n) = Ae^{j(2\pi fnt_s+\phi)} \quad (1)$$

where, A denotes the carrier amplitude, ϕ denotes the initial phase, f denotes carrier frequency, t_s denotes sampling time and for $n = 1, 2, 3..., N$ for NMOP signal.

When $n = 1, 2, 3..., \infty$ and signals are with PW more than predefined time duration T considered as continuous wave (CW). If PW is below T, they are considered as pulsed signals.

(ii) *Linear Frequency Modulation (LFM)*: LFM ascending (LFMa), LFM descending (LFMd), LFM ascending-descending (LFMad) and LFM descending-ascending (LFMda) chirp signals are considered as LFM signals. These signals are also known as Triangular FM.

(a) LFMa signal is generated as given by[29]

$$x(n) = te^{j(2\pi fnt_s+\phi+\pi\alpha n^2t_s^2)} \quad (2)$$

$$\text{for } n = \left(\frac{-N}{2}\right), \left(\frac{-N}{2}\right)+1, ..., -1.$$

where, α is the slope of the LFMa.

(b) LFMd signal is generated as given by[29]

$$x(n) = te^{j(2\pi fnt_s+\phi-\pi\beta n^2t_s^2)} \quad (3)$$

$$\text{for } n = 0, 1, 2, ..., \left(\frac{N}{2}\right)-1.$$

where, β is the slope of the LFMd. Usually, LFMa and LFMd signals have the same slope, i.e. $\beta = \alpha$.

(c) LFMad and LFMda signals are generated using a combination of the above two equations. The frequency f is the instantaneous frequency at the peak of the triangular frequency variation, which is the maximum instantaneous frequency within the observation duration in the case of LFMad. The slope α and β is calculated as $2\delta f / \tau$, where the δf is the bandwidth within the time period τ. The parameter τ is a fixed value. The waveform is characterised by f, δf, α and β.

(iii) *Non-Linear Frequency Modulation (NLFM)*: NLFM signal is generated as given by[29].

$$x(n) = Ae^{j(2\pi fnt_s+\phi+\left(\frac{\delta f}{2f_m}\right)\sin(2\pi f_m nt_s))} \quad (4)$$

where, the $\delta f / 2$ is the peak deviation, f_m is the sinusoidal modulating frequency, $n = 1, 2, 3...N$, if the signal is narrowband, it means $\delta f / 2f_m \ll 1$. It is assumed that only a fraction of the cycle is sampled over an observation time. In case of the wideband FM signal, $\delta f / 2f_m \gg 1$. NLFM forward and NLFM reverse is represented as NLFMf and NLFMr respectively.

(iv) *Stepped Frequency Modulation* (SFM): SFM is generated as below

$$x(n) = e^{j(2\pi f_h n t_s + \phi)} \quad (5)$$

for $n = 1,2,3,...,N$

where, f_h is the frequency of h^{th} step, and $h = 1,2,3,...,H$ is the number of steps. Usually H is in the sequence of $2,4,8,...$ etc. For $H = 2$, $h = 1,2$ similarly for $H = 4$, $h = 1,2,3,4$, and so on. SFM ascending and SFM descending signals are represented as SFMa and SFMd, respectively.

(v) *Phase Modulation (PM)*: Bi-Phase Modulation (BPM) is one of the phase modulations and it is generated as given by[29]

$$x(n) = Ae^{j(2\pi f n t_s + \phi + \theta(n))} \quad (6)$$

where, $\theta(n) = \pi(1-n)$, when the zero bits of the code sequences are sampled and $\theta(n) = \theta$, when the one bits of the code sequence are sampled. The phase shift θ can be 0° or 180° in the case of BPM.

3. PROPOSED DECISION TREE MODULATION IDENTIFICATION ALGORITHM

The IF signal is down-converted signal of RF signal digitised at the sampling frequency f_s which is equivalent to $f_s = 4f_c/3$, where f_c is the center frequency of the IF signal[30]. Four samples are latched into FPGA coming from ADC at the clock rate of $f_s/4$. The samples are latched at both the clock edges. All eight samples are processed in parallel at $f_s/8$ clock rate and results are combined at the output. The instantaneous frequency profile generated using the moving autocorrelation approach[31] is given by

$$F_m(n) = \left(\frac{F_s}{2\pi m}\right)\left(\Delta\Phi_m(n) + 2\pi Z_m\right) \quad (7)$$

where, F_s is the sampling frequency, $\Delta\Phi_m(n)$ is the phase difference derived from zone Z_m of phase and m is 16. The instantaneous amplitude profile is generated as given by[31]

$$X(n+1) = x(n) + |x(n+32).x^*(n+32+m)| - |x(n).x^*(n+m)| \quad (8)$$

where, x^* is a conjugate of signal *x, n* is the sample number and delay *m* is 1. The Eqn (8) is optimised by keeping $X(1) = a + jb$ where, *a* and *b* are constant values.

In Fig. 2, LFMad and FMCW signals frequency profiles are shown for presentation purposes. In the case of pulsed signals, pre-trigger and post-trigger region of the pulse is also captured to get the complete intra-pulse information including rise time and fall time. The pre-trigger region is captured based on the circular buffer memory concept which is implemented in first-in-first-out (FIFO) memory. The instantaneous frequency profile is used to extract frequency at various points. The frequency is extracted at an equal time interval at five different points from stored instantaneous frequency profile as shown in Fig. 2. These frequencies are known as leading edge frequency (F_{LE}), trailing edge frequency (F_{TE}), center frequency during the pulse (F_{CNT}), frequency at the first intermediate pint (F_{IP1}) and frequency at the second intermediate point (F_{IP2}). The F_{LE} and F_{TE} are latched at the leading edge (LE) and trailing edge (TE) of the RFP pulse. The RFP is generated using an

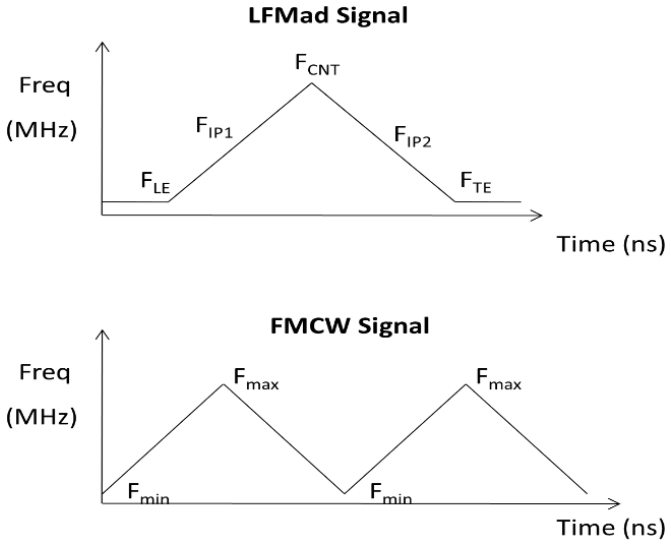

Figure 2. Frequency profiles of LFMad and FMCW signals.

instantaneous amplitude profile. Whereas to extract frequency at other three points the frequency data is stored during the pulse region in RAM which is generated using block RAM resource of FPGA. The frequency at these three points i.e. F_{IP1}, F_{CNT} and F_{IP2} are fetched from RAM based on the address calculated from the pulse region.

In the case of the FMCW signal, the maximum frequency (F_{max}) and minimum frequency (F_{min}) are computed in real-time and stored. The frequency tolerance limit (Δf) and phase tolerance limit ($\Delta\phi$) are used during comparisons and windows are fixed.

The amplitude and frequency profiles are computed from the digitised signals using the moving autocorrelation technique. The approximated standard deviation (σ_1) is computed for noise estimation[31] using the instantaneous amplitude profile $X(n)$ as given below.

$$\sigma_1 = k\sum_{n=0}^{N-1}\frac{X(n)}{N} \quad (9)$$

where, k is constant which is determined based on the minimum error between standard deviation and its approximated value and *N* is the number of samples. High-level threshold (T_H) is computed using estimated noise and accordingly, low-level threshold (T_L) is set during the noisy region. T_H is used to detect pulse leading edge (or pulse start) and T_L for the pulse trailing edge (or pulse end). The threshold is adaptive for better detection and analysis of pulses. Based on the adaptive threshold the pulse detection is carried out. The signal power and noise power is also measured[32]. Accordingly, signal-to-noise (SNR) is declared.

The flow chart for the proposed decision tree modulation recognition algorithm is shown in Fig. 3. First, the IF signal is captured and amplitude and frequency profiles are computed. The pulse start and pulse end are detected based on high and low-level threshold respectively. As per the flow chart initially, the signal is distinguished between pulsed and CW signals. If PW is greater than the predefined time limit *T*, it is declared as CW, otherwise, this is considered as a pulsed signal. If the signal is CW, the algorithm will look for frequency variations

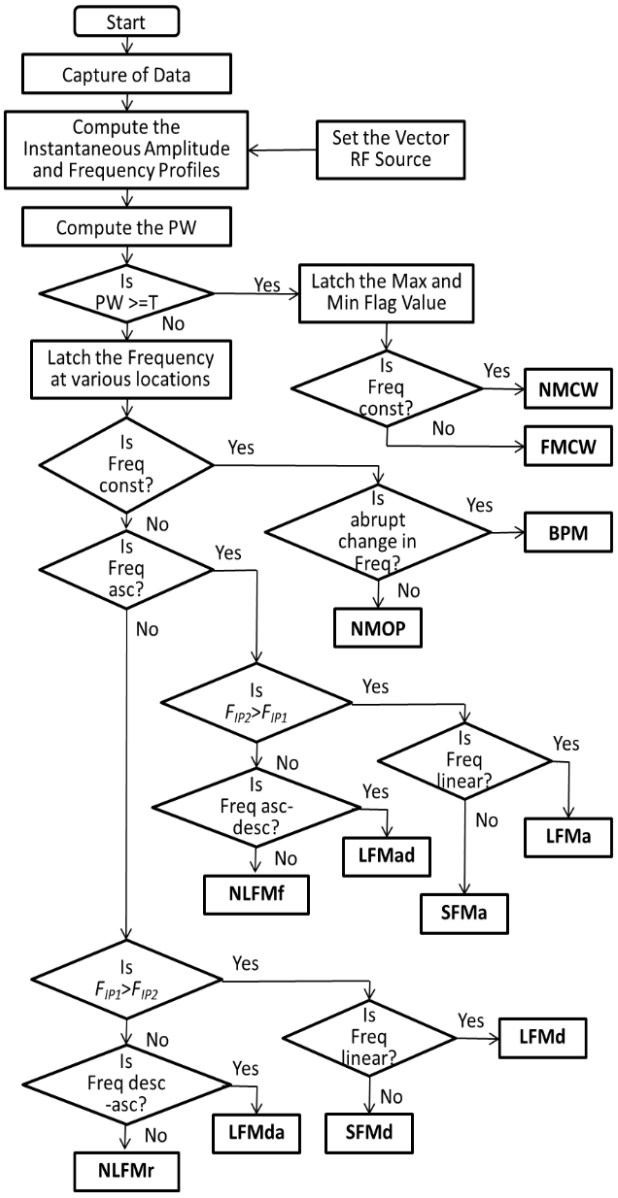

Figure 3. Proposed decision tree algorithm flow chart for modulation identification.

within that period. If F_{max} and F_{min} are within the set tolerance limit (Δf) i.e. frequency is constant, it will be declared as NMCW signal. Whereas, if the difference of F_{max} and F_{min} is more than the Δf, it will be declared as FMCW signal. When the signal PW is below predefined time limit T, it is known as a pulsed signal. If the frequency is constant in pulse region and there is no frequency discontinuity it is declared as No nodulation on pulse (NMOP). When there is an abrupt change in frequency due to sudden change in phase, it will be declared as BPM in which phase changes occur closed to pi. Phase changes and their numbers are detected. The minimum duration between two phase changes is measured and stored. The total width of the signal is divided by the minimum duration and the BPM pattern is identified. BPM pattern starts with 1's and each phase change is represented by 0's from 1's and 1's from 0's and when there is no phase change it will continue with the same 1's or 0's. The representation of the 13-bit BPM code is "1111100110101". The frequency profiles of NMCW, FMCW, NMOP and BPM are represented in Fig. 4.

The signal is declared as NLFMf when F_{IP2} is greater than F_{IP1} as well as frequency is sinusoidal. Whereas, if F_{IP1} is greater than F_{IP2} as well as frequency is sinusoidal, the signal is declared as NLFMr. SFMa is declared when F_{IP2} is greater than F_{IP1} as well as frequency changes in steps. If F_{IP1} is greater than F_{IP2} as well as frequency changes in steps, the signal is declared as SFMd. In SFM signals, there will be a step change in the frequency. NLFM signals are generated based on the approximation of SFM signals. The frequency profiles of NLFM and SFM signals are represented in Fig. 5.

When the linear change of frequency trend is ascending, descending or both in pulse region the modulation present is known as LFM. Modulation is declared as LFMa when F_{IP2} is greater than F_{IP1} as well as frequency changes linearly.

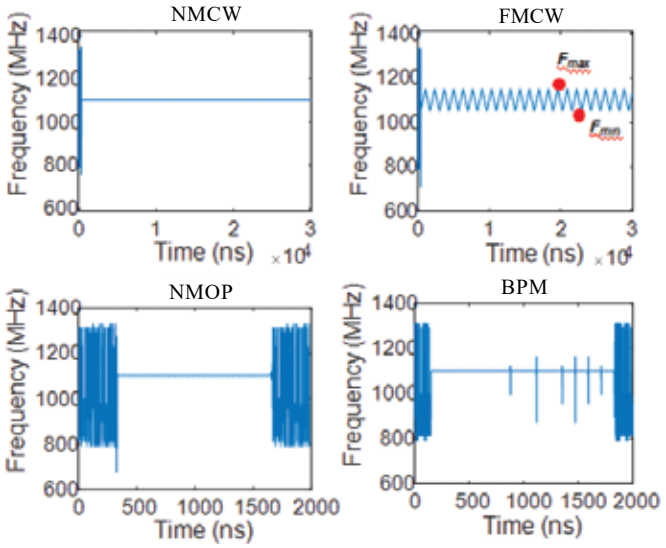

Figure 4. NMCW, FMCW, NMOP and BPM signals frequency profile.

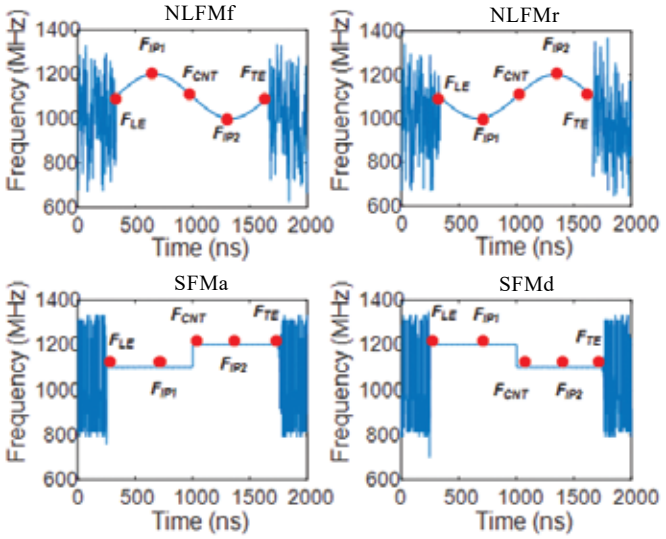

Figure 5. NLFM and SFM signals frequency profile.

Whereas, if F_{IP2} is less than F_{IP1} and frequency changes in ascending-descending order, the signal modulation is declared as LFMad. When F_{IP1} is greater than F_{IP2} and frequency changes linearly, the signal modulation is declared as LFMd. If F_{IP1} is less than F_{IP2} and frequency changes in descending-ascending order, the signal is declared as LFMda. Above mentioned LFM signals frequency profile is illustrated in Fig. 6.

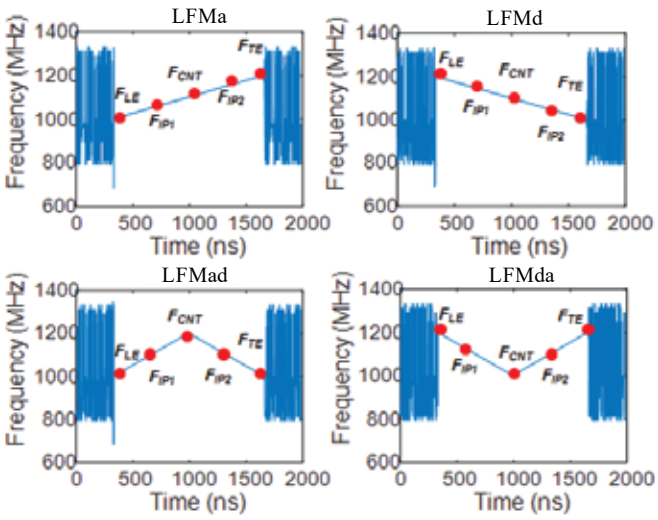

Figure 6. LFM signals frequency profile.

Once the type of modulation is found out, their parameter is also estimated like slope in the case of LFM, which is known as chirp rate in MHz/us. Similarly, the number of steps and BPM code are the parameters in the case of SFM and BPM respectively. Both modulation type (MT) and modulation parameter (MP) are represented using five nibbles in Table 1. Each MT is bit encoded and represented by one nibble, whereas, MP is represented by four nibbles. In Table, frequency deviation, frequency modulation rate, ascending chirp rate and descending chirp rate are represented as FD, FMR, ACR and DCR.

4. SIMULATION RESULTS

In this section, simulation at various SNR is presented to demonstrate the effectiveness and performance of the proposed decision tree algorithm for modulation identification. The input signal is generated with widely used additive white Gaussian noise (AWGN). A similar signal is used in the simulation for computing instantaneous frequency profile using moving autocorrelation[31] and DIQ techniques for generating results for various signals.

The detection performance of modulation identification is given in Table 2. An extensive simulation is carried out to test the performance. Total of 400 different signal sequences are generated to test each modulation. All types of modulation have been verified and the result is tabulated. The different modulations are identified at various SNR using the proposed algorithm with moving autocorrelation technique and proposed technique with DIQ technique.

Table 1. Representation of bit-pattern for modulation type (MT) and modulation parameter (MP)

MT code	Bit-pattern for				
	MT	MP			
	B2[3:0]	B1[15:12]	B1[11:8]	B1[7:4]	B1[3:0]
NMCW	0001	0000	0000	0000	0000
FMCW	0010	FMR (KHz)		FD (MHz)	
NMOP	0011	0000	0000	0000	0000
LFMa	0100	0000	0000		ACR (MHz/us)
LFMad	0101		DCR (MHz/us)		ACR (MHz/us)
LFMd	0110		DCR (MHz/us)	0000	0000
LFMda	0111		DCR (MHz/us)		ACR (MHz/us)
NLFMf	1000	0000	0000	0000	0000
NLFMr	1001	0000	0000	0000	0000
SFMa	1010	0000	0000	No. of Steps	
SFMd	1011	0000	0000	No. of Steps	
BPM	1100	BPM Code			

Table 2. Detection performance of modulation identification

Modulation type	Proposed algorithm with moving autocorrelation	Proposed algorithm with DIQ technique	Correct identification
NMCW	-2	5	99
FMCW	-1	7	98
NMOP	-2	6	99
LFM	0	7	98
NLFM	1	8	98
SFM	-2	5	99
BPM	1	8	97

The confusion matrix is extracted from the detection performance at SNR of -2 dB for the proposed algorithm with moving autocorrelation as shown in Table 3. The result shows the detection performance with 99% accuracy at -2 dB SNR for NMCW, NMOP and SFM signals. The probability of correct identification is dropped below respective SNR of all modulations. The different modulations are compared for the SNR required for set modulation and declared modulation.

Minimum SNR required using moving autocorrelation technique and DIQ technique is 1 dB and 8 dB respectively to process all types of modulated signals. Based on this, the sensitivity achieved is -87 dBm and -80 dBm using proposed algorithm with moving autocorrelation technique and DIQ technique, respectively.

Table 3. Confusion matrix of modulation identification at SNR of -2 dB

Declared MT -> Set MT (Below)	NMCW	FMCW	NMOP	LFM	NLFM	SFM	BPM
NMCW	99%	1%	-	-	-	-	-
FMCW	5%	95%	-	-	-	-	-
NMOP	-	-	99%	-	-	-	1%
LFM	-	-	-	94%	4.5%	1.5%	-
NLFM	-	-	-	3.5%	95%	1.5%	-
SFM	-	-	-	0.5%	0.5%	99%	-
BPM	-	-	4%	2.5%	1.5%	1%	91%

The comparison of this work with other similar works is not reasonable because the frequency domain techniques get the inherent processing gain. But they suffer from PW and PRI measurement accuracies. The minimum PW measurement is restricted to the number of FFT points and its percentage of overlapping. Whereas, the proposed time-domain technique measures the minimum PW of the order of 50 ns. The fact of the matter is that lower PW does not have the modulation but still, any processing method should meet all basic system requirements along with critical requirements.

Classification of modulation[27-28] presented are based on the frequency domain processing and they are implemented on DSP processor for ELINT applications. Due to the limitations of the number of MACs in the DSP processor these techniques are not suitable for tactical operations. The proposed decision-tree algorithm is implemented on FPGA hardware which provides real-time performance.

5. IMPLEMENTATION ON FPGA HARDWARE

The proposed algorithm is implemented with a system generator using Xilinx Vivado 2016.4 tool as shown in Fig. 7. The Xilinx device selected is Virtex-7 XC7VX415T FPGA. The synthesis is carried out for netlist generation, mapping for exact mapping of components, place and route is carried out.

The utilisation summary is compared for various FPGA resources with the existing DIQ technique and shown in Table 4. Mainly, DSP resources are utilised very less in the proposed algorithm with moving autocorrelation technique compared to the proposed algorithm with DIQ technique as no filter implementation is required.

The simulation result using the proposed algorithm is shown in Fig. 8 for the LFMad signal. The same input data is used which was used for Matlab simulations. Only two pulses data along with pre and post region is shown to facilitate the simulation. The Mod_Type code can be cross verified as 0x5 (i.e. 0101) with Table 1 for the LFMad signal. This code is generated after 8 clock cycles from the end of the pulse.

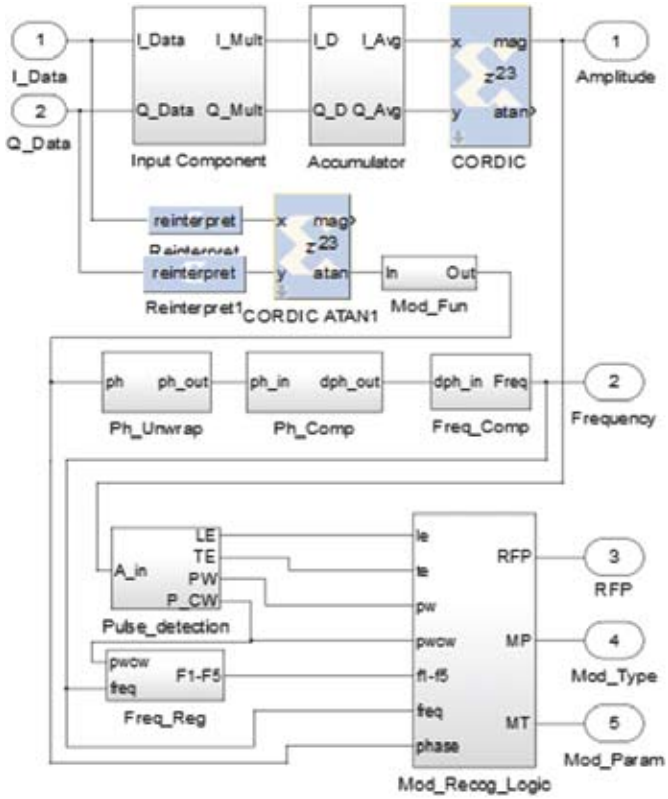

Figure 7. Model generated using system generator.

Table 4. FPGA resource utilisation summary (Device: XC7VX415T)

FPGA resource utilisation	Proposed technique with moving autocorrelation	Proposed technique with DIQ technique	Savings in %
Slice F/Fs	2334	4353	46.38
LUT (4 inputs)	2883	4136	30.29
DSP48E1	12	42	71.43
Block RAM	300	300	-
Total power (mW)	546	782	30.18

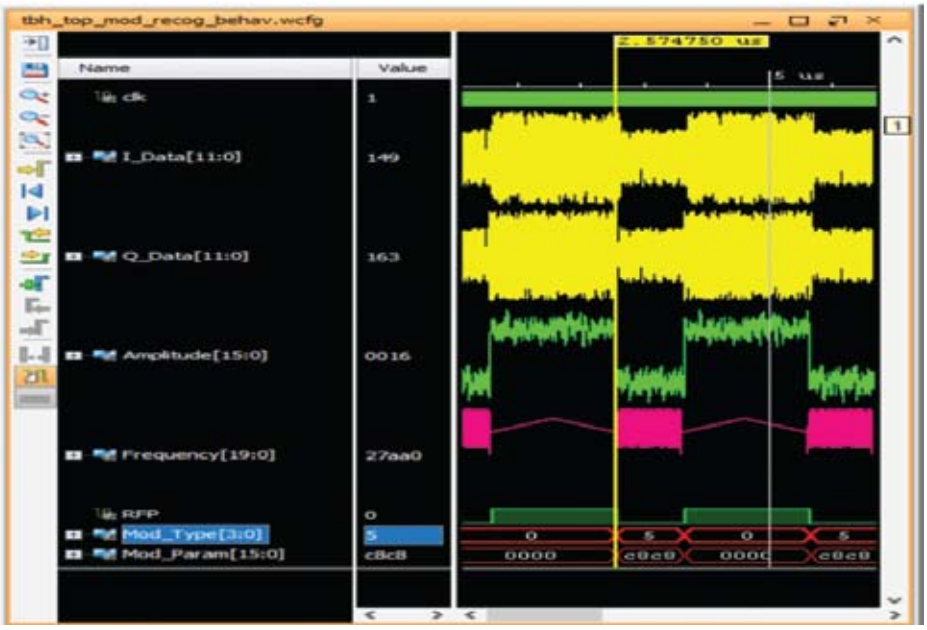

Figure 8. Simulation result for modulation identification feature.

6. CONCLUSIONS

In this work, NMCW, FMCW, NMOP, LFM, NLFM, SFM and BPM modulations have been identified using the decision tree algorithm. This decision tree algorithm used with the moving autocorrelation approach is implemented in FPGA and identified all mentioned modulated signals at 1 dB SNR. Hence, a unique time-domain digital technique for modulation identification has been proposed. The assumptions have been made that at any given point of time one modulation type is present in the input signal. The length of the input signal is assumed constant to generate a particular type of modulated signal in case of the pulsed signal. The advancement in signal processing algorithms, tied with high-performance hardware has enabled to improve the emitter identification and also to achieve a real-time performance. In the future, modulation identification work will be extended for additional signals and a combination of signals.

REFERENCES

1. Conning, M. & Potgieter, F. Analysis of Measured Radar Data for Specific Emitter Identification. *In* Proceedings of the Radar Conference, IEEE, Washington, DC, USA; 2010. doi: 10.1109/RADAR.2010.5494658.
2. Gupta, M.; Hareesh, G. & Mahla, A.K. Electronic Warfare: Issues and Challenges for Emitter Classification. *Def. Sci. J.*, 2011, **61**(3), 228-234. doi: 10.14429/dsj.61.529
3. Adamy, D.L., EW 101: A First Course in Electronic Warfare. Boston, MA, USA: Artech House, 2001.
4. Adamy, D.L. EW 102: A Second Course in Electronic Warfare. Boston, MA, USA: Artech House, 2004. 2nd Edition.
5. Richard, G.W. ELINT, the Interception and Analysis of Radar Signals. Boston, MA, USA: Artech House, 2006.
6. Niranjan, R.K. & Bhukya, R.N. Approach of Pulse Parameters Measurement Using Digital IQ Method. *IJIEE*, 2014, **4**(1), 31-35. doi: 10.7763/IJIEE.2014.V4.403
7. Mahlooji, S. & Mohammadi, K. Very High Resolution Digital Instantaneous Frequency Measurement Receiver, *In* Proceedings of International Conference on Signal Processing and Systems, IEEE, Singapore, 2009. doi: 10.1109/ICSPS.2009.43.
8. Niranjan, R.K. & Bhukya, R.N. FPGA based implementation of pulse parameters measurement. *In* Proceedings of Science and Information Conference, IEEE, London, 2014, pp. 862-867.
9. Helton, J.; Henry, C.I.; David, M.L. & Tsui, J.B.Y. FPGA-based 1.2 GHz bandwidth digital instantaneous frequency measurement receiver. *In* Proceedings of the ISQED. San Jose, CA, USA, 2008, 265-270. doi: 10.1109/ISQED.2008.4479798.
10. Gross, F.B. & Chen, K. Comparison of detectability of traditional pulsed and spread spectrum radar waveforms in classic passive receivers. *IEEE*, 2005, **41**(2), 746-751. doi: 10.1109/TAES.2005.1468765
11. Fan, X.; Li, L.; Li, T. & Chen, T. A new method for polyphase pulse compression codes modulation recognition based on IQPF and FRFT. *In* Proceedings of the Advanced Information Technology, Electronic and Automation Control Conference (IAEAC), Chongqing, *IEEE*, 2017, 1172-1176. doi: 10.1109/IAEAC.2017.8054198
12. Lbpez-Risuefio, G.; Grajal, J.; Yeste-Ojeda, O.A.; Sanz-Osorio, A. & Moreno, J.A. Two digital receivers based on time-frequency analysis for signal interception. *IEEE*, 2003, 394-399. doi: 10.1109/RADAR.2003.1278774
13. Kawalec, A. & Owczarek, R. Radar emitter recognition using intra-pulse data. *In* Proceedings of the International Conference on Microwaves, 2003. doi: 10.1109/MIKON.2004.1357059
14. Nadav, L. & Eli, M. Radar Signals. Wiley–Interscience, New York, 2004.
15. Pace, P.E. Detecting and classifying low probability of intercept radar. 2nd Edition, Artech House, 2009.
16. Tsui, J.B.Y. Digital Techniques for Wideband Receivers. 2nd Ed, Norwood, MA Artech House, 2001, pp. 265-270.
17. Azzouz, E.E. & Nandi, A.K. Automatic Modulation Recognition of Communication Signals. Kluwer Academic Publishers. Boston, MA. 1996.
18. Lin, Yun and Ma, Chunguang. Automatic Modulation Recognition of Communication Signals. *IJFGCN*, 2017, **10**(1), 83-96. doi: 10.14257/ijfgcn.2017.10.1.08
19. Park, B. & Ahn, J.M. Intra-pulse modulation recognition using pulse description words and complex waveforms. *In* International Conference on Information and Communication Technology Convergence (ICTC), Jeju, 2017, 555-560. doi: 10.1109/ICTC.2017.8191039
20. Yar, E.; Kocamis, M.B.; Orduyilmaz, A.; Serin, M. & Efe, M. A Complete Framework of Radar Pulse Detection and Modulation Classification for Cognitive EW. *In* 27th European Signal Processing Conference (EUSIPCO), A Coruna, Spain, 2019, 1-5. doi: 10.23919/EUSIPCO.2019.8903045
21. Zhang, J.; Li, Y. & Yin, J. Modulation classification method for frequency modulation signals based on the time–frequency distribution and CNN. *IET Radar, Sonar & Navigation*, 2018, **12**(2), 244-249. doi: 10.1049/iet-rsn.2017.0265
22. Azzouz, E.E. & Nandi, AK. Automatic identification of digitally modulated types. *Elsevier, Signal Processing*, 1995, **47**(1), 55-69. doi: 10.1016/0165-1684(95)00099-2
23. Nandi, A.K. & Azzouz, E.E. Automatic analogue modulation recognition. *Signal Processing,* 1995, **46**(2), 211-222. doi: 10.1016/0165-1684(95)00083-P
24. Nandi, A.K. & Azzouz, E.E. Algorithms for automatic modulation recognition of Communication signals. *IEEE Trans. Commun.,* 1998, **46**(4), 431-436**.** doi: 10.1109/26.664294

25. Dubuc, C.; Boudreau D.; Patenaude F. & Inkol R. An automatic modulation recognition algorithm for spectrum monitoring applications. *In* Proceedings of the International Conference on Communications, IEEE, Vancouver, BC., 1999, pp. 570-574. doi: 10.1109/ICC.1999.768003
26. Chan, Y.T. & Gadbois, L.G. Identification of the modulation type of a signal. *In* Proceedings of the Signal Processing, 1989, **16**(2), 149-154. doi: 10.1109/ICASSP.1985.1168289
27. You, H. Su. F. & Qu, K. A novel multiple LFM signals detection method. *In* Proceedings of the International Conference on Microwave and Millimeter Wave Technology (ICMMT), 2004, 818-821. doi: 10.1109/ICMMT.2004.1411655
28. Xu, S.W. & Shui, P.L. Nonparametric Detection of frequency modulated signals using fractional fourier transform. *Electronics Letters,* 2010, **46**(9), 649-650. doi: 10.1049/el.2010.0569
29. Sung, Stephen & Zhou, Yifeng. Modulation recognition algorithms for Intentional Modulation on Pulse (IMOP) applications, Defence R&D Canada, Patent No. CA020899.
30. Lyons, R.G. Understanding Digital Signal Processing, Boston, Addison Wesley Longman, Inc, 1997. 32-42 p.
31. Niranjan, R.K.; Singh, A.K. & Chunduri, B.R. High accuracy parameter estimation for advanced radar identification of electronic intelligence system. *Def. Sci. J.,* 2020, **70**(3), 278-284. doi: 10.14429/dsj.70.15105
32. Han, J.; He, M.; Tang, Z. & Hao. Y. A novel method for estimating the SNR of unknown emitter signal. *J. Electron.* (China), 2010, **27**(1), 134-138. doi: 10.1007/s11767-009-0031-5

ACKNOWLEDGEMENTS

It is immense pleasure to thank Director DLRL, Additional Director and Wing Head for their continuous guidance and support towards this activity. The authors also would like to thanks anonymous reviewers for making various useful suggestions and comments.

CONTRIBUTORS

Mr R.K. Niranjan, received the BE (ECE) from Dr Hari Singh Gour University, Sagar, in 1998 and ME (Systems and Signal Processing) from Osmania University, Hyderabad, in 2012. He is currently pursuing PhD from NIT, Warangal and presently working as Scientist 'F' at DRDO-Defence Electronics Research Laboratory, Hyderabad. He has been working in the area of signal processing for Electronic Warfare systems with specific interests in the area of Data Acquisitions and DSP algorithms implementations in FPGA for real time applications.
Contribution in the current study, he conceived the concept, carried out the literature survey and complete experimental work with interpretation and analysis of result.

Prof. C.B. Rama Rao, did his post-graduation from JNTU, Kakinada and PhD from IIT, Kharagpur. He has been currently working as professor in the Department of Electronics and Communication Engineering, NIT Warangal, India. His research interests primarily include adaptive signal processing, musical instrumental signal processing, speech signal processing and biomedical signal processing. He has published more than 32 papers in reputed Journals and Conferences.
Contribution in the current study, he has given the idea, reviewed the work, validated the results, continuously provided the guidance and given many valuable inputs.

Dr A.K. Singh, did ME in Digital System (ECE) and PhD from Osmania University, in 2003 and 2015, respectively. Currently working as Scientist 'G' at DRDO-Defence Electronics Research Laboratory, he was the instrumental in design and development of digital receiver. His area of interest includes high-speed board design, time-frequency signal processing, and EW Receiver design. Presently he is working for space systems design.
Contribution in the current study, he has supported in making experimental setup, reviewed the incremental work and provided various valuable inputs.

Defence Science Journal, Vol. 70, No. 6, November 2020, pp. 642-649, DOI : 10.14429/dsj.70.15619

SWaP Optimised Parameter Extraction of Radar Signals for Space Electronic Intelligence Application

R.K. Niranjan[#,@,*], A.K. Singh[#], and C.B. Rama Rao[@]

[#]*DRDO-Defence Electronics Research Laboratory, Hyderabad - 500 005, India*
[@]*Department of ECE, National Institute of Technology, Warangal - 506 004, India*
[*]*E-mail: niranjanrk2004@gmail.com*

ABSTRACT

Space-based electronic intelligence system provides wide coverage and unrestricted access to adversary radar signals. These systems play a vital role in strategic intelligence gathering for assessing electronic order of battle. These systems need to be SWaP optimized with highly efficient algorithms to extract accurate radar parameters. The realization of such a system is a persistent challenge due to the limited availability of space graded components and associated tools. Towards this, the paper deliberates upon various signal processing algorithms to achieve highly accurate direction-of-arrival (DOA), high-frequency resolution and precise timing information for pulse width and pulse repetition frequency extraction. All the proposed algorithms have been implemented, ported and tested on Xilinx Kintex Ultra Scale FPGA KU060 and being evaluated in the radiation setups to establish the performance. High DOA accuracy and frequency accuracy of the order of 0.3 degree and 0.64 MHz respectively have been achieved.

Keywords: Interferometry; Electronic intelligence; Direction-of-arrival; Interpolation; Autocorrelation

NOMENCLATURE

θ	Incident angle
ψ_{kl}	First-order virtual phase delay
ψ_{δ}	Second-order virtual phase delay
f	Radio frequency
d	Antenna separation
d_{NL}	Distance between N and L antenna's
c	Speed of light
λ	Wavelength
$\lambda_{\min}$	Wavelength of the highest frequency
d_{δ}	Virtual antenna separation
m	Peak frequency bin
S_f	Sampling rate
M	FFT number of points
p	Interpolated peak location
A_0	Magnitude of peak bin
A_1	Magnitude of previous peak bin
A_2	Magnitude of next peak bin

1. INTRODUCTION

Surveillance of radar signals is an important operation of electronic warfare (EW). It is having the significance for tactical as well as strategic use to form the electronic order of battle (EOB). In the modern EW scenario, space-based electronic intelligence (ELINT) systems playing a crucial role in gathering information of the global radar threat. They are also having the advantages of very wide coverage and an uninterrupted signal interception. The prime requirement of spaceborne systems is a small size, weight and power (SWaP). The digital techniques meeting the above requirements are preferred in designing spaceborne ELINT systems. The performance of these systems to be comparable with ground-based ELINT systems[1-3].

Basic parameters of radar signals are frequency, pulsewidth (PW), power, pulse repetition frequency (PRF) and direction-of-arrival (DOA). To extract the information of radar signals the system configuration with new signal processing algorithms has been proposed.

The DOA of a radar signal is an important parameter because it can't be camouflaged. This parameter can be exploited in many ways which include improving situational awareness, signal sorting or deinterleaving, prompt electronic attack measures (such as jammers) or electronic protection measures (such as chaff) and many more. Accurate DOA measurement is required with available space and resources. There are many contemporary directions finding methods that are suitable for implementation in microwave radar intercept receivers such as rotary direction finding (RDF), amplitude comparison direction finding (ADF), time difference of arrival (TDOA), phase difference of arrival (PDOA) and frequency difference of arrival (FDOA). The PDOA is also known as interferometry[4-5].

The baseline interferometry (BLI) approach based on four antennas is used to get less DOA error[6-7]. But the system designed using this approach will have more weight because of the requirement of 4 antennae, 4 channel down-conversion, analog-to-digital converters (ADC) and processing blocks. When processing elements are more the power consumption also will be more. Finally, size also increases based on the number of antennae and processing elements. Practically, three different types of antennae are required for coverage of 0.5 GHz to 18 GHz band which requires 12 antennae for

Received : 23 March 2020, Revised : 11 June 2020
Accepted : 15 July 2020, Online published : 12 October 2020

azimuth coverage alone. Similarly, 12 more antennas are required for coverage of elevation. The requirement of hardware increases as per system design.

A virtual antenna based BLI algorithm using three antennae and three-channel receiver are proposed for DOA extraction. The hardware requirement is further optimized with a common master antenna for azimuth and elevation. Measured DOA root-mean-square error (RMSE) using virtual 3 antennae based BLI is more compared to 4 antennae based BLI. This is compensated by using a noise cancellation technique on digitized intermediate frequency (IF) data. Smallest virtual antenna distance also can be increased beyond $\lambda_{min}/2$ due to less field-of-view (FOV) requirement of space ELINT system which improves DOA RMSE.

The frequency-domain detection based on FFT itself is frequently used in digital receivers[8]. Frequency extraction is proposed based on the FFT interpolation. Overlapped FFT is used to get the pulse width and pulse repetition interval accuracy advantage. But still, it is difficult to get the advantage equivalent to time-domain processing[9]. Moving autocorrelation algorithm is used to extract pulse repetition interval and pulse width[10]. Emitter identification is effective if parameters are measured accurately[11-12].

2. PROPOSED ALGORITHMS

The space ELINT receiver configuration is shown in Fig. 1. It uses three-antenna array in virtual BLI formation followed by three-channel superhet receiver. Three-channel ADC does the digitization of all three IFs signals which are down-converted by the superhet receiver. In this, various algorithms are applied to extract the pulse descriptor word (PDW) of the signal.

Virtual antenna based BLI algorithm for DOA extraction, FFT based interpolation algorithm for frequency extraction and autocorrelation algorithm for amplitude, PW and PRI extraction are employed. Amplitude is used for pulse detection. All proposed algorithms are described as follows.

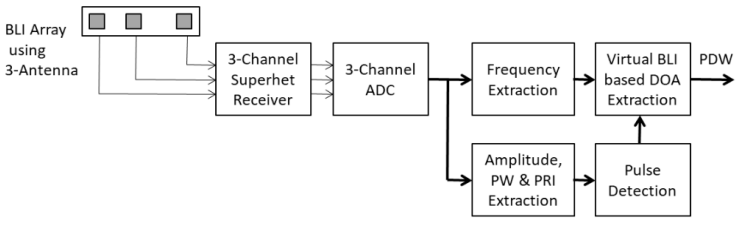

Figure 1. Space ELINT receiver configuration.

2.1 Virtual Antenna based Direction of Arrival Extraction

One advantage of Interferometry is that very accurate phase measurements can be obtained with digital hardware at a moderate sampling rate and so high accuracy DOA estimate can be obtained with shorter baselines and without the demanding timing constraints. Modern digital Interferometers achieve sub-degree accuracies. Interferometry exploits the propagation phase delay between two spatially alienated antennas to estimate the DOA of a signal. In recent decades, the advent of high-speed analog to digital converter (ADC), high-performance field programmable gate arrays (FPGAs) and digital computing had led to the development of high fidelity digital receivers. With modern technologies, the implementation of phase-coherent, multi-channel digital receivers have become increasingly more cost-effective. Furthermore, the flexibility of digital computing has allowed the implementation of higher performance algorithms compared to traditional analog counterparts. The interest to use, digital interferometers are increased in recent years to provide fast and accurate DOA estimate for military ES and ELINT systems.

The ELINT receivers are intended to provide early warning to the presence of radars. They are generally positioned at large distances from the radar. The radar signal arriving at the ELINT receiver antenna array can, therefore be reasonably approximated as a uniform plane wave. Here 1, 2, 3 …, N are the antennas, θ is the intercept angle and d_{NL} are distances between antennas.

The DOA of the signal is estimated as below, by estimating the frequency and phase delay of the signal between the two antennas outputs.

$$\hat{\theta} = \sin^{-1}\left(\frac{\lambda\hat{\psi}}{2\pi d}\right) \quad (1)$$

where wavelength $\lambda = c/f$. The baseline of the interferometer is often referred to as antenna separation d. The accuracy of DOA estimate can be improved by one of the factors such as

- Increasing the SNR of the signal,
- Increasing the signal duration (number of samples),
- Increasing the signal frequency,
- Operating closer to broadside, and
- Increasing the antenna separation.

The first three parameters can be changed by the radar as the parameters of the radar are beyond the control of the ELINT receiver.

Higher baseline Interferometers are designed to achieve higher DF Accuracy. The most popular ambiguity resolution method is based on the Chinese remainder theorem (CRT) and requires appropriately chosen interferometer baselines[13-14].

For larger aperture, unambiguous DOA estimates can generally be obtained with fewer intermediate baselines than the short baseline ambiguity resolution method. Figure 2(a) describes a simple set of interferometer baselines comprising 4 antennas whereas Fig. 2(b) describes an extended set of interferometer baselines comprising of 4 antennas[15]. The longest baseline d_{41} provides the best DOA estimation.

DOA accuracy is further increased with more number of baselines i.e. antenna. To process more number of antennas either parallel processing to be carried out that will increase the system hardware and system power or more switching to be done which decreases the probability of intercept (POI) of the radar signal. The effort has been to achieve higher DF accuracy using three channels per Antenna system with certain constraints such as a decrease in FOV and lesser phase margin than earlier configuration and also use of noise cancellation before computing the DOA.

The first constraint is possible to resolve by changing the path of the space vehicle during the predefined mission.

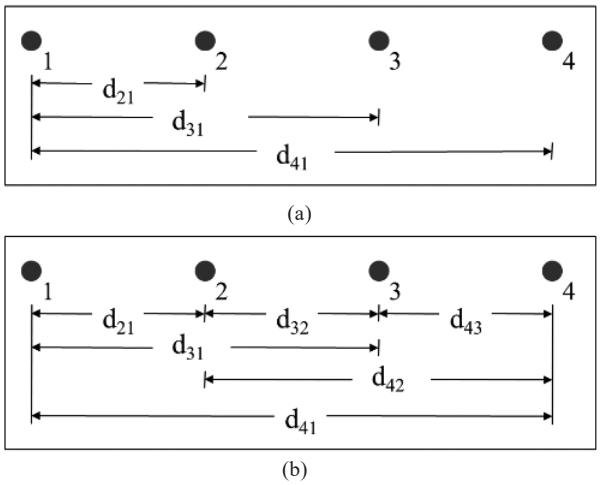

Figure 2. (a) A simple set of interferometer baselines comprising of 4 antennas and (b) An extended set of interferometer baselines comprising of 4 antennas.

Whereas the phase errors are minimized by choosing the good hardware component which is reliable for a particular phase margin of the algorithm so that it could not give wrong DOA estimates.

Based on the above constraint, there is an alternative interferometric algorithm Virtual Baseline Interferometer (VBI) which is based on a second-order difference array[16]. This VBI is computationally as fast as a conventional interferometer and also provides unambiguous DOA estimation using two long baselines.

Figure 3(a) describes the concept of the Virtual Baseline Interferometer, where only 3 antennae are required. The ambiguous first-order phase delays for d_{21} and d_{32} baselines i.e. ψ_{21} and ψ_{32} respectively are derived as below using Eqn (1),

$$\psi_{21} = \frac{2\pi d_{21}}{\lambda}\sin\theta \tag{2}$$

$$\psi_{32} = \frac{2\pi d_{32}}{\lambda}\sin\theta \tag{3}$$

It is assumed that $d_{32}>d_{21}$ and $d_{21} \gg \lambda_{min}/2$ where λ_{min} corresponds to the wavelength of the highest frequency of interest. The long baselines suggest that the phase delays are highly ambiguous. The second-order phase delay ψ_δ, can be calculated as the difference between the first-order delays using Eqns. (2) and (3),

$$\psi_\delta = \psi_{32} - \psi_{21} = \frac{2\pi(d_{32}-d_{21})}{\lambda}\sin\theta = \frac{2\pi d_\delta}{\lambda}\sin\theta \tag{4}$$

where, $d_\delta = d_{32} - d_{21}$, this is equivalent to the creation of antennae virtual pair with a baseline of d_δ as depicted in Fig. 3(b).

This virtual baseline phase delay can be unambiguous provided that the baseline is sufficiently short. It means, that it satisfied the following constraint, $0 < d_\delta \le \lambda_{min}/2$. The unambiguous estimate of DOA of the signal using the basic interferometer equation is written as

$$\hat{\theta} = \sin^{-1}\left(\frac{\lambda\hat{\psi}}{2\pi d_\delta}\right) \tag{5}$$

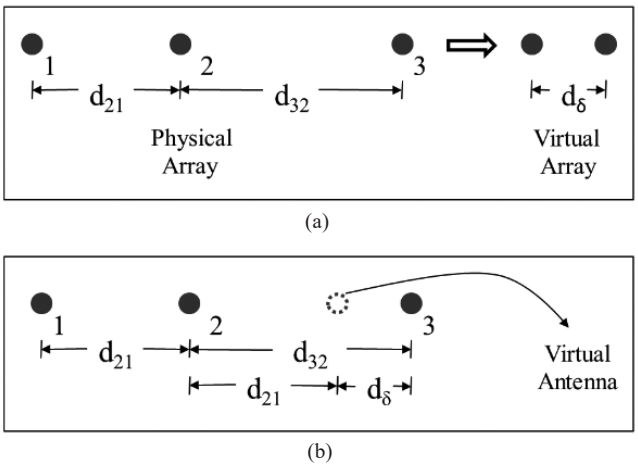

Figure 3. (a) Virtual baseline interferometer comprising of 3 antennas and (b) Physical interpretation of virtual baseline interferometer.

The RMS error of the virtual baseline interferometer is expected to be degraded compared to the first-order interferometer with a physical baseline d_δ. It is attributed to the fact that three antennae outputs are used to estimate the phase delay of a virtual two antenna interferometer. The extra antenna output is expected to introduce more noise to the phase delay estimation and hence lead to a reduction in DOA estimation performance. This error can be reduced by using the longest baseline of the antennas array. The Eqn (5) is limited to a virtual short baseline of d_δ and does not take advantage of the higher accuracy offered by the longer physical first-order baselines i.e. d_{21}, d_{32}, or d_{31}. The longest first-order baseline d_{31} offers an improvement in the DOA estimation by a factor as below:

$$\text{Improvement} = \sqrt{3} * (d_{31}/d_\delta) \tag{6}$$

At 6 GHz with d_{21} = 45 mm, d_{32} = 52.5 mm and hence d_{31} = 97.5 mm the DOA RMSE achieved is 13.7981° using virtual smallest baseline (d_δ). Whereas, DOA RMSE achieved is 0.6427° using the longest baseline (d_{31}). The factor of improvement using the longest baseline is 21.4679. The theoretical factor of improvement is 22.516 using Eqn. (6). This shows the factor of improvement is approximately matching the theoretical value. The range for 6-18 GHz is 0.2102° to 0.6432° using 3 antennas. Hence, this method provides comparable results with a less number of antennas, and hence it is an SWaP optimized approach.

2.2 Frequency Extraction

Fast Fourier transform (FFT) is used frequently to estimate the frequency of the signal. The FFT number of points is limited due to computational requirements. This restricts the frequency resolution of the FFT. The number of points is selected as a trade-off between the collected data for processing and the frequency resolution or frequency accuracy. The higher FFT number of points provides fine frequency resolution and accuracy which is hardware intensive and consumes more power.

Here Curve Fitting or Interpolation technique has been

used to achieve better frequency accuracy with less FFT number of points[17-22]. The frequency of each component is computed from their respective bin number in the spectrum with a resolution that depends on sample length. If the signal frequency is not the multiple of frequency resolution i.e. S_f/M , it will not fall on the peak. However, it will distribute near actual frequency and appear on several bins. In this case, the magnitudes of close by bins are used to estimate the actual signal frequency. The curve fitting using interpolation is used to improve the frequency resolution of the measured signal frequency component. Figure 4 shows the FFT frequency response for M points FFT spectrum. The x-axis represents the frequency bin and magnitude is represented by the y-axis. The location of the previous peak bin is represented as $m-1$, peak bin as m and next peak bin as $m+1$ of the spectrum. The A_1, A_0, A_2 are the respective magnitudes. The center point at p in fractional bins gives us an interpolated peak location.

The proposed frequency estimation using the curve fitting interpolation method calculates the offset p in frequency bin m using the three maximum amplitude samples for high accuracy frequency estimation of the signal.

The measured course frequency of the signal using FFT spectrum analysis is given as

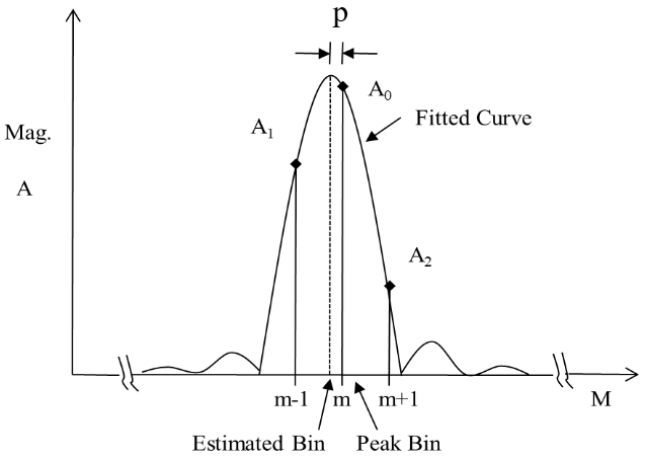

Figure 4. FFT frequency response with curve fitting interpolation.

$$\text{Course Frequency} = m*(S_f/M) \quad (7)$$

The frequency bin offset or peak location computed using interpolation is given in bins by

$$p = \frac{(A_1 - A_2)}{2(A_1 + A_2 - 2A_0)} \quad (8)$$

The estimated frequency bin is measured as

$$PeakEstimatedBin = m \pm p \quad (9)$$

And estimated frequency is measured as

$$FrequencyEstimated = (m \pm p)*(S_f/M) \quad (10)$$

The sufficient fractional number of bits is to be allocated for p to get the more advantage of estimation for hardware implementation. Accordingly, the number of bits allocation for m is also increased.

2.3 Pulse width and Time of Arrival Extraction

Measurement of time of arrival (TOA) is a critical parameter of the ELINT system. The accuracy of TOA determines the accuracy of PW and PRF. In the digital domain traditionally, FFT based approach is used to measure this parameter. But the TOA resolution is limited by the FFT size. The autocorrelation approach is used extensively to overcome this limitation. This technique requires in-phase and quadrature-phase data and carries out autocorrelation to find out TOA. The TOA resolution is improved to the order of the basic clock. This technique is optimized towards the least possible resource consumption without compromising the sensitivity and dynamic range of the ELINT system. This approach has been proposed for TOA, PW and PRF measurements[10].

3. SIMULATION RESULT AND DISCUSSIONS

Three antennae based BLI algorithm is implemented in Matlab. The first ambiguous phase is converted into an unambiguous phase from the smallest baseline unambiguous phase. Measured AOA error and RMSE are shown for ±45° FOV between 4 antennae and 3 antennae. These results are also generated using an experimental set-up for ±25° FOV. The simulation using noise cancellation technique is given for 3 antennae and comparison is shown without the noise cancellation technique. These results are shown below.

3.1 Simulation Result for Direction of Arrival

The performance of the virtual baseline interferometer algorithm has been simulated for frequency band 6 - 18 GHz. The spacing between the antennas are d_{21} = 45 mm, d_{32} = 52.5 mm. Using Eqn. (8) the $d_\delta = d_{32} - d_{21}$ =7.5 mm. The distance d_{21} and d_{32} are chosen such that $d_\delta < (\lambda_{min}/2)$. The ambiguous phase for the d_{21} baseline and d_{32} baseline is shown in Fig. 5. Whereas d_δ which is derived by virtual baseline interferometer, estimates the unambiguous phase shown in Fig. 6.

Figure 7 shows the simulation results for error at 6 GHz between set AOA and measured error and RMSE for 6 GHz to 18 GHz with ±45° FOV. It is evident that the simulation result of 4 antennae is better compared to 3 antennae interferometers. This is obvious as RMSE measured using the smallest physical antenna gives an advantage of √3 times RMSE for the smallest virtual antenna.

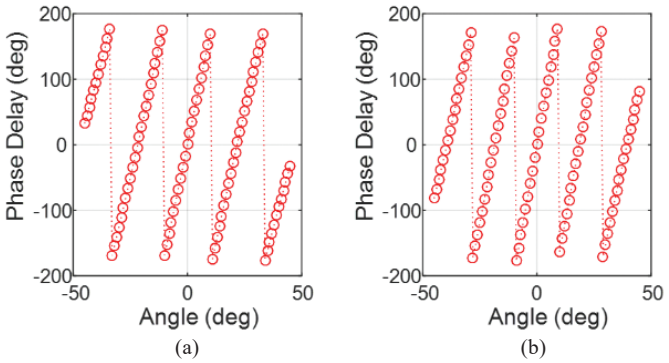

Figure 5. Ambiguous phase for (a) d_{21} (b) d_{32} baseline at 18GHz with FOV = ±45°.

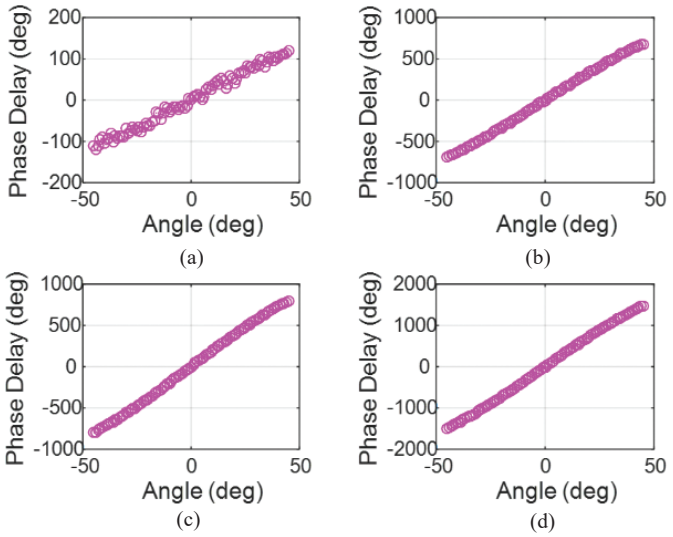

Figure 6. Unambiguous Phase for (a) d_δ (b) d_{21} (c) d_{32} (d) d_{31} Baseline at 18 GHz with FOV = ±45° using Virtual Baseline Interferometer.

Figure 8 shows the experimental result generated for ±25° FOV. The phase data is collected in radiation mode. The transmission set-up was kept at a 20 meter distance at the same height as the receiver BLI antennae. The experimental result shows the improvement compared to simulation results as shown in Fig. 7. This is because, the simulation results are generated with a maximum allowable phase error. This performance improvement is attributed to the effects of hardware perfections for space-qualified components. The experimental result is generated for ±25° FOV which is sufficient for the ELINT system for space application.

Figure 9, shows the experimental result for 3 antenna interferometer with ±25° FOV. This result is generated without and with Noise Cancellation technique[10,23]. The system noise of 200 frames is captured and computed 256 points FFT. This is carried out when input is connected to BITE port and BITE is in signal OFF condition. The estimated average of the noise spectrum is computed for all frames. In system ON condition when input is connected to antenna port and the signal spectrum is computed continuously which is noisy. The estimated noise spectrum is subtracted from the noisy input signal spectrum and an instantaneous magnitude spectrum is computed which is called a restored signal. Again restored time-domain signal is computed by inverse FFT. The SNR of 4 to 5 dB is improved when the signal is passed through this. This result shows that 3 antenna interferometer provides comparable results with 4 antenna interferometer. It shows, on reducing one antenna alone approximately one-fourth of hardware is reduced. Usually, to cover a complete 0.5 to 18 GHz band three different types of antennae are required. With 3 antennas approach, a total of 9 antennae covers complete band instead of 12 antennae. Hence, the further reduction will be there in processing electronics also.

3.2 Simulation Result for Frequency Extraction

The simulation for frequency estimation is carried out in MATLAB for 256 points FFT. The sampling frequency

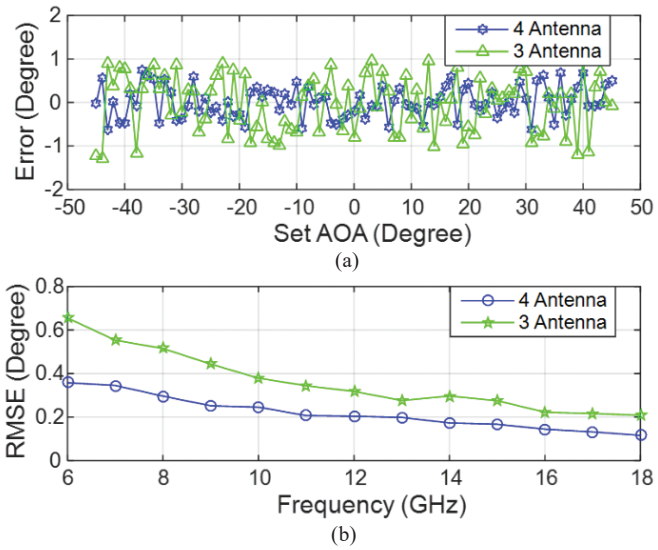

Figure 7. Simulation result with FOV = ±45° (a) Set AOA vs Error and (b) Frequency vs RMSE.

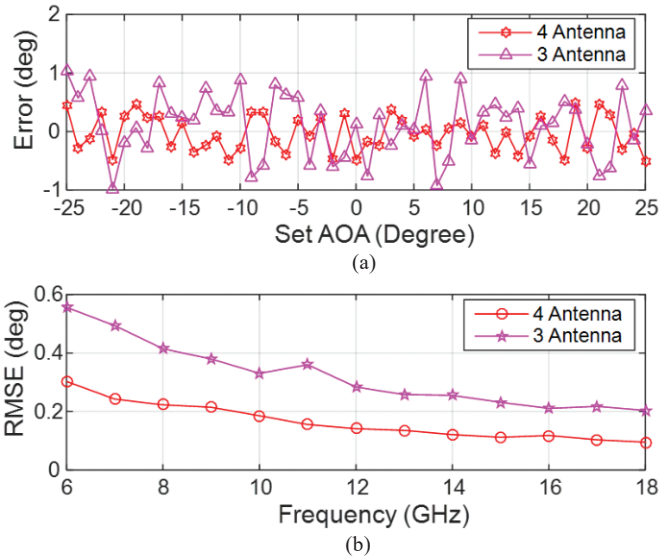

Figure 8. Experimental result with radiation set-up and FOV = ±25° (a) Set AOA vs error and (b) Frequency vs RMSE.

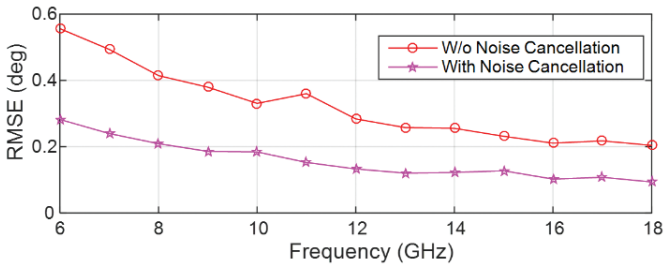

Figure 9. Experimental result with FOV = ±25° for 3 antenna.

for bandpass sampling of ADC is chosen as 1.333 GHz. The performance is validated for various power levels and pulse widths. The step size of 0.5 MHz is chosen to vary the frequency of the input signal and frequency measurement RMS error is

calculated. The input frequency of 1200 MHz and a pulse width of 200 ns are chosen for MATLAB simulation. The measured frequency error is 2.3828 MHz using normal FFT analysis whereas, the measured frequency error is 0.5218 MHz using the frequency estimation algorithm.

Figure 10 shows the MATLAB simulation output of 256 points FFT. The measurement frequency RMS error is computed in this simulation for the frequency range of 1200 to 1220 MHz. The measured frequency RMS error is 1.4905 MHz and peak frequency error is 2.5313 MHz using normal FFT analysis. Whereas, the measured frequency RMS error is 0.6399 MHz and peak frequency error is 0.9179 MHz using the frequency estimation algorithm.

4. FPGA IMPLEMENTATION

Three antennae based baseline interferometry and frequency estimation approach is implemented in field-programmable gate array (FPGA) using Xilinx system generator. The system generator design is given in Fig. 11. FFT of 256 points is computed on all three channels and phase is computed. The phase difference is computed using the phase of each channel and DOA is measured. In one of the channel frequency interpolation is implemented. The detection is carried out on the instantaneous amplitude profile which is computed from the same antenna channel. The PRI and PW are also computed using the instantaneous amplitude profile.

The design is implemented on the Xilinx Kintex Ultra Scale FPGA XCKU060-FFVA1517 which is footprint compatible with radiation tolerant device XQRKU060-CNA1509. The resources are compared with the four antennae based BLI approach and mentioned in Table 1.

Table 1. Resource comparison (Xilinx FPGA: XCKU060-FFVA1517)

FPGA resource utilisation	3 Antenna based proposed approach	4 Antenna based approach	Savings in %
Registers	16567	21355	22.4
LUTs	12893	16283	20.81
36 Kb Block RAM	757	1026	26.21
18 Kb Block RAM	1532	2042	25.02
DSP48 Slices	40	50	20.0
Total Power (mW)	16464	21152	22.16

5. CONCLUSIONS

It is evident from proposed approaches that there is an improvement in resolution and accuracy of measurement for various parameters direction-of-arrival, frequency etc. with fewer hardware resources. In case of direction finding, less number of front ends and antennas combinations can be realizable in the system that provide RMS DOA error of less than 0.3 degree with less weight and small size which is the requirement of space platform. The frequency measurement accuracies achieved is less than 0.6399 MHz RMS with this approach against 1.4905 MHz RMS with simple FFT spectrum analysis using 256 points FFT. The autocorrelation

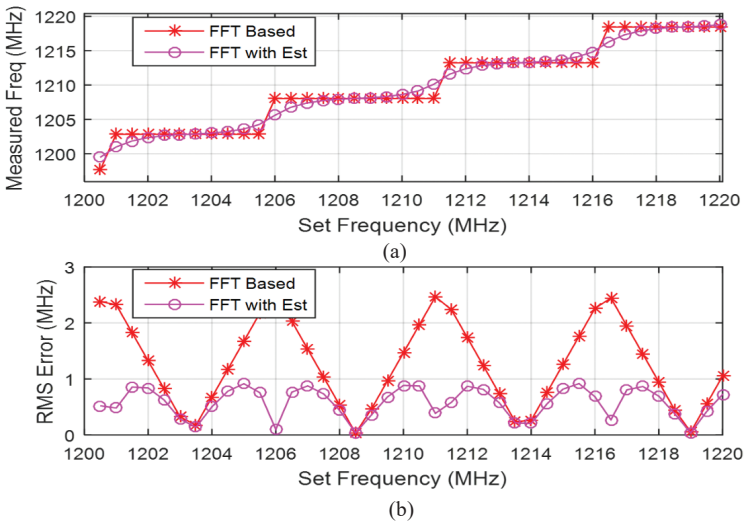

Figure 10. (a) Set Frequency vs Measured Freq (b) Set Frequency vs RMS Error for 256 Points FFT.

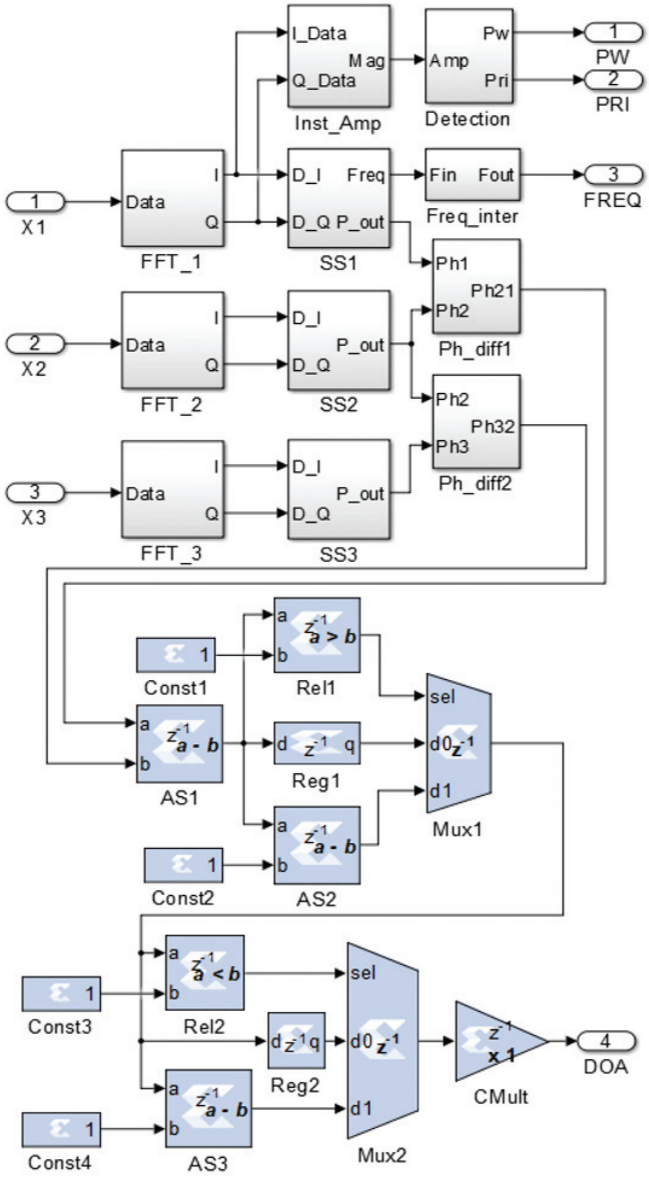

Figure 11. System generator design.

with FFT combination approach improves the PW and TOA measurements that can be measured with high accuracy with very few resources. It also helps to reduce the power consumption which is high in today's system.

Apart from the measurement of the basic parameters, there is more scope in the future to measure the more complicated parameters like intra-pulse modulation parameters information of radar. These measurement techniques will be helpful for realizing a better ELINT system based on a digital receiver for space applications.

REFERENCES

1. Adamy, D.L. EW 101: A first course in electronic warfare. Boston, MA, USA: Artech House, 2001.
2. Adamy, D.L. EW 102: A second course in electronic warfare. Boston, MA, USA: Artech House, 2004.
3. Lyons, R.G. Understanding digital signal processing. Boston, Addison Wesley Longman, Inc., 1997.
4. Wiley, R.G. ELINT: The interception and analysis of radar signals. Artech House Radar Library, Artech House, Inc., 2006.
5. Lipsky, S.E. Microwave passive direction finding. SciTech Publishing, Inc. 2004.
6. Orduyilmaz, A.; Kara, G.; Gürel, A.E.; Serin, M.; Yildirim, A. & Soysal, G. Real time four channel phase comparison direction finding method. *In* Proceedings of the Signal Processing and Communications Applications Conference (SIU), Izmir, Turkey, 2018. doi: 10.1109/SIU.2018.8404590
7. Gürel, A.E.; Orduyilmaz, A.; Yıldırım, S.A.; Kara, G.; Serin, M.; Ortatatlı, I.E. & Yildirim, A. Real time passive direction finding in FPGA environment. *In* Proceedings of the Signal Processing and Telecommunication Applications, IEEE, Antalya, 2017. doi: 10.1109/SIU.2017.7960593
8. Singh, A.K. & Rao, S.K. Digital receiver-based electronic intelligence system configuration for the detection and identification of intrapulse modulated radar signals. *Def. Sci. J.*, 2014, **64**(2), 152-158. doi:10.14429/dsj.64.5091
9. Niranjan, R.K. & Bhukya, R.N. Approach of Pulse parameters measurement using digital IQ method. IJIEE, 2014, **4**(1), 31-35. doi: 10.7763/IJIEE.2014.V4.403
10. Niranjan, R.K.; Singh, A.K. & Rama Rao, C.B. High accuracy parameter estimation for advanced radar identification of electronic intelligence system. *Def. Sci. J.*, 2020, **70**(3), 278-284. doi: 10.14429/dsj.70.15105
11. Gupta, M.; Hareesh, G. & Mahla, A.K. Electronic warfare: issues and challenges for emitter classification. *Def. Sci. J.*, 2011, **61**(3), 228-234. doi: 10.14429/dsj.61.529
12. Conning, M. & Potgieter, F. Analysis of measured radar data for specific emitter identification. *In* Proceedings of the Radar Conference, IEEE, Washington, DC, USA; 2010. doi: 10.1109/RADAR.2010.5494658
13. Xia, X.G. & Wang, G. Phase unwrapping and a robust Chinese remainder theorem. *Signal Proces. Lett.,* 2007, **14**, 247-250.
14. Sundaram, K.R.; Mallik, R.K. & Murthy, U.M.S. Modulo conversion method for estimating the direction of arrival, *IEEE Trans. Aerospace Electron. Sys.*, 2000, **36**(4), 1391-1396. doi: 10.1109/7.892687
15. Wu, Y.W.; Rhodes, S. & Satorius, E.H. Direction of arrival estimation via extended phase interferometry. *IEEE Trans. Aerospace Electron. Sys.*, 1995, **31**(1), 375-81. doi: 10.1109/7.366318
16. Peter, Q.C. Ly; Stephen, D.E.; Douglas, A. G. & Joy, Li. Unambiguous AOA Estimation Using SODA Interferometry for Electronic Surveillance. *In* Proceedings of the Sensor Array and Multichannel Signal Processing Workshop (SAM), IEEE, Hoboken, NJ, USA. doi: 10.1109/SAM.2012.6250488.
17. Tsui, J.B.Y. Digital techniques for wideband receivers. 2nd Ed, Norwood, MA Artech House, 2004.
18. Akima, H. A method of smooth curve fitting. ESSA Tech, ERL 101-ITS 73 US Government Printing Office, Washington, D.C., Jan. 1969.
19. Quinn, B.G. Estimating frequency by interpolation using Fourier coefficients. *IEEE Trans. Signal Processing*, 2014, **42**(5), 1264-1268. doi: 10.1109/78.295186
20. Voglewede, P. Parabola approximation for peak determination. *Global DSP Magazine*. 2004, **3**(5), 13-17.
21. Helton, J.; Henry, C.I.; David, M.L. & Tsui, J.B.Y. FPGA- Based 1.2 GHz Bandwidth digital instantaneous frequency measurement receiver. *In* Proceedings of ISQED. San Jose, CA, USA, 2008. 265-270. doi: 10.1109/ISQED.2008.4479798
22. Djukanovi, S. An accurate method for frequency estimation of a real sinusoid. *In* Proceedings of the Signal Processing Letters, IEEE, 2016, **23**(7). doi: 10.1109/LSP.2016.2564102
23. Saeed, V. Advanced digital signal processing and noise reduction. 4th Ed., John Wiley & Sons, 2008, pp. 321-323.

ACKNOWLEDGMENTS

It is immense pleasure to thank Director DLRL, Additional Director and Wing Head for their continuous guidance and support toward this activity. The authors are also would like to thanks anonymous reviewers for making various useful suggestions and comments.

CONTRIBUTORS

Mr R.K. Niranjan received his BE (ECE) from Dr Hari Singh Gour University, Sagar, in 1998 and ME (Systems and Signal Processing) from Osmania University, Hyderabad, in 2012. Currently pursuing his PhD from NIT, Warangal. Presently working as Scientist 'F' at DRDO-Defence Electronics Research Laboratory, Hyderabad. He has been working in the area of signal processing for electronic warfare systems with specific interests in the area of data acquisitions and DSP algorithms implementations in FPGA for real time applications.

In the current study, he conceived the concept, carried out the literature survey and complete experimental work with interpretation and analysis of result.

Dr A.K. Singh, did ME in Digital System (ECE) and PhD from Osmania University, in 2003 and 2015, respectively. Currently working as Scientist 'G' at DRDO-Defence Electronics Research Laboratory. He was the instrumental in design and development of digital receiver. His area of interest includes high-speed board design, time-frequency signal processing, and EW Receiver design. Presently he is working for space systems design.
In the current study, he has supported in making experimental setup, reviewed the incremental work and provided various valuable inputs.

Prof. C.B. Rama Rao, did his post-graduation from JNTU, Kakinada and PhD from IIT, Kharagpur. He has been currently working as Professor in the Department of Electronics and Communication Engineering, NIT Warangal, India. His research interests primarily include adaptive signal processing, musical instrumental signal processing, speech signal processing and biomedical signal processing. He has published more than 32 papers in reputed Journals and Conferences.
In the current study, he has given the idea, reviewed the work, validated the results, continuously provided the guidance and given many valuable inputs.

Defence Science Journal, Vol. 70, No. 3, May 2020, pp. 278-284, DOI : 10.14429/dsj.70.15105

High Accuracy Parameter Estimation for Advanced Radar Identification of Electronic Intelligence System

R.K. Niranjan[#,@,*], A.K. Singh[#], and C.B. Rama Rao[@]

[#]*DRDO-Defence Electronics Research Laboratory, Hyderabad - 500 005, India*
[@]*Department of ECE, National Institute of Technology, Warangal - 506 004, India*
[*]*E-mail: niranjanrk2004@gmail.com*

ABSTRACT

Radar identification is one of the vital operations in an electronic intelligence system. The conventional methods based on basic parameters comparison of unique identification of a radar in a cluster of similar radars, is prone to ambiguities. To meet the current tactical requirements of unique identification of a radar, the methodology needs to be based on better feature extraction, even in low SNR conditions. The paper explores a novel technique based on moving autocorrelation for the extraction of intra-pulse and inter-pulse radar parameters. Extensive simulation and empirical studies have been carried out to establish the approach to extend accurate radar parameters in noisy and low SNR conditions. The technique is found to be promising even in field data conditions. The paper describes the methodology, simulation results, FPGA implementation using system generator and resource utilisation summary.

Keywords: ELINT system; Electronic intelligence; Intra-pulse parameters; Autocorrelation

NOMENCLATURE

$x(n)$	Time domain signal
X_m	Restored signal spectrum
N_m	Noise spectrum
Y_m	Noisy signal spectrum
$x(m)$	Restored time domain signal
m,n	Index number
k	Bin number
θY_k	Phase of the Frequency Spectrum
F_s	Sampling Frequency
$\Phi(n)$	Phase of the signal
$\Delta\Phi(n)$	Phase difference
$F_m(n)$	Multilevel Frequency

1. INTRODUCTION

The modern electronic intelligence (ELINT) system should be capable to identify radar signal emissions uniquely in a dense environment. The evolving radar technology, utilising frequency, pulse width (PW) and pulse repetition interval (PRI) agility requires complex signal processing techniques to facilitate unique emitter identification. The dense electromagnetic environment, with complex radar waveforms, results in pulse on pulse in radar signals being overlapped in time, frequency and azimuth. It poses serious challenge to ELINT reconnaissance process.

The efficient emitter identification system is vital which extracts distinctive and accurate intra-pulse and inter-pulse parameter to handle the above challenges. The radars of the same kind exhibit slight differences in their transmitted pulses[1]. The identification system needs to classify and identify similar radars i.e. radars of the same make and model using the unintentional intra-pulse parameters in addition to the intentional parameters. These extracted features constitute the finger print or signature of the radar. Based on signature of the radar, the decision making and correct identification of the radar can be established.

The intra-pulse parameters include frequency, amplitude, rise time, fall time, type of modulation for each pulse. As part of intra-pulse analysis, instantaneous variations in frequency, amplitude, phase and their first and second order statistical variations are computed[2-4]. Instantaneous frequency is an important parameter to describe the characteristics which changes with time. The identification was presented using various methods[5-9]. Michel & Adams[10] presented the FPGA implementation aspects for radar system. Accurate measurement of parameters ensures the correct radar identification. Measurements carried out using proposed approach improve the identification as discussed[5-9].

The conventional method of handling pulse on pulse signals is given based on extraction of basic parameters, viz frequency, PW and direction of arrival (DOA)[11-12]. This method is prone to ambiguities and often result in erroneous identification. To overcome this, the intra-pulse parameters of the radar also need to be extracted. With the advent of radars exhibiting agility in frequency, PW and PRI, there is a need to measure the intra-pulse group parameters. And also with the rapid deployment of LPI radars[13-14], it is crucial to handle these radars and identify them correctly.

A better methodology is based on digital in phase and quadrature phase (DIQ) for intra-pulse analysis. This technique performs reasonably well for SNR conditions better than 12 dB as demonstrated[15]. Pulse detection approach is discussed

Received : 22 November 2019, Revised : 12 March 2020
Accepted : 20 March 2020, Online published : 27 April 2020

which needs about 3 dB SNR[16]. Digital instantaneous frequency measurement technique is presented for frequency measurement[17-20]. However they measure the frequency with high accuracy at high SNR. But their performance is not good at lower SNR.

This paper proposes for unique identification a much better methodology, in a low SNR condition of order of 0 dB. The signal is preprocessed, prior to the extraction of parameters. As part of preprocessing, noise cancellation is employed for signal enhancement to improve the quality of the signal. Noise cancellation is done by estimating the noise from electromagnetic environment. The estimated noise magnitude is subtracted from the magnitude of noisy signal without affecting the phase to get restored signal[21]. Noise cancellation is applied on both in phase and quadrature phase components and restored signal is computed for both. Thereafter, moving autocorrelation with different delays is performed on the complex signal to further enhance the signal and reduces the effect of noise. Performing autocorrelation is computationally intensive. So, an efficient technique for implementation has been devised. The intra-pulse parameters so extracted are highly accurate even at low SNR conditions.

The efficacy of the algorithms has been tested with live radar data. The analysis has been conducted on different radar modes and different radar signals to verify the robustness of the features extraction algorithm. In subsequent section, the instantaneous measurement techniques based on autocorrelation alongwith noise cancellation and noise estimation, simulation results and implementation of FPGA hardware is discussed.

2. FINE GRAIN PARAMETER MEASUREMENTS TECHNIQUES

The accurate intra-pulse information amalgamated with the inter-pulse information of RF, PRI, PW and scan provides the comprehensive characterisation of the emitter thereby arriving at the fine grain parameters of each emitter, which are highly accurate and grain parameters of each emitter and stable for identification of the emitter. Intentional parameters are measured using time domain and frequency domain techniques.

Figure 1 shows the block diagram of Fine Grain Parameter (FGP) measurement. The algorithms shown are applied on digitised baseband or IF signal and finally instantaneous amplitude profile, instantaneous frequency profile and fine grain parameters are generated using both autocorrelation approach and DIQ approach. The signal is also pre-processed using noise cancellation technique before applying these algorithms. Noise estimation is carried out for finding out the noise riding threshold which is used for pulse detection and FGP are measured.

2.1 Noise Cancellation

Subtraction of noise from the noisy signal is done to get a restored signal which reduces the SNR requirement at the input signal. Noise samples are collected from the system chain when front end is connected to built-in test equipment (BITE) port in signal off condition for minimum time of 50 us for better estimate. Then estimated average of noise spectrum N_m is subtracted from the noisy signal spectrum Y_m to get estimate of the instantaneous magnitude spectrum of restored signal X_m.

$$X_m = Y_m - N_m \tag{1}$$

Restored time-domain signal (X_m) is obtained by combining an estimate of the instantaneous magnitude spectrum of restored signal (with phase of the noisy signal), and transforming via an inverse discrete Fourier transform to the time domain[21].

$$x(m) = \sum_{n=0}^{N-1} (X_k e^{j\theta Y_k})(e^{\frac{j2\pi km}{N}}) \tag{2}$$

Noise estimate subtraction technique is applied to the input signal, to produce the output restored signal as shown in Fig. 2. The 66650 samples are taken for pre-trigger region which consists mainly noise and 8000 samples are taken for pulse signal which consists signal as well as noise. The additive white Gaussian noise (AWGN) is considered. It is visible in output restored signal that has reduced noise and thus helps in improving accuracy of further analysis. Restored signal is applied on both baseband signals of in-phase (I) and quadrature-phase (Q) components.

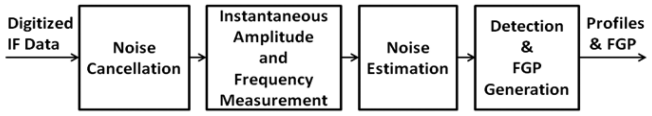

Figure 1. Fine grain parameter measurement.

2.2 Instantaneous Amplitude and Frequency Measurement

Autocorrelation is performed on the baseband signal to reduce the effect of noise[16]. Thirty two samples autocorrelation is performed in a recursive way to reduce the computational

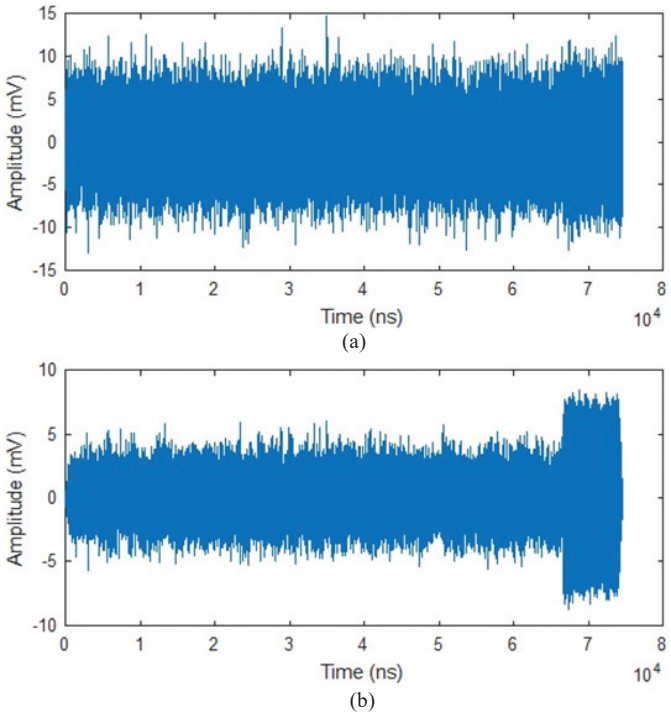

Figure 2. (a) Input at 1 GHz with 0 dB SNR and (b) Restored signal.

requirement. Thirty two samples autocorrelation is selected to cater the minimum pulse width requirement of 50 ns when sampling time is 1.5 ns. Delay m is 1 in case of amplitude measurement. First element of thirty-two samples auto correlation is calculated as:

$$X(1) = mean(x(1:32).x^*(1+m:32+m)) \quad (3)$$

where x^* is a conjugate of x. It is implemented in recursively as below:

$$X(n+1) = x(n) + |x(n+32).x^*(n+32+m)| - |x(n).x^*(n+m)| \quad (4)$$

where n varies from n to the size of samples. This equation is further optimised by replacing first element of thirty-two samples auto correlation with fixed value:

$$X(1) = a + jb \quad (5)$$

where a and b are constant values. This does not require the measurement of initial average of thirty-two samples auto correlation output. Measurement of frequency parameters involves calculation of autocorrelation variables with different delays using baseband signal. Four autocorrelation variables $X1$, $X2$, $X4$ and $X8$ with four different delays m = 1, 2, 4 and 8 are calculated from the correlated signal with different delays. Multilevel phase differences are calculated from the correlated signals with different delays, which in turn are used to compute the frequency. Frequency ($F_1(n)$) is measured as:

$$F_1(n) = F_s\left(\frac{\Delta\Phi(n)}{2\pi}\right) \quad (6)$$

where F_s is sampling frequency and $\Delta\Phi(n)$ is the phase difference derived from $X1$. Now $F_1(n)$ measurement determines the zone in which phase belongs according to the following equation.

$$Z_m = Ceil\left(\frac{mF_1(n)}{F_s}\right) \quad (7)$$

Here unwrapping of phases which is required for complex signals is not required as different phases are calculated from auto-correlated variables with different delays and are mapped to appropriate zones which are obtained with the help of frequency $F_{m-1}(n)$ [17-18]. Likewise $F_2(n)$ serves as a guide for Φ_4 by determining the zone it should be merged to. Similarly, $F_4(n)$ determines the zone for Φ_8. The final frequency parameter $F_8(n)$ is based on the mapping of Φ_8.

$$F_m(n) = \left(\frac{F_s}{2\pi m}\right)\left(\Delta\Phi_m(n) + 2\pi Z_m\right) \quad (8)$$

Using the improved instantaneous frequency, the various intra-pulse modulations. Bi-phase, quad-phase and poly-phase signals are also classified. The instantaneous frequency is median filtered to suppress impulses caused due to the noise, but to retain the main trend. The standard deviation of the median filtered instantaneous frequency profile is utilised to differentiate conventional bi-phase and quad-phase signals from poly-phase signals.

2.3 Noise Estimation

Estimation of noise is done for pulse detection which reduces the computation requirement and storage requirement. Mean of the modulus of the noise samples are taken and approximate standard deviation is computed. The absolute of input signal samples $x(n)$ are taken which makes all negative samples positive. The shape of probability density function (PDF) will be same but doubles the peak value.

$$\sigma = \sqrt{\sum_{n=0}^{N-1}\frac{(x(n)-x_{avg})^2}{N}} \quad (9)$$

$$\sigma_1 = \left(\frac{k_1}{2}\right)\sum_{n=0}^{N-1}|x(n)| \quad (10)$$

$$\sigma_2 = \left(\frac{k_2}{2}\right)|x(n)+x(n+1)| \quad (11)$$

The Eqn. (9) shows standard deviation (σ) of signal $x(n)$ which is obtained by computing mean of noise. Absolute value of signal $x(n)$ is computed and multiplied with constant $(k_1/2)$ and result (σ_1) is derived as Eqn. (10) which is approximately equivalent to standard deviation of signal $x(n)$. Similarly, based on two point averaging also approximate standard deviation (σ_2) is calculated using Eqn. (11). Constants k_1 and k_2 are decided based on minimum error. The random noise is computed and results are tabulated using both the approaches as shown in Table 1. Error is also computed with standard deviation. The error ($E1$) computed is less than 10% using first approach whereas error ($E2$) is less than 20 % using second approach. Usually, two level threshold is used which will have difference of 6 dB. Hence the first approach is appropriate as error computed is less and it is efficient also in hardware implementation.

2.4 DIQ Technique

Equations given below describes the DIQ approach for calculating instantaneous phase, frequency, and amplitude. The detection is carried out on this amplitude profile $R(n)$ and pulse is detected.

$$\Phi(n) = \tan^{-1}\left(\frac{q(n)}{i(n)}\right) \quad (12)$$

Table 1. Comparison of noise estimation approach

Iteration No.	Standard deviation A	Approach-1 (σ_1) B	Error-1 E1=A-B	Approach-2 (σ_2) C	Error-2 E2=A-C
1	5.825	5.296	0.529	5.593	0.232
2	5.784	5.343	0.441	5.339	0.445
3	4.852	5.305	-0.453	5.756	-0.904
4	5.567	5.281	0.286	5.838	-0.271
5	4.787	5.256	-0.469	5.598	-0.811
6	5.063	5.323	-0.26	6.008	-0.945
7	5.629	5.324	0.305	5.663	-0.034
8	5.276	5.196	0.08	5.576	-0.3
9	5.091	5.195	-0.104	6.023	-0.932
10	4.466	4.789	-0.323	5.213	-0.747

$$F(n)=\left(\frac{F_s}{2\pi}\right)\Delta\Phi(n) \tag{13}$$

$$R(n)=\sqrt{i^2(n)+q^2(n)} \tag{14}$$

There is a requirement of above 8 dB SNR using DIQ technique for instantaneous amplitude and frequency measurement of pulse.

A novel technique based on optimised autocorrelation and noise estimation has been developed to calculate accurate intra-pulse parameters and to overcome the effect of noise at low SNR conditions. It can be utilised for feature extraction and identification of LPI signals also. Using this technique the instantaneous amplitude and frequency parameters of a pulse can be measured with 0 dB.

3. SIMULATION RESULTS

The input signal generated at 0 dB and 9 dB SNR is plotted in Fig. 3. The same signal is used in simulation for generating autocorrelation and DIQ technique outputs.

The envelope or instantaneous amplitude is computed using correlated signal $x(n)$ at SNR conditions of 0 dB and 9 dB which is plotted in Fig. 4. First the input signal is improved using noise cancellation technique. The envelope computed using DIQ technique is plotted in Fig. 5 at SNR conditions of 0 dB and 9 dB. It is observed from Figures, that there is a improvement of 9 dB to 10 dB in the correlated signal as compared to the DIQ technique.

Figure 6 shows the instantaneous frequency output calculated from multilevel correlation coefficients and Fig. 7 shows the instantaneous frequency output as computed from the conventional DIQ technique using the same input pulse signals at 0 dB SNR and 9 dB SNR. Frequency measurement accuracy of 500 kHz at 0 dB SNR has been achieved using the multilevel correlation technique as we see in Fig. 6.

Improvement in frequency measurement accuracy with reduction in SNR requirement at the input is achieved in comparison with DIQ technique as observed through Fig. 7.

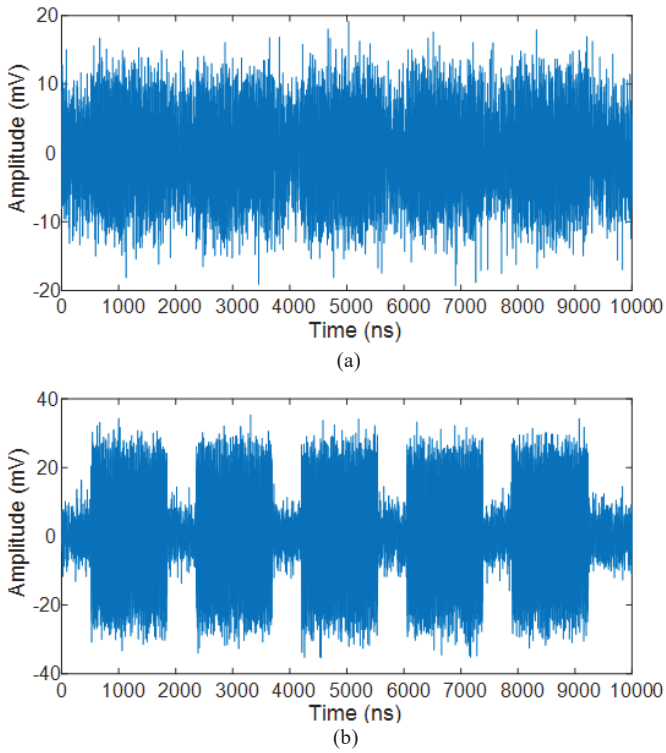

Figure 3. Input signal at (a) 0 dB and (b) 9 dB SNR.

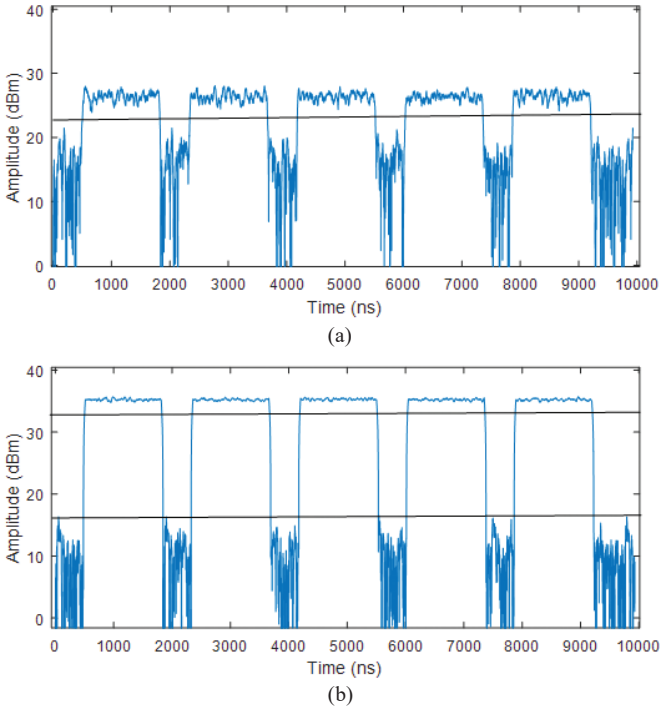

Figure 4. Amplitude profile using autocorrelation approach at 0 dB and 9 dB SNR.

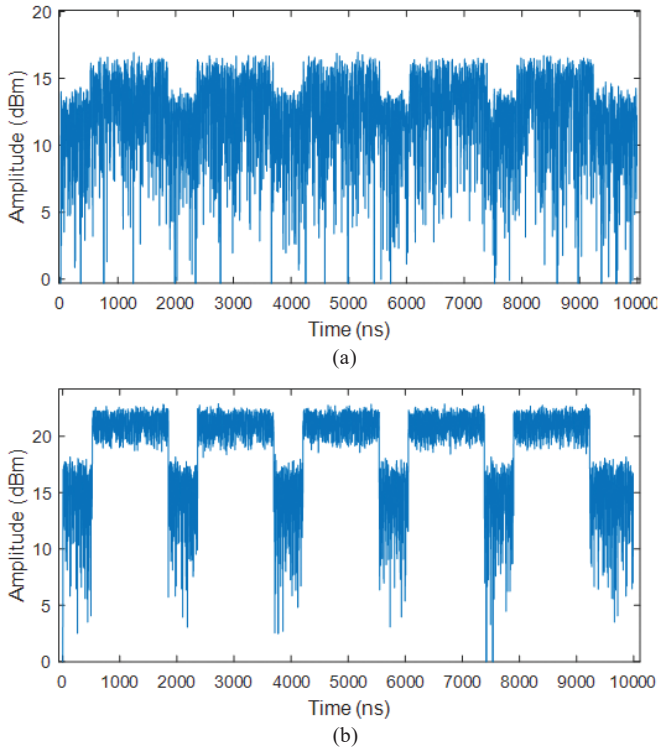

Figure 5. Amplitude Profile using DIQ approach at (a) 0 dB and (b) 9 dB SNR.

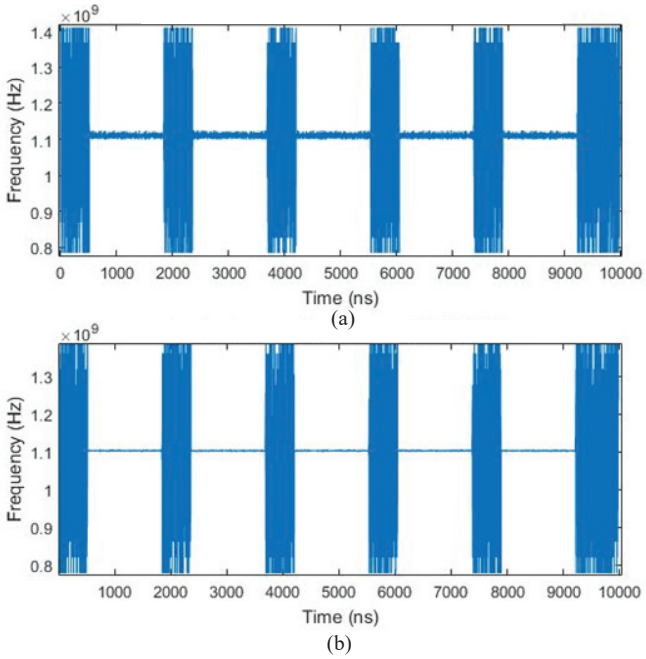

Figure 6. Frequency profile using autocorrelation approach at (a) 0 dB and (b) 9 dB SNR.

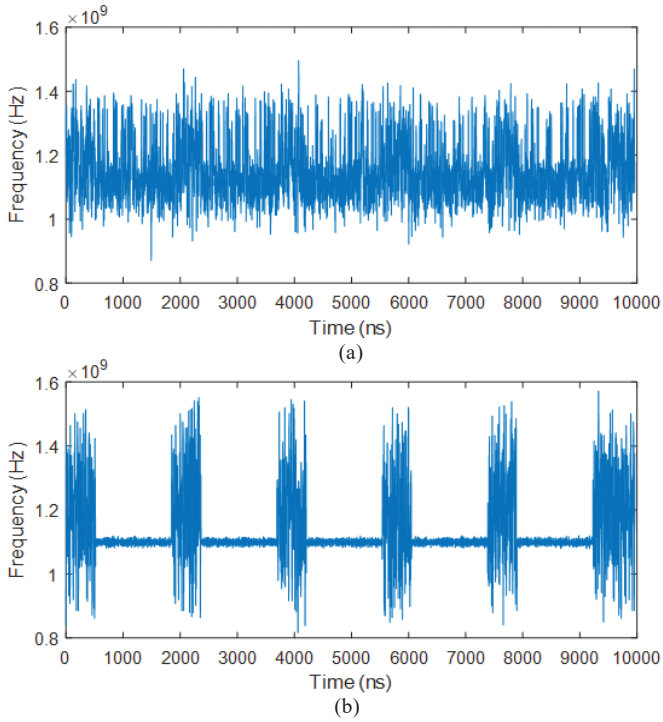

Figure 7. Frequency profile using DIQ approach at (a) 0 dB and (b) 9 dB SNR.

Figure 8 depicts the frequency accuracy with respect to SNR using both the techniques. This shows that autocorrelation technique is able to process the signal at 0 dB SNR, whereas DIQ technique fails. The DIQ technique requires the SNR more than of 9 dB.

The field data is also introduced to check the efficacy of the proposed algorithms. The same data is used for DIQ approach and results are provided as shown in Fig. 9. It is clearly evident from instantaneous amplitude and

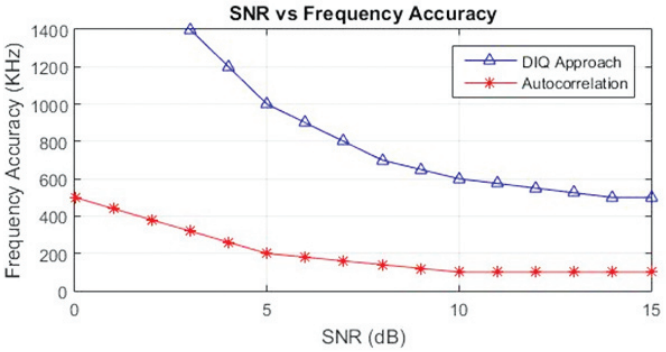

Figure 8. SNR vs frequency accuracy plot.

instantaneous frequency profiles generated using proposed approach having better results compared with DIQ approach.

4. IMPLEMENTATION ON FPGA HARDWARE AND SIMULATION RESULTS

Conventional and Proposed approaches are implemented using System generator, Matlab and Xilinx Vivado 2016.4 tools. The system generator models are generated as shown in Fig. 10. The design is implemented on Xilinx Virtex-7 XC7VX415T FPGA device. The synthesis for netlist generation, mapping, place and route is carried out. The comparison of FPGA resource utilisation summary is shown in Table 2. The overall requirements of resources are reduced in proposed approach. Total eight DSP48E1 component are required as proposed approach is having only two complex multiplications. Whereas DIQ approach requires more multiplications as it require low pass filters.

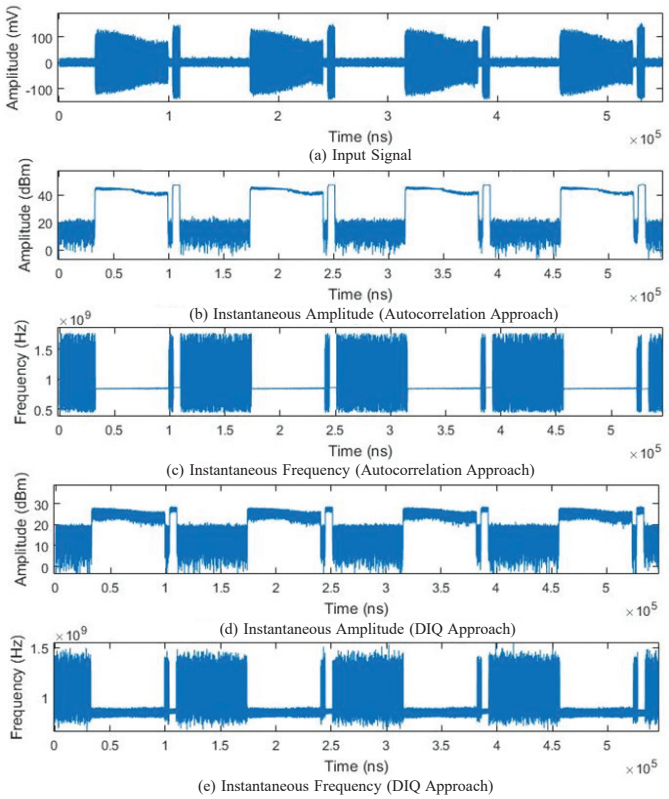

Figure 9. Field data result using Autocorrelation and DIQ approach.

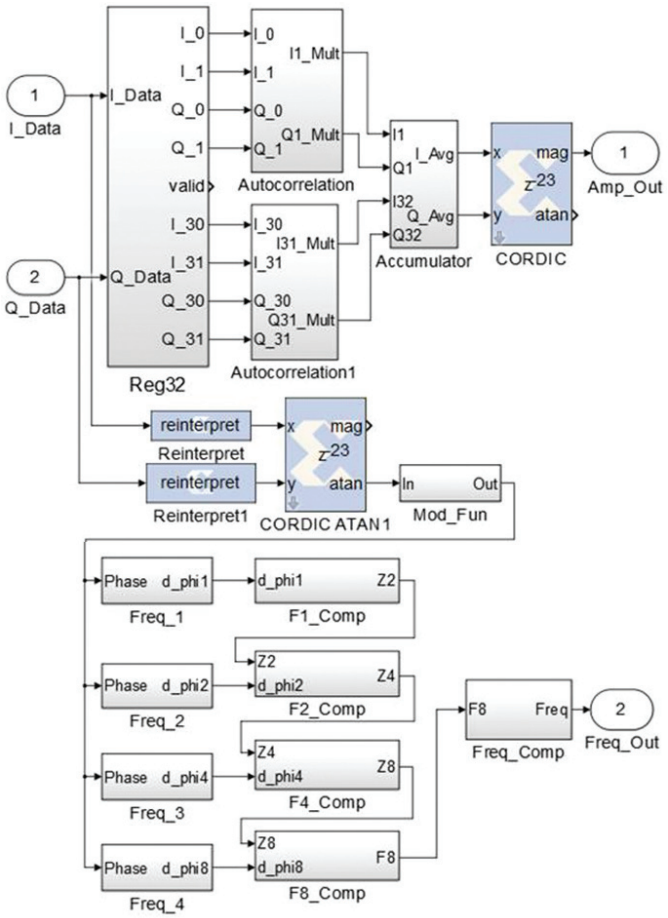

Figure 10. System generator model.

Simulation result using proposed approach is shown in Fig. 11 at 0 dB SNR. Only pulse on time along with pre and post region is shown to facilitate the simulation for multiple pulses. Amp_Out shows the instantaneous amplitude profile which is clearly visible and Freq_Out is the instantaneous frequency profile.

Table 2. FPGA resource utilisation summary (Device: XC7VX415T)

FPGA resource utilisation with max operating Freq.	Proposed approach	DIQ approach	Savings in %
Maximum clock frequency (MHz)	238.1	231.8	2.72
Slice F/Fs	2003	4052	50.52
LUT (4 Inputs)	2546	3799	32.98
DSP48E1	8	38	78.94
Total power (mW)	472	708	33.33

5. CONCLUSIONS

The proposed technique based on moving autocorrelation and noise estimation has significantly improved the measurement accuracy of intra-pulse parameters of instantaneous amplitude and instantaneous frequency at low SNR conditions. The scheme along with finger printing system has lead to a very efficient and accurate emitter identification system. The advancement in signal processing algorithms,

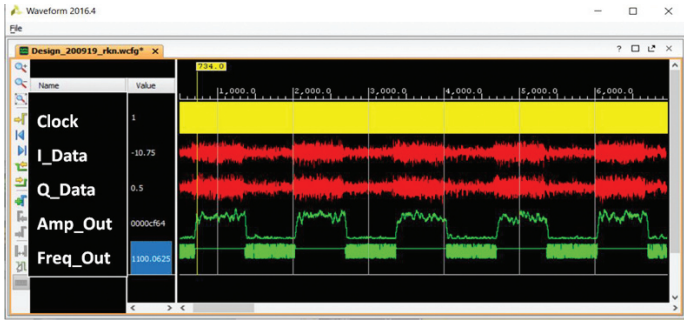

Figure 11. Simulation result at 1100 MHz.

coupled with high performance FPGA has enabled to improve the unique emitter identification and also achieves a real time performance. It is planned for real time modulation classification based on instantaneous frequency profile in future.

REFERENCES

1. Ramachandran, R.; Sharma, R. & Varughese, S. Graceful degradation: An airborne surveillance radar perspective. *Def. Sci. J.,* 2019, **69**(4), 389-395. doi: 10.14429/dsj.69.12135
2. Conning, M. & Potgieter, F. Analysis of measured radar data for specific emitter identification. IEEE Radar Conference, Washington, DC, USA; 2010. doi: 10.1109/RADAR.2010.5494658.
3. Gupta, M.; Hareesh, G. & Mahla, A.K. Electronic warfare: Issues and challenges for emitter classification. *Def. Sci. J.,* 2011, **61**(3), 228-234. doi: 10.14429/dsj.61.529
4. Singh, A.K. & Rao, S.K., Digital receiver-based electronic intelligence system configuration for the detection and identification of intrapulse modulated radar signals. *Def. Sci. J.,* 2014, **64**(2), 152-158. doi:10.14429/dsj.64.5091
5. Dudczyk, J. & Kawalec A. Identification of emitter sources in the aspect of their fractal features. *Bull. Pol. Ac.: Tech.,* 2013, **61**(3), 623–628. doi: 10.2478/bpasts-2013-0065
6. Dudczyk, J. & Kawalec A. Specific emitter identification based on graphical representation of the distribution of radar signal parameters**.** *Bulletin Polish Academy Sciences: Technical Sciences*, 2015, **63**(2), 391–396. doi: 10.1515/bpasts-2015-0044
7. Kawalec, A. & Owczarek, R. Radar emitter recognition using intrapulse data. Microwave and radar week in Poland, *In* Proceedings of MICON, Warsaw, 2004, **2**, 435-438. doi: 10.1109/MIKON.2004.1357059
8. Deng, S.; Huang, Z. & Wang, X. A novel specific emitter identification method based on radio frequency fingerprints. *In* Proceedings of ICCIA, IEEE, Beijing, 2017, 368-371. doi: 10.1109/CIAPP.2017.8167241
9. Pan, Yiwei; Peng, Hua; Li, Tianyun & Wang, Wenya. High-fidelity symbol synchronization for specific emitter identification. IEEE ITNEC, Chengdu, 2019, 393-398. doi: 10.1109/ITNEC.2019.8729181

10. Knioła, M. & Kawalec, A. Matched filter module as an application of modern FPGA in radar systems. *In* Proceedings of SPIE, **107150**, April 2018, doi: 10.1117/12.2317907
11. Adamy, D.L. EW 101: A first course in electronic warfare. Boston, MA, USA: Artech House, 2001, pp. 83.
12. Richard, G.W. ELINT, the Interception and analysis of radar signals. Boston, MA, USA: Artech House, 2006.
13. Adamy, D.L. EW 102: A second course in electronic warfare. Boston, MA, USA: Artech House, 2004, pp. 67-72.
14. Pace, P. E., Detecting and classifying low probability of intercept radar. Ed. 2nd, Boston, London, Artech House, 2008, pp. 41-63.
15. Niranjan, R.K. & Bhukya, R.N. Approach of pulse parameters measurement using digital IQ method. IJIEE, 2014, **4**(1), 31-35. doi: 10.7763/IJIEE.2014.V4.403
16. Simin, Z.; Deguo, Z. & Bin, T. A Wideband Pulse Detection Algorithm based on Autocorrelation. *In* 9th ICEMI, IEEE, **4**, Beijing, China, 2009. 287-289. doi: 10.1109/ICEMI.2009.5274088.
17. Tsui, J.B.Y. Digital techniques for wideband receivers. Ed. 2nd, Norwood, MA Artech House, 2001, pp. 265-270.
18. Mahlooji, S. & Mohammadi, K. Very high resolution digital instantaneous frequency measurement receiver. *In* IEEE Proceedings of International Conference on Signal Processing and Systems, Singapore, 2009. doi: 10.1109/ICSPS.2009.43.
19. Helton, J.; Henry, C.I.; David, M.L. & Tsui, J.B.Y. FPGA-Based 1.2 GHz bandwidth digital instantaneous frequency measurement receiver. *In* Proceedings of ISQED. San Jose, CA, USA, 2008, pp. 265-270. doi: 10.1109/ISQED.2008.4479798.
20. Pandolfi, C.; Fitini, E.; Gabrielli, G.; Megna, E. & Zaccaron. A. Comparison of analog IFM and digital frequency measurement receivers for electronic warfare. *In* IEEE, 7th European Radar Conference, Paris, France, ISBN: 978-2-87487-019-4
21. Saeed, V. Advanced digital signal processing and noise reduction. Ed. 4th, John Wiley & Sons, 2008, pp. 321-323.

ACKNOWLEDGEMENT

It is great pleasure to thank Director DLRL, Additional Director and Wing Head for their continuous guidance and support toward this activity. The authors are also would like to thanks to anonymous reviewers for making numerous useful suggestions and comments.

CONTRIBUTORS

Mr R.K. Niranjan, received his BE (ECE) from Dr Hari Singh Gour University, Sagar, in 1998 and ME (Systems and Signal Processing) from Osmania University, Hyderabad, in 2012. Currently working as Scientist 'F' at DRDO-Defence Electronics Research Laboratory, Hyderabad. He has been working in the area of signal processing for Electronic Warfare systems with specific interests in area of data acquisitions and digital signal processing algorithms implementations in Matlab and FPGA.
Contribution in the current study, he conceived the concept and carried out the complete experimental work.

Dr A.K. Singh, did ME in Digital System (ECE), in 2003 and PhD, in 2015 from Osmania University. Currently working as Scientist 'G' at DRDO-Defence Electronics Research Laboratory, Hyderabad. He was the instrumental in design and development of Digital Receiver. His area of interest includes high speed board design, Time-frequency signal processing, and EW Receiver design. Currently he is working for space systems design.
Contribution in the current study, he has supported in making experimental setup, reviewed the incremental work and provided various valuable inputs.

Prof. C.B. Rama Rao did his post-graduation from JNTU, Kakinada and PhD from IIT, Kharagpur. He has been currently working as professor in the Department of Electronics and Communication Engineering, NIT Warangal, India. His research interests primarily include adaptive signal processing, musical instrumental signal processing, speech signal processing and biomedical signal processing. He has published more than 30 papers in Journals and Conferences.
Contribution in the current study, he has given the idea, reviewed the work, validated the results, continuously provided the guidance and given many valuable inputs.

Real-Time Identification of Exotic Modulated Radar Signals for Electronic Intelligence Systems

RK Niranjan[1,2], CB Rama Rao[1] and AK Singh[2]

[1]Department of ECE, NIT, Warangal - 506004, India
[2]DLRL (DRDO), Hyderabad - 500005, India
E-mail: niranjanrk2004@gmail.com

***Abstract* :- In the modern battle field, due to proliferation of the similar radars growing demand for specific emitter identification. To identify these radars uniquely in real-time is a challenge to understand the deployment pattern. Present ELINT systems are required to decipher the exotic modulations on a pulse to pulse basis to achieve specific emitter identification of military radars. In this paper, instantaneous frequency profile is used to measure the exotic modulation and their parameter which includes linear frequency modulation (LFM) with bi-phase modulation (BPM) and stepped frequency modulation (SFM) with BPM along with other modulations. These modulation measurements contribute in de-interleaving of signals. The proposed algorithm is simulated in Matlab and results are verified with different signal-to-noise ratios. This algorithm is also implemented on FPGA to demonstrate real-time performance.**

Keywords - Intra-pulse analysis, de-interleaving, bi-phase modulation, linear frequency modulation, stepped frequency modulation.

I. INTRODUCTION

Various fire control and weapon locating radars operate nearby which makes the electronic environment very dense, especially in L and S bands. Measuring conventional parameters are not sufficient to distinguish them. Intra-pulse measurement with exotic modulation measurement is the requirement in the present scenario [1]. Electronic intelligence (ELINT) systems that are capable to measure this information will have an edge in the field.

ELINT systems estimated many parameters which together are called pulse descriptor word (PDW) includes direction-of-arrival (DOA), radio-frequency (RF), pulse-width (PW), time-of-arrival (TOA), etc. [2]. These systems do the intra-pulse analysis including modulation measurement of radar signals on a pulse-by-pulse basis using stored data to match the speed of processing hardware. Measurement of exotic modulation in real-time is a challenge along with other parameter measurements.

The fast Fourier transform (FFT) technique is extensively used to detect the radar signals, measures the PDW. Although, these techniques provide a processing gain advantage but PW and PRI measurement suffers from inaccuracies of an order of one FFT frame length. One frame of accuracy is not sufficient to measure these parameters. To improve these parameters accuracies overlap FFT is one of elucidation. Still, the sample-by-sample accuracy is a difficult task using this technique due to their high resources requirement in field-programmable gate array (FPGA) platform [3], [4]. Hence, exotic modulation measurement in real-time is also not possible. Whereas, time domain techniques have limited use due to their limited sensitivity compared to frequency domain techniques [5].

In this paper time-domain based autocorrelation algorithm is performed. The sensitivity is improved by using noise cancellation along with this technique [6]. This provides the enhancement of gain which is comparable to the frequency domain technique. These techniques are capable of instantaneous measurements of frequency and amplitude which are used for measurements. These instantaneous measurements help to measure exotic modulations using proposed identification algorithms [7].

The de-interleaving based on the basic parameters (DOA, RF, PW, and PRI) is not very effective due to the dense environment where similar radars are operating in environment [8]-[11]. The exotic modulations and their parameters will be the supportive parameters for de-interleaving in this case and similar radars can be segregated effectively.

The proposed algorithm has been tested with different signal-to-noise ratio (SNR) conditions. In section-2, modelling of exotic signals is given. Proposed algorithms are specified in section-3. In section-4 simulation results, FPGA results, and discussions are presented

II. MODELLING OF EXOTIC SIGNALS

The signals with Linear Frequency Modulation (LFM), Stepped Frequency Modulation (SFM), and Bi-Phase Modulation (BPM) are modeled as below:
(i) Linear Frequency Modulation (LFM): LFM ascending (LFMa) and LFM descending (LFMd) chirp signals are considered as LFM signals or Triangular FM.
(a) LFMa signal generation is expressed as below [12]

$$x(n) = A.exp[j(2\pi f n t_s + \phi + \pi\alpha\, n^2 t^2)] \quad (1)$$

for n = (-N/2), (-N/2)+1, …., -1. Where ϕ is the initial phase and α is the LFMa slope.

(b) LFMd signal generation is expressed as below [12]

$$x(n) = A.exp[j(2\pi f n t^2 + \phi - \pi\beta n^2 t^2)] \quad (2)$$

for n = 0, 1, 2,…., (N/2)-1. Where β is the LFMd slope.

(ii) Stepped Frequency Modulation (SFM): SFM is expressed as below

$$x(n) = A.exp[j(2\pi f_h n t_s + \phi)] \quad (3)$$

for n=1, 2, 3, …, N.
where, f_h is the frequency of h^{th} step, and h = 1, 2, 3,…., H is the number of steps. Usually, H is in the sequence of 2, 4, 8…. etc. SFM ascending and SFM descending signals are represented as SFMa and SFMd respectively.

(iii) Bi-Phase Modulation (BPM): BPM signal is modeled as given by [12],

$$x(n) = A.exp[j(2\pi f n t_s + \phi + \theta(n))] \quad (4)$$

where, θ(n) = π(1-n) when the zero bits of the code sequences are sampled and θ(n) = θ, when one bit of the code sequence are sampled. The phase shift θ can be 0^0 or 180^0 in the case of bi-phase modulation.

The exotic modulated signals are modeled as below with the combination of above signals:
(i) LFMa with BPM: LFM ascending with BPM exotic signal is generated below:

$$x(n) = A.exp[j(2\pi f n t_s + \phi + \pi\alpha\, n^2 t^2 + \theta(n))] \quad (5)$$

(ii) LFMd with BPM: LFM descending with BPM exotic signal is generated below:

$$x(n) = A.exp[j(2\pi f n t_s + \phi - \pi\beta\, n^2 t^2 + \theta(n))] \quad (6)$$

(iii) SFM with BPM: SFM with BPM exotic signal is generated below:

Error! Bookmark not defined. $x(n) = A.exp[j(2\pi f_h n t_s + \phi + \theta(n))]$ (7)

III. Proposed Identification Algorithm

The block diagram of the proposed ELINT system is given as Fig. 1. RF signals are down-converted to an intermediate frequency (IF) which is sampled by high-speed analog-to-digital converter (ADC). IF signal is the matched output to the range of ADC. This will give a dynamic range advantage. Noise cancellation technique is employed to improve the SNR of the signal by subtracting estimating averaged noise from the signal.

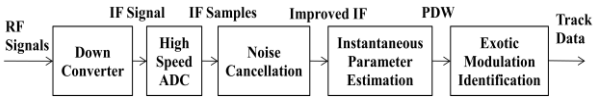

Fig. 1. Block Diagram of ELINT System.

This enhanced signal is used to estimate the instantaneous amplitude and instantaneous frequency. Instantaneous amplitude profile is generated based on the time-domain processing algorithm known as moving autocorrelation technique. This profile is generated on a sample-by-sample basis which is used for detection of the pulse and measurement of parameters. These parameters form the PDW words. Instantaneous frequency profile is also generated on the sample-by-sample basis using time-domain processing known as multilevel autocorrelation technique. Modulation on the pulse is computed using an instantaneous frequency profile. When the pulse is detected, the frequency is noted at various points and these points are used for identification of modulation [7].

The representation of flow diagram of proposed exotic modulation identification algorithm is given in Fig. 2. The proposed algorithm identifies the exotic modulation type (LFM with BPM and SFM with BPM) and their modulation parameters. Whereas the identification of other modulations are attempted using decision-tree algorithm [13].

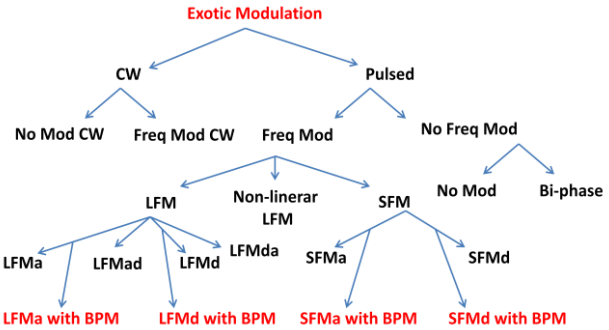

Fig. 2. Representation of Flow of Proposed Exotic Modulation Identification.

When a pulsed signal is detected and frequency modulation exists. If frequency is linear with an ascending trend and there is an abrupt change in frequency, the modulation will be declared as LFMa with BPM. Otherwise it will be declared as LFMa itself. Similarly, if frequency is linear with a descending trend and there is an abrupt change in frequency, the modulation will be declared as LFMd with BPM. Otherwise, it will be declared as LFMd alone.

If there is stepped frequency in pulsed waveform exists. If frequency is stepped with an ascending trend and there is

an abrupt change in frequency within each step. It will be declared as SFMa with BPM. Steps with ascending trend and without abrupt change in frequency will be declared as SFMa. If it is found that frequency is stepped with the descending trend and there is an abrupt change in frequency within each step. It will be declared as SFMd with BPM. Steps with the descending trend and without an abrupt change in the frequency will be declared as SFMd.

Conventionally, de-interleaving is performed based on the DOA, RF, and PW. On arrival of first PDW, first bucket is created with PDW parameter (DOA, RF, and PW). If the next PDW parameter (DOA, RF, and PW) falls within tolerance limit, they will be stored in the same bucket. If all three parameter (i.e. DOA, RF and PW) are not falling within the tolerance limit, another bucket will be created. Pulse repetition interval (PRI) is the derived parameter which is computed from time-of-arrival (TOA) of each successive pulse. This is estimated after all the buckets are created for a time slice.

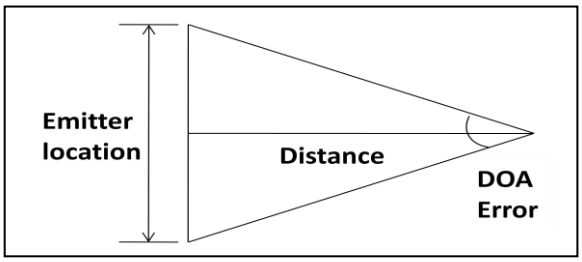

Fig. 3. Plot of Emitter Location Ambiguity versus Distance.

Considering, the DOA error value of approximately 2 degree in L and S bands. The tolerance of DOA will be ± 3 times of RMS value. The total error will be 12 degree. This total DOA error will translate into 21 Km error in azimuth from 100 Km distance. It means target available at 21 Km apart, will be considered for same basket. Fig. 3 shows the plot of emitter location ambiguity in azimuth versus distance. Similarly, the RF of 500 KHz and PW of 20 ns RMS value will translate into 3 MHz and 120 ns tolerance window respectively.

The other parameters are the modulation type and modulation parameter, which is used here for de-interleaving. This helps to improve the de-interleaving and reduces the affect of DOA inaccuracies. If signals are coming from identical DOA within tolerance, having the modulation parameter for de-interleaving is precious. Fig. 4 shows the representation of de-interleaving process.

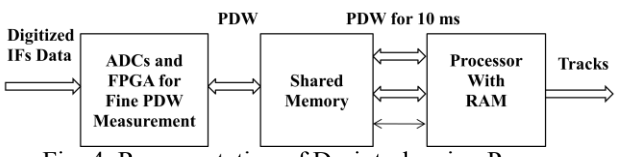

Fig. 4. Representation of De-interleaving Process.

IV. Simulation Results and Discussions

The instantaneous amplitude profile is generated for LFMa with BPM signal and shown as Fig. 5. These types of exotic modulated signals are found in ground based long range surveillance radars. The modulation information can't be measured using amplitude profile which is evident from Fig. 5.

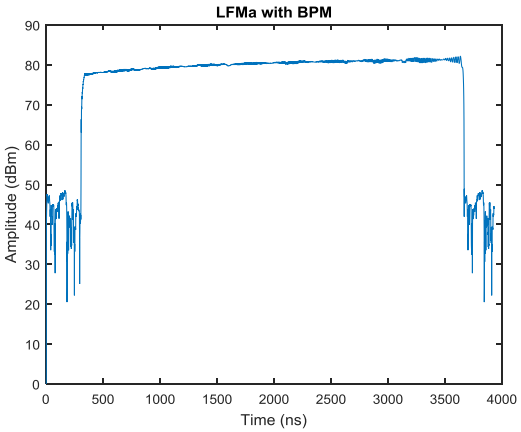

Fig. 5. Amplitude Profile of LFMa with 13-bit BPM.

The input signals are generated for various exotic modulated signals and their frequency profiles are generated. Frequency profile of LFM ascending with BPM, LFM descending with BPM, SFM ascending with BPM and SFM descending with BPM are shown as Fig. 6.

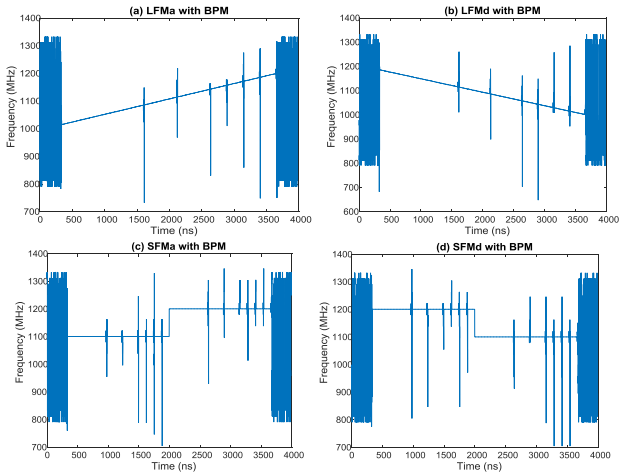

Fig. 6. Frequency Profiles of Exotic Modulated Signals

The exotic modulations were generated with different SNR and modulation measurement was carried out. The Success rate of the modulation recognition algorithm is shown in Table I. Total different 500 samples of data generated and results were captured.

TABLE I. Success Rate of Modulation Recognition Algorithm

Modulation Recognition	**Success Rate (%) # SNR (dB)**						
	3	2	1	0	-1	-2	-3
LFMa with BPM	99.2	98.0	97.2	95.4	93.6	90.4	80.6
LFMd with BPM	99.4	98.0	97.4	95.4	93.4	90.6	80.4
SFMa with BPM	99.0	98.4	97.0	95.2	93.4	90.8.	79.6
SFMd with BPM	99.2	98.6	97.0	95.4	93.6	91.0	79.4

The proposed algorithm is implemented on Xilinx RFSoC evaluation board and modulation and their parameters are measured. The resource utilization summary is shown in Table II. The utilization was compared for proposed algorithms with autocorrelation technique and digital in-phase and quadrature-phase (DIQ) technique [5], [7].

TABLE II. Resource Utilization Summary (Device ZCU111)

FPGA Resource	**Proposed Technique**		**Saving in %**
	with Autocorrelation	with DIQ Technique	
Slice F/Fs	2434	4910	50.43
LUT (4 Inputs)	2963	4328	31.54
DSP48E1	22	52	57.69
Block RAM	300	300	-

IV. CONCLUSIONS

The proposed algorithm of modulation identification is based on time-domain technique which identifies the exotic modulated signals i.e. LFMa, LFMd, SFMa, and SFMd with BPM. This technique is also implementable on FPGA as this technique consumes limited hardware resources. Such an idea to utilize modulation information will become a crucial parameter for PDW for better de-interleaving of specific emitter identification having a group of similar radars operating in the proximity.

ACKNOWLEDGMENT

It is great pleasure to thank Director DLRL, Additional Director and Wing Head for their continuous guidance and support toward this activity.

REFERENCES

[1] L. Nadav, M. Eli, Radar Signals. Wiley–Interscience, New York, 2004.

[2] R.G. Wiley, ELINT, the Interception and Analysis of Radar Signals, Artech House Radar Library, Artech House, Inc., 2006.

[3] S. Mahlooji, and K. Mohammadi, "Very High Resolution Digital Instantaneous Frequency Measurement Receiver", International Conference on Signal Processing and Systems, 2009.

[4] J. Helton, C.H. Chen, M. David, and J.B.Y. Tsui, "FPGA Based 1.2 GHz Bandwidth Digital Instantaneous Frequency Measurement Receiver", 9th ISQED, San Jose, CA, USA, 2008, pp 265-270.

[5] R.K. Niranjan, and B.R. Naik, "Approach of Pulse Parameters Measurement using Digital IQ Method", IJIEE; 2014.V4.403.

[6] V. Saeed, Advanced Digital Signal Processing and Noise Reduction, 4th Ed, John Wiley & Sons, 2008, pp. 321-323.

[7] R.K. Niranjan, A.K. Singh, C.B. Rama Rao, "High accuracy parameter estimation for advanced radar identification of electronic intelligence system", Def. Sci. J., Vol. 70, No. 3, pp. 278-284, DOI: 10.14429/dsj.70.15105.

[8] Z. Ge, X. Sun, W. Ren, W. Chen, G. Xu, "Improved algorithm of radar pulse repetition interval deinterleaving based on pulse correlation", IEEE Access, Vol. 7, 2019, pp 30126-30134, DOI: 10.1109/ACCESS.2019.2901013.

[9] V. Iglesias, J. Grajal, O. Yeste-Ojeda, M. Garrido, M.A. Sánchez, M. López-Vallejo, "Real-time radar pulse parameter extractor", IEEE Radar Conference, Cincinnati, OH, 2014, pp 371-375, DOI: 10.1109/RADAR.2014.6875617.

[10] M. Bagheri, M.H. Sedaaghi, "A new approach to pulse deinterleaving based on adaptive thresholding", Turk J Elec Eng & Comp Sci, Vol. 25, 2017, pp 3827 – 3838, DOI: 10.3906/elk-1606-415.

[11] L. Zhang-Meng, "Online pulse deinterleaving with finite automata, IEEE Transactions on Aerospace and Electronic Systems", Vol. 56, No. 2, 2020, pp 1139-1147, DOI: 10.1109/TAES.2019.2925447.

[12] S. Sung, Y. Zhou, "Modulation recognition algorithms for intentional modulation on pulse (IMOP) applications", Defence R&D Canada, 2001, Patent No. CA020899.

[13] R.K. Niranjan, C.B. Rama Rao, A.K. Singh, "FPGA based Identification of Frequency and Phase Modulated Signals by Time Domain Digital Techniques for ELINT Systems", Def. Sci. J., Vol. 71, No. 1, pp. 79-86, DOI: 10.14429/dsj.70.15705.

2021 International Conference on Advances in Electrical, Computing, Communication and Sustainable Technologies (ICAECT) | 978-1-7281-5791-7/20/$31.00 ©2021 IEEE | DOI: 10.1109/ICAECT49130.2021.9392569

Improved Parameters Estimation of Radar Pulses using Autocorrelation

[1,2]RK Niranjan, [1]CB Rama Rao and [2]AK Singh

[1]Department of ECE, NIT, Warangal - 506004, India
[2]DLRL (DRDO), Hyderabad - 500005, India
Email: niranjanrk2004@gmail.com

***Abstract* - Electronic Intelligence (ELINT) system provides significant advantages with enhanced range, high coverage, and portability. It has various challenges and is highly demanding. These systems should have a highly sensitive receiver with a capability to intercept, characterize and distinctly identify ground-based, shipborne, and airborne radars to meet the platform requirement. This paper describes an approach with low computations for real-time radar signal detection and pulse parameter estimation based on autocorrelation. The detailed feature extraction is carried out on the detected pulse data, leading to distinct identification of radar referred to as specific emitter identification.**

Keywords - Detection, parameter estimation, autocorrelation, sensitivity, pulse repetition interval, signal-to-noise ratio.

I. INTRODUCTION

The ELINT systems do the information gathering of signals emitted from radars. Modern radar systems transmit complex waveforms with low power [1]. Signal detection is an essential requirement of these systems at low signal-to-noise ratio (SNR).

One of the important operations in electronic warfare (EW) is radar emitter identification. It is having significance for strategic use. To distinguish the emitters from the same class or same type in an increasingly dense environment is a challenging task for the ELINT receiver. Conventional radar identification is based on the basic pulse parameters angle-of-arrival (AOA), radio frequency (RF), pulse repetition interval (PRI), pulse width (PW) are unable to characterize the nature of the emitter radar effectively. The extraction of radar signal fine features becomes an important task for the ELINT receiver. The extraction of fine features includes intentional and unintentional, followed by classification and identification is referred to as specific emitter identification [2]. The concept of specific emitter identification has evolved over the years and is an important aspect of ELINT and ES systems. It is a primary supplier of information to the pre-programmed libraries meant for countermeasures. The pace of technological advancement in the field of radars has been rapid. The challenge is to act against new, unknown, and adaptive radar threats. A high performance computing platform is needed to realize ELINT receiver coupled with signal processing capability.

Many digital receiver configurations are used as part of ELINT systems. The requirement of hardware resources is varied based on their architecture and processing technique [3]-[5].

To realize such an ELINT receiver requires a lot of resources, solid-state memories. The signal processing approach is applied to the signal detection itself. It has become possible due to an availability of high speed, high density, signal processing intensive Field Programmable Gate Array (FPGA). Still due to the usage of low computational approaches requires fewer resources and minimizes the power requirement.

This paper describes the various signal processing detection approaches for radar signal detection. The techniques are compared in terms of computations, resources, and speed. The optimum technique is elaborated along with its hardware implementation using FPGA. The performance benchmarks in terms of achieved PW, TOA accuracy, and SNR are also described.

II. VARIOUS TECHNIQUES FOR PARAMETER ESTIMATION

It is very important to detect the radar signals in real-time and get accurate TOA and PW estimation in the field of electronic reconnaissance. The accurate TOA and PW estimation are pre-requisites for measuring amplitude, frequency, phase, and other parameters using signal processing techniques. The accuracies of these parameters will directly affect the performance and efficiency in exploring the EM environment.

Initially, the radar pulse has to be detected correctly to estimate the pulse parameters. The radar pulse has to be digitized and to be captured for detection. These are different ways by which pulse can be detected and parameters are estimated either in time-domain or the frequency domain.

(a) Internal Trigger

The intermediate frequency (IF) signal is the down-converted radio frequency (RF) signal. The trigger is called internal as it is generated based on the IF signal itself. The IF signal is digitized by high-speed analog to digital (ADC) converter. The internal trigger is high for the pulse on time. The trigger pulse is used to detect the pulse and IF samples during the pulse on time along with TOA are stored for further measurements.

(b) External Trigger

The external trigger is generated based on log video. The log video is the logarithmic scale detector output of the IF signal. It indicates the envelope of the IF signal [6]. It covers the complete dynamic range of the IF signal. The trigger signal of a fixed level is generated if it crosses the threshold.

In the above techniques, no signal processing is involved and hence no processing gain is achieved. These techniques do not require any kind of processing. The techniques below are based on signal processing and processing gain is achieved.

(c) Digital IQ technique

The following equations are described the standard digital IQ techniques for calculating instantaneous amplitude profile which is synthetic amplitude profile. This amplitude profile describes the envelope of the IF signal.

$$R(n) = \sqrt{x_i{}^2(n) + x_q{}^2(n)} \tag{1}$$

The trigger signal is generated based on the amplitude profile. But, it requires a signal-to-noise ratio (SNR) of more than 12 dB.

(d) FFT Based

The 256 points FFT is computed continuously on the digitized IF signal. The FFT output is compared with the threshold and a trigger signal is generated. The trigger signal represents the pulse envelope of the IF signal. The output of FFT is generated with a 3 dB loss if at least half of the frame (i.e. 128 samples) is full. The maximum delay of trigger signal to pulse IF samples will be two frames and each frame is with 256 samples. So, the total of two frames of pulse IF samples is stored in FIFO to avoid the loosing of pulse IF data [7]. The FFT based detection gives the processing advantage compared to other techniques. But this technique requires more hardware resources compared to any other techniques.

III. PROPOSED AUTOCORRELATION BASED PULSE PARAMETER ESTIMATION

The proposed approach is computationally efficient and occupies fewer FPGA resources. It also provides a detection advantage. It is performed on the signal x(n).

The received signal is expressed in complex form as

$$\mathrm{x(n)} = \mathrm{Ae}^{\mathrm{j2\pi fnt_s}}\mathrm{e}^{\mathrm{j\emptyset}} + \mathrm{w(n)} \tag{2}$$

Where $\mathrm{Ae}^{\mathrm{j2\pi ft_s}}$ is the received signal, A is the signal amplitude, $\emptyset$ is the initial phase, $\mathrm{t_s}$ is the sampling interval, f is the carrier frequency. w(n) is the sampled zero-mean, Gaussian additive white noise.

The autocorrelation result is computed based on the absolute value of the pulse and according to the features of a digital wideband pulse. The autocorrelation function is given by [8],

$$\begin{aligned} S_n(n) &= \textstyle\sum_{i=0}^{N-1}|x(n+i)|\,|x^*(n+i+1)| \\ &= \textstyle\sum_{i=0}^{N-1}\big|A^2 e^{j2\pi f n t_s} e^{j\emptyset} + \\ &\quad Ae^{j\emptyset}e^{j2\pi f_{(n+i)}t_s}\, w^*(n+i+1) + \\ &\quad Ae^{-j\emptyset}e^{-j2\pi(n+i+1)t_s}\, w(n+i) + \, w(n+i)\big| \end{aligned} \tag{3}$$

$\mathrm{S_n(n)}$ can be updated by iterated means and can be easily implemented on hardware by using,

$$\begin{aligned} S_n(n+1) &= S_n(n) + |x(n+N)x^*(n+N+1)| - \\ &\quad |x(n)x^*(n+1)| \end{aligned} \tag{4}$$

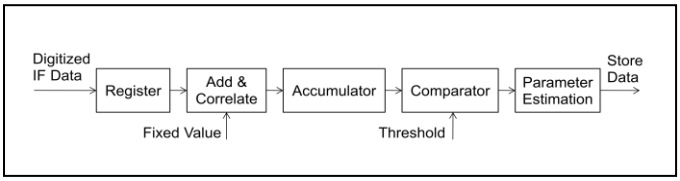

Fig. 1. Block Diagram of Autocorrelation based Parameter Estimation.

Initial autocorrelation will be performed with length N samples. Then subsequently new autocorrelation output will be obtained by subtracting the first sample autocorrelation output and adding new sample autocorrelation to the correlation value. N samples autocorrelation is performed in a recursive way to reduce the computational burden. The block diagram of autocorrelation based parameter estimation is shown in Fig. 1.

Autocorrelation output will be compared with a threshold to check for start of the pulse. If the start of a pulse is detected, then IF data will be stored and the time of arrival will be stored. N should be selected in such a way that it should detect minimum pulse width. As N increases noise reduction is improved. So a selection of N is a trade-off between minimum pulse width and noise suppression. Value of N, more than 16 is optimum. The following equation is rewritten and simplified as below,

$$x(n) = x_i\,(n) + jx_q\,(n) \tag{5}$$

$$S_N(n) = \textstyle\sum_{n=0}^{N}\big[x_i(n) + jx_q(n)\big]\big[x_i(n+1) + jx_q(n+1)\big] \tag{6}$$

$$\begin{aligned} S_N(n+1) &= S_N(n) + \big[x_i(n+N-1) + jx_q(n+N-1)\big] \\ &\quad \big[x_i(n+N) + jx_q(n+N)\big] - \\ &\quad \big[x_i(n) + jx_q(n)\big]\big[x_i(n+1) + jx_q(n+1)\big] \end{aligned} \tag{7}$$

$$\begin{aligned} Y_N(n) &= \big[x_i(n+N-1) + jx_q(n+N-1)\big] \\ &\quad \big[x_i(n+N) + jx_q(n+N)\big] \end{aligned} \tag{8}$$

$$Y_1(n) = \big[x_i(n) + jx_q(n)\big]\big[x_i(n+1) + jx_q(n+1)\big] \tag{9}$$

$$S_N(n+1) = \frac{S_N(n) + Y_N(n) - Y_1(n)}{N} \tag{10}$$

$S_N\,(n)$ is computed for every new sample. Here only four real multiplications are required for every new sample.

$$S_N(n+1) = \; k + \frac{Y_N(n)}{N} - \frac{Y_1(n)}{N} \tag{11}$$

Proposed Approach vs FFT for detection

In present days, FFT is frequently used for pulse detection. N point FFT requires $(N)\log_2(N)$ complex multiplications. Total 2K complex multiplications are required for 256 points FFT. Whereas, the proposed approach requires 512 multiplications for 256 samples are averaged. Minimum Overlapping of 75% is used to improve TOA accuracy but in that case total a 8K multiplications are required. The multiplications are performed in DSP48 slice of FPGA. Therefore, FFT requires a huge number of DSP48 slice operations whereas the proposed technique requires only 12 DSP slices operations for 1 sample. The TOA error in case of 75% overlapping also will be of the order of 64 samples whereas, 4 samples TOA accuracy is achieved with the proposed approach.

Implementation Architecture

Autocorrelation is performed on the IF signal. The IF signal is then converted to in-phase (I) and quadrature-phase (Q) samples. The complex multiplication is performed to compute the autocorrelation. After complex multiplication is performed all real and imaginary values are added separately as shown in Fig. 2.

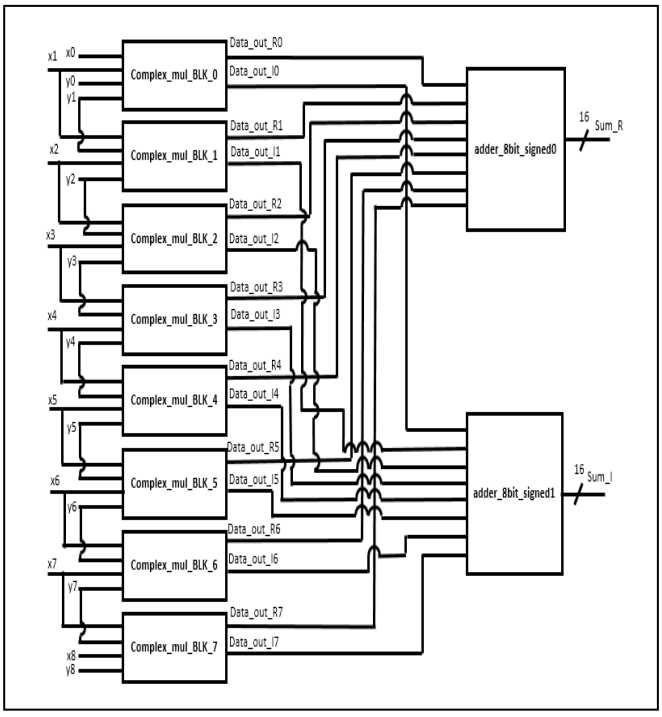

Fig. 2. Complex Multiplication of 8 samples in single block

Complex multiplication is computed based on "(6)". The final correlation value is compared with the defined threshold and a trigger is generated when it crosses the given threshold value.

Resource Utilisation and Performance Comparison

The autocorrelation based pulse detection is implemented on the Xilinx Virtex-7 XC7VX415T FPGA using Vivado 2018.3 tool. The summary of resource utilization is shown in Table I and the performance comparison is shown in Table II. Table II shows the proposed approach is appropriate compared to other approaches.

TABLE I. RESOURCE UTILIZATION SUMMARY

Resources	**FFT Approach**	**IQ Approach**	**Proposed Approach**
Slice F/Fs	4836	3965	1492
LUT (4 Input)	3526	2380	1022
DSP48E1	42	38	12
Total Power (mW)	812	708	528

TABLE II. PERFORMANCE COMPARISON

Resources	**FFT Approach**	**IQ Approach**	**Proposed Approach**
Algorithm Complexity	More	More	Less
Hardware Requirement	More	More	Less
Processing SNR Requirement at Sensitivity	8 dB	12 dB	4 dB
Dynamic Range Achieved	42 dB	39 dB	47 dB
TOA Accuracy	64 samples	10 samples	4 samples
PW Accuracy	64 samples	8 samples	8 samples
Ability to measure Rise/Fall Time	No	Yes	Yes
Ability for Intra -pulse Modulations measurement	No	Yes	Yes

IV. SIMULATION RESULTS AND DISCUSSIONS

The simulation is carried out using Xilinx Simulator tool for various pulse widths. It is varied from very narrow PW of 50 ns to 1ms and trigger pulse is generated i.e. pulse is detected correctly. Fig. 3 to Fig. 5 depicts the trigger pulse generation for pulse widths 50 ns, 200 ns and 1 us. Simulation is shown for two pulses only due to visibility. Three sequential autocorrelations are performed to meet the input sample data rate and accordingly, three triggers are generated. Finally, based on the three triggers single trigger is generated.

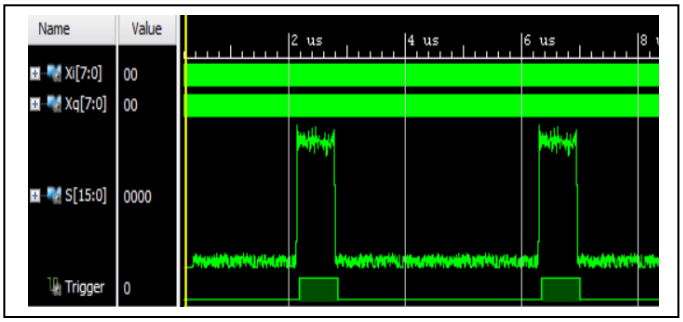

Fig. 3. Trigger generation (Pulse detection) for PW of 50 ns

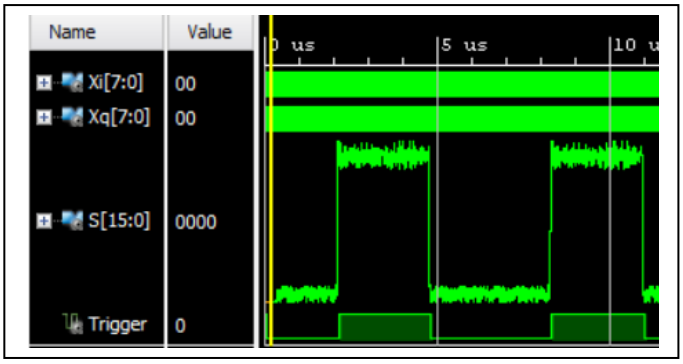

Fig. 4. Trigger generation (Pulse detection) for PW of 200 ns

Fig. 5. Trigger generation (Pulse detection) for PW of 1 us

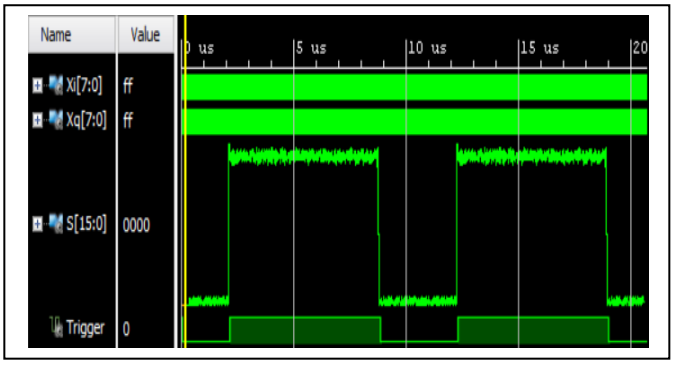

V. CONCLUSIONS

This paper describes the algorithm for signal detection based on autocorrelation which is more resistant to noise and computationally less intensive. The proposed technique has been implemented on the Xilinx Virtex-7 XC7VX415T FPGA which has DSP slices to carry out signal processing functionality. The efficacy of the technique has been tested for various Pulse Widths, under varying SNR conditions and modulated pulses. It has also been tested with real radar signals and results were positive with correct pulse detection and without false detection and missed detection.

ACKNOWLEDGMENT

It is great pleasure to thank Director DLRL, Associate Director, and Wing Head for their continuous guidance and support toward this activity.

REFERENCES

[1] M.I. Skolnik, “Introduction to Radar Systems”, Tata McGraw Hill, First Edition, 1980, pp. 376-382, pp. 420-434.

[2] Y. Qun, C. Heng, and G. Moyun, Radar Specific Emitter Identification Using Carrier Frequency Feature, 2019 IEEE International Conference on Signal, Information and Data Processing (ICSIDP), Chongqing, China, 2019, pp. 1-4..

[3] H. Pekau, and J.W. Haslen, A Comparison of Analog Front End Architectures for Digital Receivers, CCECE/CCGEI, Saskatoon, May 2005, IEEE.

[4] S. Mahlooji, and K. Mohammadi, Very High Resolution Digital Instantaneous Frequency Measurement Receiver, International Conference on Signal Processing and Systems, 2009.

[5] J. Helton, C. In, H. Chen, M. David, Lin, and B.Y.T. James, "FPGA-Based 1.2 GHz Bandwidth Digital Instantaneous Frequency measurement Receiver", ISQED 2008, 9th International Symposium on Quality Electronic Design, San Jose, CA, USA, 2008, pp. 568-571.

[6] J.B.Y. Tsui, Microwave Receivers with Electronic Warfare Applications, SCRW PUBLISH1, INC., SciTech Publishing, Inc, Raleigh, NC.

[7] J.B.Y. Tsui, “Digital Techniques for Wideband Receivers”, 2nd Ed., Norwood, MA: Artech House, 2001.

[8] Z. Simin, Z. Deguo, and T. Bin, A Wideband Pulse Detection Algorithm based on Autocorrelation, The Ninth International Conference on Electronics Measurement Instruments, ICEMI, IEEE, vol. 4, 2009, pp. 287-289.

2021 International Conference on Advances in Electrical, Computing, Communication and Sustainable Technologies (ICAECT) | 978-1-7281-5791-7/20/$31.00 ©2021 IEEE | DOI: 10.1109/ICAECT49130.2021.9392605

Performance Comparison of FFT based Frequency Estimation using different Interpolation Techniques for ELINT Systems

[1,2]RK Niranjan, [1]CB Rama Rao and [2]AK Singh

[1]Department of ECE, NIT, Warangal - 506004, India
[2]DLRL (DRDO), Hyderabad - 500005, India
Email: niranjanrk2004@gmail.com

***Abstract* - Fast Fourier Transform (FFT) is widely used in Electronic Intelligence (ELINT) systems for detection as well as for frequency measurement. Measurement of the frequency with high accuracy is a challenge within the trade-off of hardware resources, and without affecting other parameter measurements. In this paper, interpolation techniques are used at the output of N-point FFT, and frequency is estimated. These techniques are implemented in Matlab and results are verified for the band of input frequencies.**

Keywords - Detection, FFT, Estimated frequency, Windowing, Interpolation, Curve fitting.

I. INTRODUCTION

Electronic Support (ES) and Electronic Intelligence (ELINT) are part of Electronic Warfare (EW) systems. These systems are used to detect, acquire, measure, and store the radar signal information for intention of tactical as well as to form the electronic order of battle (EOB). ES systems are required to be wideband to detect signals from the entire frequency band simultaneously. Whereas, ELINT systems are meant for high sensitivity to detect signals from a large distance. Electronic Attack (EA) systems are used to protect our resources by jamming action. Electronic Protection (EP) is the capability built into radar itself to protect radar systems against enemy jamming. EP and EA are also part of EW systems [1].

Various parameters are measured by ES and ELINT systems. These parameters form pulse descriptor word (PDW) which includes direction of arrival (DOA), radio frequency (RF), pulse width (PW) and pulse repetition interval (PRI), type of PRI, etc [2]. These systems measure the low probability radar (LPI) signals [3]. The LPI signals contain low power and modulations within the pulse. It becomes difficult to detect these signals due to these characteristics.

Time-domain techniques have restricted use due to their less sensitivity compared to frequency domain techniques. The sensitivity is further improved if the noise-cancellation technique is used along with time-domain techniques [4]. These techniques are capable of instantaneous measurements of frequency and amplitude which are suitable for intra-pulse measurements [5-8]. But frequency domain techniques are commonly used to get their inherent processing gain.

Digital receivers are configured based on Fast Fourier Transform (FFT) which is generally used in ELINT systems. Intermediate frequency (IF) signal coming from the front-end of systems is digitized using a high-speed analog-to-digital converter (ADC). IF signal is the down-converted output of the RF signal. FFT is used to detect the activity and measure the parameters. This provides the frequency resolution of f_s/N MHz, where f_s is the sampling frequency. Interpolation is required to perform to enhance the frequency accuracy.

Frequency accuracy can be improved by increasing the FFT number of points. But more FFT number of points requires more multiplications and results in various processing complexities. To avoid this, interpolation is the correct choice to improve the frequency accuracy. This provides the advantage for detecting the radar pulses also.

Four different interpolation techniques have been tested with the same input band of signal frequency to check the performance of each technique. In section-2, the interpolation techniques are discussed. The Matlab simulation results are given in section-3.

II. FREQUENCY ESTIMATION USING DIFFERENT INTERPOLATION TECHNIQUES

IF signal is digitized at the f_s of 1333 MS/s which is equivalent to $4f_c/3$, where f_c is the centre frequency of the IF signal [9]. The IF signal is varied from 750 to 1250 MHz with f_c of 1 GHz and bandwidth of 500 MHz. Demuxed 8 samples are latched into FPGA coming from ADC at the dual-edge clock rate of $f_s/4$ MS/s. The total collection time for 256 samples is 256*0.75 ns = 192 ns. The processing of 256 point FFT completes before next set of data arrives. Once the data is processed, it will be sent to the output stage of FFT. Interpolation is performed on this output data. Two parallel FFT engines and interpolation blocks are used and the real-time performance is achieved. Both the FFT engines work in ping-pong mode. Fig. 1 shows the block diagram of interpolation technique.

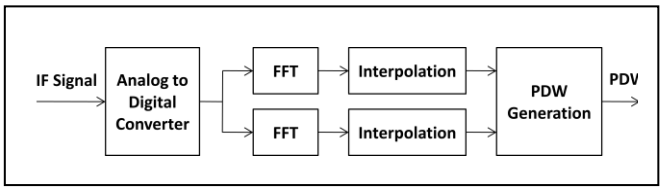

Fig. 1. Block Diagram of Interpolation Technique.

The FFT equation is given by

$$S_p = \sum_{n=0}^{N-1} x(n) e^{-j2\pi pn/N} \quad (1)$$

where p=0,1,2,….,N-1. The limits of p can also be written as -N/2 to N/2. The measured frequency is equivalent to p*f_s/N where the spectrum is having the highest value for that peak p. Fig. 2 shows the FFT spectrum

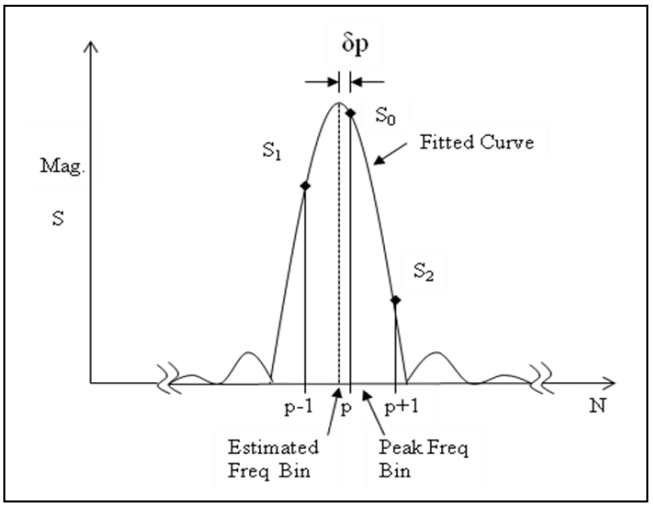

Fig. 2. FFT Spectrum

Interpolation technique is used to improve the frequency accuracy without increasing the FFT number of points. Different techniques namely Rectangular window based, Hanning window based, curve fitting based and curve fitting when FFT is performed with Hanning window are used for this purpose. The frequency is estimated by all four methods. The FFT output spreads across the bins due to the presence of non-coherent signal and white Gaussian noise. Since the input frequency or set frequency is not always the multiple of FFT resolution or least significant bit (LSB) of f_s/N. The spectral component spreads and reported peak frequency will not be exactly the same as the set frequency. Amplitude is extracted from the spectrum at three different bins. The highest peak (S_0) at bin p, the second highest peak (S_1) at p-1, and third highest peak (S_2) at p+1 is extracted from the spectrum. The delta bin which is away from the peak by $\pm\delta p$ is computed. The delta bin for the rectangular window is given by [10]

$$\delta p = (S_1 - S_2)/(S_1 + S_2) \quad (2)$$

The delta bin for the Hanning window is given by [10]

$$\delta p = (2S_1 - S_0)/(S_0 + S_1) \quad (3)$$

These techniques are similar to zero padding. The windowing methods don't change the shape of the spectrum. But it provides a better estimation of the peak frequency. These techniques provide an accurate result when only a single frequency is available at the input signal.

When S_0 is very close to the main peak above two techniques are sensitive to noise. Under this situation, S_1 and S_2 are very close to the minima and noise may reverse their amplitudes. The peak will move in the wrong direction using the above equations. When the amplitudes of S_1 and S_2 are reversed then there will be more errors [10].

Similarly, the delta bin can be written as using the curve fitting technique [11-13]

$$\delta p = (S_1 - S_2)/(S_1 - 2S_0 + S_2) \quad (4)$$

Finally, the estimated frequency is computed using the delta bin δp as $(p + \delta p)$*f_s/N.

Hanning window is applied on IF data and FFT is performed. Curve fitting technique is applied on FFT output to get the delta bin δp from "(4)". The modified interpolation technique block diagram is shown in Fig. 3.

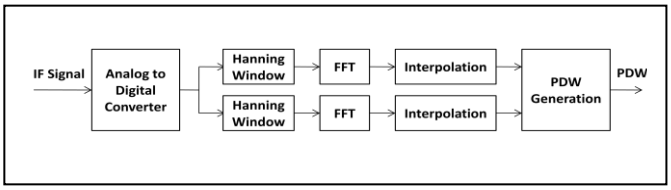

Fig. 3. Block Diagram of Modified Interpolation Technique.

III. Simulation Results and Discussions

The input signal is generated for the band of input frequencies. The set frequencies are varied from 1100 MHz to 1120 MHz with the step of 0.5 MHz to check the accuracy of algorithms.

Fig. 4 shows the frequency estimation using the rectangular window interpolation technique using 256 points FFT. The FFT frequency and estimated frequency versus set frequency is shown in Fig. 4(a). Fig. 4(b) shows the root mean square error (RMSE) versus set frequency for both FFT reported frequency and estimated frequency. Fig.5, Fig. 6, and Fig.7 show the result for Hanning window interpolation technique, curve fitting interpolation technique and curve fitting with Hanning window interpolation technique respectively.

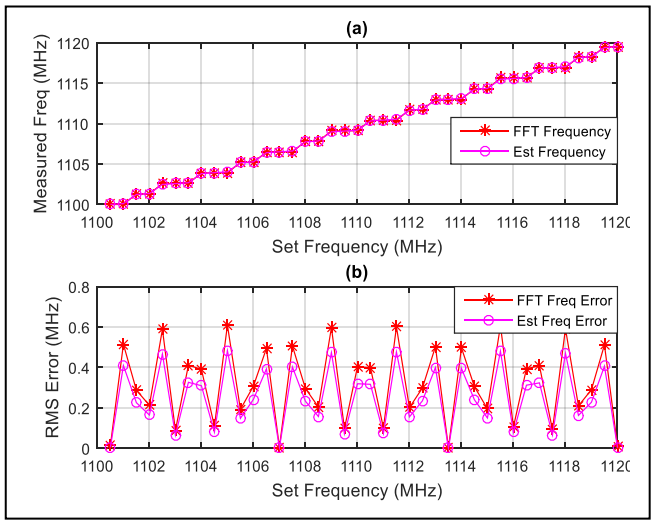

Fig. 4. Frequency Estimation using Rectangular Window (a) Measured Frequency vs. Set Frequency and (b) RMSE vs. Set Frequency

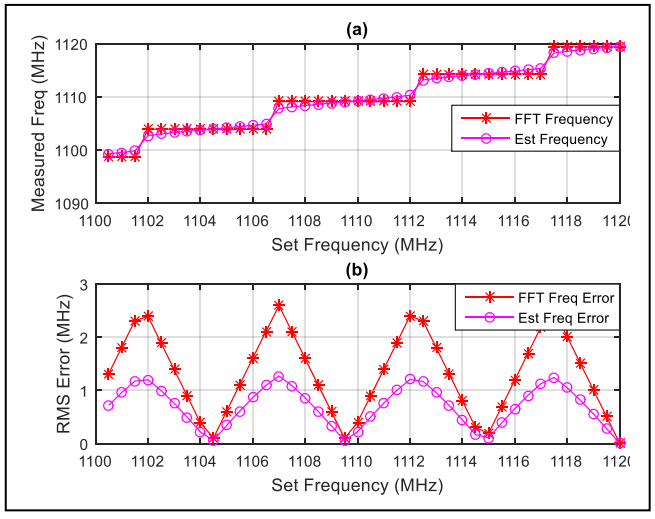

Fig. 5. Frequency Estimation using Hanning Window (a) Measured Frequency vs. Set Frequency and (b) RMSE vs. Set Frequency

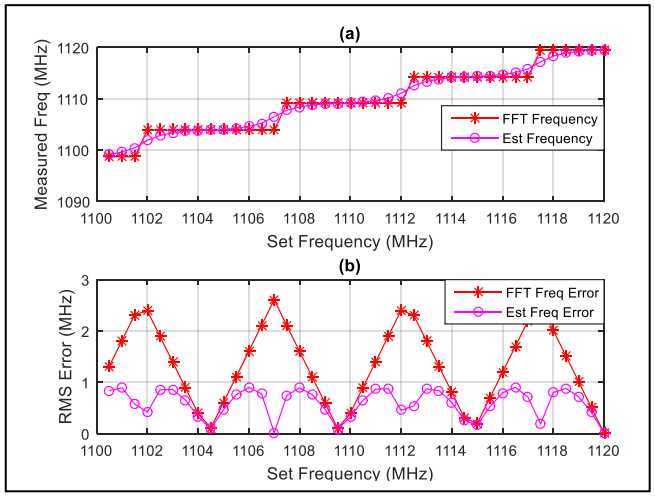

Fig. 6. Frequency Estimation using Curve Fitting (a) Measured Frequency vs. Set Frequency and (b) RMSE vs. Set Frequency

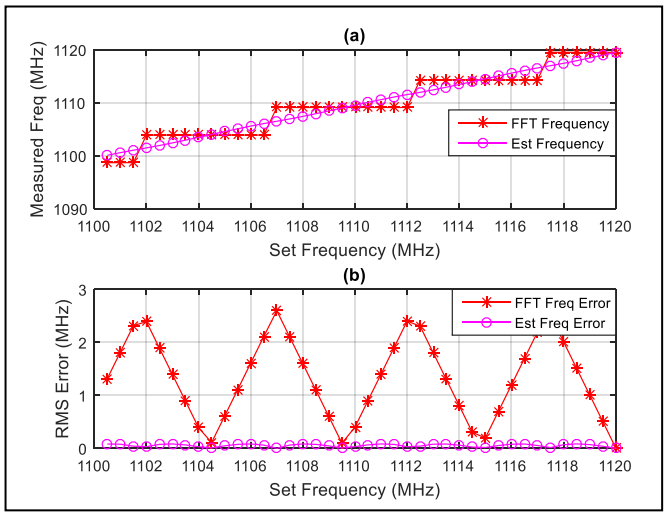

Fig. 7. Frequency Estimation using Curve Fitting with FFT along with Hanning Window (a) Measured Frequency vs. Set Frequency and (b) RMSE vs. Set Frequency

Based on the frequency accuracy error computed using different interpolation techniques the RMSE and peak error are calculated and tabulated as Table I and Table II respectively. It is found from the result that RMSE calculated from measured frequency using 256 points FFT is 1.528 MHz. In case of the rectangular window interpolation technique, Hanning window interpolation technique, Curve fitting interpolation technique, and Curve fitting interpolation technique with Hanning window the RSME is 1.0954 MHz, 0.7969 MHz, 0.6561 MHz, and 0.0609 MHz respectively. The RMSE is lowest in the case of the curve fitting interpolation technique with the Hanning window. The peak error is also lowest 0.0820 MHz in the case of the curve fitting interpolation technique with the Hanning window. This performs equivalent to multiple times the number of points FFT results without interpolation.

TABLE I. RMSE OF ESTIMATED FREQUENCY FOR INTERPOLATION TECHNIQUES

Interpolation Technique	**RMSE (MHz) # N Point FFT**				
	256	**512**	**1024**	**2048**	**4096**
FFT Measured Frequency	1.5280	0.7566	0.3702	0.1843	0.0916
Rectangular Window	1.0954	0.5742	0.2929	0.1503	0.0765
Hanning Window	0.7969	0.4584	0.2467	0.1308	0.0681
Curve Fitting Technique (CFT)	0.6561	0.3169	0.1573	0.0787	0.0402
CFT with Hanning window	0.0609	0.0297	0.0148	0.0074	0.0038

TABLE II. PEAK ERROR OF ESTIMATED FREQUENCY FOR INTERPOLATION TECHNIQUES

Interpolation Technique	Peak Error (MHz) # N Point FFT				
	256	**512**	**1024**	**2048**	**4096**
FFT Measured Frequency	2.5977	1.2988	0.6094	0.3076	0.1567
Rectangular Window	1.8745	0.9872	0.4832	0.2512	0.1309
Hanning Window	1.2722	0.7577	0.3982	0.2149	0.1148
Curve Fitting Technique (CFT)	0.9051	0.4423	0.2197	0.1093	0.0545
CFT with Hanning window	0.0820	0.0418	0.0209	0.0104	0.0052

IV. CONCLUSIONS

Simulation results of all four interpolation techniques are taken and their performance is compared. The curve fitting interpolation technique gives the lowest RMSE compared to rectangular window, and Hanning window techniques. The RMSE is further improved when FFT is computed with the Hanning window and the curve fitting technique is applied. This technique is also implementable for real-time applications and hence it is useful for ELINT systems where better frequency accuracy is required. The estimated frequency is further improved if FFT points are increased. But for more number of FFT points, the data collection time, and processing time increases. Processing hardware should also support the resource requirements for implementation.

ACKNOWLEDGMENT

It is great pleasure to thank Director DLRL, Associate Director and Wing Head for their continuous guidance and support toward this activity.

REFERENCES

[1] D.L. Adamy, EW 101: A First Course in Electronic Warfare, Boston, MA, USA: Artech House, 2001.

[2] R.G. Wiley, ELINT, the Interception and Analysis of Radar Signals, Artech House Radar Library, Artech House, Inc., 2006.

[3] D.L. Adamy, EW 102: A Second Course in Electronic Warfare, Boston, MA, USA: Artech House, 2004.

[4] V. Saeed, Advanced Digital Signal Processing and Noise Reduction, 4th Ed, John Wiley & Sons, 2008, pp. 321-323.

[5] S. Mahlooji, and K. Mohammadi, "Very High Resolution Digital Instantaneous Frequency Measurement Receiver", International Conference on Signal Processing and Systems, 2009.

[6] Z. Simin, Z. Deguo, and B. Tang, "A Wideband Pulse Detection Algorithm based on Autocorrelation", 9th ICEMI, vol. 4, IEEE, 2009, pp. 287-289.

[7] R.K. Niranjan, and B.R. Naik, "Approach of Pulse Parameters Measurement using Digital IQ Method", IJIEE; 2014.V4.403.

[8] J. Helton, C.H. Chen, M. David, and J.B.Y. Tsui, "FPGA Based 1.2 GHz Bandwidth Digital Instantaneous Frequency Measurement Receiver", 9th ISQED, San Jose, CA, USA, 2008, pp 265-270.

[9] R.G. Lyons, Understanding Digital Signal Processing, Boston, Addison Wesley Longman, Inc, 1997, pp. 32-42.

[10] J.B.Y. Tsui, Special Design Topics in Wideband Digital Receivers, 2nd Ed, Norwood, MA, Artech House 2004.

[11] H. Akima, A method of smooth curve fitting, ESSA Tech, ERL 101-ITS 73 US Government Printing Office, Washington, D. C., Jan. 1969.

[12] B.G. Quinn, "Estimating Frequency by Interpolation Using Fourier Coefficients," IEEE Trans. Signal Processing, Vol. 42, May 1994, pp. 1264-1268.

[13] P. Voglewede, Parabola Approximation for Peak Determination Global DSP Magazine, 3(5), May 2004, pp. 13-17.